NOVA SCHOOL OF SCIENCE & TECHNOLOGY

DEPARTMENT OF CHEMISTRY

DEVELOPMENT OF MIXED MATRIX IONGEL MEMBRANES FOR CO_2 SEPARATION

ANA RITA MILEU MOTA NABAIS

Master in Chemical and Biochemical Engineering

DOCTORATE IN CHEMICAL AND BIOLOGICAL ENGINEERING

NOVA University Lisbon

March, 2023

DEPARTMENT OF
CHEMISTRY

DEVELOPMENT OF MIXED MATRIX IONGEL MEMBRANES FOR CO_2 SEPARATION

ANA RITA MILEU MOTA NABAIS

Master in Chemical and Biochemical Engineering

Adviser: Luísa Alexandra Graça Neves
Assistant Researcher, NOVA University Lisbon

Co-advisers: Liliana Sofia Carvalho Tomé
Assistant Researcher, NOVA University Lisbon

João Paulo Serejo Goulão Crespo
Full Professor, NOVA University Lisbon

Examination Committee:

Chair: Susana Filipe Barreiros,
Full Professor, FCT-NOVA

Rapporteurs: Jason Edward Bara,
Professor, University of Alabama

Adélio Miguel Magalhães Mendes,
Full Professor, University of Porto

Adviser: Luísa Alexandra Graça Neves,
Assistant Researcher, FCT-NOVA

Members: Ana Maria Antunes Dias,
Assistant Researcher, University of Coimbra

Isabel Alexandra de Almeida Canento Esteves Esperança,
Assistant Professor, FCT-NOVA

DOCTORATE IN CHEMICAL AND BIOLOGICAL ENGINEERING

NOVA University Lisbon
March, 2023

Development of Mixed Matrix Ionogel Membranes for CO_2 Separation

To my family.

ACKNOWLEDGMENTS

The accomplishment of this work was only possible due to the contribution of many people, to whom I am immensely grateful, both professionally and personally.

To my supervisors, Doctor Luísa Neves, Doctor Liliana Tomé and Professor João Crespo, for accepting to guide me over these last 4 years, for allowing me to develop this work at the Laboratory of Membrane Processes (LMP) and for all the guidance, scientific discussions, dedication and patience to bring it to a successful conclusion. For knowing me well enough to give me the freedom to develop this work "in my own way", but at the same time being there whenever necessary. For all the opportunities they have given me to share my work at numerous conferences, which was, without a doubt a very important step in my education and in building the foundations for my future. A special acknowledgement to Doctor Luísa Neves, for taking this journey with me, since my master's thesis, in 2016, and for trusting me to continue this work.

To *Fundação para a Ciência e a Tecnologia* (FCT), for the financial support through the fellowship SFRH/BD/136963/2018.

To my institution, NOVA University of Lisbon, which I have been a part of for the past 12 years and where I completed my entire academic journey.

To Professor Vítor Alves (*Instituto Superior de Agronomia*), for the availability to help me with the mechanical experiments, and for the kindness and generosity in always giving a valuable contribution to the work. To Rosa Huertas, for all the help with the TGA experiments at ITQB.

To Rute Francisco, for all the work she developed that led to one of the chapters of this thesis.

A special acknowledgement to Professor David Mecerreyes, for having me in his group, at POLYMAT (University of the Basque Country, Spain), which was, without a doubt, a turning point in this thesis. It was a great opportunity to develop part of this work, in such a dynamic group. I will always be grateful for the generosity and help during lockdown, when I could not return home.

To Professor Lilia Ahrné, from the University of Copenhagen, for having me in her group and sharing so much knowledge and experience with me. To Mikkel, Anne, Gabriele, Ester and Yuan for making me feel part of the group in such a short time. To Arthur, for his patience, company and for sharing everything he knows with me, and for all the coffees and beers, that made me feel at home.

To all my colleagues from the LMP group, for the mutual help and companionship both inside and outside of the lab. I would like to particularly acknowledge Rosa Nascimento, Noémi, Suchintan, Usman and Bhavna, for the companionship, friendship and all the good moments spent together throughout these years. Finally, to Inês Ferreira and Paloma Ortiz, for being much more than lab colleagues. I am grateful for you, for all the moments we shared, for all the lessons we learned and taught each other and for sharing this journey with you.

To Gonçalo Martins, for being the best friend I could ask for at every moment of the last 11 years.

To my friends, Flávia Gaio, Tiago Santos, João Valentim, Clarinda Costa, Gonçalo Marcelo, Mónica Carvalheira, Eliana Guarda, Mário Sousa, André Loureiro, José Gomes, Catarina Martins and Diogo Mendonça.

To Bruno Cardoso, for all the 7 a.m. workouts and for putting up with my grumpy face and complaints.

To Paula and Nuno, for welcoming me into their family with open arms and for making me feel part of it from day one.

To the most important people in my life. To my parents, to whom I owe everything. There are not enough words for me to express the gratitude, love, and admiration I have for you. Your unconditional support, love, sacrifices, dedication, and belief in me were the biggest motivators for me to reach this point. To my brother, who has always been an example of hard work and dedication. For always being there when needed, no questions asked and for giving me my beautiful nephew and nieces, who are the joy of any family gathering. To my husband, João, for the endless patience, precious help, love, and emotional support. For sharing the best and worst moments of my life with me. For showing me the positive side in every situation, for never judging or doubting me and always encourage me during my confidence crises. For being one of the most genuine and generous people I've ever met and for sharing a life with me for the past 10 years. Everything I am today I owe it to all of you. This thesis, and what it represents, is also yours.

To all of you who contributed to the completion of this thesis, my most sincere "Thank You"!

“Science is a way of thinking much more than it is a body of knowledge.”

Carl Sagan

ABSTRACT

The climate crisis and the strategies to mitigate it are, undoubtedly, some of the most relevant and discussed issues in today's society. The continuous increase in greenhouse gas emissions, particularly CO_2, and consequent global warming can pose severe risks to the environment and the population. Due to the urgent need to mitigate CO_2 emissions, numerous strategies have been considered, particularly the implementation of a Carbon Capture, Utilization and Storage (CCUS) technology. In terms of carbon capture, membrane separation processes offer a variety of advantages, compared to other processes, in terms of lower energy consumption, maintenance requirements, and capital investment.

The designable nature of Ionic Liquids (ILs) opens up a wide range of possible chemical structures, targeting specific applications, especially CO_2 capture processes. Considering the broad range of tunable chemical and physical properties of ILs and the undeniable advantages of membrane processes, from an economical and environmental point of view, this thesis explores the development of iongel membranes, which are a specific class of IL-based materials, for CO_2 separation. Throughout this thesis, different polymer matrices and solid fillers were used to design Mixed Matrix Iongel Membranes (MMIMs) with the intent of, not only enhance their gas separation performance, but also to improve their mechanical, thermal, and chemical stabilities. A fast and solvent-free method was employed to fabricate MMIMs, by free-radical UV polymerization, as an alternative to longer and more complex preparation methods previously used.

The main idea throughout the presented thesis is to fine-tune the design of iongel membranes and to address some of the major challenges regarding the use of these IL-based materials, for CO_2 separation, in terms of thermal and mechanical properties and stability under different experimental conditions. In this thesis, CO_2/N_2 (flue gas) and CO_2/CH_4 (biogas) are the target separations, due to their relevance at an industrial level. Therefore, and considering the importance of evaluating the potential of the iongel membranes in a more realistic scenario, the developed materials were tested under different and relevant experimental conditions, in terms of temperature, pressure and humidity.

The data presented throughout Chapters 2 to 6, clearly show that the chemistry and properties of the selected component materials has a significant impact on the MMIMs' properties and overall

performance. Moreover, it is expected that the obtained results will be a step towards the design of new and alternative IL-based materials for CO_2 separation.

Keywords: Ionic Liquids, Iongel, Membranes, Nanoclay, Porous Organic Polymers, Metal Organic Frameworks, CO_2 separation.

RESUMO

As mudanças climáticas e as estratégias para as mitigar são, indiscutivelmente, algumas das questões mais relevantes na sociedade atual. O aumento contínuo das emissões de gases com efeito de estufa, em particular CO_2, e consequente aquecimento global podem representar graves riscos para o ambiente e para a população. Devido à urgente necessidade de mitigar as emissões de CO_2, têm sido consideradas inúmeras estratégias, em particular, a implementação de tecnologias de captura, utilização e armazenamento de carbono (CCUS). Relativamente à captura de carbono, os processos de separação com membranas oferecem uma variedade de vantagens em termos de consumo energético, requisitos de manutenção e investimento de capital.

A possibilidade de desenhar Líquidos Iónicos (LIs) permite obter uma ampla gama de estruturas químicas, direcionadas a aplicações específicas, especialmente para processos de captura de CO_2. Considerando a ampla gama de propriedades químicas e físicas dos LIs e as inegáveis vantagens dos processos de membranas do ponto de vista económico e ambiental, esta tese explora o desenvolvimento de membranas ditas "iongel", que são uma classe específica de materiais baseados em LIs, para a separação de CO_2. Ao longo desta tese, foram utilizadas diferentes matrizes poliméricas e materiais sólidos para desenvolver membranas iongel de matriz mista (MMIMs) como uma forma de, não só melhorar o seu desempenho na separação de gases, mas também melhorar a sua estabilidade mecânica, térmica e química. Esta tese apresenta um método rápido e sem recurso a solventes para preparar MMIMs, através da polimerização UV de radicais livres, como alternativa a métodos de preparação mais longos, complexos e poluentes, utilizados anteriormente.

A ideia subjacente a este trabalho é afinar/otimizar o desenho das membranas "iongel" e abordar alguns dos principais desafios em relação à utilização destes materiais, para separação de CO_2, em termos de propriedades térmicas e mecânicas e estabilidade em diferentes condições experimentais. Nesta tese, foram consideradas as separações CO_2/N_2 e CO_2/CH_4, devido à sua relevância a nível industrial. Desta forma, e tendo em conta a importância de avaliar o potencial das membranas "iongel" num cenário mais realista, os materiais desenvolvidos foram testados sob diferentes condições experimentais, em termos de temperatura, pressão e teor de humidade.

Os dados apresentados ao longo dos capítulos 2 a 6 mostram claramente que a natureza dos materiais selecionados tem um impacto significativo nas propriedades e desempenho das MMIMs.

Além disso, é esperado que os resultados obtidos representem um avanço no desenvolvimento de materiais novos e alternativos à base de LIs para a separação do CO_2.

Keywords: Líquidos Iónicos, *Iongel*, Membranas, *Nanoclay*, Polímeros Orgânicos Porosos, Redes Metálico-Orgânicas, Separação de CO_2.

CONTENTS

LIST OF FIGURES

LIST OF TABLES

ABBREVIATIONS

Abbreviation	Meaning
ALP	Azo-linked Polymers
ASAP	Accelerated Surface Area and Porosimetry
ATR	Attenuated Total Reflectance
BET	Brunauer-Emmett-Teller
BTC	Benzenetricarboxylic acid
CP	Cross Polarization
CCUS	Carbon Capture Utilization and Storage
DN	Double Network
DSC	Differential Scanning Calorimetry
FTIR	Fourier Transform Infrared
GC	Gas Chromatography
GO	Graphene Oxide
IL	Ionic Liquid
IPN	Interpenetrating Polymer Network
MIL	Materials of Institut Lavoisier
MMIM	Mixed Matrix Iongel Membrane
MMM	Mixed Matrix Membrane
MMT	Montmorillonite
M_n	Molecular Weight
MOF	Metal Organic Framework
MOP	Microporous Organic Polymers
M_w	Molecular Weight
NMR	Nuclear Magnetic Resonance

PA	Polyamide
PDMAAm	Poly(N,N-dimethylacrylamide)
PEG	Poly(ethylene glycol)
PEGDA	Poly(ethylene glycol) Diacrylate
PEO	Poly(ethylene oxide)
PIM	Polymer of Intrinsic Microporosity
PIL	Poly(Ionic Liquid)
POF	Porous Organic Framework
POP	Porous Organic Polymer
PVDF-HFP	Poly(vinylidene fluoride-co-hexafluoropropylene)
SAPO	Silicoaluminophosphate
SEM	Scanning Electron Microscopy
SILM	Supported Ionic Liquid Membrane
sIPN	Semi-Interpenetrating Network
TGA	Thermogravimetric Analysis
TR	Thermally Rearranged
UV	Ultra-Violet
ZIF	Zeolitic Imidazolate Framework

VARIABLES

Variable	Meaning	Units
α	Selectivity	-
β	Geometric parameter of permeation cell	m^{-1}
ε	Elongation at break	%
σ	Puncture strength	MPa
σ_n	Normalized puncture strength	MPa mm^{-1}
A	Area	m^2
a_w	Water Activity	-
d	Distance from the point of contact to the point of puncture	m
F	Applied force	N
F^f	Gas molar flow rate	mol s^{-1}
h	Radius of the sample exposed in the sample holder	m
j_i	Molar flux of gas	mol m^{-2} s^{-1}
l	Membrane thickness	m
P	Permeability	Barrer
p_{feed}	Feed pressure	Bar
p_{perm}	Permeate pressure	Bar
r	Radius of the probe	m
t	Time	s
T_{dec}	Decomposition Temperature	K
T_{onset}	Onset Temperature	K
V_{feed}	Feed volume	m^3
V_{perm}	Permeate volume	m^3
y	Gas molar fraction	-

IONIC LIQUIDS SHORT NAMES

Cations	Meaning
$[C_2mim]^+$	1-ethyl-3-methylimidazolium
$[C_4mim]^+$	1-butyl-3-methylimidazolium
$[C_4mpyr]^+$	1-butyl-1-methylpyrrolidinium
$[Ch]^+$	Cholinium
$[EtNH_3]^+$	Ethylammonium Nitrate
$[Pyr_{11}]^+$	Poly(diallyldimethylammonium)
$[Pyr_{14}]^+$	1-butyl-1-methylpyrrolidinium
$[smim]^+$	Poly(1-styrenemethyl-3-methylimidazolium)

Anions	Meaning
$[B(CN)_4]^-$	Tetracyanoborate
$[BETi]^-$	Bis(pentafluoroethylsulfonyl)imide
$[BF_4]^-$	Tetrafluoroborate
$[C(CN)_3]^-$	Tricyanomethanide
$[CF_3SO_3]^-$	Trifluoromethanesulfonate
$[ClO_4]^-$	Perchlorate
$[FAP]^-$	Tris(pentafluoroethyl)trifluorophosphate
$[FeCl_4]^-$	Tetrachloroferrate
$[FSI]^-$	Bis(fluorosulfonyl)imide
$[Gly]^-$	Glycolate
$[Mal]^-$	Malonate
$[MSPM]^-$	Monomer Sulfopropyl Methacrylate
$[MSS]^-$	Monomer Styrenesulfonate

[MTFSI]$^-$	Sulfonyl(trifluoromethane sulfonyl)imide Methacrylate
[Lac]$^-$	Lactate
[Lev]$^-$	Levulinate
[N(CN)$_2$]$^-$	Dicyanamide
[NO$_3$]$^-$	Nitrate
[PF$_6$]$^-$	Hexafluorophosphate
[TFSI]$^-$	Bis(trifluoromethylsulfonyl)imide

1

INTRODUCTION

Chapter 1 comprises parts of the author's publication: A. R. Nabais, L. A. Neves and L. C. Tomé, "Mixed-matrix iongel membranes for gas separation", ACS Appl. Polym. Mater., 2022, 4, 3098.

In the present dissertation, the use of membranes for gas separation is considered. For many years, the use of membranes for CO_2 separation has been considered the most promising technology, as an alternative to those already existing and implemented on a large scale. However, this process still needs to overcome relevant limitations, from the choice of the materials to the technological scale-up. From polymer to inorganic, including a combination between both, there is a wide variety of materials and configurations that can be used to design the most suitable membrane process for a specific gas separation.

The present dissertation focuses on the development of mixed matrix iongel membranes (MMIMs), comprising different fillers in an attempt to improve not only the gas separation performance of iongel membranes, but also combine it with thermal, chemical and mechanical stabilities. Specific parts of the scientific work here presented were achieved in collaboration with POLYMAT, University of the Basque Country (Spain) and the Beijing Institute of Technology (China).

The following subsections provide a detailed description of the concept behind the development of ionic liquid-based membranes as well as a state-of-the-art of the most relevant achievements reported so far in the literature. It should be noted that the works described throughout be following subsections report permeation results that may be expressed in different units (Barrer and GPU). The permeability of a membrane can be expressed in Barrer (10^{-10} cm^3(STP) cm cm^{-2} s^{-1} $cmHg^{-1}$), which is an intrinsic material property, that can be obtained as the product of gas solubility and diffusivity. On the other hand, the permeance is, by definition, the ratio between permeability and membrane thickness and it is typically expressed in GPU (10^{-6} cm^3(STP) cm^{-2} s^{-1} $cmHg^{-1}$).

Starting with ionic liquids, this chapter reports the evolution of ionic liquid-based membranes, describes some of the most relevant works available in the literature and sets the goals and objectives of this PhD thesis.

1.1 Ionic Liquids

The first ionic liquid (IL), ethylammonium nitrate - $[EtNH_3][NO_3]$ was proposed in 1914 by Paul Walden.[1] Since then, ILs have gained more and more relevance, especially in the last 25 years.

Ionic liquids represent a specific class of salts, composed entirely of ions (organic cations and either organic or inorganic anions), which are usually in the liquid state at room temperature, with melting points below 373 K. This feature arises from the asymmetry of the ions, that lead to weak interactions and low packing efficiency, and by the delocalization of their charges.[2] Since ILs are composed by a cation and an anion, in theory, there are an almost endless number of possible combinations to prepare these materials. This feature also provides a unique characteristic to ILs, which is their tunability. The choice of the most suitable cation-anion pair allows for the preparation of ILs with specific characteristics towards a specific application. Moreover, ILs are also known for their high thermal stability, low or negligible volatility and capability of being recycled.[1,3] This features enable the amount of waste generated during the technological process to be reduced. For many years, ILs were regarded as "green" alternatives to commonly used volatile organic solvents. However, even though ILs are considered environmentally friendly due to above-mentioned properties, their use can still raise some concerns due to a possible accumulation in the environment and in organisms, if they reach ground or surface waters or soils by accidental spills or effluents.[4] Moreover, it was found that the degree of toxicity of ILs is mainly related to the nature of the cation and the length of the alkyl side chain.[4]

Throughout the years, ILs have been widely studied in the fields of chemical synthesis and catalysis.[3] Nonetheless, taking into account their versatility and the vast amount of possible structures, ILs have also been explored for other applications, one of the most relevant being CO_2 capture. The practical application of ILs for CO_2 capture depends mostly on their effectiveness compared to other solvents, such as aqueous solutions of amines. ILs can be tailored to have a CO_2 adsorption capacity comparable to those of aqueous solutions of amines, without the disadvantages associated with amine-based solvents, mainly their volatility.[5] In this context, ILs have been widely studied mainly due to the quadrupole moment of the CO_2 molecules that interact with the electrical charges of the IL. In general, both ions can influence the CO_2 capture capacity of ILs, however the anion has been found to have the most significant influence on this parameter.[2] The most commonly used cations include imidazolium, pyrrolidinium, pyridinium, ammonium and phosphonium, while the anions can be fluorinated, cyano-based, sulfonates, acetates, carboxylates, halogens and sulfonates. In imidazolium-based ILs, increasing alkyl chain length leads to higher CO_2 solubility, due to a decrease in the interactions between the ions in the IL, leaving more free volume to accommodate the CO_2 molecules, that will become more available to interact with the IL's anions.[2] The common structures of the most used ILs for CO_2 separation can be found in Figure 1.1.

Even though adjusting the cation-anion pair in the IL structure could enhance the CO_2 solubility, their CO_2 capture capacity is still low, compared to the more conventional carbon capture technologies using aqueous solutions of amines. To overcome this drawback, task-specific or functionalized ILs have been developed. In this case, suitable moieties, such as amines, are incorporated into the IL structure.[6]

In sum, CO_2-philic functional groups are attached to ILs, to significantly increase their CO_2 capture capacity. Nonetheless, complicated synthesis and purification steps, high viscosity and high production costs represent the major challenges for this class of ILs to be used for the CO_2 capture .[7,8] Hence, it became clear that a different strategy should be studied, to develop new materials, to take advantage of the best properties of ILs, while overcoming the mentioned drawbacks associated with their use.

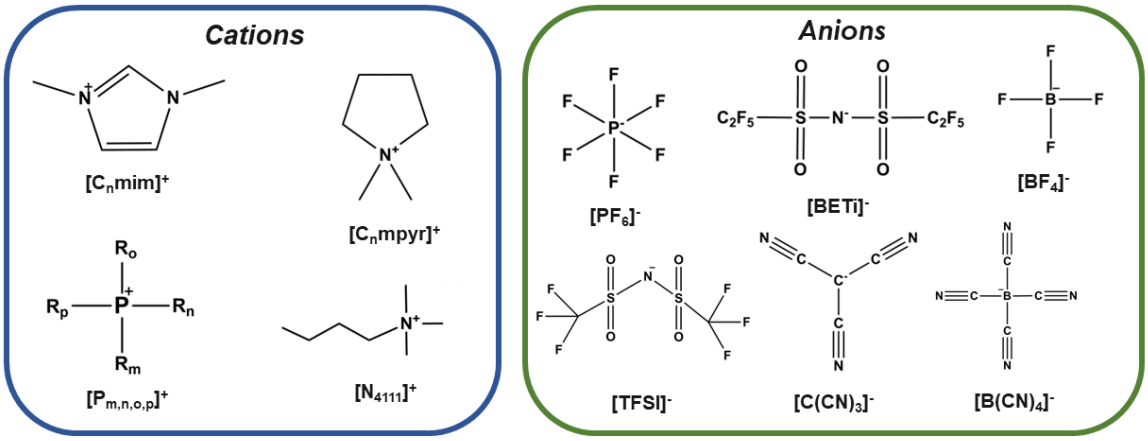

Figure 1.1 – Examples of common IL cations and anions.

1.2 Designing IL-based Membranes for CO_2 Separation

During the last 25 years, the potential of ionic liquid materials to improve membrane-based gas separation processes has been demonstrated through the exploitation of numerous membranes with diverse configurations, chemical functionalities, properties, morphologies, and separation efficiencies. Remarkable CO_2 solubilities and designer nature are essential features of the versatile and unique IL platform. The research progress on ionic liquid-based membranes for gas separation, particularly for CO_2 separation applications, has been reviewed in recent years.[2,9–11]

1.2.1 Supported Ionic Liquid Membranes (SILMs)

The easiest way to combine ILs and membrane technology is through the preparation of supported ionic liquid membranes (SILMs), in which the selected IL phase is immobilized into the pores of an inert solid membrane supported by capillary forces (Figure 1.2).[12]

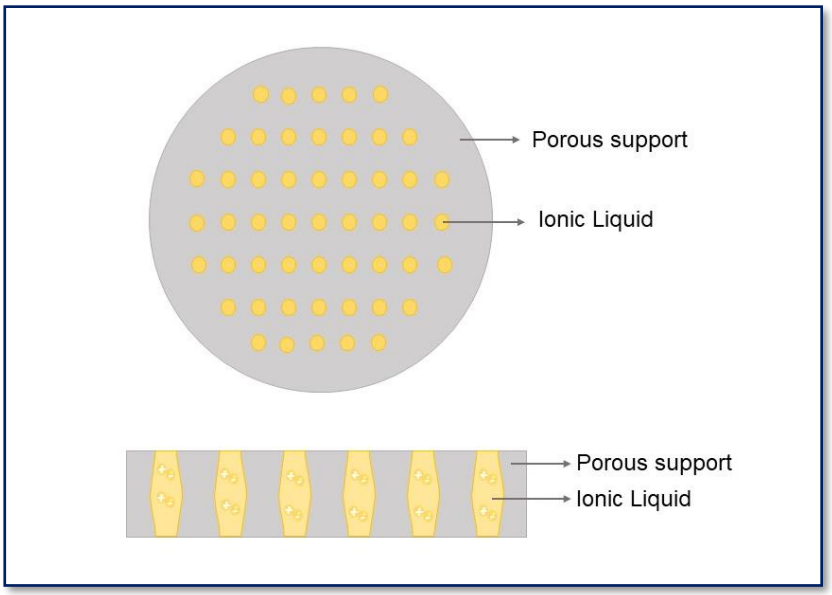

Figure 1.2 - Schematic representation of a supported ionic liquid membrane (SILM).

Compared to organic solvents, the low volatility and high viscosity of ILs are advantageous for SILM configuration, since the use of these materials helps preventing the loss of solvent by evaporation and pressure displacement, at low pressures. SILMs are considered an attractive approach, as much smaller quantities of IL are needed, compared to the use of bulk ILs for CO_2 absorption. The preparation method of SILMs plays a vital role in the quality of IL immobilization and overall membrane stability. Typically, SILMs can be fabricated by three different methods: (i) immersion, which consists in soaking the porous support in the selected IL for a few hours;[13,14] (ii) pressure, where the IL immobilization is obtained by putting the porous support in an ultrafiltration unit, the IL is added and pressurized (i.e. with nitrogen) to ensure that the IL is immobilized into the pores of the support, [15] and (iii) vacuum, where initially the porous support is placed inside a vacuum chamber to remove the air inside the pores and then drops of IL are spread on the membrane surface and vacuum is again applied to guarantee that the IL is trapped within the pores of the support.[16] The supports can be either polymer or ceramic, and must be selected considering the compatibility with the IL, the pore size as well as their mechanical stability.[2,17,18]

SILMs for CO_2 separation were reported, for the first time, by Scovazzo *et al.* [19] and, since then, different configurations have been tested,[20–22] including flat sheet,[16,23–30] which is the simplest approach.

A wide variety of ILs, with different characteristics/properties have already been used to fabricate SILM systems.[31,32] Considering the cation, several studies have focused on imidazolium-based

ILs, since these materials are widely commercially available and can be easily modified for CO_2 separation. As stated before, in imidazolium-based ILs, the CO_2 solubility is highly influenced by the alkyl chain length. Neves *et al.* [25] studied the effect of increasing the alkyl chain length of imidazolium-based ILs (C_4, C_6 and C_8) containing the $[PF_6]^-$ anion. The authors found that the increase in the alkyl chain length of the IL cation led to a two-times increase in gas permeability (from 171 to around 370 Barrer).[25] Several authors have also reported improvements in the SILMs' gas separation performance through modifications on the imidazolium cations. The functionalization of imidazolium cations with oligo(ethylene glycol) was reported by Bara *et al.*,[33] where improvements in CO_2/N_2 and CO_2/CH_4 selectivities of the resulting ILs were observed, compared to the alkyl analogues.[33] Later, the same authors reported the use of different imidazolium-based ILs containing fluoroalkyl substituents. The authors found that as the fluoroalkyl substituent increased in length, the CO_2/N_2 and CO_2/CH_4 ideal selectivities decreased but presented higher CO_2/CH_4 selectivity compared to the alkyl-functionalized analogues.[34] Other cations have also been explored for the preparation of SILMs, such as, for example, pyridinium, [35,36] pyrrolidinium, [35,37,38] thiazolium [39,40] and ammonium.[41–43]

The IL anion has also been the subject of study, as it is known that it has the most influence on the gas solubility of ILs. For instance, Mahurin *et al.*[44] compared the performance of SILMs containing either the $[TFSI]^-$ or cyano-based anions, such as $[C(CN)_3]^-$ or $[B(CN)_4]^-$. It was found that cyano-based ILs not only had higher solubilities for CO_2 than those based on the $[TFSI]^-$ anion, but also the SILMs performance improved when the number of cyano groups in the structure increased.[44] Tomé *et al.*[45] studied the use of IL mixtures containing sulfate and/or cyano-functionalized anions as the liquid phase of SILMs for the CO_2/N_2 and CO_2/CH_4 separations. Remarkably, the SILMs containing IL mixtures exceeded the 2008 upper bound for the CO_2/N_2 separation.[45] The same group studied the combination of the cholinium cation $[Ch]^+$ with environmentally friendly anions such as levulinate ($[Lev]^-$), lactate ($[Lac]^-$), glycolate ($[Gly]^-$) and malonate ($[Mal]^-$). The results showed that, although good CO_2 permselectivities and high CO_2 solubilities were achieved, the permeability of cholinium-based SILMs was limited by the high viscosities of the ILs.[23]

Additionally, task-specific ILs with amine groups have also been used to fabricate SILMs for CO_2 facilitated transport, where amine functional groups act as the gas carriers.[13,46–49]

It should be noted that throughout the years, SILMs have shown good CO_2 separation performances, with permeabilities and selectivities close or above the 2008 upper bounds for CO_2/N_2 and CO_2/CH_4. In fact, SILMs have shown better ideal separation performance than the industrial standard, by polymer membranes.[14,50,51]

Despite that SILMs usually yield good gas separation performances at low feed pressures, their stability is still an issue. The use of SILMs is restricted by the experimental conditions, such as temperature, pressure and water vapour content on the gas stream. When the pressure difference across the membrane is high enough or when the high temperature lowers the IL viscosity, the liquid phase can be displaced from the pores of the support, which will compromise the membrane operation, separation performance and long-term stability.[24,45,50] To overcome this challenge, ionic liquid-based

membranes with higher stabilities needed to be developed, where the IL should be embedded in tighter structures, and not free to flow.[9]

1.2.2 Polymer/IL Composite Membranes

Polymer/IL composite membranes

The strategy consisting of incorporating ILs into polymer matrices was developed as a way to overcome the drawbacks associated with the use of SILMs, in particular the stability of the ILs in the pores of the support, under specific conditions of high temperature and pressure difference. In polymer/IL composite membranes, the IL is entrapped within the free space between the polymer chains (Figure 1.3).

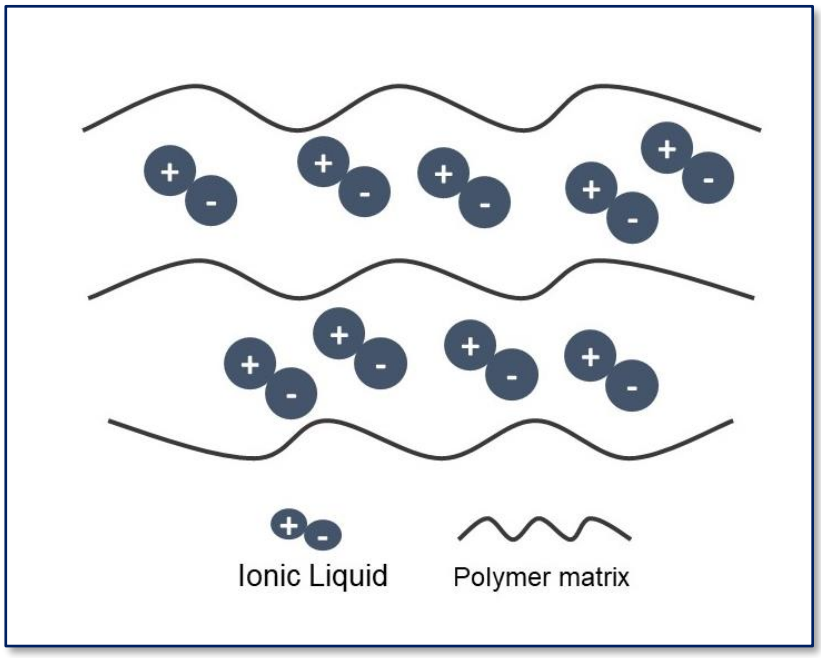

Figure 1.3 - Schematic representation of a polymer/IL composite membrane.

Polymer/IL composite membranes are usually prepared by two distinct methods: solvent evaporation and phase inversion. In solvent evaporation, the solvent present in the solution is left to evaporate at a slow rate, under a controlled atmosphere, to ensure that a dense and defect-free free structure is obtained.[52,53] On the other hand, in phase inversion, the solution is casted on a proper supporting layer/plate and then submerged in a coagulant bath containing a non-solvent. The exchange between the solvent and non-solvent leads to the precipitation of the final membrane.[54] Ideally, the polymer should possess high thermal, mechanical and chemical stability, while the IL should present a high affinity for CO_2 and low viscosity to minimize the resistance to gas transport. A critical aspect in the fabrication of polymer/IL composite membranes is the compatibility between the polymer and the IL phase, since low compatibility can lead to phase separation and leakage of the IL from the membrane.[2]

The incorporation of ILs into a polymer matrix can significantly increase the permeability of all gases, especially compared to pure polymer membranes. Mass transport in ILs is much faster than in solid polymer materials. Thus, higher gas fluxes and faster separations can be achieved in polymer/IL composite membranes. However, the incorporation of increasing amounts of IL can also decrease the CO_2/N_2 and CO_2/CH_4 selectivities, following the well-known trade-off relation between permeability and selectivity.[55]

The first polymer/IL membrane was reported by Hong *et al.*,[56] in 2009, where different amounts of [C_2mim][BF_4] IL were incorporated in the poly(vinylidene fluoride-hexafluoropropyl) (PVDF-HFP) copolymer. Remarkably, the results obtained were able to surpass the CO_2/N_2 upper bound (CO_2 permeability of 400 Barrer and CO_2/N_2 selectivity of 60), coming very close to the results obtained for the SILMs containing the same IL, while being thermally stable at high temperatures.[56] Since then, PVDF-HFP has been the most used copolymer in the fabrication of polymer/IL membranes, mainly due to its high free volume and successful use in gas separation.[2] A variety of other polymers have also been explored, such as polyether-polyamide block-copolymer (Pebax®), poly(vinylidene difluoride) (PVDF) and polyimides (PIs). The most common ILs used are those that have already been studied in SILMs configurations, containing fluorinated anions, namely $[TFSI]^-$,[57–61] $[BF_4]^-$,[62] $[CF_3SO_3]^-$,[52,59] and $[FAP]^-$ [59] or containing the $[B(CN)_4]^-$ anion,[63] showing better separation performances than the neat polymer membranes. These anions are usually combined with imidazolium cations, with variable alkyl chain lengths.

Besides the improvement in gas separation properties, the incorporation of ILs into polymer matrices can also reduce the polymer crystallinity, making the membranes more flexible and less brittle, compared to neat polymer membranes. For instance, Liang *et al.*[64] prepared polymer/IL composite membranes comprising poly(pyromellitimide-*co*-4,4'oxydianiline) (PMDA-ODA PI) and polybenzimidazole (PBI) mixed with [C_4mim][TFSI] IL. The prepared membranes could withstand pressure gradients of up to 6 bar and temperatures as high as 473 K.[64]

The polymer also plays a significant role in the gas separation properties of polymer/IL membranes. As an example, lower permeation results were obtained for Pebax®/[C_2mim][BF_4], when compared to PVDF-HFP/[C_2mim][BF_4] containing the same IL. The same conclusion was drawn by Erdni-Goryaev *et al.*,[59] who found very similar results in terms of CO_2/N_2 separation performance for poly(ethylene glycol) mono and dimethacrylates (DMPEG)-based membranes comprising ILs such as [C_2mim][TFSI], [C_2mim][CF_3SO_3] or [C_2mim][FAP].[59]

Overall, polymer/IL composite membranes can provide a mechanically and thermally stable alternative to the use of SILMs. It has been demonstrated that the incorporation of ILs into polymer matrices has undeniable benefits regarding the gas transport, mechanical and thermal properties of the resulting composite membranes. Even so, the obtained permeabilities are generally lower than those obtained with SILMs and can be limited by the Robeson upper bound.[11,18]

Polymer/IL-based Mixed Matrix Membranes

Mixed Matrix Membranes (MMMs) composed of a polymer and inorganic/organic solid particles have been one of the most studied topics in the membrane research field. A broad variety of solid fillers, such as zeolites, metal organic frameworks (MOFs), metals and silica nanoparticles have been investigated for the fabrication of MMMs.[65,66] A schematic representation of a polymer/IL/filler MMM and the different fillers used is shown in Figure 1.4. It is known that the simple blend of polymers and solid fillers can originate the formation of non-selective voids between the materials, leading to higher gas permeabilities but considerably lower selectivities. The incorporation of ILs offers an interesting strategy to improve the morphology of MMMs, by acting as a wetting-agent between the polymer and solid particles, enhancing their interfacial adhesion.[65,67] This approach allows for the polymer matrix to be

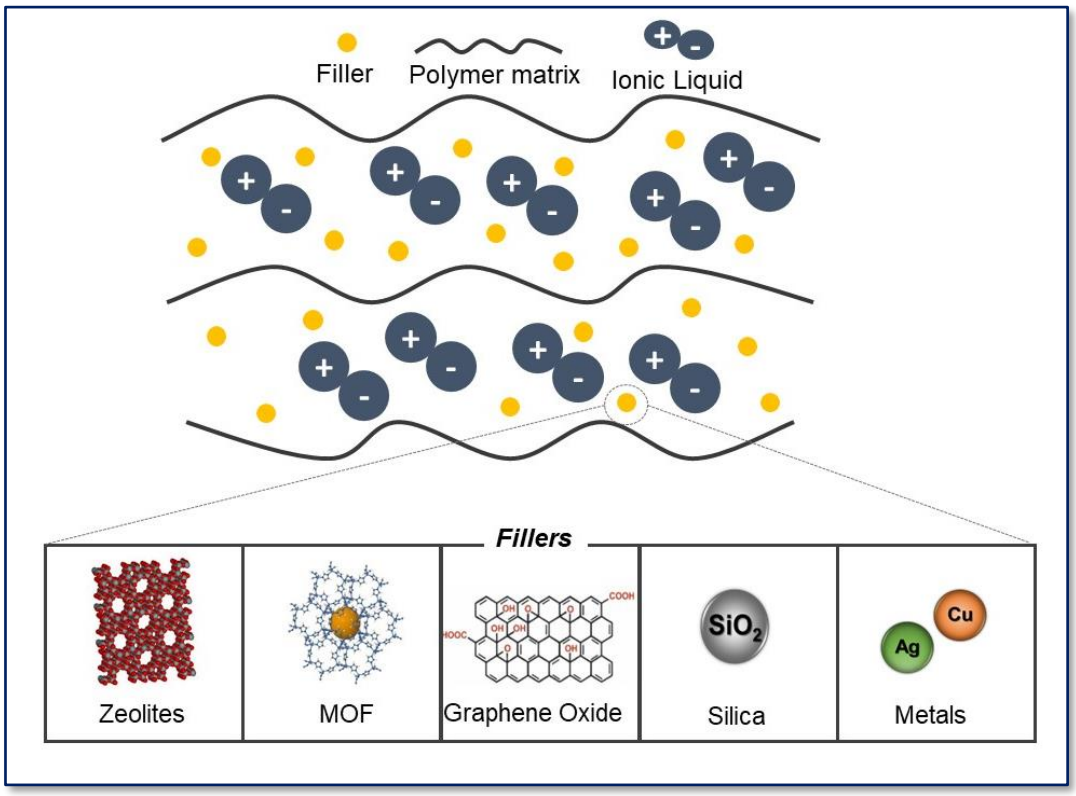

Figure 1.4 - Schematic representation of a polymer/IL/filler mixed matrix membrane and different fillers.

more flexible and better interact with the surface of the solid fillers, avoiding the formation of non-selective voids and improving the overall performance of the MMMs.

Among the various ILs available, imidazolium-based ILs are frequently investigated to improve the morphology and performance of three-component MMMs, mainly due to the good CO_2 affinity and lower cost compared to other commercially available ILs.[68,69]

The first type of fillers used in the development of MMMs were zeolites, which are versatile microporous materials with a three-dimensional structure, composed of SiO_4 and AlO_4 as elementary

building units. These materials can present an almost infinite variety of structures, sizes and shapes, and tailored for a specific application.[70] Membranes fabricated entirely of zeolites generally have superior separation performances, compared to polymer membranes.[71] The sieving mechanism ensures an excellent selectivity, while the high thermal and chemical stabilities of zeolites confirm the potential of these materials for gas separation processes.[72,73] However, the complexity in the large-scale production of defect-free zeolite membranes changed the approach towards these materials. Hence, particular attention has been given to the use of zeolites in MMMs, mainly due to the promising zeolites' transport properties.[74] The crucial factor here is undoubtedly the compatibility between the organic and inorganic phases.

The first studies towards this approach focused on the incorporation of imidazolium-based ILs into polymer-zeolites systems. For instance, Shindo *et al.*[75] developed 6FDA-TeMPD/[C_4mim][TFSI]/[ZSM-5] MMMs, where the increasing IL content was found to play an important role in the morphology of the membrane, by filling the interfacial defects. As a consequence, the ideal CO_2/H_2 and CO_2/N_2 selectivities of the three-component MMMs were higher than those obtained for the pristine polymer membrane and 6FDA-TeMPD/ZSM-5 composite MMM.[75] More recently, Moshim *et al.*[76] developed defect-free MMMs combining [C_2mim][TFSI] IL, SAPO-34 particles and PES as polymer matrix. Besides the good CO_2 affinity, the incorporation of the IL eliminated the non-selective voids, resulting in higher ideal CO_2/CH_4 separation performances, compared to the SAPO-34/PES membranes.[76]

Metal Organic Frameworks (MOFs) have also been studied in the preparation of MMMs containing ILs.

MOFs are a class of porous, crystalline materials, constructed from a metal ion or a cluster of metal ions, coordinately linked to organic ligands, to form two- or three-dimensional structures.[77] MOFs are known for their high surface areas and porosity, tunable pore sizes and topologies and high thermal stability.[78] The higher porosity and easier tunability of MOFs sets them apart from zeolites, which generally have lower porosity and a more complicated tunability due to their fully inorganic nature.[79,80] Due to their partially organic nature, MOFs have shown a better compatibility with polymers when compared to zeolites, enhancing the properties and separation performance of the resulting membranes.[81] Nevertheless, some MOFs can still originate the "sieve-in-a-cage" morphology, arising from a poor interfacial adhesion between the MOF particles and the polymer.[82] Similar to the case of zeolites, ILs can be used in MOF-containing polymer membranes to eliminate morphological defects and improve both separation and mechanical performance.

For instance, Casado-Coterillo *et al.*[76] investigated the CO_2 separation performance of MMMs based on chitosan (CS), ZIF-8 and HKUST-1 and [C_2mim][Ac] IL. The selected IL showed a good affinity for CO_2 and, as expected, contributed to the enhanced interaction and adhesion of the fillers with the polymer matrix. A remarkable CO_2 permeability of 5413 Barrer was achieved with 10 wt% ZIF-8, while the highest CO_2/N_2 selectivity (19) was obtained at 5 wt% HKUST-1.[76]

Analogous conclusions to the ones described above were also drawn by several authors, regarding the use of different fillers to develop MMMs, such as metal oxides [76] and two dimensional materials (graphene oxide - GO, boron nitride - BN and MOF nanosheets).[67,83,84]

In sum, it is clear that the development of three-component MMMs is an interesting strategy to improve their gas separation properties and overall stability. This class of membranes benefit for the easy processability of polymer membranes, the high thermal and chemical stabilities of the solid fillers and from the high CO_2 solubility and wetting-capacity of ILs. Nonetheless, contrary to the ILs, the polymers presented in this subsection are not electrically charged, which can possibly lead to lower compatibilities with the ILs, phase separation and the absence of ionic interactions between the materials. Moreover, if higher IL contents are used, high pressure differentials across the membrane can compress the material, causing IL leakage. The use of electrically charged polymers can help improve the gas separation properties of MMMs, due to a higher affinity of the polymer to CO_2 molecules, arising from their quadrupole moment.

1.2.3 Poly(ionic liquid)-based Membranes

Poly(ionic liquid) Membranes

Poly(ionic liquid)s or polymerized ionic liquids (PILs) are a subclass of polyelectrolytes prepared from polymerizable ionic liquid monomers. This class of polymers are composed by monomer repeating units bearing IL species, connected through a polymer backbone. PILs are a class of versatile materials, combining the tunability and CO_2 affinity of ILs with the intrinsic macromolecular properties of polymers.[65] The polymerizable group can be located either on the cation or the anion, depending on the desired structure. In addition, the variation of the structure type, chemical composition and ability to bond with other polymer species to form PIL block copolymers allows for the design of a broad variety of different polymers.[85]

The development of PILs followed the same trend as ILs, where the first structures to be synthesized combined halides or fluorinated counter anions and polycations based on imidazolium,[86–88] pyridinium,[89] pyrrolidinium,[90,91] piperidinium[90] or ammonium moieties. PILs are usually synthesized by either direct polymerization of IL monomers or chemical modification of existing polymers. Most of the synthesized PILs are polycations, bearing the above-mentioned cationic backbones, combined with counter anions such $[BF_4]^-$, $[PF_6]^-$, $[TFSI]^-$, $[N(CN)_2]^-$, $[CF_3SO_3]^-$, $[NO_3]^-$, $[FeCl_4]^-$, $[C(CN)_3]^-$ and $[ClO_4]^-$.[92]

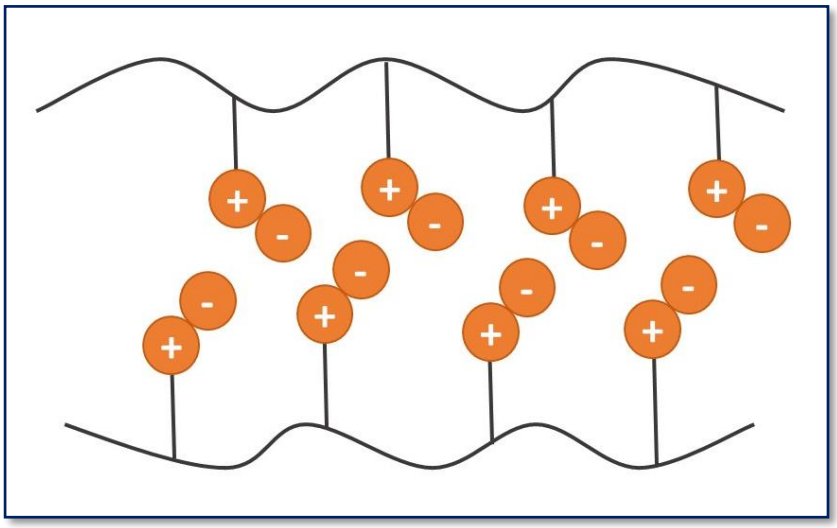

Figure 1.5 - Schematic representation of a neat PIL membrane.

Given their versatility and tunability, PILs emerged as an alternative to more conventional polymers to fabricate membranes for CO_2 separation (Figure 1.5).

The first neat PIL membrane was reported by Noble's group, with the study of the effect of modifying the PIL structures on the gas separation properties.[93] By varying the length of the *n*-alkyl substituents on the IL monomers, CO_2/N_2 and CO_2/CH_4 selectivities of 32 and 38 were respectively obtained. Moreover, the authors observed that the CO_2 permeability increased (from 9 to 32 Barrer) with the increasing length of the *n*-alkyl substituent. Inspired by the versatility of these polymers, valuable work regarding the development of membranes based on PILs containing functionalized imidazolium cations was performed by different authors.[94–97] In particular, Bara *et al.* [94] proposed a generation of functionalized imidazolium-based PILs, bearing polar groups, namely oligo(ethylene glycol) and alkyl-terminated nitrile. The addition of nitrile groups was found to decrease the CO_2 permeability (between 4 and 8 Barrer), while PILs containing oligo(ethylene glycol) pendant units showed higher CO_2 permeabilities (ranging from 16 to 22 Barrer), that were similar to those obtained with their alkyl analogues.[94]

In order to design PIL-membranes with better film-forming ability, the backbones of conventional polymers, such as PPO and PBI were also modified to design new and versatile PILs. As an example, Cong *et al.*[98] studied the modification of the PPO backbone by attaching imidazolium, pyridinium and ammonium moieties to the methyl position of the PPO unit. However, the overall CO_2/N_2 selectivities (between 4 and 12) obtained for the PPO-based PIL membranes were significantly lower than those of other PILs.[98]

Several strategies have been attempted to improve the properties of neat PIL membranes. This class of materials provide solid stable membranes and the knowledge acquired from studies concerning neat PIL membranes were an important step towards the development of PILs. However, the fabrication of neat PIL membranes cannot provide the CO_2 permeabilities and gas selectivities comparable to those of their analogous liquid phases in SILMs, mainly due to the reduced gas diffusivity caused by the solid

polymer matrix. Ideally, a membrane should combine the high CO_2 permeability and selectivity of a SILM, with the mechanical robustness of a polymer. Therefore, different approaches have been explored to enhance the gas transport properties of IL-based membranes, including the design of PIL/IL composite membranes.

PIL/IL Composite Membranes

The goal behind the concept of PIL/IL composite membranes (Figure 1.6) is to prepare membranes that can achieve higher permeabilities than neat PIL membranes while maintaining their mechanical stability.

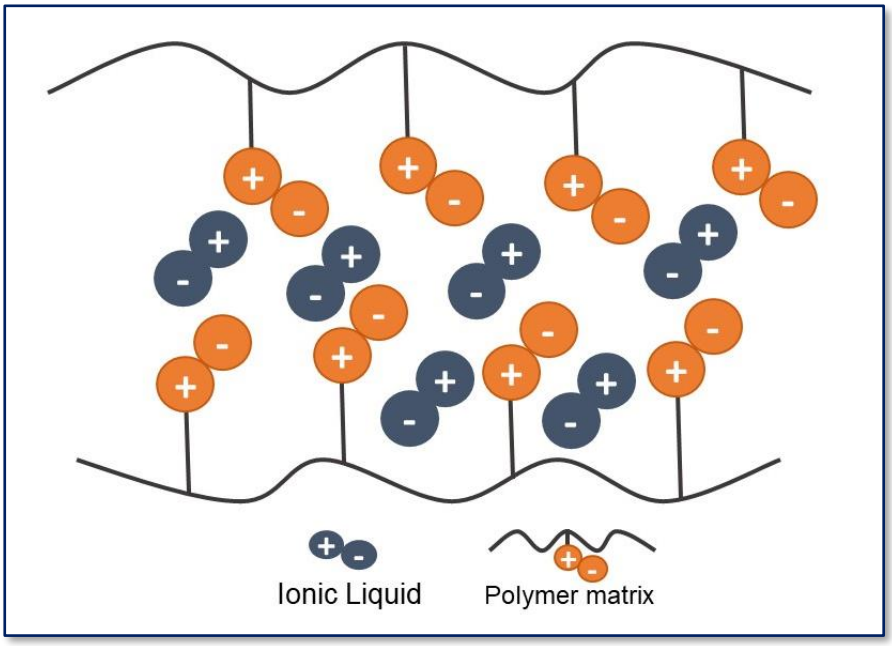

Figure 1.6 - Schematic representation of a PIL/IL composite membrane.

In PIL/IL membranes, the ILs differ from traditional plasticizers in conventional polymers due to their low/negligible vapour pressure, and to the strong electrostatic interactions between the IL and the charged PIL backbone. The large degree of interactions between the PIL and IL components allows to hold the free IL within the membrane structure, even when high transmembrane pressures are applied.[2]

The proof-of-concept of PIL/IL membranes was reported by Bara *et al.*,[99] that prepared membranes by photopolymerization of imidazolium-based IL styrene monomer, in the presence of a non-polymerizable IL, [C_2mim][TFSI]. Remarkably, the incorporation of 20% (molar fraction) of [C_2mim][TFSI] IL provided an increase of around 400% in the CO_2 permeability, as well as 33% increase in CO_2/N_2 selectivity, compared to the neat PIL membrane.[99] Following the same strategy, Bara *et al.*,[100] focused on changing the anion of the imidazolium-based IL to study the effect on the membranes' separation performance. It was found that the PIL/IL composite membrane containing 20 mol%

[C_2mim][TFSI] exhibited the highest CO_2 permeability (60 Barrer). This result was attributed to the higher molar volume of [C_2mim][TFSI], which resulted in a membrane with higher free volume, having higher gas diffusion. Moreover, only a slightly decrease in the CO_2/N_2 (39-36) and CO_2/CH_4 (27-24) selectivities were observed, compared to those of the corresponding neat PILs.[100] The same group studied the functionalization of imidazolium-based cations with alkyl, ether, nitrile, fluoroalkyl and siloxane groups.[101] A remarkable increase of 243% in CO_2 permeability (from 16 to 55 Barrer) was achieved for the PIL/IL membranes containing siloxane-functional groups, while the highest CO_2/N_2 and CO_2/CH_4 selectivities (40 and 28, respectively) were obtained in the presence of nitrile groups.

Throughout the years, Noble's research group made significant advances in the development of PIL/IL composite membranes, which have been described in detail in a published review.[10] This group studied several approaches towards the fabrication of PIL/IL membranes, containing free [C_2mim][TFSI] IL. Initially, linear PIL/IL composite materials were prepared, allowing for the fabrication of 100 nm-thick and defect-free membranes with high performance (> 6000 GPU of CO_2 permeance and CO_2/N_2 ideal selectivity of around 22).[102] Further research led to the development of cross-linked PIL/IL blends able to retain large amounts of IL in the structure, while maintaining mechanical strength and high gas transport properties (CO_2 permeability of 500 Barrer and ideal CO_2/N_2 of 24).[103] Considering the above-mentioned works, it became clear that the best CO_2 separation performances in terms of both permeability and selectivity were achieved in PIL/IL membranes containing higher amounts of IL (between 58 and 80 wt%). These types of membranes are usually classified as iongel membranes, due to the presence of high quantities of IL in the structure. A detailed description of the concept of iongel membranes, as well as an overview of the existing literature will be presented in the next topic.

Since most of the studies concerning PIL/IL membranes were mainly focused on the use of imidazolium-based PILs, Tomé *et al.*[93,104] studied pyrrolidinium-based PILs to prepare membranes for gas separation. Comparatively, the synthetic pathway and purification of imidazolium-based PILs is more complex and requires more controlled polymerization conditions. In their first work, Tomé *et al.*[105] prepared a series of composite membranes based on poly[pyr_{11}][TFSI] combined with 20-80 wt% of free [pyr_{14}][TFSI] IL. The authors found that the permeability/selectivity properties of the pyrrolidinium-based PIL membranes were the same order of magnitude as those of imidazolium-based ones containing the same $[TFSI]^-$ anion.[105] Moreover, Tomé *et al.*[106] synthesized four PIL random copolymers with pyrrolidinium cation pendant units combined with different counter-anion mixtures, and blended it with 20 wt% [pyr_{14}][TFSI] IL to fabricate PIL/IL membranes. The results showed that the CO_2 separation performance of the membranes can be tuned by using PILs with different counter-anions mixtures.[106] The authors also found in another study that the gas permeability is strictly dependent on the number of cyano-functional groups present in the anion of the pyrrolidinium-based PIL.[107] Later, Tomé *et al.* [108] studied the influence of using PILs with different molecular weights (M_w) to prepare PIL/IL membranes containing between 20 and 60 wt% [C_2mim][$C(CN)_3$] IL. Interestingly, only the use of high and medium M_w provided stable and free-standing membranes. The smaller chains of medium M_w PIL enabled higher chain mobility within the composite, resulting in lower resistance to gas transport and higher gas

permeabilities.[108] More recently, the authors explored the potential of PIL/IL composite systems in the purification of biohydrogen, with promising results above the CO_2/H_2 upper bound being achieved.[109,110]

PIL/IL-based Mixed Matrix Membranes

Similar to what was described for polymer/IL/filler MMMs in section 1.2.2, the CO_2 separation efficiency, as well as other chemical and physical properties of PIL/IL membranes can also be tuned by the incorporation of solid fillers (Figure 1.7). Zeolites and MOFs have been the most studied fillers in this regard. This strategy allows for the preparation of MMMs that combine the high CO_2 affinity and thermal/chemical stabilities of the fillers with the mechanical robustness and CO_2 affinity of the charged PILs, as well as the wetting-capacity of ILs to eliminate possible defects caused by the incorporation of inorganic particles.

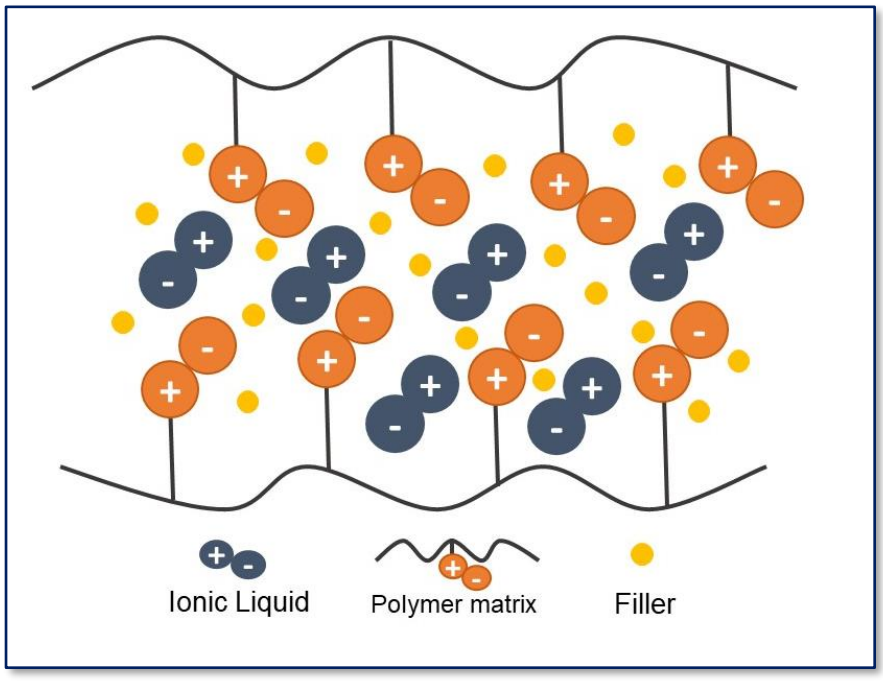

Figure 1.7 - Schematic representation of a PIL/IL/filler mixed matrix membrane.

The first study on MMMs based on PIL/IL composites was conducted by Hudiono *et al.*,[111] where SAPO-34 (zeolite) particles were incorporated into a imidazolium-based PIL/[C_2mim][TFSI] IL system. As expected, the IL acted as a wetting agent, to mitigate polymer-filler defects on the structure. MMMs containing 10 wt% SAPO-34 achieved a CO_2 permeability of 72 Barrer, with only a slight decrease in CO_2/CH_4 selectivity, compared to the PIL/SAPO-34 membrane, which was attributed to the intrinsically lower selectivity of the IL.[111] Later, Singh *et al*.[112] combined SAPO-34 particles with poly([smim][TFSI]) and [C_2mim][TFSI] ILs to study and optimize the factors affecting the gas separation performance of

these MMMs by systematically varying the filler loafing and cross-linker density. The IL behaved mainly as a lubricant to facilitate the uniform dispersion of the filler particles and eliminate interfacial voids, while SAPO-34 provided the necessary pathways for gas diffusion. At 30 wt% [C_2mim][TFSI] and 40 wt% SAPO-34, the CO_2/CH_4 upper bound was surpassed, with a CO_2 permeability of 260 Barrer and an ideal CO_2/CH_4 selectivity of 90.[112] Dunn *et al.*[113] developed three-component MMMs based on curable IL prepolymers of controlled length. The MMM combining 64 wt% of curable prepolymer, 16 wt% [C_2mim][TFSI] IL and 20 wt% SAPO-34 exhibited a CO_2 permeability of 47 and a CO_2/CH_4 selectivity of 42. Moreover, the proposed MMM system also exhibited faster curing gelation times and resistance to support penetration when casted on top of porous polymer supports.[113]

In our previous works, we investigated a series of PIL/IL/filler MMMs combining poly([pyr_{11}][TFSI]), [C_4mpyr][TFSI] IL and different MOFs. Three different MOFs (Cu(BTC), MIL-53 and ZIF-8) with different loading (up to 30 wt%) were used to prepare dense and defect-free MMMs.[114] The continuous increase in MOF loading resulted in overall better CO_2/H_2 separation performances (CO_2 permeability up to 97 Barrer for 30 wt% ZIF-8 and CO_2/H_2 ideal selectivity of 13 for 30wt% MIL-53). The obtained results surpassed the CO_2/H_2 upper bound. More recently, Sampaio *et al.*[115] proposed PIL/IL/filler MMMs containing MOF-5 for biogas upgrading. The same poly([pyr_{11}][TFSI]) PIL was blended with [C_2mim][BETi] IL and 10-30 wt% MOF-5. The highest CO_2 permeability (282 Barrer) was achieved at 20 wt% MOF-5 loading, corresponding to a CO_2/CH_4 ideal selectivity of 15. However, at the highest loading, there is a dramatic decrease in selectivity, due to the large cavity size of the filler.[115]

The efforts made throughout the years have boosted the use of IL-based membranes for gas separation, with continuous improvements in the design of the materials and, consequently on the membranes' overall performances. At the same time, it became clear that increasing the IL content in the membranes is one of the most straightforward strategies to improve their properties, not only in terms of separation performance, but also in terms of thermal and chemical stabilities. In the case of MMMs, the presence of ILs play a vital role in enhancing the compatibility between the fillers and the polymer matrix.

1.2.4 Iongel Membranes

The Concept

Another approach to develop ionic liquid-based membranes with higher stabilities, compared to SILMs, is to prepare iongel membranes. Usually, in an iongel system, the liquid phase (*i.e.* IL), is the predominant component, making up for more than half of the total iongel mass, while a solid phase/gelator is used to trap the IL, forming a three-dimensional structure, and providing the necessary mechanical support, [116] as illustrated in Figure1.8. Looking at the literature, it is clear that there is not a common spelling and fundamental definition to refer to this type of membranes. Although many spellings have been adopted, such as ion gel, ionogel, iongel or ionic liquid gel, throughout this dissertation the term "iongel" will be employed, for the sake of pronunciation and spelling. Moreover, the term iongel has been broadly used to describe polymer composite membranes where an IL is present in the structure,

regardless of its content. Many works employ this term to describe membranes in which their structure is composed predominantly by an IL, while others use it even when small amounts of IL are present. To clearly distinguish the concept of iongel from the ones described above (polymer/IL and PIL/IL composites) in this thesis, the term iongel will be used solely to describe composite membranes in which the IL is the predominant phase (*i.e.* for IL contents > 50 wt%).

Iongels can be classified as physical or chemical gels. In physical gels, the internal network is cross-linked through interactions such as hydrogen bonds, hydrophobic interactions, or crystalline junctions. Physical iongels can be obtained by using an organic gelator (polymers or molecular species of low molecular mass) or a divided solid that coagulates the whole system (*e. g.* fumed silica particles).[117] In chemical iongels the cross-linkage consists of covalent bonds, and can be created by confining the IL in a covalently interconnected network.[117]

Two-component Iongel Membranes

Due to the versatile nature and almost unlimited structural possibilities, the research on hybrid iongel materials have gained unprecedented importance in the development of devices for a wide range of other applications,[118–120] such as batteries,[121] supercapacitors,[122] actuators,[123,124] and sensors.[125] In an iongel system (Figure 1.8), the intrinsic properties of the ILs are preserved, such as the negligible vapour pressure, thermal stability, high solubility and selectivity for specific gases. This makes iongels a suitable strategy to prepare pseudo-solid membranes retaining liquid-like gas transport properties, while unveiling improved mechanical strength and higher burst pressures compared to SILMs.[126] In theory, the use of a high amount of IL brings the performance of iongel membranes closer to those observed for SILMs.

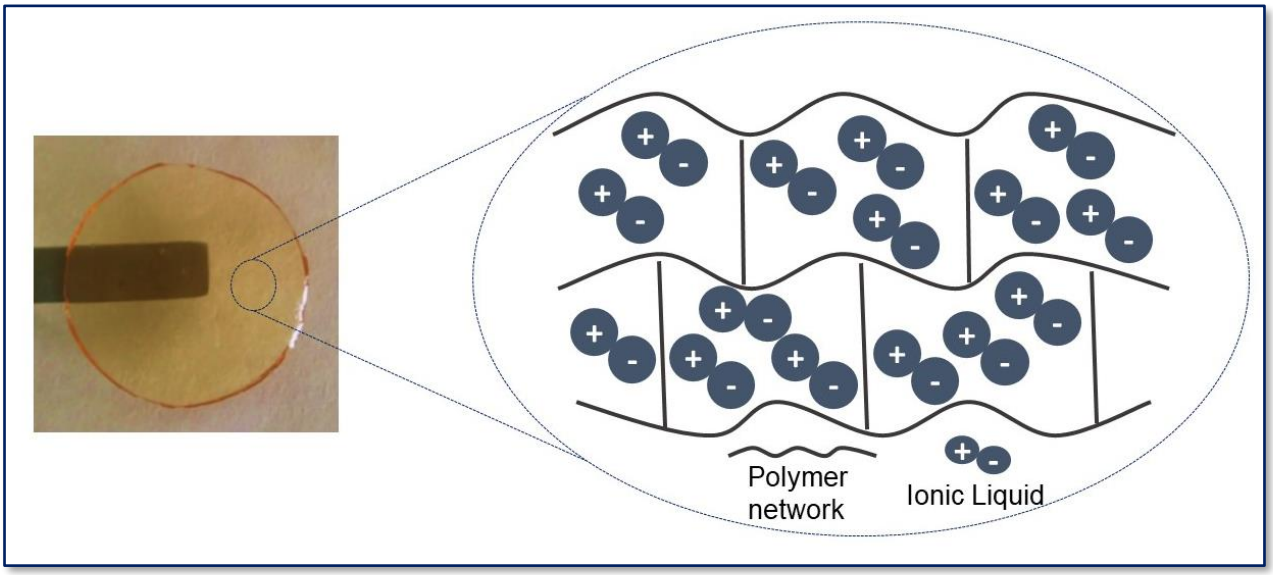

Figure 1.8 - Schematic representation of a neat cross-linked iongel membrane.

Iongels can usually be fabricated by solvent evaporation methods or by free-radical UV or thermal polymerization. In fact, thermal or UV-initiated polymerization is a particularly promising single-pot strategy to fabricate iongel membranes, able to overcome the other multi-step methods. This strategy also allows to rapidly treat large areas of materials at once, reducing the cost and time associated with other preparation methods, which is also a relevant issue when considering the process scale-up.

Regarding the development of iongel membranes, the most used ILs have been those already studied in the SILM context, and that are known for their high gas permeabilities or selectivities, such as ILs bearing fluorinated ($[TFSI]^-$, $[CF_3SO_3]^-$, $[FSI]^-$, $[BF_4]^-$, $[PF_6]^-$, and $[BETI]^-$) or cyano-functionalized anions ($[N(CN)_2]^-$, $[C(CN)_3]^-$, and $[B(CN)_4]^-$), combined with imidazolium, pyrrolidinium or phosphonium cations having variable alkyl chain lengths.[2] Some authors have also reported iongels based on ILs with amino acid anions, which act as CO_2 carriers, reversibly reacting with CO_2.[127]

Several approaches considering different types of gelators have been adopted in the preparation of iongel-based gas separation membranes,[116] including the use of low molecular weight gelators,[128] or ABA-triblock copolymers,[129] mixing ILs with non-charged polymers,[61,130] poly(ionic liquid)s,[96,107,131,132] or ionic polyimides,[133,134] and the fabrication of cross-linked iongels based on non-ionic polymer networks,[135,136] IL or PIL monomers.[103,137–139] Particularly, the development of iongel membranes combining characteristics of ILs and PILs take advantage of their strong electrostatic interactions and stability, enabling the use of higher ILs content, as discussed in section 1.2.3. [105–108,140]

Particular interest has also been given to the development of cross-linked iongel membranes, using polymer networks, since this approach enables the preparation of membranes with higher free IL contents, while preserving solid-like mechanical properties.[10] Particularly, the use of poly(ethylene glycol)-based (PEG) polymer networks has raised much interest since it contains several ether groups, known for having high affinity for CO_2, [92] with good results already reported in the literature.[135,141,142] Kusuma *et al*.[135] studied the compatibility between a selection of different ILs at moderate loadings (40 vol%) and different cross-linked polymer networks, poly(ethylene glycol) diacrylate (PEGDA) and PEGDA copolymer with a thiol functionalized polysiloxane. ILs combining imidazolium and pyridinium cations combined with the $[TFSI]^-$ anion provided the most thermally stable and compatible iongel membranes.[135] Later on, the same authors incorporated $[TFSI]^-$-based ILs and 1,3-subsituted imidazolium cations into a cross-linked PEG polymer network.[142] The presence of shorter alkyl substituents enhanced the gas permeability, due to higher polymer chain mobility. Furthermore, at 60 vol% $[C_2mim][TFSI]$, a CO_2 permeability of 530 Barrer and a CO_2/N_2 selectivity of 31 was achieved.[142] Recently, in a previous work that preceded the research developed in this PhD thesis, we studied the influence of the anion structure on the thermal, mechanical and CO_2 solubility properties of UV cross-linked iongel membranes based on PEGDA network.[136] The iongels were prepared by the fast and solvent-free UV polymerization of PEGDA in the presence of imidazolium-based ILs (between 60 and 90 wt%) bearing different anions, $[TFSI]^-$, $[FSI]^-$, $[(C(CN)_3]^-$ and $[B(CN)_4]^-$. It was found that the thermal and mechanical properties of the iongel membranes were highly dependent on the IL content and anion. The iongel containing 70 wt% $[C_2mim][C(CN)_3]$ supported on a porous filter was able to surpass the

CO_2/N_2 upper bound, with a CO_2 permeability of around 583 Barrer and ideal selectivity of 66. Nonetheless, iongel membranes containing the fluorinated anions showed better mechanical and thermal properties than the ones based on cyano-functionalized anions.

The diversity of IL chemical structures and gelators that have been used so far provided soft ionic membranes with varying composition, physical/chemical properties and gas separation performances. There are several excellent reviews describing the progress and the most important aspects of these two-component iongel membranes.[2,10,65,127,143,144] Overall, there are a few general points regarding these materials that should be point out:

- The main driving force behind the development of iongels for gas separation is to have a membrane with the improved gas transport properties of ILs and the mechanical properties and processability of solids;

- Regarding separation efficiency, the potential of iongel materials to outperform conventional polymer membranes has been shown, especially for CO_2/N_2 separation;

- The gas transport properties can be tuned by synthetically adjusting the chemical structure of both components, the ionic liquid and gelator, as well as their ratios. It is worth noting that the amount of IL is one of the most important parameters affecting the gas transport. As the IL content increases, the gas separation performances of the iongels approaches those of their parent SILMs;

- High amount of IL (> 50 wt%) means that the gelator content is low (< 50 wt%) and the mechanical stability of the iongels is generally compromised. To circumvent this problem, iongels were supported in porous membranes that acted as mechanical supports.

Despite the promising results obtained so far with two-component iongel membranes, some even coming close or surpassing the Robeson upper bounds, additional efforts should be made in order to further improve the gas separation performance of iongel materials. Additionally, other concerns such as the thermal and mechanical stability of these iongels should also be addressed. In this context, an emerging class of membrane materials is mixed matrix iongel membranes, in which fillers are embedded into iongel matrices. The rich diversity of iongels and inorganic fillers allows for a wide variety of mixed matrix iongel membranes to be tailor-made by combining different components with varying compositions.

Mixed Matrix Iongel Membranes

The successful development of mixed matrix iongel membranes (MMIMs), schematically illustrated in Figure 1.9, with improved gas separation performances, as well as thermal and mechanical

properties, depends primarily on the rational design/selection and optimal matching of fillers and iongel matrices, which can directly affect the filler dispersion and the filler-iongel interfacial morphology. While the type of filler, its size and dispersion are important issues, the most significant challenge in the design of suitable mixed matrix materials for gas separation is the good adhesion and interfacial compatibility between the organic phase and the different fillers.[145,146] In this case, iongels can play a strategic role, considering that ILs have been used as interface agents to heal polymer/filler interfacial defects.[82]

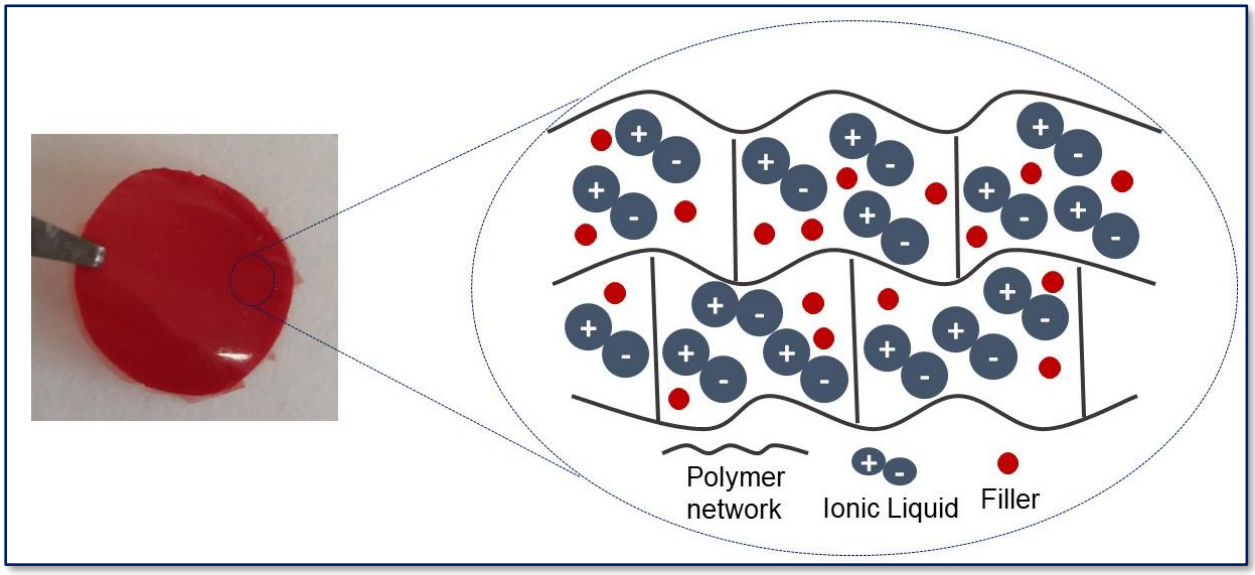

Figure 1.9 - Schematic representation of a mixed matrix iongel membrane.

The number of studies available in the literature regarding the use of a third component in iongel membranes is still limited, compared to other two-component systems. Among all the available fillers than can be used (*i.e.* zeolites, MOFs, silica, metal salts and nanoparticles and graphene oxide) in the preparation of MMIMs, zeolites were the first ones to be studied. Shindo *et al.*[75] prepared a series of MMIMs comprised of 6FDA-TeMPD polyimide (PI), [C_4mim][TFSI] IL (between 9 and 66 wt%) and ZSM-5 (15 wt%), by solvent evaporation. The authors were able to analyse how the interfacial voids between the polymer and zeolite phases decreased with increasing IL content, being completely filled at 66 wt% IL. It was also reported that the thermal stability of the membranes was improved up to 816 K by the incorporation of 15 wt% ZSM-5 and 66 wt% [C_4mim][TFSI] IL, which is well above the typical temperature range of gas streams, at an industrial level. The PI/IL/ZSM-5 iongel membrane with 60 wt% IL was able to withstand a 24 h permeation experiment at 10 bar, due to an additional strength and flexibility provided by the zeolite and IL, respectively.[75]

Li *et al.*[147] studied the influence of different imidazolium-based IL anions ($[TFSI]^-$, $[BF4]^-$, $[N(CN)_2]^-$), as well as ZIF-8 loading and IL content (between 5 and 80 wt%), in the performance of block copolymer, Pebax®1657-based membranes, prepared by solvent evaporation. All membranes revealed an excellent thermal stability, with degradation temperatures above 603 K. The authors found that the

anions of ILs played a significant role in gas permeability, similar to what happens in pure ILs. The addition of ZIF-8 reduced the polymer crystallinity and increased both CO_2 diffusivity and solubility coefficients, resulting in a two-fold increase of CO_2 permeability. As expected, the increase in IL content decreased the interfacial voids between ZIF-8 particles and the polymer phase. At 80 wt% of [C_4mim][TFSI] IL, a completely amorphous structure was achieved. The increase in IL content promoted a higher chain mobility of the polymer and fractional free volume, facilitating gas diffusion. The permeability of the Pebax®1657/ZIF-8(15 wt%)/IL(80 wt%) iongel membrane was found to be 4.3 times higher than the pure Pebax®1657 membrane, without sacrificing the CO_2/N_2 and CO_2/CH_4 selectivities.[147]

In what concerns the development of silica-containing iongel membranes, Matsuyama's group carried out significant work in this area, particularly using silica nanoparticle networks. The research group fabricated a series of double-network (DN) iongel membranes, comprising remarkably high contents of different ILs. [119,148–152] For instance, Kamio *et al.*[119] developed an optimized method to fabricate robust double-network (DN) ion gels with a high amount of IL (80 wt%), using polydimethylacrylamide (PDMAAm) as polymer matrix and silica particles. The DN ion gels exhibited excellent mechanical stability, sustaining more than 28 MPa of compressive stress, higher than the PDAAMm/IL single-network, which was attributed to the silica content on the iongel membrane.[119] Very recently, the same authors [150] were able to increase the IL content of the inorganic/organic DN iongels up to 95.2 wt% IL, achieving a CO_2 permeability of 1380 Barrer, while maintaining the CO_2/N_2 selectivity (around 22). Conversely, a significant decrease in the fracture stress and Young's modulus at 95.2 wt% IL was also obtained. Consequently, the authors suggested the use of a PEG-based organic network instead of PDMAAm to further improve the mechanical strength of these iongel membranes.[150]

The use of metal salts and metal nanoparticles that can act as carriers in iongel membranes for gas separation is a promising strategy to improve both selectivity and permeability. Due to their negligible vapour pressure, ILs have shown to be a very promising media for facilitated transport through mobile carriers as metal salts or nanoparticles.[153–155] For instance, Fam *et al.*[156] studied the influence of different inorganic salts ($NaSO_4$, NaCl and $CaCl_2$) and [C_4mim][BF_4] IL in Pebax®1657-based membranes for CO_2/N_2 separation. The $CaCl_2$-containing membranes showed the highest increase in the CO_2 permeance (around 500 GPU) when the IL content was raised to 80 wt%, however at the expense of their selectivity and mechanical stability.[156] In the context of iongel membranes containing metal nanoparticles, only the separation of CO_2 from N_2 and CH_4 has been reported. Estahbanati *et al.*[157] prepared a series of membranes containing Pebax®1657, 25-50 wt% [C_4mim][BF_4], and 0.5-1.5 wt% Ag nanoparticles. The authors observed that best separation performance for both CO_2/N_2 and CO_2/CH_4 gas pairs was achieved for the iongel containing 50 wt% IL and 0.5 wt% Ag nanoparticles.[157]

Graphene-based materials have also been extensively studied for a variety of applications, including gas separation.[158] These materials benefit from a set of important features, such as an easy and flexible functionalization, high thermal stability, ease of processing and compatibility with organic solvents. In the context of iongel membranes, Fam *et al.*[130] studied the impact of [C_2mim][BF_4] and

graphene oxide (GO) at different loadings in the performance of Pebax®1657-based iongels. The GO sheets loadings were varied between 0.2-2 wt% and the IL+GO content accounted for 80 wt% of the whole iongel composition. CO_2 permeance of 773 GPU and CO_2/N_2 ideal selectivity over 60 were achieved at a 0.5 wt% GO loading. The authors also investigated the iongel membranes' stability through mixed-gas permeation experiments. Remarkably, after an ageing process, the authors observed that no change in the CO_2/N_2 selectivity was detected, compared to the freshly tested iongels, meaning that the IL remained stable and trapped in the iongel material.[130]

Two-component iongel membranes have already shown promising results regarding CO_2 separation. However, it is clear that the incorporation of a third component into the iongel matrix can result in an improvement in, not only the gas separation performance, where remarkably high CO_2 permeabilities were achieved with different fillers , but also in the thermal stability (as it was shown for zeolites[75]) and mechanical properties (*e.g.* with silica particles[119]). These findings represent an important step forward in the development of advanced materials for CO_2 separation.

Considering all the literature mentioned and discussed above in section 1.2, it is clear that the development of IL-based membranes, particularly iongels, for gas separation revealed undeniable advantages and offers great potential to emerge as a viable alternative membrane material to CO_2 separation. In fact, some of the reported IL-based membranes were able to surpass the 2008 Robeson upper bound, but the factors considered to determine the potential of these IL-based membranes should not be limited to their gas transport properties alone. Other parameters, such as the morphology, membrane thickness, thermal properties and mechanical stability must also be more frequently addressed. Besides the nature of the polymer and IL, the fillers can also promote significant modifications on the membranes' properties, which can unveil numerous possibilities towards the development of MMIMs, able to overcome the major challenges associated with this class of membranes.

1.3 Research Strategy and Objectives

Considering the potential of mixed matrix membranes, and the clear advantages of developing ionic liquid-based materials for gas separation, the main focus of this PhD thesis is to combine these two approaches to prepare novel advanced membranes for CO_2 separation.

It is known that the nature and structure of the filler selected to fabricate MMMs has a major impact on the morphology and overall performance of the membranes, not only in terms of the gas separation properties, but also on their thermal and mechanical stabilities. Therefore, several characteristics should be considered when selecting the fillers, such as their nature (e. g. organic or inorganic materials), their structure, and their porosity parameters.

This thesis aims at answering specific questions regarding the development of MMIMs:

1. ***How can the mechanical stability of iongel membranes be improved?*** Considering that iongel membranes are predominantly composed of a liquid phase (IL), their mechanical stability can be severely compromised, specially under experimental conditions as those of the industrial gas streams. In this thesis, the design of MMIMs contemplated the importance of fabricating mechanically stable membranes for gas separation.

2. ***How can the polymer matrix and the fillers affect the gas separation performance of iongel membranes?*** The nature of the polymer matrix as well as the morphology, pore parameters, adsorption capacity and nature (organic/inorganic) of the different fillers has a significant impact on the gas separation performance of MMIMs. Therefore, different materials with diverse characteristics were considered.

3. ***Can the fillers help maintain the iongel membrane's stability under harsh conditions?*** Even though there are a few works published reporting the use of iongel membranes under different experimental conditions, there is still lack of information regarding the stability of these materials under different pressures, higher temperature or in the presence of water. The incorporation of a solid filler could help maintain the stability of the membranes under varying experimental conditions, which was also studied throughout this thesis.

To tackle these questions, different materials were studied, based on their nature and potential towards the proposed application: (*i*) inorganic nanoclays, able to, not only improve the CO_2 transport but also enhance the mechanical stability of the prepared iongel membranes. In this particular case, the nanoclay Montmorillonite (MMT) was chosen due to its easy dispersibility in polymer matrices, low cost and proved ability of clay minerals to enhance the mechanical stability of membranes;[159,160] (*ii*) new organic porous organic polymers (POPs), with specific azo functional groups (azo-POPs) with high affinity towards CO_2 and good compatibility with a variety of polymers and ILs due to their entirely organic nature. These properties are expected to improve the morphology and separation performance of the iongel membranes, as well as provide a good thermal stability. The use of entirely organic fillers can also provide a way to reduce the fabrication costs of MMMs, compared, for example, to the use of other inorganic materials; (*iii*) "hybrid" organic/inorganic metal organic frameworks (MOFs) with high CO_2 adsorption capacities and thermal stabilities. MOFs have been one of the most studied classes of porous materials for the development of mixed matrix membranes. In this thesis, different MOFs were specifically selected taking into account their availability and several characteristics, such as CO_2 adsorption capacity, porosity parameters and thermal stability, also based on one of our previous work;[114] and (*iv*) a semi-interpenetrating polymer network was developed, combining PEGDA and a poly(ionic liquid) (PIL) with a polymerizable $[MTFSI]^-$ monomer, to increase the affinity of the electrically

charged polymer matrix towards CO_2 and, consequently, enhance the separation performance of MMIMs and the stability of the IL in the iongel matrix.

In this thesis, all iongel membranes were prepared by a free-radical UV polymerization process. This method allows for the fast preparation of iongel membranes, without the intrinsic need of additional solvents (as in the case of solvent evaporation or phase inversion), making the preparation of iongel membranes a more environmental-friendly procedure. In addition, the use of solvent-free fabrication procedures facilitates the processing of large areas of material. Consequently, the chosen preparation procedure provides a mean to reduce time and costs associated with the fabrication of membranes, which is especially relevant when considering the scale-up of the process. Besides the undeniable advantages of using membrane processes (in terms of lower energy consumption and capital investment), the fabrication of the materials also plays an important role. Hence, the search for more efficient preparation methods (such as UV polymerization) should also be considered.

The separation of CO_2 from different gas mixtures can be a challenging process, due to the experimental conditions, in terms of temperature, pressure and feed gas composition. In order to evaluate the potential of the prepared groups of MMIMs, for CO_2 separation applications, a number of characterization techniques were performed aiming to obtain information about: *(i)* morphology, to determine if the selected fillers and respective loadings could promote the formation of agglomerates and hinder the gas separation performance; *(ii)* thermal stability with increasing temperature, to determine if the prepared MMIMs can be used at temperatures similar to those of the industrial gas streams; *(iii)* mechanical properties to evaluate the effect of the polymer matrix and fillers on the mechanical strength and flexibility of MMIMs; *(iv)* pure gas permeation, for CO_2/N_2 and CO_2/CH_4 gas pairs to make a first evaluation of the gas transport properties and ideal selectivities of the different polymer matrices and fillers that compose the MMIMs; and *(v)* to make a more realistic assessment of the potential of the prepared iongel membranes, the best performing MMIMs were tested under experimental conditions similar to those of the industrial flue gas and biogas streams.

The results obtained give an insight into the influence of different polymer matrices and fillers on the separation performance of iongel membranes.

1.4 Thesis Outline

This thesis is divided into seven chapters. Chapters 2 to 6 include a summary of the work performed, a short review/state-of-the-art, description of the materials and methods used in the respective chapter, a discussion of the results obtained, and the main final conclusions.

Chapter 1 introduces this thesis, which includes the background, context and motivation behind this work, a review of the state-of-the-art, and the objectives of this PhD work.

In **Chapter 2**, a strategy to improve the mechanical stability of iongel membranes with a high IL content is proposed. Accordingly, different loadings of nanoclay montmorillonite (MMT) were incorporated into iongels and the resulting mixed matrix iongel membranes (MMIMs) were characterized. The influence of the MMT loading on the mechanical properties of the iongel membranes

was studied through puncture tests, while its influence on the morphology was analyzed by Scanning Electron Microscopy (SEM). Finally, the CO_2/N_2, CO_2/CH_4 and CO_2/H_2 separation performance of the MMIMs containing different loadings of MMT was also assessed by carrying out pure gas permeation experiments.

To further improve the gas separation performance of MMIMs, in **Chapter 3**, azo-porous organic polymers (azo-POPs) were used as fillers. Four structurally different and completely organic azo-POPs were synthesized, and their structure, thermal stability and CO_2 adsorption capacity were determined. A low loading of each azo-POP was incorporated into the MMIMs and their morphology, thermal and mechanical stabilities and hydrophilicity was assessed. Finally, the separation performance of the prepared iongels membranes containing azo-POPs was also investigated for the CO_2/N_2, CO_2/CH_4 and CO_2/H_2 separations.

Following the results obtained in the previous chapter, the aim of **Chapter 4** was to study the effect of temperature, pressure, gas composition and presence of water vapour on the separation performance of the best performing MMIMs containing azo-POPs, for CO_2/N_2 and CO_2/CH_4 binary gas mixtures.

Chapter 5 is dedicated to the study of metal organic frameworks (MOFs), a class of hybrid materials, as fillers to prepare MMIMs. Three different MOFs were selected, based on their affinity towards CO_2. The thermal and mechanical stabilities, as well as the morphology, structure, and hydrophilicity of the MMIMs containing different MOF loadings are presented. The influence of the MOF type and loading on the separation performance of the prepared MMIMs was also evaluated for the CO_2/N_2 and CO_2/CH_4 gas pairs, through pure gas permeation experiments. Finally, the best performing MMIM was subjected to the permeation experiments using gas mixtures, under experimental conditions near those of the industrial streams, in terms of temperature, pressure and composition.

In **Chapter 6**, a semi-interpenetrating polymer network (sIPN), was prepared and used as polymer matrix of the MMIM systems designed in the previous chapters. The synthesis of three PILs bearing structurally different polymerizable anions was first attempted. Afterwards, a sIPN, combining PEGDA and a PIL bearing a polymerizable anion was used to prepare MMIM with the best performing fillers identified in the previous chapters. The prepared membranes were characterized in terms of their pure CO_2 permeability and CO_2/N_2 and CO_2/CH_4 ideal selectivities. The separation properties of the best performing MMIM were also assessed under experimental conditions near those of the industrial streams, in terms of temperature, pressure and composition.

Chapter 7 includes the main results obtained throughout this PhD project and the main conclusions are discussed. Moreover, challenges and suggestions for future work are also provided.

2

POLY(ETHYLENE GLYCOL) DIACRYLATE IONGEL MEMBRANES REINFORCED WITH NANOCLAYS FOR CO_2 SEPARATION

Published as: A. R. Nabais, R. O. Francisco, V. D. Alves, L. A. Neves and L. C. Tomé, "Poly(ethylene glycol) diacrylate iongel membranes reinforced with nanoclays for CO_2 separation", Membranes, 2021, 11, 998.

Summary

Despite the fact that iongels are very attractive materials for gas separation membranes, they often show mechanical stability issues mainly due to the high ionic liquid (IL) content (≥60 wt%) needed to achieve high gas separation performances. This work investigates a strategy to improve the mechanical properties of iongel membranes, which consists in the incorporation of montmorillonite (MMT) nanoclay, from 0.2 to 7.5 wt%, into a cross-linked poly(ethylene glycol) diacrylate (PEGDA) network containing 60 wt% of the IL 1-ethyl-3-methylimidazolium bis(trifluoromethylsulfonyl)imide ([C_2mim][TFSI]). The iongels were prepared by a simple one-pot method using ultraviolet (UV) initiated polymerization of poly(ethylene glycol) diacrylate (PEGDA) and characterized by several techniques to assess their physico-chemical properties. The thermal stability of the iongels was influenced by the addition of higher MMT contents (>5 wt%). It was possible to improve both puncture strength and elongation at break with MMT contents up to 1 wt%. Furthermore, the highest ideal gas selectivities were achieved for iongels containing 0.5 wt% MMT, while the highest CO_2 permeability was observed at 7.5 wt% MMT content, due to an increase in diffusivity. Remarkably, this strategy allowed for the preparation and gas permeation of self-standing iongel containing 80 wt% IL, which had not been possible up until now.

2.1 Introduction

In the last 25 years, numerous studies have been focusing on ionic liquids (ILs), a material with exceptional features that keeps stimulating researchers' curiosity today. Besides being liquid salts at room temperature due to their melting points below 373 K, ILs are characterized by distinct tunable properties.[161,162] The most appealing property of ILs is their designable nature, which allows the preparation of task-specific materials for the envisioned application by the combination of different ions and the addition of specific functional groups.[161] Regarding energy-related applications, their ionic conductivity, low volatility, electrochemical and thermal stability serve as advantages in the development of batteries,[163] fuel cells,[164] and chemical sensors.[165] On the other hand, considering the unique properties of some ILs, such as biocompatibility, biodegradability, and bioactivity, biomedical applications such as biosensors [166] and drug delivery systems [167] have also been developed. This work focuses on the use of ILs for carbon dioxide (CO_2) separation from light gases taking advantage of the interactions established between the electrical charges of the IL and the quadrupole of CO_2 molecules, and combining them with membrane technology, an economic and environmentally friendly approach to CO_2 capture.[2,18,65]

In the last years, diverse ionic liquid-based membranes have been developed. In particular, iongel membranes have shown promising results for CO_2 separation, with performances similar to those of supported ionic liquid membranes (SILMs), surpassing the 2008 Robeson upper bound.[2] However, SILMs often have stability issues brought up by operation conditions (e.g., high pressures and high temperatures) that can cause the IL displacement from the porous support.[2,11] Instead, iongels are soft solid materials that present a gel-like nature, as they are mainly composed of ILs, retaining a liquid-like gas transport.[168] For the fabrication of iongels, there is a wide variety of materials that can be selected, as well as diverse routes to approach their preparation.[168] In order to ensure that high IL contents (>50 wt%) are efficiently retained within the iongel structure, different types of gelators can be used,[168] such as polymer networks,[136] block copolymers,[129] biopolymers,[169] supramolecular gelators,[170] organosilane networks,[171] or inorganic nanoparticles.[172] The combination of ILs with polymers, which are commercially available such as poly(vinylidene fluoride) (PVDF) [63] or poly(ethylene glycol) (PEG),[173] and poly(ionic liquid)s (PILs) with imidazolium [10] or pyrrolidinium [105] cations and a variety of counter anions, is perhaps the most straightforward approach to fabricate iongel membranes. PIL-based membranes can hold up to 60 wt% IL due to the advantage of establishing strong electrostatic interactions between their charged PIL and IL components.[2] In order to further improve their CO_2 separation performance along with other properties, some researchers also reported the incorporation of porous fillers, such as zeolites [174] and metal organic frameworks (MOFs) [114] to produce mixed matrix membranes (MMMs). Additionally, significant efforts have been made in the fabrication of iongels using cross-linked PIL-based networks since this strategy provides extra mechanical stability and allows the incorporation of higher IL contents.[103] Nevertheless, the preparation routes of cross-linked PIL-based

iongels are often complex, involving multi-pot polymerization procedures or several steps of synthesis and purification at the monomer level.

A simpler strategy is the preparation of iongels by single-pot polymerization using commercially available non-ionic polymer networks, such as poly(ethylene glycol) (PEG)-based networks, due to their high affinity towards CO_2.[135] The polymerization can be thermal or UV initiated. Recently, Martins *et al*.[136] studied the influence of the anion structure on the CO_2/N_2 separation performance of UV-cross-linked poly(ethylene glycol) diacrylate (PEGDA) iongels. Using imidazolium-based ILs with cyano-functionalized ($[C(CN)_3]^-$ and $[B(CN)_4]^-$) or fluorinated anions ($[TFSI]^-$ and $[FSI]^-$), self-standing iongels containing between 60 and 90 wt% of IL were obtained. Although the PEGDA iongel with 70 wt% $[C_2mim][C(CN)_3]$ IL showed CO_2 permeability of 583 Barrer and ideal CO_2/N_2 selectivity of 66,[136] further improvements are needed to circumvent the use of a porous support and preserve the iongel mechanical stability while increasing the IL content.

One popular strategy used to improve the mechanical stability of polymer membranes is the incorporation of fillers.[175] A wide variety of fillers, porous or nonporous, have been reported in the literature,[176,177] including the use of nanoclays.[178] Nanoclays are natural, nonporous inorganic materials that have been considered to enhance the mechanical properties of polymer membranes, as well as their gas separation performances.[159,160] Several studies revealed that the addition of low contents of nanoclay particles (≤10 wt%) can improve the thermal, mechanical, electrical, and barrier properties of MMMs,[179] because of the attractive properties of nanoclays such as ion exchange capacity and specific surface area, besides being widely available at low cost.[180] Montmorillonite (MMT) is one of the most commonly used nanoclays, mainly due to its ability to be dispersed into polymer matrices. This nanoclay has a 2:1 phyllosilicate structure, composed of 1 nm layers of alumina octahedra sheets placed between two sheets of silica tetrahedra.[181,182]

This work focuses on the development of robust PEGDA-based mixed matrix iongel membranes (MMIMs) reinforced with MMT nanoclay particles, considering a simple one-pot preparation method. The $[C_2mim][TFSI]$ IL was selected and firstly used at 60 wt% IL content, seeing that previously reported PEGDA iongels have shown higher storage modulus when comprising this IL rather than other ILs having different anions (i.e., $[FSI]^-$, $[C(CN)_3]^-$ and $[B(CN)_4]^-$).[136] Moreover, low contents of MMT nanoclay particles were used, between 0.2 and 7.5 wt%, in order to fabricate self-standing iongels with good mechanical properties. All the prepared iongel materials were characterized by several techniques to study their physico-chemical properties. Pure gas permeation experiments were also carried out to evaluate the potential of PEGDA iongels reinforced with nanoclays as CO_2 separation membranes.

2.2 Experimental Section

2.2.1 Materials

The ionic liquid 1-ethyl-3-methylimidazolium bis(trifluoromethylsulfonyl)imide ($[C_2mim][TFSI]$, 99 wt% pure) was acquired from IoLiTec GmbH (Heilbronn, Germany). Sigma-Aldrich (Madrid, Spain)

supplied the poly(ethylene glycol) diacrylate (PEGDA, M_n 575 g mol^{-1}) and 2-hydroxy-2-methylpropiophenone (DAROCUR®, 97 wt% pure). The nanoclay Nanomer® I.34TCN, montmorillonite (MMT) clay surface modified with 25–30 wt% methyl dihydroxyethyl hydrogenated tallow ammonium was obtained from Sigma-Aldrich (Taufkirchen, Germany). The gases carbon dioxide (CO_2, 99.998 wt% pure), nitrogen (N_2, 99.99 wt% pure), and methane (CH_4, >99.99 wt% pure) were provided by Praxair (Almada, Portugal). Hydrogen (H_2, 99.99 wt% pure) gas was obtained from Air Liquide (Almada, Portugal).

2.2.2 Preparation of the Iongels

The neat iongel and MMIMs reinforced with different MMT contents (0.2, 0.5, 1.0, 2.5, 5.0, and 7.5 wt%) were prepared by UV-initiated free radical polymerization (Figure 2.1). First, the desired amounts of MMT were added to 60 wt% of [C_2mim][TFSI] IL. The solutions were left stirring overnight at room temperature on a magnetic stirrer plate (Magnetic Emotion Mix 15 eco, from 2mag, Munich, Germany) and sonicated for 1 h in an ultrasonic bath (Sonorex Digitec, from Bandelin, Berlin, Germany). Afterwards, the necessary content of PEGDA was added into the solutions and magnetically mixed for 1 h at room temperature. Next, the radical photoinitiator DAROCUR® (3 wt% to PEGDA) was added, and the solutions were mixed and poured between two Rain-X™ coated quartz plates. The plates were separated by a spacer to assure the desired thickness (around 100 µm) and diameter of the iongel membrane and secured in place using clips. The solutions were then exposed to UV radiation with a wavelength of 365 nm and an intensity of 1.7 mW cm^{-2} for 10 min. Lastly, the iongels were carefully peeled from the plates and stored in Petri dishes until characterization. The MMIMs samples are systematically designated as “XX PEGDA-60 TFSI-YY MMT”, according to PEGDA (XX) and MMT (YY) content.

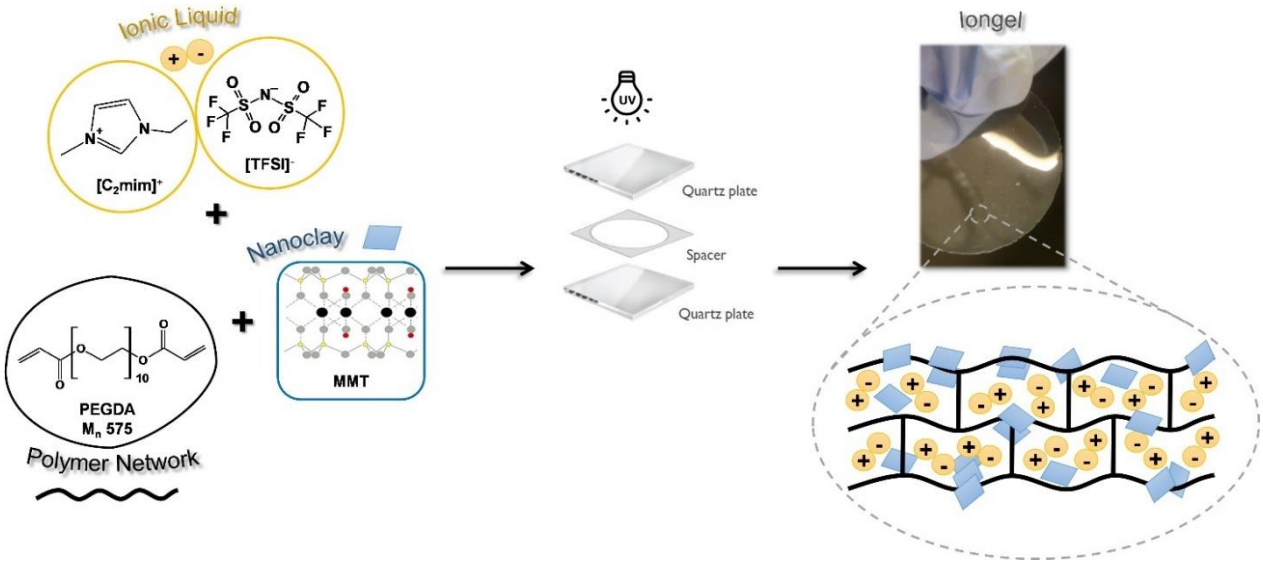

Figure 2.1 - Schematic representation of the preparation of the iongels reinforced with MMT.

2.2.3 Characterization Methods

Scanning Electron Microscopy (SEM) was carried out in order to examine the morphology of the neat 40 PEGDA-60 TFSI iongel and MMIMs. The samples were covered with a thin layer of Au-Pd before the acquisition of the images by a JOEL scanning electron microscope, model 7001F (USA) with an electron beam intensity of 10 kV.

Fourier-Transform Infrared-Attenuated Total Reflectance (FTIR-ATR) spectroscopy was performed to confirm the incorporation of the IL, PEGDA, and MMT into the MMIMs, verify possible interactions established between them, and confirm the occurrence of the photopolymerization reaction. The spectra were obtained using a Perkin Elmer Spectrum Two spectrometer that collected 10 scans from 400 to 4000 cm^{-1}.

The contact angles were measured to assess the hydrophilicity of the neat 40 PEGDA-60 TFSI iongel and MMIMs, using a sessile drop method. A drop of distilled water was manually deposited on the surface of each sample. For each sample, 10 frames were acquired with an intercalation of 1 s and processed by CAM100 (KSV Instruments LTD, Helsinki, Finland) software. The mean contact angle was obtained when the drop shape was fitted to mathematical equations.

Thermogravimetric Analysis (TGA) addressed the thermal stability of samples (ca. 10 mg) of the starting materials and the iongel membranes by determining their onset temperatures (T_{onset}). The measurements were performed using a Lass Evo TGA-DTA/DSC 1600 °C PG from Setaram KEP Technologies (Caluire, France) from 298 to 873 K, at a heating rate of 10 K min^{-1}, under an argon atmosphere.

The mechanical properties of the neat 40 PEGDA-60 TFSI iongel and MMIMs were determined by puncture tests. The tests were performed using a TA XT Plus Texture Analyzer (Stable Micro Systems, Godalming, UK) by puncturing each membrane through a hole (diameter of 10 mm) with a

cylindrical probe with 2 mm of diameter at a constant velocity of 1 mm s^{-1}, at room temperature. The data obtained allowed the determination of the puncture strength according to Equation (2.1)

$$\sigma = \frac{F}{A} \tag{2.1}$$

where σ is the puncture strength (Pa), F is the maximum force applied by the probe (N) and A is the cross-sectional area of the probe (m^2). In order to compare the results rigorously, the puncture strength was normalized with thickness following Equation (2.2)

$$\sigma_n = \frac{\sigma}{l} \tag{2.2}$$

where σ_n is the normalized puncture strength (MPa mm^{-1}) and l is the thickness of the iongel (mm). The elongation at break given by Equation (2.3) was also determined.

$$\varepsilon\,(\%) = \left(\frac{\sqrt{h^2 - d^2} - h}{h}\right) \times 100 \tag{2.3}$$

where ε is the elongation at break (%), h is the radius of the iongel exposed in the cylindrical hole of the sample holder (mm) and d is the distance of the probe from the point of contact to the point of puncture (mm). The Young's modulus of all prepared iongels was obtained from the initial slope of the graphic representation of the puncture strength (σ) as a function of the elongation at break (ε (-)). For each sample, at least four replicates were performed and the mean values of puncture strength, elongation at break, and Young's modulus were calculated.

2.2.4 Gas Permeation Experiments

Pure gas permeation experiments using CO_2, N_2, CH_4, and H_2 were performed on a gas permeation setup described elsewhere.[28] The setup is composed of a cell immersed in a water bath maintained at 303 K by a thermostat (Julabo Corio C, Germany). The pressure of each cell compartment is measured over time by a transducer (Jumo type 404327, Germany) and recorded by the software PicoLog. The compartments were pressurized with pure gas and, when the pressure was stable, the experiments began with the application of a transmembrane driving force of around 0.7 bar of relative pressure. The data collected allowed the determination of the permeability of the iongels according to Equation (2.4)

$$\frac{1}{\beta} \times ln\left(\frac{\Delta p_0}{\Delta p}\right) = P \times \frac{t}{l} \tag{2.4}$$

where Δp_0 and Δp (bar) are the pressure variations between the feed and the permeate compartments of the cell at the beginning of the experiment and over time, respectively, P is the permeability ($m^2\ s^{-1}$)

of the iongel (where 1 Barrer = 1×10^{-10} cm^3 (STP) cm cm^{-2} s^{-1} $cmHg^{-1}$ = 8.3×10^{-13} m^2 s^{-1}), *t* is time (s), *l* is the thickness of the iongel (m) and β is the geometric parameter of the cell (m^{-1}), given by Equation (2.5).

$$\beta = A \times \left(\frac{1}{V_{feed}} + \frac{1}{V_{perm}} \right) \tag{2.5}$$

where *A* is the membrane area (m^2), V_{feed} and V_{perm} are the volumes of the feed and permeate compartments (m^3), respectively. The permeability of the iongel was obtained from the slope when $1/\beta \ ln(\Delta p_0/\Delta p)$ was plotted as a function of *t*/*l*. The ideal selectivity of the iongels is given by Equation (2.6).

$$\alpha = \frac{P_A}{P_B} \tag{2.6}$$

where α is the ideal selectivity, P_A and P_B are the permeabilities of the most permeable gas and the least permeable gas, respectively. For each membrane, three replicates were tested, under the same experimental conditions.

2.3 Results and Discussion

2.3.1 Scanning Electron Microscopy (SEM)

SEM images of the cross-section of the MMIMs containing 0, 0.2, and 7.5 wt% MMT are displayed in Figure 2.2 a), b) and c), respectively. The images obtained for the remaining MMIMs are represented in Figure A.1 of Appendix A. Dense morphologies were obtained in all MMIMs, regardless of the MMT content. As the MMT content increased, the small inorganic particles became more visible, and at 7.5 wt% MMT, some agglomerates were clearly distinguishable. This morphology was a consequence of, not only the high MMT concentration, but also the absence of a solvent during iongel preparation, which can difficult the dispersion of MMT particles. Despite the agglomerates, no major defects that could compromise the performance of the iongels reinforced with MMT were observed. It should also be noted that, apart from the neat iongel image, some reliefs were observed in the iongels structure, due to the fracturing process, under liquid nitrogen.

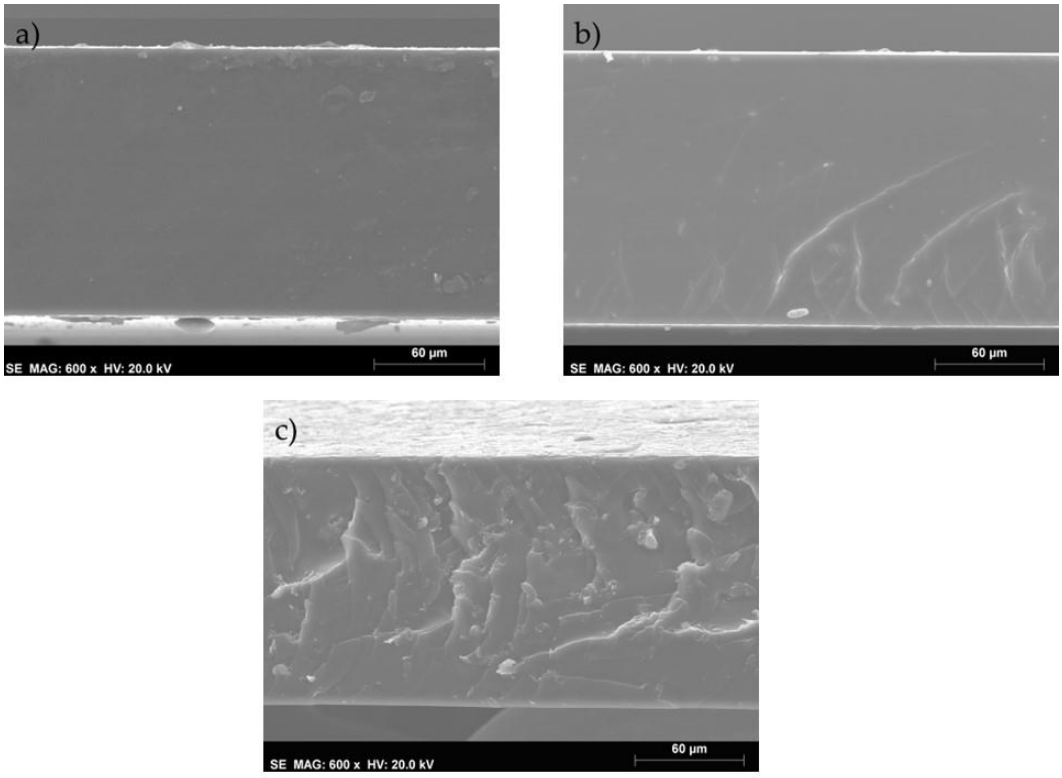

Figure 2.2 - SEM images of the (a) 40 PEGDA-60 TFSI iongel and iongels reinforced with (b) 0.2 and (c) 7.5 wt% MMT.

2.3.2 Fourier Transform Infrared-Attenuated Total Reflectance spectroscopy (FTIR-ATR)

FTIR-ATR spectroscopy was used to confirm the structure of the MMIMs components, as well as to detect any possible interactions being established between them. The obtained FTIR spectra of the 40 PEGDA-60 TFSI iongel, MMT powder, and 32.5 PEGDA-60 TFSI-7.5 MMT iongel are displayed in Figure 2.3. In the 40 PEGDA-60 TFSI spectrum, the peaks detected at 1053, 1133 and 1179 cm^{-1} corresponded to the $[TFSI]^-$ anion, while the bands at 3120 and 3160 cm^{-1} corresponded to the CH_3 bending and CH_2 stretching vibrations of the $[C_2mim]^+$ cation, respectively. The peak at 1732 cm^{-1} was attributed to the C=O symmetric stretching, while the bands between 2866 and 2936 cm^{-1} were attributed to the C-H stretching of PEGDA. The FTIR-ATR spectra of the pristine $[C_2mim][TFSI]$ IL and PEGDA can be found in Figure A.2 of Appendix A. The absence of visible peaks at wavenumbers of 1619 and 1635 cm^{-1}, arising from the terminal acrylate groups of PEGDA indicated the high extension of the polymerization reaction. The same peaks and bands were also observed on the 32.5 PEGDA-60 TFSI-7.5 MMT iongel spectrum. Regarding the MMT spectrum, peaks at 517 and 1012 cm^{-1} were representative of the Si-O bending and stretching of the silica tetrahedra sheets, respectively. At 779, 885, and 918 cm^{-1} the peaks observed were attributed to the bending of AlMgOH, AlFeOH, and AlAlOH functional groups, respectively. The observed peaks at 2851 and 2924 cm^{-1} were attributed to the stretching of the C-H bending of the CH_2 groups and bending of CH_3 functional groups, respectively,

while at 3630 cm^{-1} a peak from the stretching of OH groups was associated with Al-OH and Si-OH from alumina and silica sheets. Due to overlapping, the characteristic peaks of MMT were not easily distinguishable in the spectrum of the reinforced iongel. Nonetheless, the influence of MMT in the 32.5 PEGDA-60 TFSI-7.5 MMT iongel spectrum was observed at 450, 1053, and 2924 cm^{-1}.

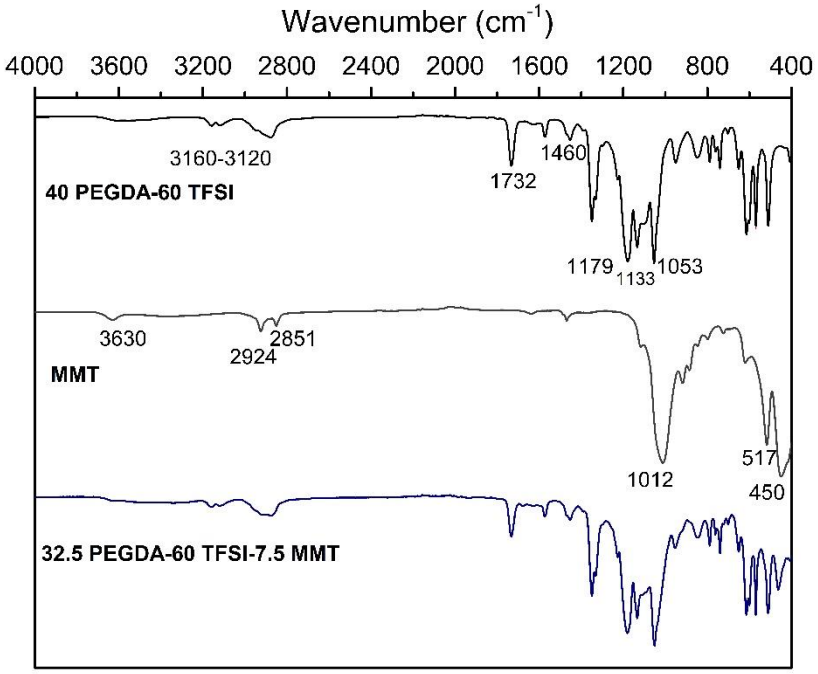

Figure 2.3 - FTIR spectra of the 40 PEGDA-60 TFSI iongel, MMT and 32.5 PEGDA-60 TFSI-7.5 MMT iongel.

2.3.3 Contact Angle Measurements

The water contact angles of MMIMs reinforced with different MMT contents were determined and the results are depicted in Figure 2.4. A contact angle of 41.3° was obtained for the 40 PEGDA-60 TFSI iongel membrane. As it can be seen, at lower contents (≤ 1 wt%), the incorporation of the MMT particles did not have a significant impact on this parameter. On the other hand, at higher contents, there was a clear increase in the contact angle, from 46.9° for the 37.5 PEGDA-60 TFSI-2.5 MMT iongel, up to 58° for the highest MMT content (7.5 wt%). These variations at higher MMT contents may be attributed to two reasons; first, a tendency for the MMT to lower the hydrophilicity of the iongels, and/or the decrease in the PEGDA content. PEGDA is composed of hydrophilic ethylene oxide units and hydrophobic acrylate units. Longer PEGDA networks, like the one used in this work, present higher contents in ethylene oxide groups, making the material more hydrophilic. A decrease in the hydrophilic PEGDA content, while maintaining the (hydrophobic) IL composition, resulted in a decrease in the hydrophilic character of the iongels reinforced with MMT. Nonetheless, all the prepared MMIMs presented a hydrophilic nature, regardless of the MMT content. This comes as an advantage for gas transport since the solubility of CO_2 in hydrophilic polymers is reported as being higher than in hydrophobic ones.[183]

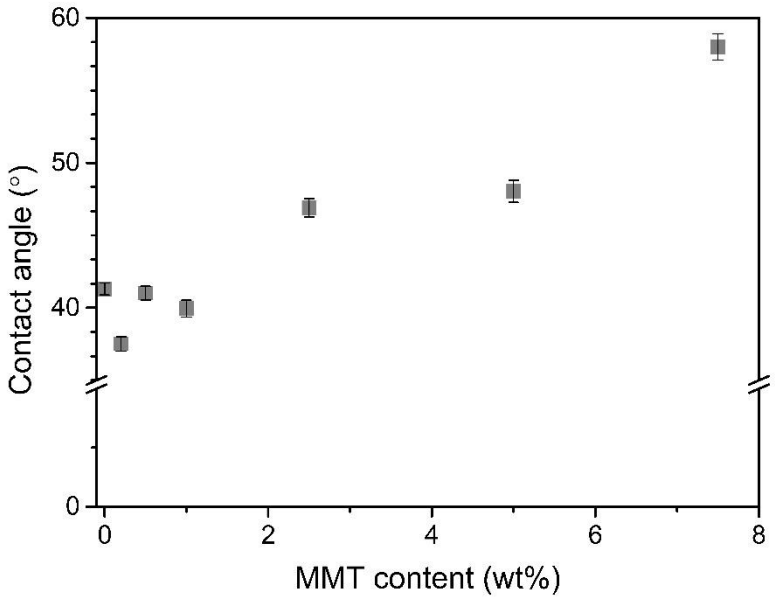

Figure 2.4 - Water contact angle of the neat 40 PEGDA-60 TFSI and MMIMs reinforced with MMT.

2.3.4 Thermogravimetric analysis

The T_{onset}, considered as the temperature at which the baseline slope changes, of MMT, [C_2mim][TFSI] IL, PEGDA and all prepared MMIMs with different MMT contents are listed in Table 2.1. The respective thermogravimetric profiles of all the starting materials and iongels prepared in this work, can be found in Figure A.3 a) and b) of Appendix A, respectively. The T_{onset} obtained for [C_2mim][TFSI] IL, PEGDA and MMT were in accordance with previous reports.[136,184–186] The degradation of MMT started around 473 K and from this point until around 803 K this degradation step was associated to the release and decomposition of the MMT organic modifier, methyl dihydroxyethyl hydrogenated tallow ammonium. The two decomposition steps observed in this temperature range were related to the different sites where the functionalization of the nanoclay may occur: at the external surface and at the edges (first step) and in the interlayer space (second step).[184] As it can be seen from Table 2.1, until 2.5 wt% of MMT content there was no significant change in the T_{onset} of the prepared MMIMs reinforced with nanoclays, due to its low content. However, at temperatures up to 473 K, a more pronounced decomposition of around 5% was noticed in the MMIMs, compared to the neat iongel (Figure A.3 b) of Appendix A). This happened probably due to the lower thermal stability of the MMT nanoclay, which started to decompose at around 473 K. For all the iongels, a second decomposition step was observed at around 673–683 K, which was associated to the degradation of both PEGDA and IL. The T_{onset} decreased from around 612 K for the iongels with up to 2.5 wt% MMT to 604 and 599 K for the iongels with 5 and 7.5 wt% MMT content, respectively, due to the higher content of MMT with a lower thermal

stability. In sum, it can be concluded that the thermal stability of the iongels was influenced by the incorporation of higher contents of MMT. Furthermore, the chosen nanoclay can be considered appropriate to be incorporated into iongels since its weight remained constant up to 423 K.

Table 2.1 - Onset temperature of the neat iongel components and the iongels reinforced with MMT.

Membrane Sample	T_{onset} (K)
[C_2mim][TFSI]	685
PEGDA	642
MMT	473
40 PEGDA-60 TFSI	612
39.8 PEGDA-60 TFSI -0.2 MMT	612
39.5 PEGDA-60 TFSI -0.5 MMT	613
39 PEGDA-60 TFSI -1 MMT	612
37.5 PEGDA-60 TFSI -2.5 MMT	613
35 PEGDA-60 TFSI -5 MMT	604
32.5 PEGDA-60 TFSI -7.5 MMT	599

2.3.5 Mechanical properties

The normalized puncture strength, elongation at break, and Young's modulus of the MMIMs with different MMT contents can be found in Figure 2.5 a)–c), respectively. It is known that the incorporation of nanoparticles, such as nanoclays, into a polymer matrix, can improve the mechanical stability of the resulting materials. As such, it could be expected an increase of puncture strength and deformation of the iongels prepared in this work, if the MMT particles are well dispersed within the polymer matrix.

From Figure 2.5 a), it is clear that the puncture strength increased in MMIMs with low MMT contents (between 0.2 and 1 wt%), where a maximum increase of 49% was achieved for 1 wt% MMT (6.0 MPa mm^{-1}). This suggests that the MMT particles were evenly dispersed throughout the iongel, acting as a reinforcement, while the material became more resistant to the external force applied during the puncture tests. On the other hand, MMT contents higher than 1 wt% resulted in a reduction in the puncture strength to 2.98 MPa mm^{-1} for a content of 7.5 wt% MMT, even lower than the neat iongel. It seems that higher MMT contents can result in a lower level of dispersion of the particles and a higher number of agglomerates, as it can be seen in Figure 2.2. The appearance of weak spots due to the aggregation of MMT sheets consequently resulted in lower mechanical resistance of the material. In previous works, where MMT particles were incorporated into polymer matrices, such as polyethersulfone and cellulose, higher MMT contents (>5 wt%) also resulted in deprived mechanical performances.[187,188]

A similar trend was obtained regarding the elongation at break of the prepared iongels, as presented in Figure 2.5 b). The elongation at break increased 57%, from 10.7% deformation for the neat

iongel to 16.8% for the MMIM reinforced with 1 wt% MMT. At lower MMT contents, and consequently homogeneous dispersion of the particles, there is a possible rearrangement of the clay sheets in the direction of the deformation, allowing higher elongation.[187] Similar to what was observed for the puncture strength, higher MMT contents decreased the ability of the iongels to elongate before rupture, due to the aforementioned lower degree of dispersion of MMT particles.

Figure 2.5 c) represents the variation in Young's modulus with the MMT content incorporated into the iongels. Young's modulus, defined as the ratio between the puncture strength and deformation is, in its essence, the resistance of the material to deformation when a force is applied. A significant increase in Young's modulus was achieved for all the MMIMs reinforced with MMT, compared to the neat iongel, with a maximum of 5.1 MPa for 1 wt% content. This improvement was attributed to the good dispersion and alignment of MMT sheets within the iongel and the additional cohesive strength provided by the inorganic particles. The slight decrease in Young's modulus at higher contents (>1 wt%) was again attributed to a reduced level of dispersion of the MMT particles. Nonetheless, the iongels

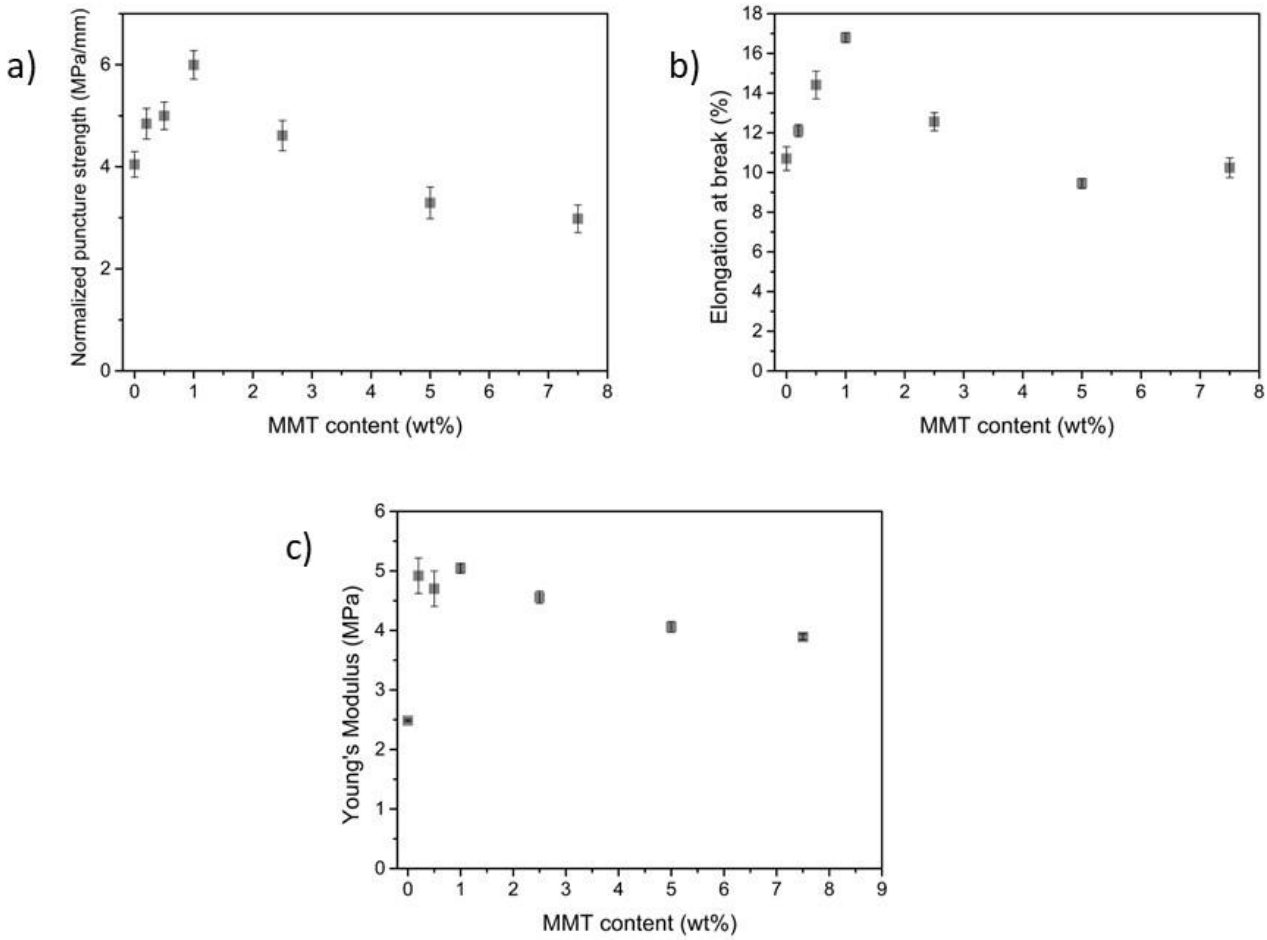

Figure 2.5 – (a) Normalized puncture strength, (b) elongation at break and (c) Young's Modulus obtained for all prepared MMIMs, as a function of the MMT content.

reinforced with MMT particles revealed better overall mechanical performances, compared to the 40 PEGDA-60 TFSI iongel, with stronger membranes upon puncture achieved for 1 wt% MMT content.

2.3.6 Gas permeation experiments

The CO_2 permeability, as well as the ideal CO_2/N_2, CO_2/CH_4, and CO_2/H_2 selectivities are plotted in Figure 2.6 and Figure 2.7, respectively. At 0.2 wt% MMT content, there were no significant variations in the CO_2 permeability, probably due to such lower MMT content. The further increase in the MMT content resulted in a continuous increase in gas permeability. The CO_2 permeability increased from 40 Barrer for the 40 PEGDA-60 TFSI iongel up to 98 Barrer at 7.5 wt% MMT content. Following the same trend, the N_2, CH_4, and H_2 also increased with higher MMT concentrations (Figure A.4, of Appendix A).

In order to study the effect of the MMT particles in the gas transport of the prepared MMIMs, the CO_2 solubility of the MMT powder was also measured, following a pressure decay method, described elsewhere.[28] It was not possible to observe any pressure decay over time (40 h), so it can be assumed that the MMT particles do not show affinity towards CO_2. Therefore, the incorporation of MMT particles likely provided an increase in diffusivity, without any substantial influence in terms of solubility. Nonetheless, the CO_2 permeability was considerably higher than that of the remaining gases. The CO_2 is a highly condensable gas and has a high affinity for the iongels, due to the fact that the quadrupole moment of the CO_2 molecules interacts favorably with the electrical charges of [C_2mim][TFSI] IL, which is the major component of the iongels.[2] Apart from the solubility, the smaller kinetic diameter and linear molecular shape of CO_2 are also advantageous for fast diffusion of the gas across the iongel.[160] It can be concluded that, while the CO_2 permeability was governed by a combination of diffusivity and solubility, the permeation of the remaining light gases in this case was mainly controlled by diffusivity.

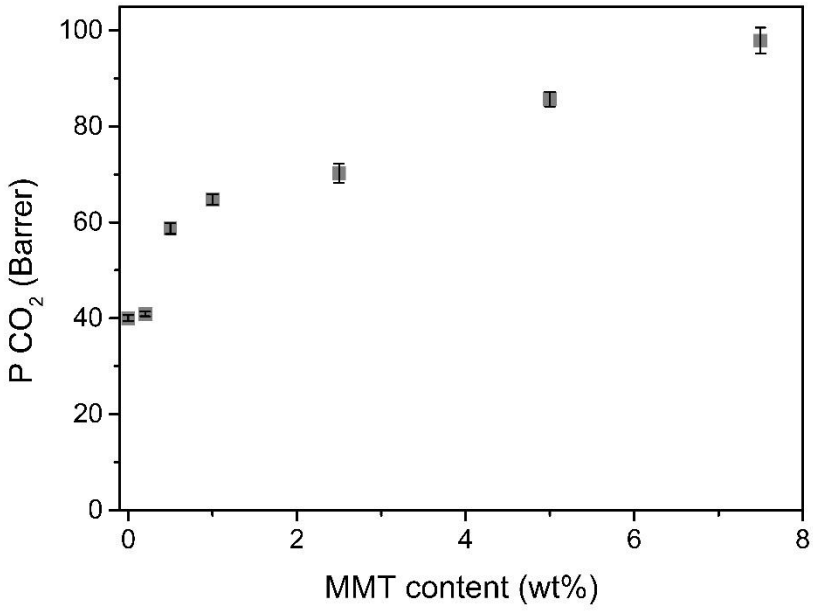

Figure 2.6 - CO_2 permeabilities obtained for the neat 40 PEGDA-60 TFSI iongel and MMIMs, as a function of the MMT content.

Looking at Figure 2.7, it can be seen that the ideal selectivities of all gas pairs were improved by the incorporation of up to 0.5 wt% MMT. In this work, the use of a modified MMT clay was expected to improve the compatibility between this inorganic filler and the polymer phase, allowing a more even distribution of the particles across the iongel matrix.[189] At lower contents and good MMT particles distribution, the selectivity can be enhanced by a shape and size discrimination of gases passing between the intercalated clay layers.[186] On the other hand, at higher contents, the MMIMs reinforced with MMT suffered a decline in selectivity. The formation of agglomerates (Figure 2.2) increased the free volume of the reinforced iongels, thus increasing gas diffusion. This allowed all gases to be transported more easily across the MMIMs, resulting in the observed decrease in CO_2/N_2, CO_2/CH_4, and CO_2/H_2 selectivities.[160] Similar results have also been reported in the literature. For instance, Jamil *et al*.[190] found an optimal modified-MMT content at 2 wt% to prepare polyetherimide-based mixed matrix hollow fiber membranes. Hashemifard and co-workers[186] found out that an increase in selectivity and CO_2 permeance could be achieved by incorporating up to 1 wt% of Cloisite 15A. However, at higher contents, a dramatic decline in the separation performance was observed, due to an increase in clay agglomeration.[186]

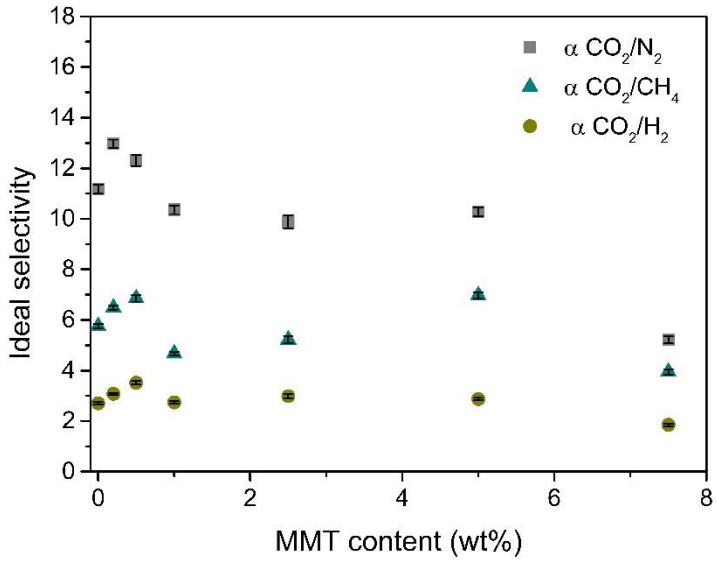

Figure 2.7 - CO_2/N_2, CO_2/CH_4 and CO_2/H_2 ideal selectivities obtained for the neat 40 PEGDA-60 TFSI iongel and MMIMs, as a function of the MMT content.

To study the possibility of further increasing the IL content, two additional MMIMs were prepared with 80 wt% [C_2mim][TFSI] IL, and 0.5 and 7.5 wt% MMT, and the obtained CO_2 permeabilities are illustrated in Figure 2.8. These specific MMT contents were chosen based on the results obtained for the iongels containing 60 wt% IL, where the 60 TFSI-39.5 PEGDA-0.5 MMT iongel showed the highest gas selectivity, while the 32.5 PEGDA-60 TFSI-7.5 MMT iongel achieved the highest CO_2 permeability. Remarkably, both free-standing iongel membranes reinforced with MMT and containing 80 wt% IL were able to withstand the gas permeation experiments, which had not been possible without the incorporation of MMT.[136] The CO_2 permeabilities of the MMIMs containing 80 wt% [C_2mim][TFSI] IL were considerably higher than those of the MMIMs with 60 wt% IL content. At 0.5 wt% MMT content, the CO_2 permeability increased from 60.3 to 115.3 Barrer, while for MMIMs reinforced with 7.5 wt% MMT it increased up to 132.3 Barrer. This behaviour can be attributed to the higher IL content, resulting in a higher affinity of the iongel towards CO_2, as expected.

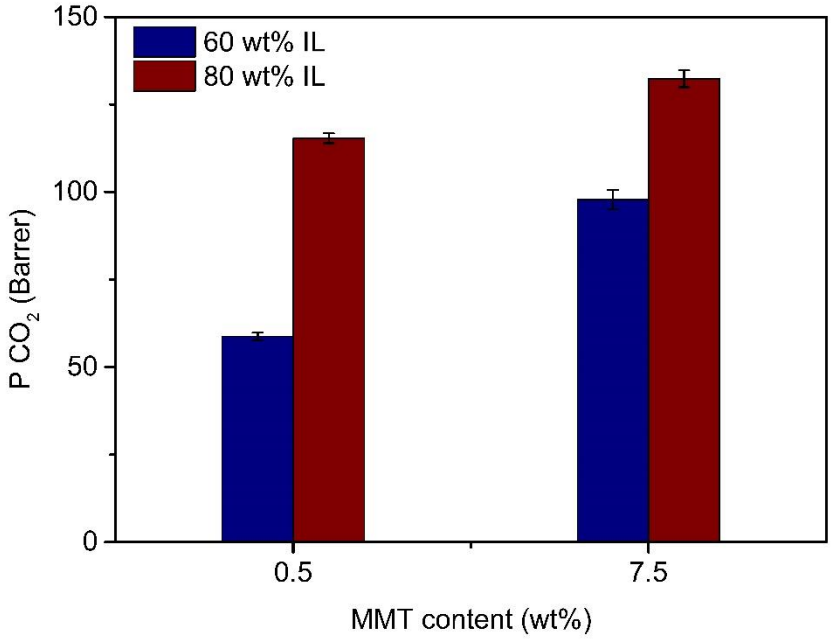

Figure 2.8 - Influence of the IL content in the CO_2 permeability of the MMIMs reinforced with 0.5 and 7.5 wt% MMT.

The influence of increasing the IL content in the ideal selectivities of the MMIMs reinforced with 0.5 and 7.5 wt% MMT can be found in Figure 2.9 a) and b), respectively. For the MMIM with 0.5 wt% MMT, a decrease in the CO_2/N_2 selectivity was obtained when the IL content was increased to 80 wt%. For CO_2/CH_4 and CO_2/H_2, the variations in selectivity were not as significant. Interestingly, the opposite behaviour was observed at the highest MMT content. For all gas pairs studied, the ideal selectivity increased with increasing IL content, at 7.5 wt% MMT. This was most likely attributed to the higher IL content in the MMIM, which helped prevent the formation of agglomerates. A more even dispersion of MMT particles in the iongel matrix along with the higher solubility provided by the IL will promote CO_2 transport, thus improving the selectivity.

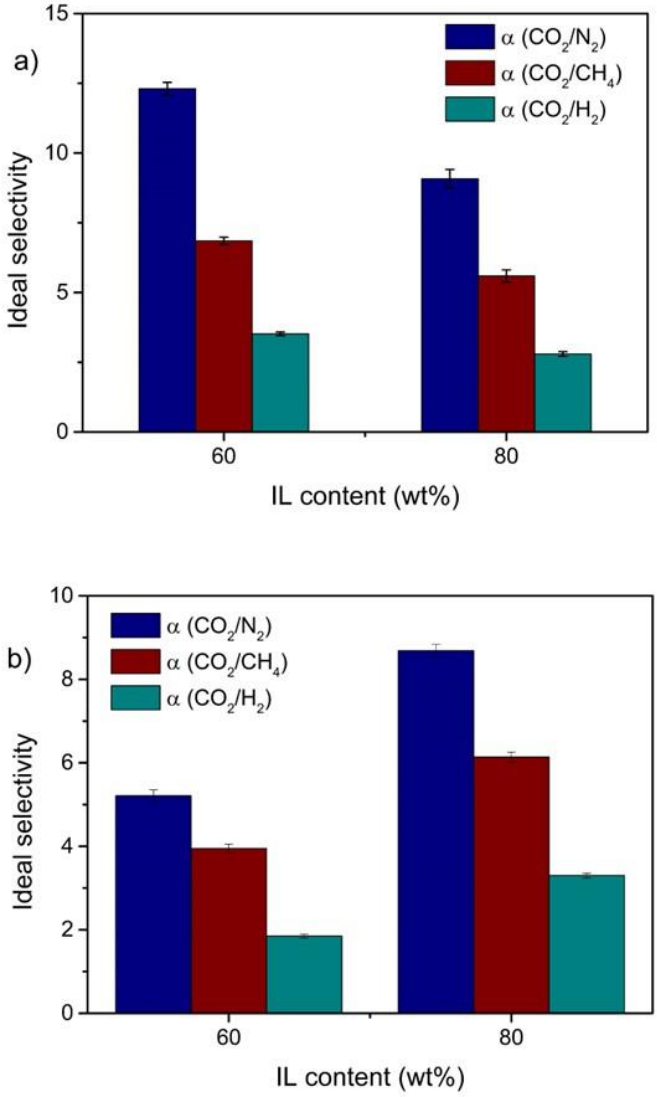

Figure 2.9 - Influence of the IL content in the CO_2/N_2, CO_2/CH_4 and CO_2/H_2 ideal selectivities of the MMIMs reinforced with (a) 0.5 and (b) 7.5 wt% MMT.

2.3.7 Comparison with other iongel membranes

In order to provide an overview of how the performance of the MMIMs prepared in this work are comparable with other iongel membranes reported in the literature, the experimental results were plotted in the 2008 Robeson upper bounds for CO_2/N_2 and CO_2/CH_4 separation, as well as on the CO_2/H_2 upper bound developed by Rowe and co-workers, in Figure 2.10 a)–c), respectively.[55,191] The results for both two- and three-component iongels reported in the literature are also included.[56,63,133,136,137,140,142,147–151,75,157,174,192–199,105,200,201,107,109,113–115,119]

It is clear that for the CO_2/N_2 and CO_2/CH_4 separations, the MMIMs reinforced with MMT generally presented lower CO_2 permeabilities and selectivities compared to those of other iongel membranes reported in the literature. The fact that MMT does not present affinity towards CO_2 highly contributes to the low permeabilities and selectivities observed. On the other hand, for the CO_2/H_2 separation, the obtained results were placed among the ones reported in the literature. It should be mentioned that even though the separation performances of the iongels reinforced with MMT were not as good as those reported for other iongels, the main goal of this work was to improve the mechanical stability of iongels, so they could be tested in their self-standing form. Different materials to prepare iongels should be considered, as long as their mechanical stability is preserved or enhanced.

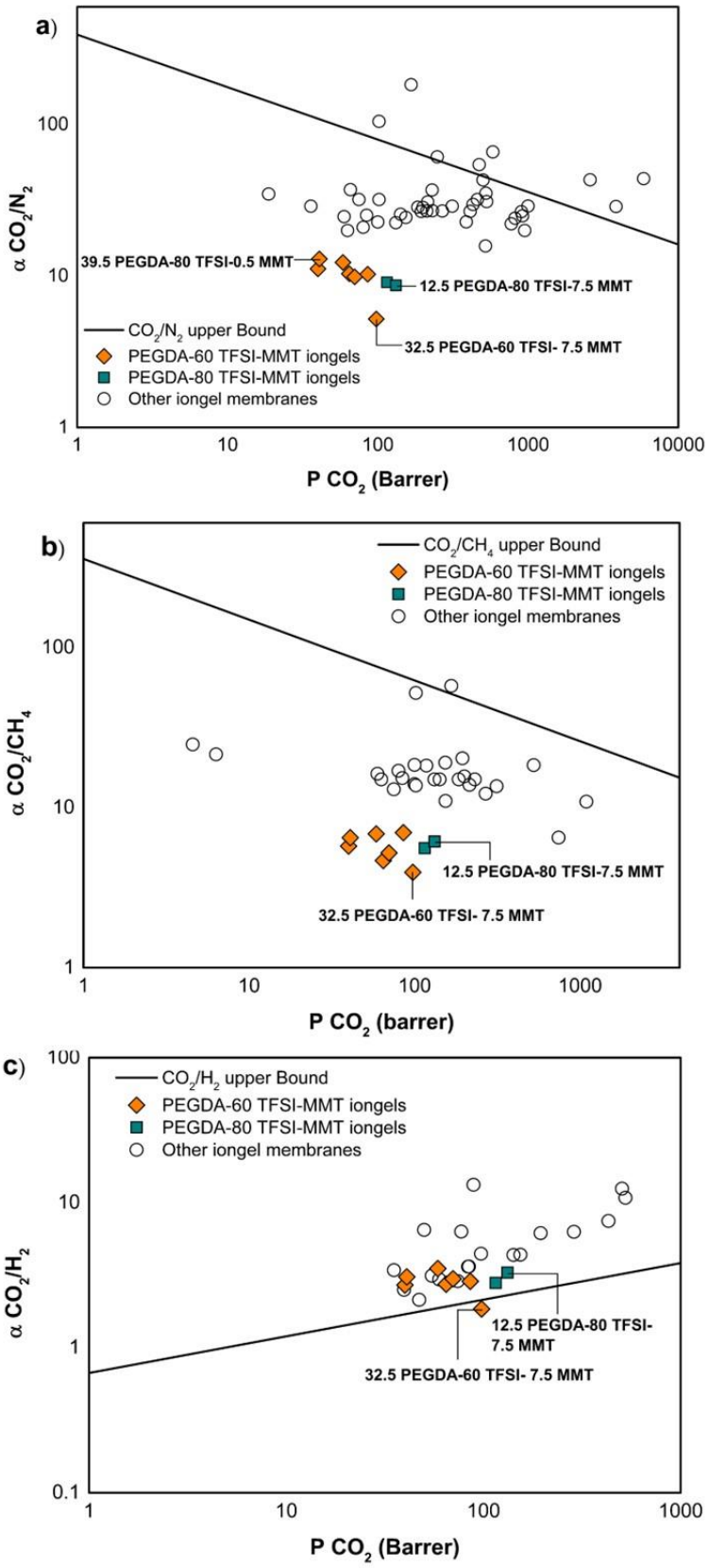

Figure 2.10 – (a) CO_2/N_2, (b) CO_2/CH_4 and (c) CO_2/H_2 ideal selectivities as a function of the CO_2 permeability for all iongels prepared in this work, as well as other iongel membranes reported in the literature.

2.4 Conclusions

In an attempt to improve the mechanical properties, MMIMs reinforced with different contents of MMT nanoclay (0.2–7.5 wt%) were prepared. The influence of increasing MMT content on the thermal and mechanical stabilities, as well as on the gas transport properties of the iongels was assessed. Dense, flexible, and freestanding MMIMs were successfully obtained, through a solvent-free UV polymerization process. Agglomerates were visible in the MMIMs, especially at higher MMT contents, however, no major defects were detected in the membranes structures. FTIR spectroscopy confirmed the high extent of the photopolymerization process of the PEGDA network. The thermal stability of the iongels was influenced by the incorporation of MMT particles, since the T_{onset} decreased at MMT contents >5 wt%. Both puncture strength and elongation improved in the MMIMs reinforced with up to 1 wt% MMT (up to 6 MPa mm^{-1} and 16.8%, respectively), further decreasing at higher contents, due to the observed MMT agglomerations. A significant increase in gas diffusivity with increasing MMT content resulted in the highest CO_2 permeability being achieved for the MMIM containing 7.5 wt% MMT (98 Barrer). On the other hand, the highest gas selectivities were obtained for the MMIM reinforced with 0.5 wt% MMT. Due to the mechanical reinforcement provided by the MMT particles, it was possible to increase the IL content up to 80 wt%, which allowed for better dispersion of the MMT particles, increasing the ideal selectivity for all gas pairs, compared to the MMIMs composed of 60 wt% IL.

It is clear that the incorporation of MMT particles into the iongel is a suitable strategy to improve the mechanical stability of these materials, as long as a good dispersion is assured. Nevertheless, further research regarding different nanoparticles to improve the mechanical stability of iongels containing high IL contents should be carried out.

3

MIXED MATRIX MEMBRANES BASED ON IONIC LIQUIDS AND POROUS ORGANIC POLYMERS FOR SELECTIVE CO_2 SEPARATION

Published as: A. R. Nabais, S. Ahmed, M. Younis, J-X. Zhou, J. R. Pereira, F. Freitas, D. Mecerreyes, J. G. Crespo, M-H. Huang, L. A. Neves and L. C. Tomé, "Mixed matrix membranes based on Ionic liquids and porous organic polymers for selective CO_2 separation", Journal of Membrane Science, 2022, 660, 120841.

Summary

The development of more efficient materials is a crucial step in the development of gas separation membranes. In this work, we combine ionic liquids (ILs) and porous organic polymers (POPs) for the first time to fabricate a new type of mixed matrix iongel membranes (MMIMs), which are entirely composed of organic materials. The new azo-POPs reported in this work were specifically designed due to their "CO_2-philic" feature to be incorporated in iongel materials. The membranes, comprising 80 wt% of [C_2mim][TFSI] IL and 20 wt% of poly(ethylene glycol) diacrylate (PEGDA) network, were prepared using a solvent-free UV curing method. The unique properties of azo-POPs within the iongel material resulted in the fabrication of dense and defect-free membranes with improved gas separation performances, in terms of both CO_2 permeability (62.3–90.6 Barrer) and CO_2/CH_4 (9.9–12.0), CO_2/H_2 (6.0–12.1) and CO_2/N_2 (16.8–53.1) ideal selectivities, with the latter revealing to be highly dependent on the morphological properties of the azo-POPs. Furthermore, iongel characterization in terms of morphology, chemical structure and thermal properties, confirmed the potential of the novel mixed matrix iongels for CO_2 separation processes.

3.1 Introduction

The growing interest in understanding the full potential of membranes has led this class of materials to be considered a promising technology in processes such as the removal of CO_2 from flue gas streams (CO_2/N_2), natural gas/biogas upgrading (CO_2/CH_4) and hydrogen purification (CO_2/H_2).[9,202–205] Despite their unquestionable advantages, the use of membranes for the separation of industrial gas streams at a large scale still needs to overcome some challenges in order to become a competitive technology. In this context, the search and development of more efficient materials is a crucial step in the development of advanced membranes, capable of combining high permeability and selectivity for specific gases with good thermal/chemical resistance, suitable mechanical properties, and long-term stability.[206]

Among the different materials studied throughout the years, ionic liquids (ILs) have established themselves as one of the most versatile class of materials. The easy design and functionalization and the remarkable gas solubility of ILs have been essential features in the growth of IL-based membranes, either through the preparation of supported ionic liquid membranes (SILMs),[16,24,25,207] combination of ILs with poly(ionic liquids) (PILs),[108,112,114] or through the development of iongels, also called ionogels, iongels or ionic liquid gel membranes.[10,61,193,208] Iongels are soft solid materials composed of a dispersed IL phase, which is usually the predominant component, and a solid continuous phase to form a three-dimensional structure, preserving the main properties of ILs and enabling the preparation of membranes with high IL content (> 60 wt%).[168]

One simple and efficient way to prepare iongels is by single-pot UV initiated polymerization of a polymer network in the presence of the desired IL. In a previous work, we demonstrated a fast and simple methodology to prepare cross-linked iongel membranes, based on poly (ethylene glycol) diacrylate (PEGDA) and imidazolium-based ILs with different anions, namely $[TFSI]^-$, $[FSI]^-$, $[C(CN)_3]^-$ and $[B(CN)_4]^-$.[136] Self-standing iongel membranes were prepared containing up to 90 wt% IL and the influence of the IL content and anion structure on the thermal and mechanical stability, as well as on the CO_2 solubility of the iongels, was studied. Finally, looking at the overall performance of the prepared iongels, it was possible to conclude that, although the cyano-based iongels presented higher CO_2 loading capacities, the iongels containing the $[C_2mim][TFSI]$ IL showed the best compromise between CO_2 solubility and thermal/mechanical properties.[136] The conclusions drawn from this motivated us to further improve the performance of these materials through the incorporation of a third component. In the context of iongels, works related with the study of the incorporation of porous materials in an iongel composed predominantly of ILs are just in infancy.[75,111,147,209,210]

Metal Organic Frameworks (MOFs), zeolites and graphene oxide (GO), are among the available and known materials, that can be used as a third porous component in the so-called mixed matrix membranes (MMMs).[211–213] Recently, new synthetic routes are following the development of versatile and all-organic materials such as porous organic polymers (POPs).

POPs are a class of porous materials known for their high surface area, tuneable chemical functionalities and outstanding physicochemical stability, that have been used in several applications, such as catalysis,[214–216] optoelectronics,[217–219] chemical sensors,[220–222] gas adsorption,[223–225] and gas separation.[226] However, the use of POPs in gas separation membranes, particularly in membranes based on ILs, is yet to be explored.

In particular, azo-linked POPs, containing azo functional groups (R–N–N-R'), have shown large potential towards CO_2 capture for several reasons: the "CO_2-philic" nature of these materials arising from the Lewis acid-base interactions between CO_2 and azo groups leads to high CO_2 sorption capacity/selectivity, up to 5.36 mmol g^{-1} for ALP-1;[227] they are composed of light elements (usually H, B, N, C and O) and are lightweight materials, therefore their gravimetric CO_2 capture capacities tend to be high and their BET surface areas are comparable to other porous materials, ranging from 400 to 1235 m^2 g^{-1}.[227,228] Depending on the synthetic route, and due to their easy functionalization, it is possible to design azo-POP structures and tailor their properties towards a specific separation.[228] Moreover, azo-POPs have a higher stability due to the nature of their covalent bonds, when compared to MOFs, which are linked through coordination bonds.

Structurally different azo-POPs and their potential towards CO_2 capture has been assessed throughout the recent years. For instance, Lu *et al*.[229] reported a facile synthesis of two different azo-linked POFs (azo-POF-1 and azo-POF-2) with moderate BET surface areas (up to 712 m^2 g^{-1}), but good CO_2 sorption capacities (up to 131 mg g^{-1} at 273 K) were obtained. Interestingly, the authors discovered that the highest CO_2/N_2 selectivity was achieved for the azo-POF with the largest average pore width.[229] This shows that different porosity parameters should also be considered when analyzing the affinity of these materials towards specific gases.[229] A simple and efficient preparation method was also reported by Yang and co-workers,[230] where azo-functionalized microporous organic polymers (azo-MOPs) were synthesized at room temperature with yields over 95%. The resultant azo-MOPs, with a BET surface area around 706 m^2 g^{-1}, showed good thermal stabilities and high sorption capacity for CO_2 (up to 134.8 mg g^{-1}), once again unveiling the potential of these materials for gas separation applications.[230] More recently, He *et al*.[231] highlighted the CO_2-philic properties of azo-POPs, by preparing mixed matrix membranes based on low molecular weight polyethylene glycol (PEG) 400 and Pebax®1657 with azo-POPs. PEG 400 and azo-POPs were combined through hydrogen bonding to effectively separate CO_2 from N_2, by enhancing the CO_2 permeability, from 94 Barrer achieved by the unfilled Pebax®1657 membrane to 392 Barrer, at 1 bar and 303 K for the membrane with 1 mg mL^{-1} azo-POP.[231]

Bearing in mind the potential shown by azo-POPs and the easy preparation of iongels, this work aims at providing a new approach regarding the preparation of mixed matrix membranes, by a solvent-free method, where it is possible to combine a high amount of IL (80 wt%) with an entirely organic filler, specifically designed for CO_2 separation. This work focuses on three main objectives: (i) the use of an efficient synthetic pathway to prepare four different azo-POPs; (ii) the fabrication and characterization of new UV cross-linked mixed matrix iongel membranes (MMIMs) combining a polymer network (poly(ethylene glycol) diacrylate, PEGDA), 80 wt% [C_2mim][TFSI] IL and four structurally different azo-

POPs, using a straightforward solvent-free method; and (iii) understand how the azo-POP structures and their functional azo groups can impact CO_2 separation, which had only been explored through adsorption experiments or molecular simulation studies, so far. Besides the improvement in the separation performance of the MMIMs containing azo-POPs, it is expected that a high compatibility between all the materials can be achieved, due to the organic nature of the azo-POPs, which is a common challenge in the use of inorganic or organic-inorganic filler materials.

The novel MMIMs were characterized in terms of gas transport properties, through pure gas permeation experiments (CO_2, N_2, CH_4 and H_2) and the influence of the azo-POP structure in the separation performance was assessed. The morphology, chemical structure and thermal stability of these materials were also investigated through several characterization techniques.

It is worth mentioning that we describe here the synthesis of three new azo-POPs, as well as their characterization in terms of structural properties. Furthermore, to the best of our knowledge, this is the first time that azo-POPs are used as porous fillers in MMIMs for CO_2 separation.

3.2 Experimental Section

3.2.1 Materials

para-nitrofluorobenzene, para-nitrochlorobenzene, sodium hydride (60% in mineral oil), para-phenylenediamine, benzidine, 4,4″-diamino-p-terphenyl and dimethylsulfoxide (C_2H_6OS) were purchased from Energy Chemical. Co (China), and used without further purification, unless otherwise noted. The tetra(p-nitrophenyl)methane (TNPM) and N,N′ ,N″ ,N‴-tetra(p-nitrophenyl)phenyldiamine (TNPPDA), N,N′,N″ ,N‴-tetra(pnitrophenyl) bisphenyldiamine (TNPBPDA), N,N′,N″ ,N‴-tetra(p-nitrophenyl) trisphenyldiamine (TNPTPDA) were synthesized using modified literature methods.[232–234] Poly(ethylene glycol) diacrylate (PEGDA, M_n 575 g mol^{-1}) and 2-hydroxy-2-methylpropiophenone (DAROCUR®, 97 wt% pure) were purchased by Sigma-Aldrich (Portugal). Ionic Liquid 1-ethyl-3-methylimidazolium bis(trifluoromethylsulfonyl) imide ([C_2mim][TFSI], 99 wt% pure) was supplied by Iolitec GmbH (Germany). Carbon dioxide, CO_2 (99.998% purity), nitrogen, N_2 (99.99% purity), methane, CH_4 (99.99% purity) and hydrogen, H_2 (>99.99% purity) gases were supplied by Praxair (Portugal).

3.2.2 Preparation and Characterization of Azo-linked Porous Organic Polymers (Azo-POPs)

The detailed description of the synthesis of azo-POP monomers can be found in Appendix B. The synthesis of azo-POPs was carried out using a time-efficient synthetic method reported by Huang *et al*.[232], via $NaBH_4$-mediated coupling on four-folded monomers containing nitro groups. The synthesis and characterization of azo-POP-1 has already been reported.[232] In the present study, three other monomers (monomer 2, monomer 3 and monomer 4, schematically represented in Figure 3.1 containing tetra-nitro groups were prepared by n-arylation of diamines with p-nitrobenzene, in order to synthesize

the three new azo-POPs. To obtain the desired azo-POPs, also represented in Figure 3.1, a solution of 1 mmol tetranitro monomer in 10 mL of DMF was gradually mixed with a solution of 20 mmol $NaBH_4$ and the resulting mixture was stirred for 1 h at 358 K. Afterwards, the prepared solution was poured into 100 mL of water and the obtained solid particles were filtered and washed with water and ethanol (3x100 mL). Azo-POP-1, azo-POP-10, azo-POP-11 and azo-POP-12 were obtained as yellow to red solids, with yields over 90%, which structures were confirmed by ^{13}C CP/MS Nuclear Magnetic Resonance (NMR), Fourier Transform Infrared spectroscopy (FTIR) and elemental analysis.

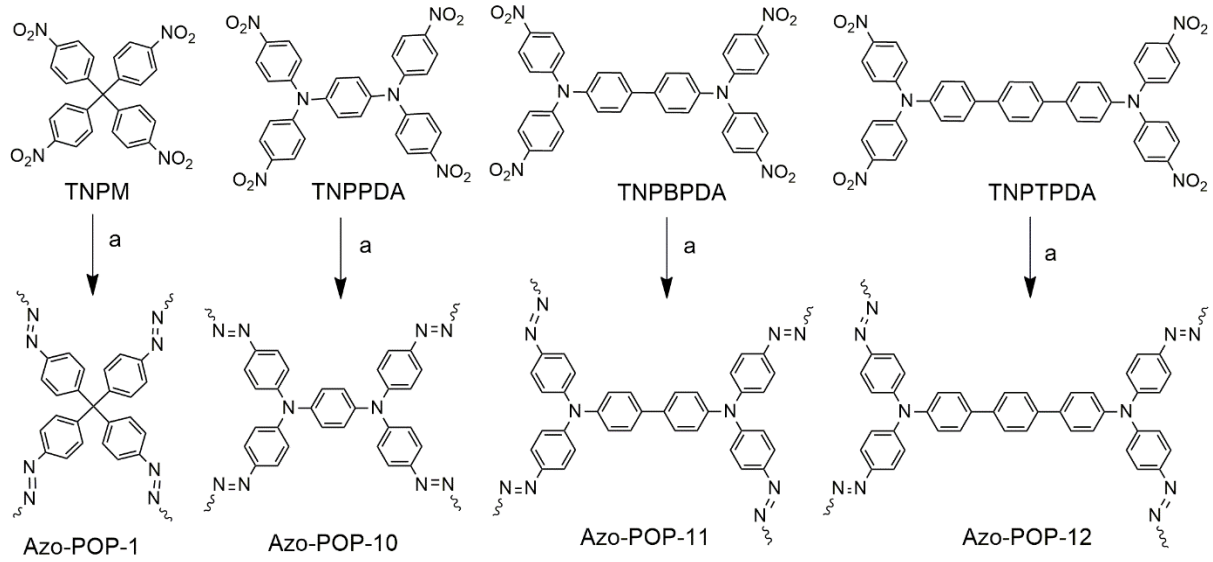

Figure 3.1 - Synthesis of the different azo-POPs from the corresponding monomers. Condition (a) corresponds to: $NaBH_4$, DMF, 0.5h at 358 K.

3.2.3 Adsorption Isotherms and Morphological Characterization of Azo-POPs

The morphological characterization of all azo-POPs was performed according to standard procedures. The porous volume and Brunauer-Emmet-Teller (BET) surface area, in the range of P/P_0 = 0.0–1.0, were determined by N_2 adsorption/desorption measurements at 77K, using Accelerated Surface Area and Porosimetry System (ASAP 2010). All powdered samples were degassed before each sorption equilibrium experiment, under vacuum at 393 K for 24h. This ensures that any moisture or contaminants adsorbed on the materials' surface are removed before the experiments. Carbon dioxide adsorption-desorption experiments were carried out at 273 and 298 K, using a BELSORP-MAX II (BEL Inc., Japan). The azo-POP samples were degassed at 373 K for 12 h, under vacuum before analysis.

3.2.4 Preparation of Mixed Matrix Iongel Membranes

Bearing in mind our previous results on PEGDA/IL iongels,[136] the azo-POP iongel membranes studied in this work were prepared containing 80 wt% IL to maximize their CO_2 loading capacity. Moreover, a low concentration of azo-POP (0.5 wt%) was chosen to make an initial study of the influence

of these solid particles on the MMIMs performances and avoid the need for solvents to disperse the solid particles in the mixture during their preparation.

The MMIMs were prepared by UV-initiated free radical polymerization. Initially, 80 wt% of IL was mixed with 0.5 wt% (above the total iongel solution) of azo-POP. The obtained solutions were sonicated for 1 h and magnetically stirred overnight to ensure a good dispersion of the solid particles. Afterwards, 20 wt% of PEGDA and around 3 wt% (relative to PEGDA) of DAROCUR® as photo initiator were added, and the solutions were left stirring until they were completely homogeneous. The resulting mixtures were casted between two Rain-X™ coated quartz plates, with a 100 µm spacer in between and exposed to a UV light using a UVC-5 UV Curing Conveyor System with 800 mW cm^{-2}, at a wavelength of 365 nm. The distance from sample to lamp was 1 cm and the belt speed was set at 1 m min^{-1}. The resulting MMIMs were peeled off from the plates and characterized. Figure 3.2 shows a schematic illustration of the preparation of MMIMs containing azo-POPs.

Composite membranes were prepared to carry out the gas permeation experiments without compromising the mechanical integrity of the iongels. The iongel was supported on a pre-wetted porous polyamide (PA) filter (Sartorius™, supplied by Fisher Scientific) with a pore size of 0.22 µm. The support was immersed in deionized water before the solution was casted on top of it, in order to minimize the pore filling from the iongel solution to the porous support. The chosen hydrophilic PA support was found to be compatible with the iongel solution, assuring a good adhesion between the two layers.

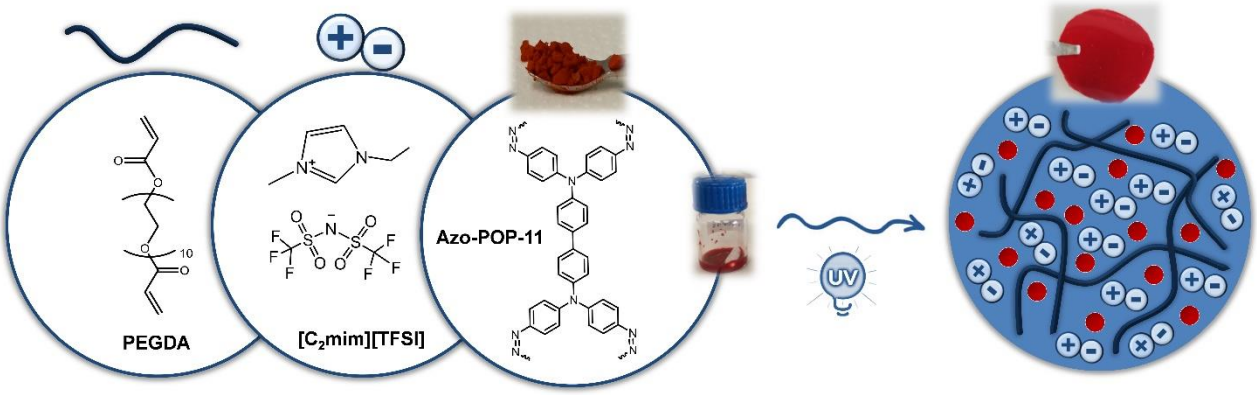

Figure 3.2 - Schematic illustration of the preparation of MMIMs containing azo-POP.

3.2.5 Scanning Electron Microscopy (SEM)

Scanning Electron Microscopy images of the surface and cross section of the self-standing and composite MMIMs (iongel supported onto porous polyamide filter) were acquired using an analytical JEOL 7001F scanning electron microscope (FEG-SEM), equipped with a field emission gun operated at 15 kV. All samples were coated with a thin Pd/Au layer to induce charge under the electron beam.

3.2.6 Fourier Transform Infrared-Attenuated Total Reflectance spectroscopy (FTIR-ATR)

FTIR-ATR analysis was performed for all the iongel membranes and azo-POPs to confirm their chemical structure, as well as to determine if there were any interactions being established between the materials used. The FTIR-ATR spectra were acquired in a PerkinElmer Spectrum two spectrometer. The spectra were collected using 10 scans, from 4000 to 400 cm^{-1}, with a resolution of 4 cm^{-1}.

3.2.7 Contact Angle Measurements

The contact angle of the neat PEGDA-80 TFSI iongel and MMIMs were measured to evaluate their hydrophilic/hydrophobic nature. A drop of distilled water was manually deposited on the surface of each membrane sample, and three replicates were performed to obtain the mean contact angle. For each replicate, 10 frames were acquired, with an interval of 1 s between each, and all images were processed by CAM100 (KSV) software, where the water drop was fitted to mathematical functions.

3.2.8 Thermogravimetric Analysis

Thermogravimetric analysis was carried out using a TA Instrument model TGA Q50. MMIMs and azo-POPs samples of around 10 mg were heated from room temperature to 873 K, at a constant heating rate of 10 K min^{-1}, under a nitrogen flow of 40 mL min^{-1}, to prevent thermo-oxidative degradation of the samples. The obtained data was analysed using a Universal Analysis 4.5A software to determine the onset temperature, (T_{onset}), defined as the temperature at which the baseline slope changes and degradation temperature, (T_{dec}), defined as the temperature at 50% weight loss.

3.2.9 Mechanical Properties

The mechanical properties of the prepared composite MMIMs (iongel supported onto porous polyamide filter) were evaluated through tensile tests, using a TMS-Pro texture analyser, where the samples were stretched until their rupture. All samples were prepared with 1.5 × 6 cm and thickness of around 200 μm. Each sample was placed between two testing clamps and the testing speed was set at 1 mm s^{-1}, until the rupture of the sample. For each sample, at least four replicates were performed and the mean values of the tension at break, deformation at break and Young's modulus were determined.

3.2.10 Single Gas Permeation Experiments

Gas permeation experiments were carried out for pure CO_2, N_2, CH_4 and H_2, at 0.7 bar and 303 K, using an experimental setup, fully described elsewhere.[16] The system is composed by a stainless-steel cell with two similar compartments, designated as feed and permeate, separated by the membrane. The detailed procedure to carry out a gas permeation experiment can be found in our previous work.[16] For each membrane, three replicates were tested The permeability of a pure gas

through the membrane was calculated from the obtained pressure data over time, on both compartments, according to the following equations.[235]

$$\frac{1}{\beta}\ln\left(\frac{[p_{feed}-p_{perm}]_0}{[p_{feed}-p_{perm}]}\right)=\frac{1}{\beta}\ln\left(\frac{\Delta p_0}{\Delta p}\right)=P\,\frac{t}{l} \tag{3.1}$$

Where p_{feed} and p_{perm} are the pressures (bar) in the feed and permeate compartments, respectively, P is the membrane permeability ($m^2\,s^{-1}$, where 1 Barrer = $1x10^{-10}$ cm^3 cm cm^{-2} s^{-1} $cmHg^{-1}$ = $8.3x10^{-13}$ m^2 s^{-1} [235]), t is the time (s) and l is the membrane thickness (m). β (m^{-1}) is a geometric parameter, characteristic of the geometry of the cell, given by:

$$\beta = A\left(\frac{1}{V_{feed}}+\frac{1}{V_{perm}}\right) \tag{3.2}$$

Where A is the membrane area (m^2) and V_{feed} and V_{perm} are the volumes (m^3) of the feed and permeate compartments, respectively. The gas permeability is obtained from the slope represented by ploting $\frac{1}{\beta}ln\left(\frac{p_0}{p}\right)$ versus t/l. The ideal gas selectivity was calculated by dividing the permeabilities of the two different gases (A and B), according to the following equation:

$$\alpha_{A/B}=\frac{P_A}{P_B} \tag{3.3}$$

It should be noted that, in this work, the permeability data obtained from Equation 3.1, as well as the thickness considered for these calculations, are related to the global permeability of the membrane, considering the polymer support and the iongel layer.

To understand the contribution of the iongel layer alone to the gas transport of the membrane, the iongel permeability was calculated using the resistance in series model (RSM).[236,237] According to the RSM, the gas transport on a layered membrane and the electric current flow in the serial connection to conductors are equivalent since the different layers of a composite membrane can be described in terms of their resistance to gas transport. The resistance (R) to the gas flow is proportional to the thickness (l) and inversely proportional to the permeability (P) and surface area (S), and the total resistance is equal to the sum of resistances originating from each layer.

The resistance of a specific layer can be calculated using the following equations:

$$R=\frac{l}{P.S} \tag{3.4}$$

$$R_t = R_i + R_s \tag{3.5}$$

$$\frac{l_t}{P_t.S} = \frac{l_i}{P_i.S} + \frac{l_s}{P_s.S} \tag{3.6}$$

The permeability of the double layer composite membrane is described by the following equation:

$$P_t = \frac{(l_i + l_s).P_i.P_s}{(P_s.l_i) + (P_i.l_s)} \tag{3.7}$$

Consequently, by knowing the gas permeability of the composite membrane and pre-wetted support layer (s) obtained from Equation 3.1, as well as the respective thickness of each of these layers, it is possible to predict the permeability of the iongel layer (*i*). In this work, even though porous supports were used in the preparation of the membranes, it was observed that, due to the pre-wetting step, they offered resistance to the gas transport, which did not occur when the supports were dry. For that reason, gas permeation measurements for all gases were also performed on the pre-wetted support to determine the permeability, P_s, of this layer.

For the gases studied in this work, the permeability of the double layer structure can be described by the following equations:

$$P_t^{CO_2} = \frac{(l_i + l_s).P_i^{CO_2}.P_s^{CO_2}}{(P_s^{CO_2}.l_i) + (P_i^{CO_2}.l_s)} \tag{3.8}$$

$$P_t^{N_2} = \frac{(l_i + l_s).P_i^{N_2}.P_s^{N_2}}{(P_s^{N_2}.l_i) + (P_i^{N_2}.l_s)} \tag{3.9}$$

$$P_t^{CH_4} = \frac{(l_i + l_s).P_i^{CH_4}.P_s^{CH_4}}{(P_s^{CH_4}.l_i) + (P_i^{CH_4}.l_s)} \tag{3.10}$$

$$P_t^{H_2} = \frac{(l_i + l_s).P_i^{H_2}.P_s^{H_2}}{(P_s^{H_2}.l_i) + (P_i^{H_2}.l_s)} \tag{3.11}$$

Where $P_i^{CO_2}$, $P_i^{N_2}$, $P_i^{CH_4}$ and $P_i^{H_2}$ are the CO_2, N_2, CH_4 and H_2 permeability of the iongel layer, and $P_s^{CO_2}$, $P_s^{N_2}$, $P_s^{CH_4}$ and $P_s^{H_2}$ are the CO_2, N_2, CH_4 and H_2 permeability of the support layer, respectively.

The ideal selectivity of each gas pair can be calculated, for the composite membrane or for each layer, by dividing the correspondent permeability of the more permeable species (CO_2) by the permeability of the least permeable species (N_2, CH_4, and H_2), according to the previously described Equation 3.3.

3.3 Results and Discussion

3.3.1 Azo-POPs Characterization and N_2 Adsorption Isotherms

In this work, four different azo-POPs were synthesized according to Figure 3.1, azo-POP-1 and the new porous polymers azo-POP-10, azo-POP-11 and azo-POP-12. The structures of azo-POPs were evidenced by their solid-state ^{13}C CP/MS NMR (Figure B.3 of Appendix B), which showed the common chemical shifts in the range of 100–160 ppm for sp^2 carbons and characteristic broad peak of –C–N–N– bond at 152 ppm. In the case of azo-POP-1, the peak around 65 ppm indicated the presence of a quaternary carbon. The exact ratio between the masses of C and N for azo-POPs was determined by elemental analysis (see Table B.1, Appendix B), and the obtained data showed that C/N ratio of all the azo-POPs samples was well consistent with theoretical values.[229,238]

Looking at the N_2 sorption isotherms of the prepared azo-POP-10, azo-POP-11 and azo-POP-12 shown in Figure 3.3, the rapid uptake at low pressure (0–0.1 bar) indicated the presence of permanent micropores. The apparent hysteresis between adsorption and desorption suggested that the prepared azo-POPs are networks enclosing both meso- and micropores, which were assigned to the pore network effects.[239,240] The same behaviour had already been observed for azo-POP-1 in a previous work.[232] The BET surface area and porous volume obtained for the prepared azo-POPs are displayed in Table 3.1. The BET surface areas were calculated as 1100 $m^2 g^{-1}$ (azo-POP-1), 439 $m^2 g^{-1}$ (azo-POP-10), 478 $m^2 g^{-1}$ (azo-POP-11) and 298 $m^2 g^{-1}$ (azo-POP-12), while the porous volumes were obtained between 0.57 $cm^3 g^{-1}$ for azo-POP-1 to 0.29 $cm^3 g^{-1}$ for azo-POP-12. These BET SA were generally higher than those reported for azo-POP-7, azo-POP-13 and azo-POP-14 and within the range of values obtained for azo-POP-2 and azo-POP-3.[241,242] Moreover, it was found that azo-POP-1 presented the most narrow pores (2.8 nm, average), while azo-POP-12 encloses the biggest pores in its structure (around 7.8 nm), compared to the other azo-POPs studied.

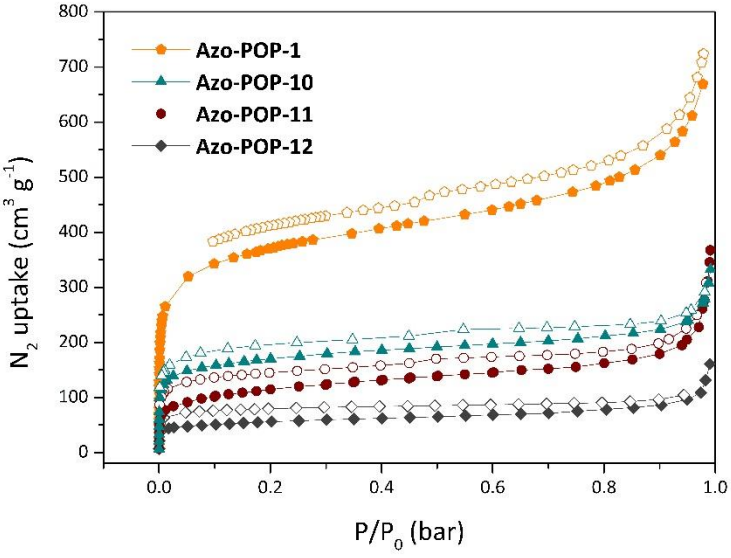

Figure 3.3 - N_2 sorption isotherms of the prepared azo-POPs.

Table 3.1 - Morphological characterization of the azo-POPs studied in this work.

Azo-POP	BET surface area ($m^2\ g^{-1}$)	Porous volume ($cm^3\ g^{-1}$)	Mean Pore size (nm)
Azo-POP-1	1100	0.57	2.8
Azo-POP-10	439	0.35	3.4
Azo-POP-11	478	0.34	3.6
Azo-POP-12	298	0.29	7.8

3.3.2 Single Gas CO_2 Adsorption Isotherms

Figure 3.4 a) and b) illustrates the single gas CO_2 sorption isotherms obtained at 273 and 298 K, respectively, for synthesized azo-POP-1, azo-POP-10, azo-POP-11 and azo-POP-12. All sorption isotherms were type I, according to the IUPAC classification, which is characteristic of microporous materials.[243] Except for azo-POP-1 at 298 K, where a small hysteresis was observed, no hysteresis were found for the remaining isotherm curves, showing a completely reversible behaviour and possible full regeneration of the materials after the sorption experiments. The smooth adsorption-desorption cycles showed that the interactions between the azo-POPs and CO_2 molecules are weak enough to regenerate the materials. This finding is of great importance for cyclic sorption gas separations processes, where the adsorbent material should be able to fully regenerate to prevent residual adsorbed gas onto the material.

The adsorption capacities obtained at 273 K, were 2.3 mmol g^{-1} for azo-POP-1, 1.51 mmol g^{-1} for azo-POP-10, 0.66 mmol g^{-1} for azo-POP-11 and 1.55 mmol g-1 for azo-POP-2, which decreased at 298 K to 1.95 mmol g^{-1}, 0.82 mmol g^{-1}, 0.37 mmol g^{-1} and 0.91 mmol g^{-1}, respectively. As expected, the adsorption capacity decreased with increasing temperature since this is an exothermic process. The adsorption capacity obtained for the synthesized azo-POPs were lower than the values obtained for other azo-POPs previously reported in the literature, having similar structures.[238,244] However, their performance as fillers in membranes for gas separation was not assessed.

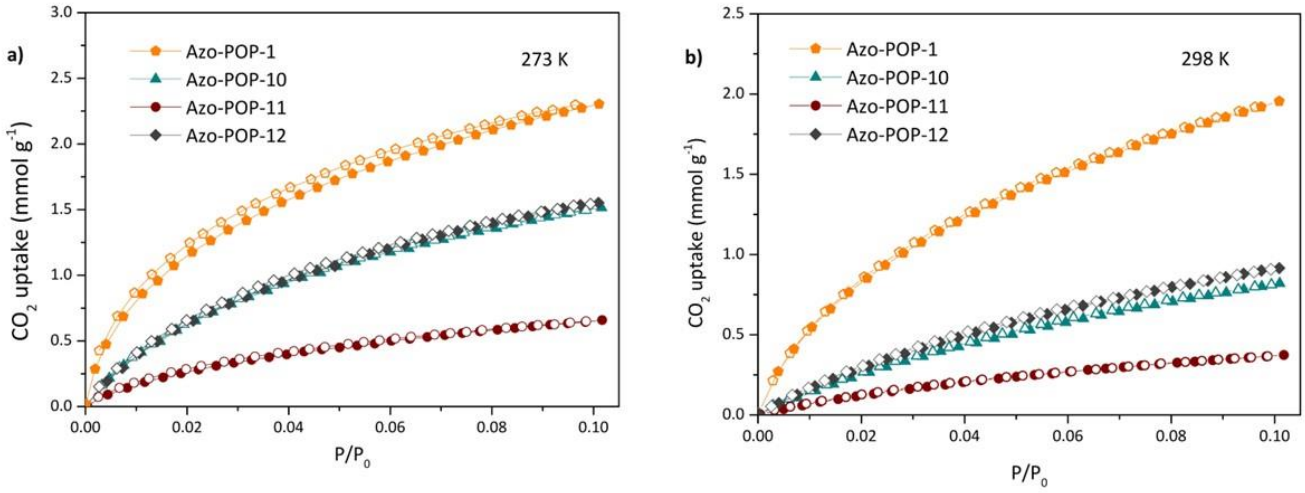

Figure 3.4 - CO_2 sorption isotherms in azo-POP-1, azo-POP-10, azo-POP-11 and azo-POP-12, at (a) 273 and (b) 298 K. Closed and open symbols denote adsorption and desorption data, respectively.

3.3.3 Membrane Preparation and Characterization

As illustrated in Figure 3.2 and described in the experimental section, the MMIMs were prepared by UV-photopolymerization of PEGDA in the presence of 80 wt% of IL and 0.5 wt% of azo-POP. We selected this PEGDA/IL formulation based on our previous work.[136] The powdery azo-POPs were easily dispersed in the liquid PEGDA/IL mixture before photopolymerization without the need of additional organic solvent.

3.3.3.1 Scanning Electron Microscopy (SEM)

As a typical example, Figure 3.5 a) and b) show the SEM images of the surface and fractured cross-section of the self-standing MMIMs containing the azo-POP-11. A non-porous and defect free membrane morphology was obtained, since no deformations, agglomerations or phase separation were detected. Such morphology indicates not only a good miscibility between the different components, but also a good dispersion of the azo-POP particles in the MMIM. It should be noted that the reliefs seen in

the cross-section image were probably due to the plastic deformation caused by liquid nitrogen during the fracturing process. The same type of morphology was found for all the MMIMs prepared in this work. Figure. 3.5 c) and d) shows the SEM images of the respective composite membrane, composed by the PEGDA-80 TFSI-0.5 POP-11 iongel and the porous polyamide support. Similarly, the iongel layer of the composite membrane also presented a dense and defect-free surface, while in the cross-section image it was possible to distinguish the support (top) from the iongel layer (bottom).

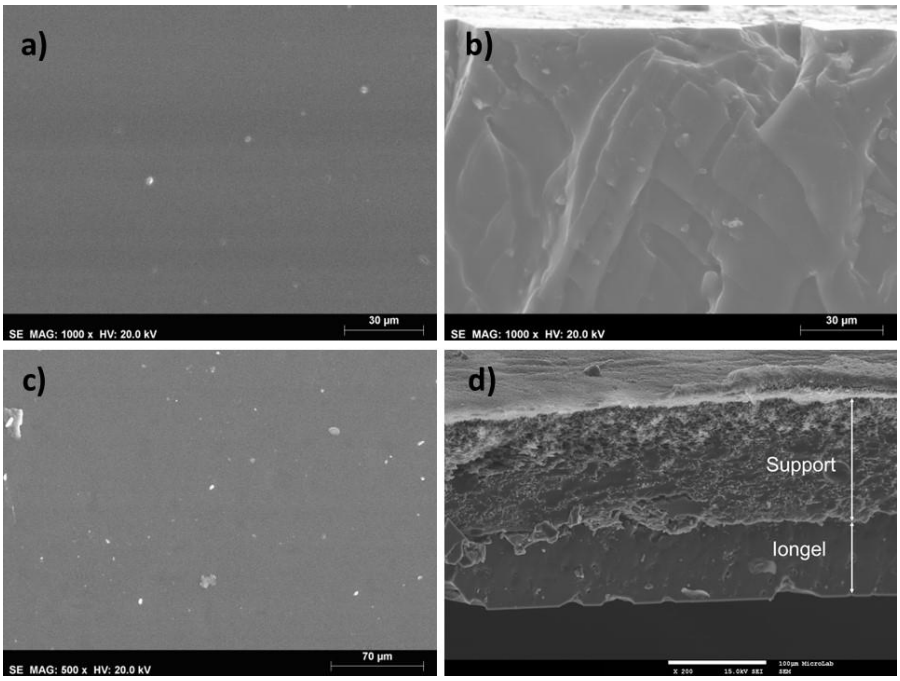

Figure 3.5 - SEM images of the (a,c) surface and (b,d) cross section of the (a,b) self-standing and (c,d) composite MMIMs composed by PEGDA-80 TFSI-0.5 POP-11.

3.3.3.2 FTIR-ATR spectroscopy

The chemical structure of the azo-POPs and prepared iongel membranes were confirmed by FTIR-ATR spectroscopy, as shown in Figure B.4 (Appendix B) and Figure 3.6, respectively.

The presence of the azo group in azo-POP-1, azo-POP-10, azo-POP-11 and azo-POP-12 (Figure B.4, Appendix B) was confirmed by the absorption peaks at 1480 and 1410 cm^{-1}, corresponding to the N=N stretching vibrations. The peaks observed at 1270 and 1305 cm^{-1} were attributed to the C-N stretching vibrations of the aromatic compounds present in the azo-POP structures.[232]

In Figure 3.6, the presence of PEGDA in the iongel was confirmed by the peaks at 1730 cm^{-1}, arising from the C=O symmetric stretching and the bands at around 2878 and 2940 cm^{-1}, attributed to the C-H stretching. Moreover, the absence of visible peaks at 1619 cm^{-1} and 1635 cm^{-1} (C=C asymmetric and symmetric stretching, respectively), attributed to the presence of terminal acrylate groups from PEGDA, confirmed the occurrence of the polymerization reaction.[136] The peak at 1460 cm^{-1} and the

bands at 3120 and 3160 cm^{-1} were assigned to the CH_3 bending vibrations and CH_2 stretching vibrations, respectively, originated from the imidazolium-based cation of the IL. On the other hand, the bands at 1049 cm^{-1}, 1132 cm^{-1}, 1178 cm^{-1} and 1343 cm^{-1} are typical of the $[TFSI]^-$ anion.[136] The characteristic peaks of azo-POPs, described above, were not detected in the iongels spectra, due to the low azo-POP content in the iongel or possible overlapping of peaks.

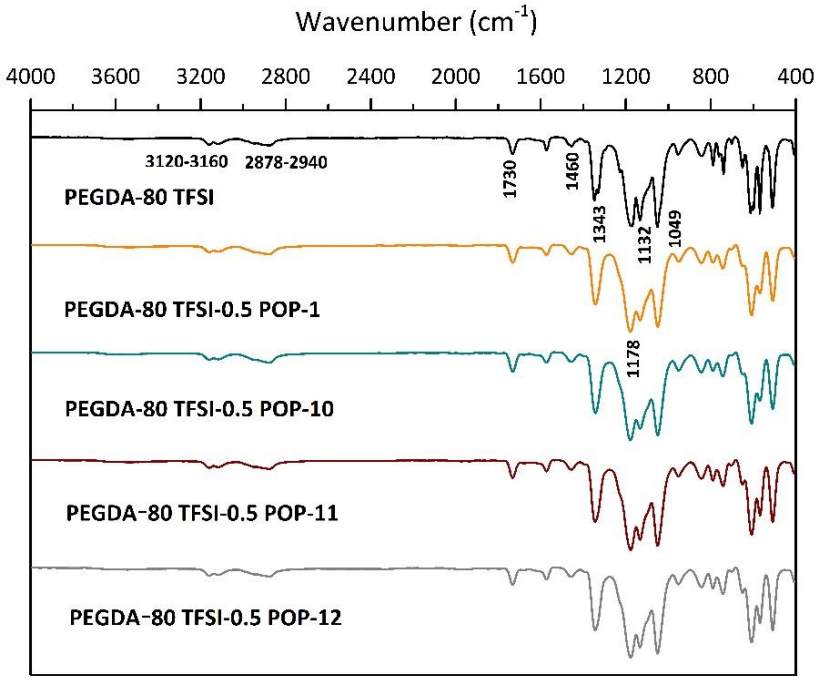

Figure 3.6 - FTIR spectra of the PEGDA-80 TFSI iongel and the different MMIMs containing different azo-POPs.

3.3.3.3 Contact Angle Measurements

The water contact angle of each iongel membrane sample was measured, and the respective mean values and corresponding errors are displayed in Figure 3.7. The PEGDA-80 TFSI iongel presented the highest water contact angle at 61.9°, and this value decreased upon the incorporation of different azo-POPs, down to 42.5° for PEGDA-80 TFSI-0.5 POP-1, suggesting that the addition of azo-POPs accentuated the hydrophilic character of these materials. For the different MMIMs containing azo-POPs, the water contact angles were similar, probably because the azo-POP structures are also similar between them and thus, the azo-POPs used do not have a major impact in this parameter.

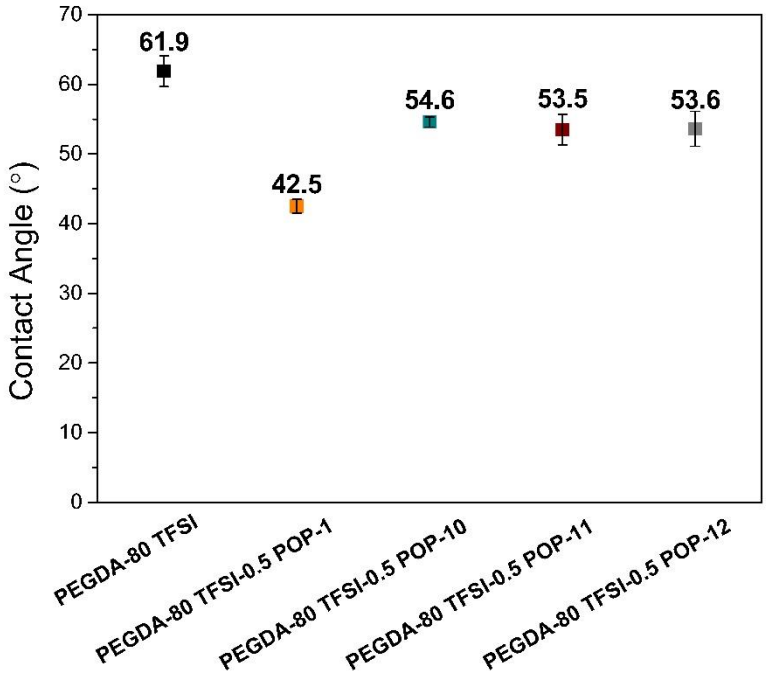

Figure 3.7 - Water contact angles obtained for the PEGDA-80 TFSI iongel and the MMIMs containing different azo-POPs.

3.3.3.4 Thermogravimetric Analysis

Figure 3.8 presents the TGA profiles of the prepared neat PEGDA-80 TFSI iongel and MMIMs. The MMIMs containing the different azo-POPs present a similar behaviour when compared to that of the PEGDA-80 TFSI iongel. Until around 473 K, only trapped moisture was removed. Considering that PEGDA has a lower thermal stability compared to the neat [C_2mim][TFSI] IL, the PEGDA-TFSI iongel exhibited T_{onset} and T_{dec} values between those of the neat materials. After the incorporation of the different azo-POPs, both T_{onset} and $T_{dec,}$ presented in Table B.2 (Appendix B), decreased from 661 K for the PEGDA-80 TFSI iongel to 610 K for the PEGDA-80 TFSI-0.5 POP-1 MMIM. Above these temperatures there was a continuous weight loss, which resulted in the total degradation of the iongels. The decrease observed after the incorporation of azo-POPs was attributed to a lower thermal stability of these materials, compared to PEGDA or the IL. The T_{onset} of azo-POP-1, azo-POP-10, azo-POP-11 and azo-POP-12 were detected at 514, 558, 583 and 563 K, respectively, as observed in Figure B.5 (Appendix B).[232] Nonetheless, the TGA results here presented confirmed that the proposed MMIMs containing azo-POPs possess a suitable thermal stability within the typical temperature range of the CO_2/N_2, CO_2/CH_4 and CO_2/H_2 streams, with weight losses < 3 wt% up to 473 K.

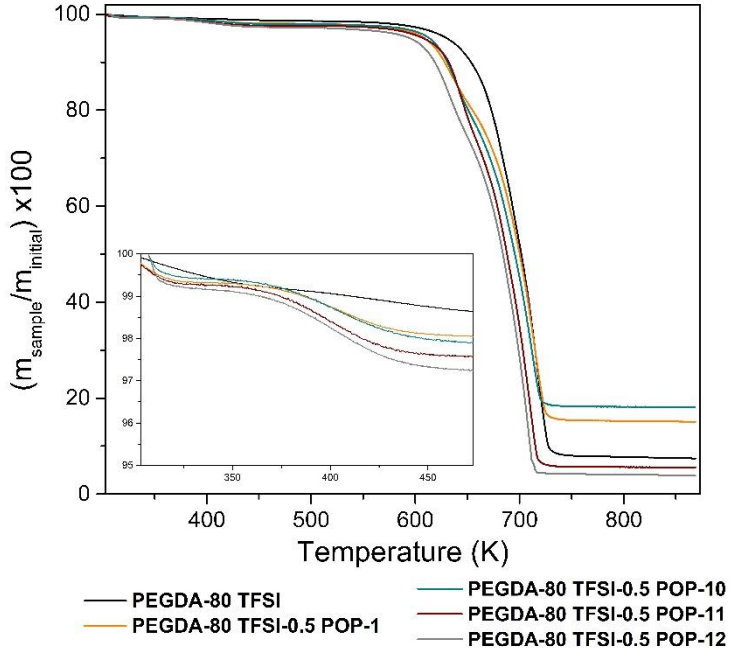

Figure 3.8 - Thermogravimetric profiles of the PEGDA-80 TFSI iongel and the MMIMs containing different azo-POPs.

3.3.3.5 Mechanical Properties

Table 3.2 shows the tension at break, deformation at break and Young's modulus obtained for all composite iongel membranes, in which the iongel was supported on top of a porous polyamide filter. The self-standing MMIMs were too mechanically fragile to be tested since they broke easily when placed between the testing clamps of the equipment. Thus, only the porous polyamide support and the respective composite iongel membranes were tested. The results concerning the tension at break and Young's Modulus showed that the polymer support alone could withstand a higher stress before breaking and had a higher resistance to elastic deformation, compared to the composite iongel membranes. The pre-wetting step and the casting of the iongel solution on the polyamide support surface may decrease the stiffness of this layer, by acting as a plasticizer that reduces the entanglement and bonding between molecular chains, resulting in the variations of the mechanical parameters observed in Table 3.2.[245,246] It was also observed that, as the tension increased, the iongel layer began to crack while the support was stretched, finally resulting in its rupture. This happened because the iongel layer was mechanically weaker when compared to the polyamide support. Small cracks in the iongel started to be observed during the plastic deformation region of the samples. Looking at the data obtained for the composite iongel membranes, it is possible to perceive that the composition of the azo-POP iongel layer had no significant impact in the mechanical parameters determined from these experiments, since the main contribution to the membrane's strength was made by the support layer. This explains the use of a support layer to provide mechanical resistance for the MMIMs containing azo-

POPs during the gas permeation tests. Even though the iongel layers started to crack at a lower tension, they did not detach from the polyamide support, showing a good adhesion between the two materials and also the successful preparation of these composite membranes.

Table 3.2 - Tension at break, deformation at break and Young's modulus of the polymer PA support and the different MMIMs prepared in this work.

Membrane Sample	Tension at break (MPa)	Deformation at break (%)	Young's Modulus (MPa)
Porous PA support	21.1 ± 0.3	19.6 ± 0.4	5.8 ± 0.1
PEGDA-80 TFSI	12.1 ± 0.9	16.5 ± 0.9	3.1 ± 0.2
PEGDA-80 TFSI-0.5 POP-1	13.3 ± 1.3	16.7 ± 1.7	3.3 ± 0.3
PEGDA-80 TFSI-0.5 POP-10	12.2 ± 0.6	24.6 ± 0.9	2.5 ± 0.1
PEGDA-80 TFSI-0.5 POP-11	13.5 ± 1.6	16.7 ± 0.3	3.4 ± 0.2
PEGDA-80 TFSI-0.5 POP-12	13.1 ± 1.5	19.6 ± 2.0	2.9 ± 0.3

3.3.3.6 Pure Gas Permeation Experiments

Pure gas permeation experiments were carried out for CO_2, N_2, CH_4 and H_2, to study the influence of the incorporation of different azo-POPs on the permeability and selectivity of MMIMs. It is important to emphasize once again that, to the best of our knowledge, this is the first time that a class of POPs is incorporated in iongel membranes for gas separation.

The gas transport in MMIMs follows the same mechanism of other dense membranes, where the permeability is a combined effect of the gas diffusivity and solubility ($P=S\times D$) and the incorporation of porous materials has a direct influence on these parameters. For nonpolar gases, such as CH_4, N_2 and H_2, the solubility depends primarily on the properties of the gas molecules, while for CO_2 this coefficient is more dependent on the membrane material and its interactions with the gas molecules. Moreover, the presence of specific functional groups can help increase the solubility coefficient. On the other hand, the diffusivity is primarily governed by the gas molecule size and the free volume in the membrane structure. The porosity induced by the incorporation of porous materials, such as azo-POPs, can restrict or facilitate the diffusion of gas molecules, depending on their size.

Table B.3 (Appendix B) presents the global CO_2 permeabilities and the CO_2/N_2, CO_2/CH_4 and CO_2/H_2 ideal selectivities of the prepared composite membranes, considering the iongel deposited on top of the polyamide support. To better understand the separation performance of the MMIM layer, Table 3.3 presents the CO_2 permeabilities and the CO_2/N_2, CO_2/CH_4 and CO_2/H_2 ideal selectivities of the iongel layers, calculated according to Equation 3.8 and Equation 3.3, respectively, and the following discussion will be focused on these results.

From Table 3.3, it can be seen that the CO_2 permeability was favoured by the incorporation of azo-POP in the MMIM, even at such a low concentration (0.5 wt%), since these membranes were able to outperform the one composed by only PEGDA and 80 wt% of IL. This improvement in CO_2 permeability resulted from the incorporation of an extra porous network provided by the azo-POPs, the physical nature of their pores and the azo functional groups present in their structures, as previously revealed by both theoretical and experimental studies.[231,238,244] It has been demonstrated that porous frameworks with nitrogen-rich functionalities provide "CO_2-philic" properties to the membrane and high CO_2 uptake capacity. These features are believed to arise from enhanced CO_2-framework interactions through strong dipole-quadrupole interactions. Azo groups can act as a Lewis basic site, while the carbon atom in CO_2 acts as an acid, originating dipole/quadrupole interactions between the two sites, thus resulting in a higher affinity of the azo-POP pore surface for CO_2.[230] It is also interesting to see that, for the MMIMs, the CO_2 permeability was higher when the contact angle was lower (Figure 3.7), as the solubility of CO_2 in more hydrophilic materials is generally higher than in less hydrophilic/hydrophobic ones.

The highest CO_2 permeability was achieved for the MMIM with azo-POP-1 (91 Barrer), while the lowest was obtained for the one with azo-POP-12 (68 Barrer). These CO_2 permeability values followed a trend similar to that of the BET surface area (1100 $m^2\ g^{-1}$, and 298 $m^2\ g^{-1}$, respectively) and porous volume (0.57 $cm^3\ g^{-1}$ and 0.29 $cm^3\ g^{-1}$, respectively) parameters obtained for these materials (Table 3.1). Moreover, stronger CO_2-framework interactions are expected in azo-POPs having more narrow pores, due to a higher number of interactions between the adsorbed CO_2 molecules and the pore walls.[227] Additionally, from the CO_2 sorption experiments (section 3.3.2) it was also possible to conclude that the higher CO_2 permeability of the MMIM containing azo-POP-1 was favoured by the higher sorption capacity of this material. Therefore, the narrower pores of azo-POP-1 combined with its higher surface area and CO_2 sorption capacity led to the highest CO_2 permeability. Looking at the CO_2 sorption isotherms obtained for the studied azo-POPs, it is possible to conclude that the CO_2 permeabilities of the respective MMIMs did not follow the same trend. This indicates that the gas transport across the MMIM was primarily governed by the porosity parameters of the organic fillers, rather than their intrinsic CO_2 adsorption capacity.

Regarding the ideal selectivities obtained for the prepared MMIMs, it can be seen that the CO_2/CH_4 and CO_2/H_2 separations showed similar results which were considerably lower than the ones obtained for the CO_2/N_2 separation. It is known that CH_4 is a more soluble gas, compared to N_2 and that H_2 has the smallest gas molecules (2.9 Å), among all studied gases. A higher solubility of CH_4 and diffusivity of H_2 gas molecules, compared to N_2, promoted their permeability, which led to lower selectivities. Nonetheless, for all gas pairs considered, the selectivities of the azo-POP-containing MMIMs were higher than those obtained for the neat PEGDA-80 TFSI iongel. The MMIM containing azo-POP-12 showed the highest CO_2/N_2 selectivity, originating from its low BET surface area, which led to a low N_2 uptake. Even though azo-POP particles induced a higher porosity in the iongels structure, facilitating the diffusion of the gas molecules, their high affinity towards CO_2 overcame this effect, increasing the separation efficiency. The higher CO_2/N_2 selectivities in the MMIMs were a direct

consequence of the presence of the azo groups in the POPs structures. The differences in the affinity of azo functional groups towards N_2 and CO_2 were the key factor for the improved selectivity. Patel and co-workers [238] showed, through Monte Carlo simulations, that the binding affinity of the azo groups towards N_2 (9.0 kJ mol^{-1}) is considerably lower than for CO_2 (17.0 kJ mol^{-1}). These findings unveil the possibility of designing highly selective azo-POPs to be used as fillers in membranes for gas separations.

Table 3.3 - CO_2 permeability and CO_2/N_2, CO_2/CH_4 and CO_2/H_2 ideal selectivities of the MMIM layers containing different azo-POPs.

Iongel layer	P_i CO_2 (Barrer)	α_i (CO_2/N_2)	α_i (CO_2/CH_4)	α_i (CO_2/H_2)
PEGDA-80 TFSI	62 ± 2	167 ± 1	10 ± 0	6 ± 1
PEGDA-80 TFSI-0.5 POP-1	91 ± 3	28 ± 1	11 ± 0	12 ± 1
PEGDA-80 TFSI-0.5 POP-10	79 ± 2	19 ± 1	12 ± 1	11 ± 1
PEGDA-80 TFSI-0.5 POP-11	80 ± 3	41 ± 2	12 ± 0	11 ± 0
PEGDA-80 TFSI-0.5 POP-12	68 ± 2	53 ± 3	10 ± 0	12 ± 1

In order to better understand the overall separation performance of the prepared MMIMs containing azo-POPs, the experimental data obtained from this work was plotted against the well-known upper bound limits for CO_2/N_2 (Figure 3.9 a)), CO_2/CH_4 (Figure 3.9 b)) and CO_2/H_2 (Figure 3.9 c)) separations, at 303 K, where the ideal selectivity for each separation was represented as a function of the CO_2 permeability.[191] It is worth mentioning that the first upper bound limits developed based on experimental data for the H_2/CO_2 separation, at low temperatures, considered that the permeability of H_2 was much higher than that of CO_2.[55] However, it is known that depending on the materials and their interactions with the gas molecules, it is also possible to achieve a higher permeability for CO_2 compared to H_2, as we show in this work, which led to the development of a new upper bound limit for CO_2/H_2.[191] The available data reported for other three-component membranes, containing high IL content (> 60 wt%) and other third component solid materials, such as silica nanoparticles,[119,149,193] zeolites,[75] and MOFs,[147] at higher concentrations (between 8 and 15 wt%), is also plotted against the upper bound limits, in order to provide a general idea of the performance of the novel MMIMs containing azo-POPs proposed herein.

Looking at Figure 3.9 a), the experimental results of this work came closer to the CO_2/N_2 upper bound limit, after the incorporation of the different azo-POPs, with the MMIMs based on azo-POP-11 and azo-POP-12 showing the best results. It was also possible to conclude that overall, the CO_2 permeabilities obtained with third component solid materials, such as silica nanoparticles,[119,149,193] zeolites [75] and MOFs [147] were higher, compared to those obtained in this work with azo-POPs. However, the CO_2/N_2 ideal selectivities obtained in this work were generally higher, bringing the experimental

results closer to the CO_2/N_2 upper bound limit than those reported in the literature. In contrast, for the CO_2/CH_4 separation, depicted in Figure 3.9 b), the relation between permeability and selectivity found in the MMIMs containing azo-POPs was not as promising as it was for the other membranes with higher filler concentrations, mainly due to lower ideal selectivity. Interestingly, the exact opposite behaviour was observed for CO_2/H_2 separation (Figure 3.9 c)), where even the unfilled iongel composed of only PEGDA and IL exhibited a remarkable performance, and all experimental points were able to overcome the respective upper bound limit.

It is also worth noting that the azo-POP concentration used in the MMIMs (0.5 wt%) is considerably low when compared to the literature data available for iongels containing silica, [119,149,193] zeolites [75] and MOFs [147] (between 8 and 15 wt%). Therefore, we can expect that an increase in the azo-POP loading will probably improve the iongels' permeabilities.[114,115,247]

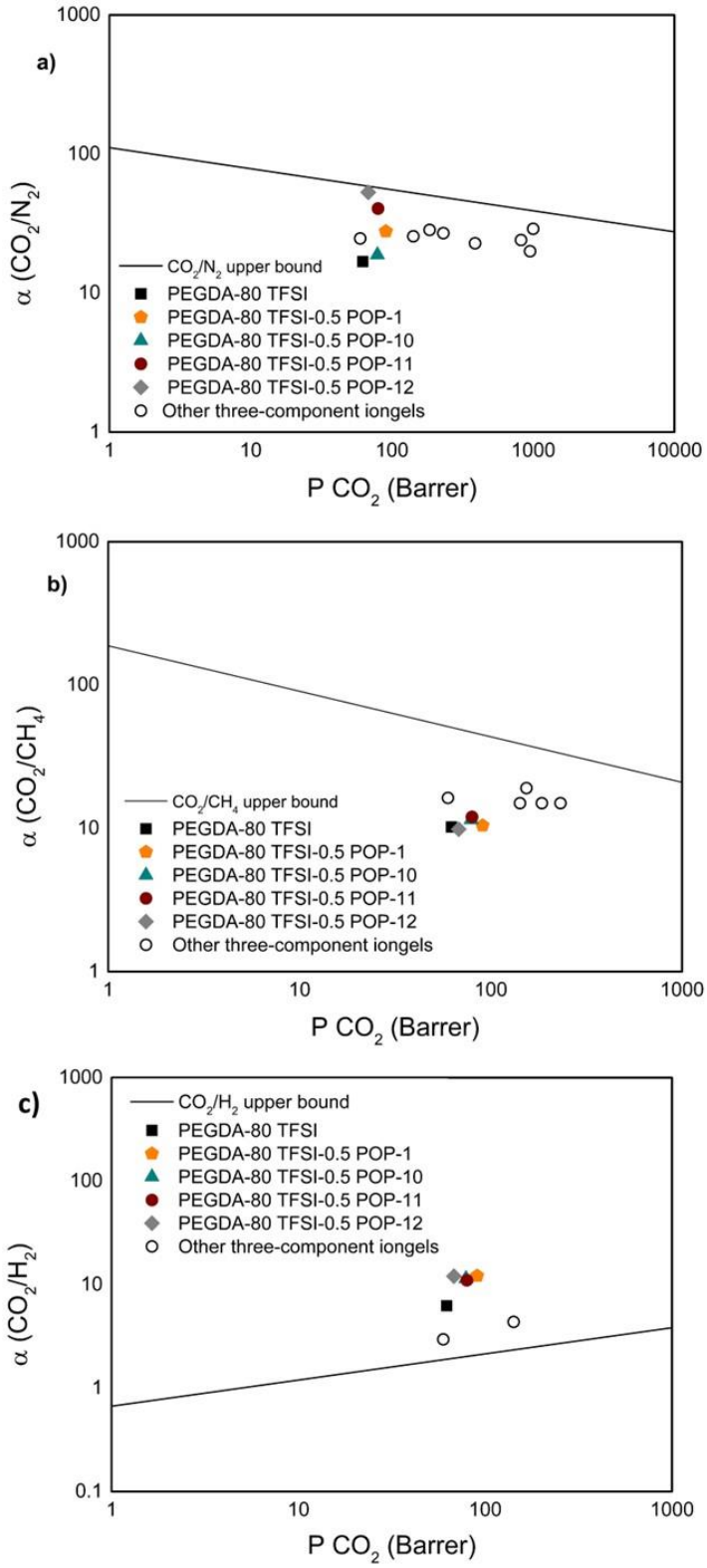

Figure 3.9 - (a) CO_2/N_2, (b) CO_2/CH_4, (c) CO_2/H_2 ideal selectivities of the prepared neat PEGDA-80 TFSI iongel and MMIMs containing different azo-POPs as a function of CO_2 permeabilities. Literature data are also illustrated for comparison purposes.

3.4 Conclusions

Mixed matrix iongel membranes, which are entirely composed of organic materials (PEGDA, 80 wt% [C_2mim][TFSI] IL and four different azo-POPs) were successfully prepared, for the first time, by a fast and simple solvent-free UV polymerization process. The SEM analysis demonstrated that dense and defect-free MMIMs with a good dispersion of azo-POP particles were obtained. All the iongel membranes presented high thermal stabilities (>603 K). Furthermore, the pure gas permeation experiments showed that with only 0.5 wt% of azo-POP, it was possibly to improve both CO_2 permeability (from 6 to 91 Barrer) and CO_2/N_2, CO_2/CH_4 and CO_2/H_2 ideal selectivities, mainly due to the "CO_2-philic" nature of azo-POPs. In fact, it was found that the azo-POP structure had a significant influence on the CO_2/N_2 ideal selectivity, since the "N_2-phobicity" of these materials is strictly dependent on porosity parameters. Remarkably, all the prepared iongels were able to surpass the CO_2/H_2 upper bound limit.

Overall, the results of this work clearly indicate that the incorporation of different azo-POPs in iongels with high IL content is a promising strategy that should be taken into consideration regarding the design of membrane materials with improved CO_2 separation properties. Moreover, besides the separation performance, it is also worth highlighting the straightforward and solvent-free method used in the preparation of these MMIMs, as well as the novelty in the combination of the different organic materials.

Future work will be focused on evaluating the gas separation performance of these MMIMs at experimental conditions that mimic those of industrial gas streams, in terms of composition, temperature, pressure and water vapour content.

4

MIXED MATRIX IONGEL MEMBRANES CONTAINING AZO-POROUS ORGANIC POLYMERS: INFLUENCE OF TEMPERATURE, PRESSURE AND WATER VAPOUR ON CO_2 SEPARATION

This chapter is part of the following publication: A. R. Nabais, P. Ortiz-Albo, J-X. Zhou, M-H. Huang, D. Mecerreyes, J. G. Crespo, L. C. Tomé and L. A. Neves, "Mixed matrix membranes containing azo-porous organic polymers: Influence of temperature, pressure and water vapour on CO_2 separation" (submitted to Journal of Membrane Science)

Summary

The effect of temperature, pressure, and humidity content in the gas separation performance of iongel membranes are crucial parameters that should be assessed to determine the real potential of these materials to be used in CO_2 separation processes. In this work, we present a detailed study on the impact of temperature (303, 323 and 353 K), pressure (2 and 4 bar), gas composition and water vapour content (between 11 and 21% of relative humidity) on the performance of iongels containing azo-porous organic polymers (azo-POPs), for CO_2/N_2 and CO_2/CH_4 binary gas separations. The iongels combining 80 wt% of the ionic liquid (IL) [C_2mim][TFSI], 20 wt% of poly(ethylene glycol) diacrylate (PEGDA) and 0.5 wt% of different azo-POPs were prepared by a solvent-free UV curing method. At the lower temperature, the pressure increase seems to have a negative impact on the CO_2 permeability of the prepared mixed matrix iongel membranes (MMIMs). However, the opposite behaviour was found when the temperature increases. Moreover, the presence of humidity in the feed gas stream affects the gas separation performance of the studied iongels, since the CO_2 permeability greatly increases with increasing humidity in the gas mixture, while the selectivity decreases, for both gas separations under

study. In general, the high pressure and temperature, and the presence of humidity have a significant influence on the separation performance of the studied iongel membranes, due to induced alterations in their structure and overall stability.

4.1 Introduction

Throughout the years, membrane processes have established themselves as one of the most promising strategies to purify gas streams. Compared to other processes, such as absorption using aqueous amine solutions, pressure swing adsorption and cryogenic distillation, the use of membranes can offer several advantages, namely in terms of energy-saving, continuous operation mode, low maintenance required and the inherent simplicity of the process.[248,249] However, despite the attractiveness of this process, the use of membranes still faces some challenges, namely in terms of the materials used. The challenging experimental conditions of some of the most common industrial gas separations, either in terms of temperature, pressure, or separation performance requirements, may represent a setback in the development of membrane processes at large scale. Therefore, the performance of membranes in harsh industrial conditions (e. g. high pressure and high temperature) should be properly assessed before the process can be scaled up.

The pressure increase, for example, in natural gas and syngas streams, might have a significant effect on the membranes' separation performance, especially if highly condensable gases such as CO_2 and heavy hydrocarbons are present in the gas mixture. Highly sorbing gases can induce swelling of the polymer chains, also known as plasticization, leading to a significant increase of the fractional free volume and gas diffusion rate. As a consequence of the higher gas diffusivity, the gas permeability increases while selectivity usually decreases.[250] On the other hand, depending on the membrane's material, elevated temperatures can also have a significant impact on the membranes' separation performance, usually by increasing the permeability at the expense of the gas selectivity.[251] Besides the effect of pressure and temperature, the presence of water vapour in some gas streams can also influence the separation performance of membranes. The presence of water molecules in the gas stream can lead to the formation of water clusters that fill the membranes' free volume or promotes a competitive sorption effect with other gas molecules, decreasing their permeability. The opposite effect can also be observed if the water vapour molecules are able to change the membrane's structure by inducing a plasticization effect.[252]

The selection of the most suitable materials to fabricate membranes for gas separation is the key factor behind a successful separation performance, under harsh conditions. In the last few years, a variety of new materials have been proposed as alternatives to prepare membranes with superior gas separation performance. Among them, ionic liquid (IL)-based membranes have been looked at as one of the most versatile classes of materials that can be used to achieve high gas separation performances.[2] These materials take advantage of, not only their high affinity for specific gases, such as CO_2, but a high thermal and chemical stability.[9,127] In particular, iongel membranes, containing a high

amount of IL and a polymer network to provide the necessary mechanical support, can take benefit from these intrinsic IL properties, to achieve high gas permeabilities and selectivities.[116,136] To improve the separation performance of these iongels, a third component, such as metal organic frameworks (MOFs), zeolites and silica particles, can also be added to prepare MMIMs.[66] Over the past years, the development of MMIMs has shown promising results towards the separation of CO_2. Noble's group carried out pioneer work regarding mixed matrix membranes with zeolite particles, such as SAPO-34, poly(ionic liquid)-based membranes and moderate contents of [C_2mim][TFSI] IL, for CO_2/N_2 and CO_2/CH_4 separations.[111,113,174,192] Even though the membranes prepared by the authors do not fall under the definition of iongel considered in this work, the results showed that there was a clear advantage when combining a solid filler with an IL, unveiling the potential of using MMIMs for gas separation. Later on, Matsuyama's group developed silica containing iongel membranes, with not only good separation performances but also remarkable mechanical properties, able to withstand up to 28 MPa of compressive stress.[119,149,150] Moreover, we studied the influence of different MOFs (MOF-5, Cu(BTC), MIL-53 and ZIF-8) loadings and ILs ([C_2mim][BETI] and [C_4mpyr][Tf_2N]) incorporated in poly([pyr_{11}][TFSI]-based membranes for CO_2 separation. It was clear that the CO_2 permeability was significantly improved, however at the expense of the ideal selectivity.[114,115] Following a similar approach, a nanoclay (Nanomer®1.34TCN, montmorillonite – MMT) was used to reinforce poly(ethylene glycol) diacrylate (PEGDA) iongel membranes in a self-standing form. The additional mechanical resistance provided by the inorganic particles, at 7.5 wt% loading, allowed for the preparation of free-standing iongels with 80 wt% [C_2mim][TFSI] IL and an increase in permeability and in CO_2/N_2 and CO_2/CH_4 ideal selectivities, due to the higher IL content.[253]

More recently, azo-porous organic polymers (azo-POPs) have also attracted much attention regarding their use in CO_2 separation applications.[228,230] The use of totally organic fillers such as azo-POPs combined with ILs, can help to overcome the compatibility issues between the filler particles and the polymer materials, which is known for being one of the main challenges regarding the fabrication of mixed matrix membranes. We recently reported an efficient synthetic pathway to prepare four different azo-POPs (azo-POP-1, azo-POP-10, azo-POP-11 and azo-POP-12) to be used as fillers and improve the CO_2 separation performance of PEGDA iongel membranes bearing [C_2mim][TFSI] IL.[254] The results obtained in pure gas permeation experiments showed a considerable improvement on the iongels' permeability and selectivity upon the incorporation of azo-POP-1 and azo-POP-11.[254] However, the performance of MMIMs under conditions similar to those of the most relevant industrial gas streams (Table 4.1) is yet to be fully assessed.[66] In this work, we started by evaluating the influence of different water activities in the pure gas permeation of the iongel membranes containing the different azo-POPs. Additionally, we evaluated the CO_2/N_2 and CO_2/CH_4 separation performance of the previously proposed MMIMs iongels containing azo-POP-1 and azo-POP-11 under different experimental conditions. To make a more realistic evaluation, the effect of temperature, pressure, gas composition and presence of water vapour on the iongels' performance was assessed.

Table 4.1 - Typical conditions of the CO_2/N_2 and CO_2/CH_4 industrial gas streams

	Separation	Temperature (K)	Pressure (bar)	References
Flue gas	CO_2/N_2	308-393	1	[255–258]
Natural Gas	CO_2/CH_4	298-308	30-50	[258–260]
Biogas	CO_2/CH_4	298-308	1	[258,261]

4.2 Experimental Section

4.2.1 Materials

Poly(ethylene glycol) diacrylate (PEGDA, M_n 575 g mol^{-1}) and 2-hydroxy-2-methylpropiophenone (DAROCUR®, 97 wt% pure) were purchased from Sigma-Aldrich (Portugal). 1-ethyl-3-methylimidazolium bis(triuoromethylsulfonyl) imide ([C_2mim][TFSI], 99 wt% pure) was supplied by Iolitec GmbH (Germany). Carbon dioxide, CO_2 (99.998% purity), nitrogen, N_2 (99.99% purity), methane, CH_4 (99.99% purity) and helium, He (>99% purity) gases were supplied by Praxair (Portugal). Azo-POP-1, azo-POP-10, azo-POP-11 and azo-POP-12 were synthesized according to a previously described procedure.[254]

4.2.2 Preparation of Mixed Matrix Iongel Membranes

The MMIMs containing azo-POP-1 (PEGDA-80 TFSI-0.5 POP-1), azo-POP-10 (PEGDA-80 TFSI-0.5 POP-10), azo-POP-11 (PEGDA-80 TFSI-0.5 POP-11) and azo-POP-12 (PEGDA-80 TFSI-0.5 POP-12) were tested in this work.[254] The iongels were prepared by mixing 0.5 wt% (above the total iongel mass) of the selected azo-POP with 80 wt% of [C_2mim][TFSI] IL and left stirring overnight. Afterwards, 20 wt% of PEGDA was added and the solution was left stirring for 1 hour before adding 3 wt% (relative to PEGDA mass) of DAROCUR® as photoinitiator. The final solution was then placed on top of a pre-wetted hydrophilic polyamide (PA) support (Sartorius™, supplied by Fisher Scientific), with a pore size of 0.22 µm and then between two Rain-X® coated quartz plate, with a 100 µm spacer in between. The solutions were exposed to a UV light using a UVP Cross-linker CL-3000 (Analytik Jena, Germany), with a wavelength of 365 nm and an intensity of 1.9 mW cm^{-2} for 10 minutes. Before testing, the resulting membranes were then dried at 333 K to remove the water trapped inside the polymer support. Therefore, it was considered that the permeability results obtained in this work, from the pure and mixed gas permeation experiments, correspond to the iongel layer without the resistance of the porous support (as it was confirmed when trying to perform permeation experiments on the support alone and no resistance to gas transport was observed). This means that, in the present work, it was not necessary to use the Resistance in Series Model (RSM) as previously reported. [254] A schematic representation of the fabrication of the MMIMs can be found in Figure 4.1.

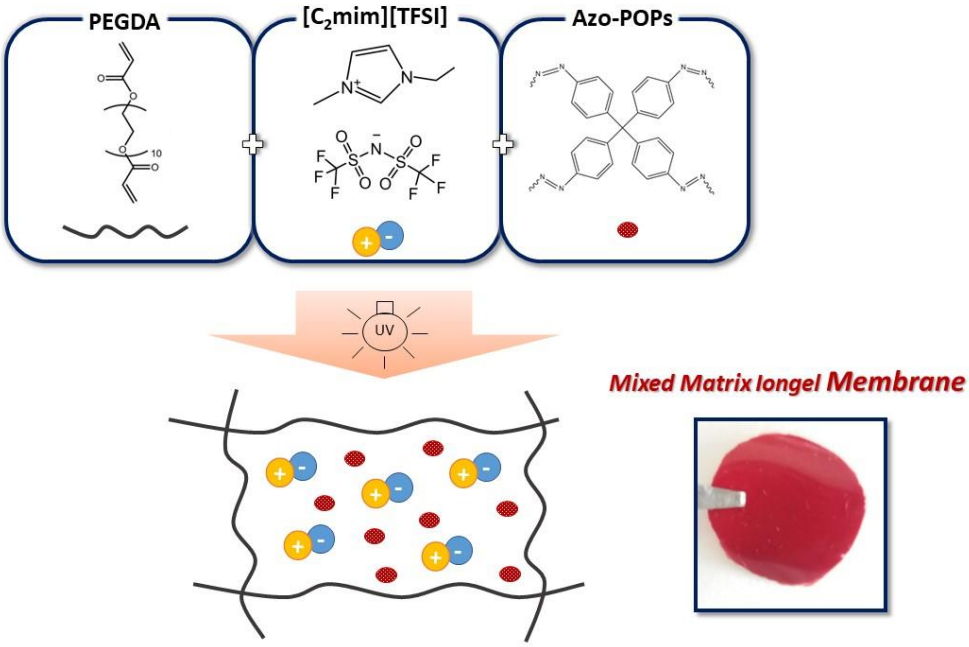

Figure 4.1 - Schematic representation of the preparation of the MMIMs studied in this work.

4.2.3 Effect of Water Activity

The prepared iongels were conditioned at different water activities (a_w). Saturated salt solutions were used to equilibrate the iongel membranes at a defined water activity through the vapour phase, as listed in Table 4.2. Specific amounts of different inorganic salts were mixed with distilled water and the iongels were placed in four different desiccators, each with a well-defined water activity at 303 K. A thermohygrometer equipped with a HM42 probe (Vaisala, Finland) was used to confirm the RH inside each desiccator. The weight and thickness of each sample were measured every 5 days until these parameters remained constant, after approximately 3 weeks, meaning that the iongels were equilibrated at the desired RH before being tested for pure and mixed gas experiments.

Table 4.2 - Saturated salt water activities, at 303 K .[262]

Salt	Water activity (a_w)
Lithium chloride, LiCl	0.113
Potassium acetate, CH_3CO_2K	0.216
Sodium bromide, NaBr	0.560
Sodium chloride, NaCl	0.751

4.2.4 Gas Permeation

4.2.4.1 Pure Gases

Pure gas permeation experiments were carried out for pure CO_2, N_2 and CH_4, to evaluate the influence of the presence of water inside the iongels structure on their separation performance, according to a previously described procedure.[16] The iongel membranes were placed inside a stainless-steel cell composed of two compartments, designated as feed and permeate. The cell was placed inside a water bath, where the temperature was maintained at 303 K. All permeation experiments were performed at a transmembrane pressure of 0.7 bar and three replicates of each membrane were tested.

The permeability of the pure gas through the iongel membrane equilibrated at the desired RH was calculated from the acquired pressure data over time, on both compartments, according to the following equations:

$$\frac{1}{\beta}\ln\left(\frac{[p_{feed}-p_{perm}]_0}{[p_{feed}-p_{perm}]}\right)=\frac{1}{\beta}\ln\left(\frac{\Delta p_0}{\Delta p}\right)=P\ \frac{t}{l} \quad (4.1)$$

Where Δp_0 and Δp (bar) represent the pressure variations between the feed and permeate compartments of the cell at the beginning of the experiment and over time, respectively, P (m^2s^{-1}) is the permeability of the iongel membrane (where 1 Barrer = 1x10-10 cm^3 cm cm^{-2} s^{-1} $cmHg^{-1}$ = 8.3x10^{-13} m^2 s^{-1}),[235] t is the time (s) and l is the iongel layer thickness (m). β (m^{-1}) is a geometric parameter, characteristic of the geometry of the cell, given by:

$$\beta = A\left(\frac{1}{V_{feed}}+\frac{1}{V_{perm}}\right) \quad (4.2)$$

Where A is the iongel membrane area (m^2) and V_{feed} and V_{perm} are the volumes (m^3) of the feed and permeate compartments, respectively. The permeability of the iongel membrane was obtained from the slope represented by plotting $\frac{1}{\beta}\ln\left(\frac{p_0}{p}\right)$ versus $\frac{t}{l}$.

The ideal gas selectivity was calculated by dividing the permeabilities of the two different gases (A and B), according to the following equation:

$$\alpha_{A/B}=\frac{P_A}{P_B} \quad (4.3)$$

4.2.4.2 Binary Gas Permeation Experiments

Binary gas mixtures experiments for CO_2/N_2 and CO_2/CH_4 mixtures were performed using an experimental set-up, schematically represented in Figure 4.2, to determine the permeability and real selectivity of the prepared iongel membranes, under mixed gas conditions. The setup is composed by a stainless-steel cell, divided in two compartments (feed and permeate) separated by the membrane to be tested, placed inside an oven (Venticell MMM, Germany) with a controlled temperature (TC). The flow rate of each gas (CO_2 and N_2 or CH_4) was controlled by two mass flow controllers, MFC1 and MFC2 (Alicat Scientific, USA) connected to the gas bottles, which were then mixed, inside the oven, before entering the feed compartment of the membrane module. The experimental pressure was controlled by a back pressure regulator (BPR). Helium (He) was used as sweep gas on the permeate compartment (MFC3) during the experiment, in counter current, with a flow rate of 5 mL min^{-1} and pressure around 1 bar. Retentate and permeate compositions were analysed using an Agilent gas chromatograph (GC) 7890B (in which He was used as the gas carrier), equipped with a thermal conductivity detector (TCD) and maintained at 473 K. For the analysis, an isothermal method was used, with a PoraPlot U column connected to a Molsieve 5A column, purchased from Soquimica Lda. (Lisbon, Portugal). Each experiment was carried out until a constant permeate flow and composition were achieved.

The experiments were carried out at different temperatures, pressures, and gas compositions, as listed in Table 4.3, to achieve experimental conditions similar to those of flue gas (CO_2/N_2) and biogas upgrading (CO_2/CH_4) streams. Three replicates of each membrane were tested.
The permeability of each gas was calculated according to:

$$j_i = \frac{F^f_{total} \cdot y^f_i}{A} \tag{4.4}$$

$$\Delta p_i = p^f \cdot y^f_i - p^p \cdot y^p_i \tag{4.5}$$

$$P_i = \frac{j_i \cdot l}{\Delta p_i} \tag{4.6}$$

Where j_i is the molar flux of gas i (mol m^{-2} s^{-1}), F is the gas molar flow rate (mol s^{-1}), y^f and y^p are the gas molar fractions on the feed and permeate side, respectively, A is the iongel membrane area (m^2), Δp represents the driving force between feed and permeate sides (Pa), p^f and p^p are the pressures (Pa) in the feed and permeate sides, respectively, l is the thickness of the iongel layer (m) and P is the iongel membrane permeability towards gas i (mol m^{-1} Pa^{-1} s^{-1}).

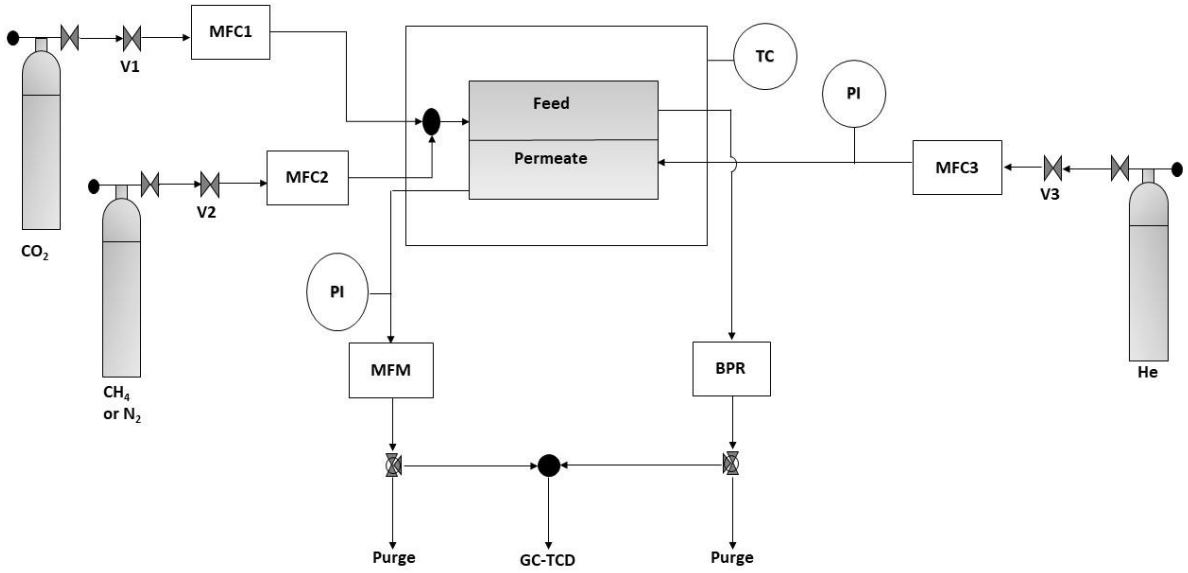

Figure 4.2 - Schematic representation of the experimental setup used for the mixed gas permeation experiments (dry conditions): BPR – back pressure regulator; MFC1-MFC3 – mass flow controllers; MFM – mass flow meter; PI – pressure indicator; TC – temperature controller; V1-V3 – valves.

Table 4.3 - Experimental conditions for the binary gas mixture permeation experiments.

Gas stream	Temperature (K)	Pressure (bar)	Gas composition
CO_2/N_2	303, 323 and 353	2 and 4	5-30 vol% CO_2
CO_2/CH_4	303	2 and 4	10-40 vol% CO_2

4.2.4.3 Humidified mixed gas permeation experiments

The experimental setup schematically represented in Figure 4.3 was used to evaluate the effect of relative humidity (RH) present in the stream on the gas separation of the iongels membranes, under mixed gas conditions. To obtain a humidified feed gas stream, a fraction of N_2 or CH_4 (MFC3) was passed through a water container, using a bypass (V5 and V6), to obtain the desired RH content (RH = 11 and 21 vol%) before being mixed with the other components of the gas mixture. The RH present in the gas stream was confirmed using a Vaisala thermohygrometer, equipped with a HM42 probe, placed on the retentate stream, outside of the oven. The membranes to be tested were properly conditioned at the desired water activity, as described in Section 2.3, for a_w=0.11 and a_w=0.21, prior to the experiments. All experiments were carried out following the procedure described in Section 4.2.4.2.

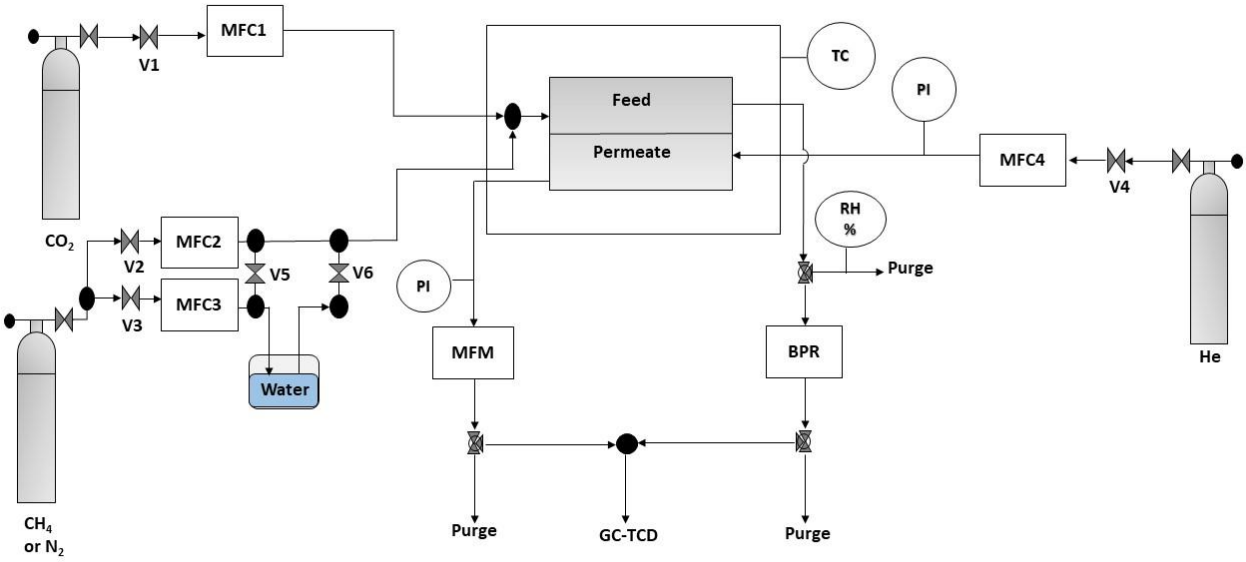

Figure 4.3 - Schematic representation of the experimental setup used for the mixed gas permeation experiments (humidified conditions): BPR – back pressure regulator; MFC1-MFC4 – mass flow controllers; MFM – mass flow meter; PI – pressure indicator; RH% - relative humidity indicator; TC – temperature controller; V1-V6 – valves.

4.3 Results and Discussion

In this work, gas permeation experiments were performed using two different systems, to evaluate different parameters. First, the effect of water activity in the MMIMs structure was evaluated by single gas permeation experiments, with dry gases (section 4.3.1). The objective was to understand how a specific water activity/water content inside the membrane can affect its structure and, consequently, its gas transport properties without the influence of other parameters (humidity of the gas stream, type of gas mixture, etc.). Due to the short duration of these experiments, it was assumed that the water activity inside the membrane did not change significantly during each test.

In the second part of this work (section 4.3.2), gas mixtures permeation experiments were performed, considering three variables: temperature, pressure, and RH in the gas stream. In this case, besides the water activity inside the MMIMs (that were also pre-equilibrated), the influence of a specific water content in the gas stream, as well as temperature and pressure were evaluated.

4.3.1 Effect of Water Activity on Pure Gas Permeation

4.3.1.1 Gas Permeability

Figure 4.4 displays the pure CO_2 permeability of the neat PEGDA-80 TFSI and respective MMIMs containing azo-POPs, equilibrated at different water activities. In this way, this section discusses the impact of the presence of water content inside the structure of the membranes. The CO_2 permeability greatly increased from a_w=0 to a_w=0.21, further decreasing at higher a_w. Similar to what was observed in our previous work (a_w=0)[254], the MMIM containing azo-POP-1 presented the highest CO_2 permeability, regardless of the a_w value, while the neat PEGDA-80 TFSI iongel showed the lowest. This means that the azo-POPs incorporated in the iongels were able to maintain their performance even at different water activities inside the iongel structure, still acting as enhancers of the gas permeability. The neat PEGDA-80 TFSI iongel presented a CO_2 permeability of around 62 Barrer for a_w=0, which increased to 320 Barrer at a_w=0.21 and then decreased down to 207 Barrer at higher values of a_w. The CO_2 permeability of the PEGDA-80 TFSI-0.5 POP-1 increased from 91 Barrer for a_w=0 up to 479 Barrer at a_w=0.21, further decreasing down to 375 Barrer at a_w=0.76. In fact, the CO_2 diffusion increased with increasing a_w, which could be primarily associated with the absorption of water molecules in the polymer matrix. At low a_w, the water molecules are more likely to interact with the polymer rather than with other water molecules, behaving as a plasticizing agent, increasing the free volume in the membrane and, consequently, the gas diffusion. On the other hand, higher a_w (between 0.57 and 0.76), were found to counter this effect, by significantly decreasing the CO_2 permeability.[263] This phenomenon can be attributed to a reduction in diffusivity when the water molecules started to aggregate, creating water clusters that occupy the free volume of the polymer. This hinders the transport of gas species since the water clusters provide a significant obstruction to gas diffusion.[264] As the a_w increased, more water molecules were absorbed leading to the formation of aggregates, as long as the membrane was able to swell and accommodate such water clusters.[263] Also, the CO_2 solubility is much higher in the IL [C_2mim][TFSI] (S CO_2=2.40 cm^3 (STP) cm^{-3} atm^{-1} at 298 K) than in water (S CO_2=0.76 cm^3 (STP) cm^{-3} atm^{-1} at 298 K), which also contributed to the observed decrease in the iongels permeability at higher a_w.[265] Overall, the highest increase in CO_2 permeability was achieved with the MMIMs containing azo-POP-1 and azo-POP-11, since these were also the most hydrophilic materials, as shown in our previous work, while the less hydrophilic iongel (PEGDA-80 TFSI) showed the lowest increase in permeability, when compared to the results obtained in the dry state (a_w=0).[254]

Overall, it can be concluded that the presence of water, at low concentrations, can benefit the CO_2 transport of the studied iongel membranes, particularly when azo-POPs are incorporated in the matrix.

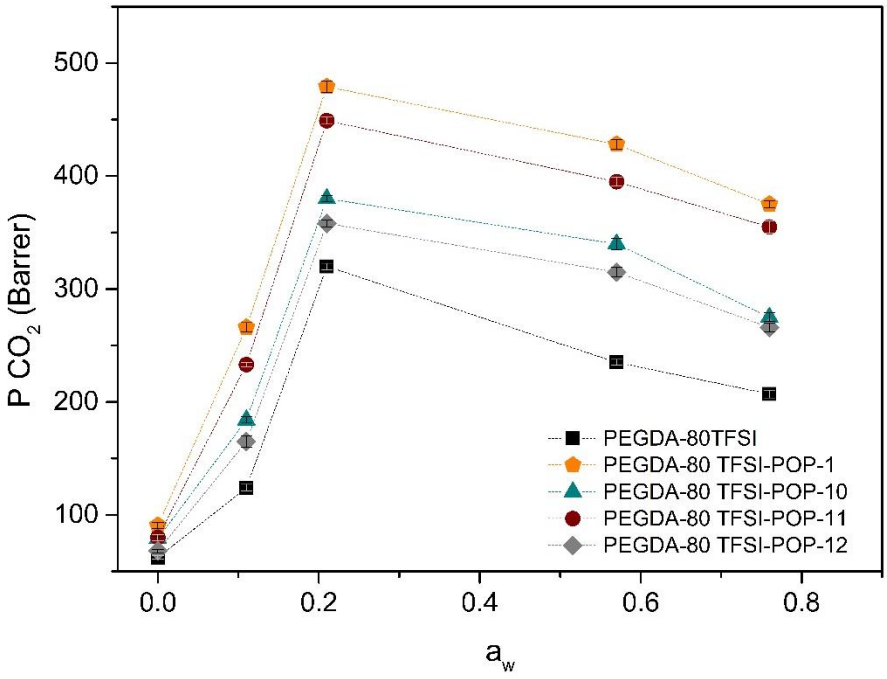

Figure 4.4 - CO_2 permeability obtained for the neat PEGDA-80 TFSI and MMIMs as a function of the water activity (a_w).

4.3.1.2 Ideal Selectivity

Figure 4.5 a) and b) displays, respectively, the CO_2/N_2 and CO_2/CH_4 ideal selectivities of the neat iongel and MMIMs containing azo-POPs, as a function of the water activity. Similar to what was observed for the CO_2 permeability, the ideal selectivities increased with an increase in the a_w (up to 0.21) for all the studied iongel membranes. The solubility of CO_2 in water (3.4×10^{-4} mol m^{-3} Pa^{-1}) is considerably higher than that of N_2 (6.4×10^{-6} mol m^{-3} Pa^{-1}) and CH_4 (1.45×10^{-5} mol m^{-3} Pa^{-1}).[265] These differences contributed to an increase in the CO_2 permeability, which was more significant than for the other less soluble gases (N_2 and CH_4) and thus, ideal selectivity increased. It should also be noted that the azo functional groups acted as selective binding sites for CO_2, hence the MMIMs containing azo-POPs presented higher ideal selectivities compared to the neat PEGDA-80 TFSI iongel membrane. On the other hand, as the a_w increased (from 0.21 to 0.76), there was a notorious decrease in the ideal selectivity for both gas separations. This can be attributed to the clustering effect caused by the presence of more water molecules in the structure that hindered the gas diffusivity. The presence of a higher water content also decreased the gas solubilities because the studied gas species are less soluble in water that in the IL. Considering that CO_2 has the highest solubility coefficient among all the studied gases, CO_2 will suffer a higher decrease in solubility, which coupled with the decrease in diffusivity, resulted in the observed loss of ideal selectivity.

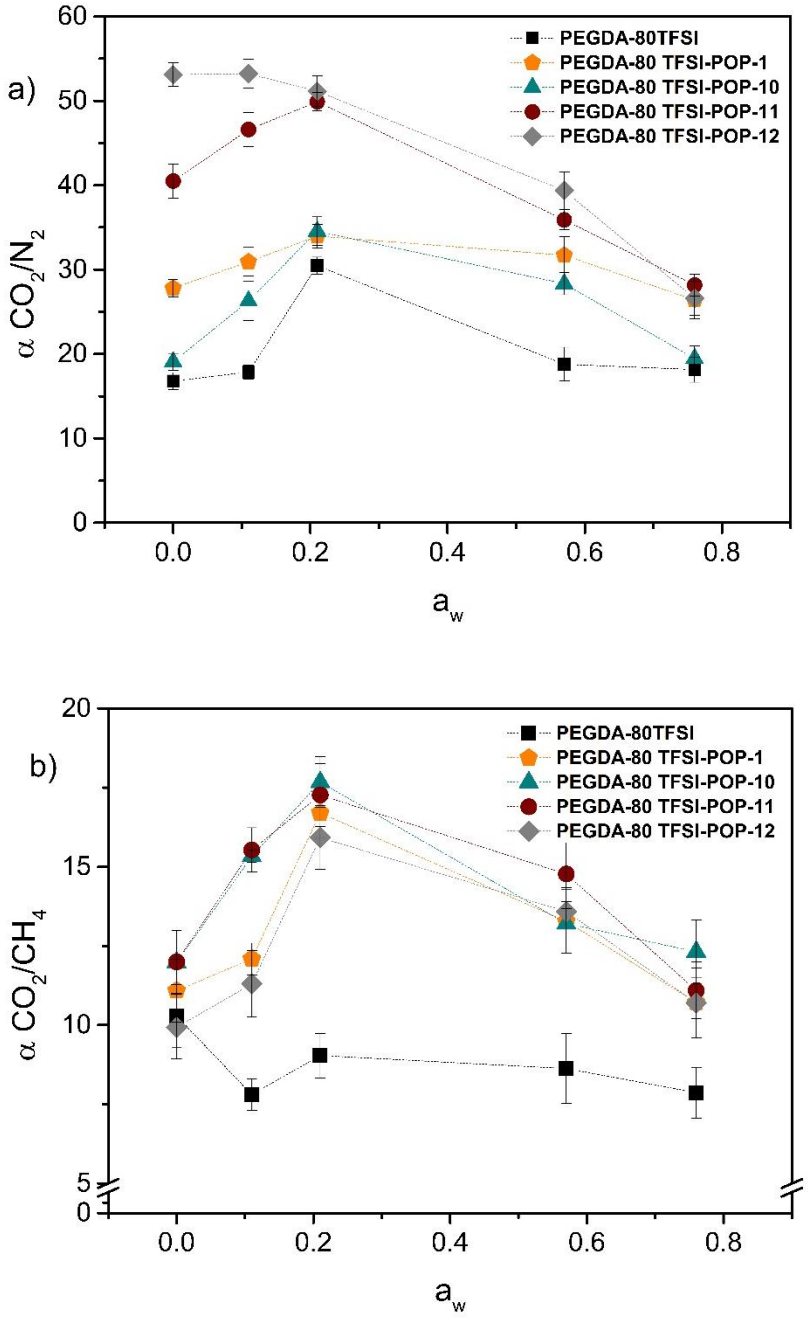

Figure 4.5 - (a) CO_2/N_2 and (b) CO_2/CH_4 ideal selectivities of the neat and MMIMs as a function of the water activity (a_w).

4.3.2 Binary Gas Mixture Permeation Experiments

Taking into account not only the results of the pure gas permeation experiments previously obtained,[254] but also the ones presented in section 4.3.1 regarding the effect of the water activity on the iongels pure gas permeation, the MMIMs containing azo-POP-1 and azo-POP-11 were selected and evaluated under mixed and humidified gas conditions, for CO_2/N_2 and CO_2/CH_4 separations. Regarding CO_2/N_2 separation, the influence of temperature (303, 323 and 353 K), pressure (2 and 4 bar), gas composition (5-30 vol% CO_2), and RH (11 and 21%) was studied. Additionally, the influence of pressure (2 and 4 bar), gas composition (10-40 vol% CO_2) and RH (11 and 21%) was assessed for the CO_2/CH_4 separation. The results obtained as a function of the vol% CO_2, temperature, pressure and RH for both separations are provided in Appendix C (Tables C.1-C.12).

The influence of gas composition on the CO_2/N_2 and CO_2/CH_4 separation performance of the neat PEGDA-80 TFSI iongel and MMIMs containing azo-POP-1 and azo-POP-11 can be perceived from the results presented in Table C.1-C.3 and Table C.4-C.6 of Appendix C. Overall, the CO_2 permeability in the CO_2/N_2 binary gas mixture was not significantly influenced by the variation in the feed gas composition between 5 and 15 vol% CO_2. However, at 30 vol%, the CO_2 permeability decreased for all studied iongel membranes. For the CO_2/CH_4 separation, the CO_2 permeability did not present a significant dependence on the feed gas composition.

4.3.2.1 Effect of Temperature

The results regarding the influence of temperature on the CO_2/N_2 separation of the studied iongel membranes, with a CO_2 feed composition of 15 vol%, can be found in Table 4.4. For all iongel membranes, regardless of the experimental pressure, the CO_2 permeability increased with increase in temperature. At 2 bar, the CO_2 permeability increased from 115 Barrer at 303 K to 127 Barrer, for the neat PEGDA-80 TFSI iongel, while the MMIM containing azo-POP-1 presented a CO_2 permeability ranging from 144 to 172 Barrer, under the same experimental conditions. These findings were in agreement to what was previously observed,[254] *i.e*. the MMIMs containing azo-POP-1 had the highest CO_2 permeability, while the neat PEGDA-80TFSI membrane presented the lowest. The same tendency was observed at 4 bar, where the CO_2 permeability consecutively increased with increasing temperature. Higher temperatures led to an increase in the average kinetic energy and, consequently, in the movement of the gas molecules, improving the rate of diffusion.[251,266] Similar results have also been reported in the literature. [266–268]

The permeation of gases through a dense membrane can be considered as an activated process, usually following an Arrhenius type temperature-dependent equation, as follows:[269]

$$P = P_0 \, . \, e^{-\frac{Ea}{RT}} \tag{4.7}$$

Where P is the permeability (cm^3(STP) cm cm^{-2} s^{-1} $cmHg^{-1}$), P_0 is the pre-exponential factor (cm^3(STP) cm cm^{-2} s^{-1} $cmHg^{-1}$), E_a is the activation energy (kJ mol^{-1}), R is the ideal gas constant (kJ mol^{-1} K^{-1}) and T is the temperature (K). To investigate the temperature dependence of the CO_2 permeability, the activation energy was calculated, by plotting *ln P* as a function of 1/*T* for every composition, and the mean values are provided in Table 4.5. It can be seen that the activation energies obtained for the MMIMs containing azo-POPs were higher than those of the neat PEGDA-80 TFSI iongel. This means that the MMIMs were more sensitive to temperature variations, which was probably attributed to the temperature-dependent intrinsic properties of the azo-functional groups of the POP structure. In fact, previous studies showed that the separation performance, particularly for CO_2/N_2, achieved with azo-POPs can be enhanced when the temperature increases.[238] The effect of temperature on the CO_2 permeability presents two contradictory effects: on one hand, it is known that the CO_2 solubility decreases with increasing temperature while, on the other hand, the diffusivity increases. This means that the CO_2 permeability was more solubility-controlled at low temperatures and diffusion-controlled at higher temperatures.[266,269]

Although the temperature did not have a significant impact on the CO_2/N_2 selectivity at 2 bar, the MMIMs containing azo-POPs maintained higher separation factors in comparison with the neat PEGDA-80 TFSI iongel, due to the affinity of the azo groups towards CO_2. Moreover, azo-POP-11 provided the highest selectivity, in agreement to what was observed in our previous work.[254] On the other hand, at 4 bar, the selectivity followed the order α (323 K) > α (303 K) > α (353 K). The lower selectivity at 303 K might be explained by a decrease in the CO_2 permeability, at higher pressure, which was not as pronounced for N_2, as it will be discussed in the next section.

Table 4.4 - Effect of temperature and pressure on the CO_2 permeability and CO_2/N_2 selectivity of the neat iongel and MMIMs containing azo-POPs, at 15 vol% CO_2.

	***P* CO_2 (Barrer) (α CO_2/N_2)**					
	2 bar			**4 bar**		
Membrane Sample	**303 K**	**323 K**	**353 K**	**303 K**	**323 K**	**353 K**
PEGDA-80 TFSI	115 ± 1	124 ± 2	127 ± 2	116 ± 2	147 ± 3	168 ± 2
	(14 ± 1)	(11 ± 1)	(12 ± 1)	(9 ± 1)	(16 ± 1)	(6 ± 1)
PEGDA-80 TFSI-0.5 POP-1	144 ± 2	158 ± 2	172 ± 2	140 ± 2	168 ± 2	174 ± 3
	(20 ± 1)	(19 ± 1)	(17 ± 1)	(15 ± 1)	(16 ± 1)	(10 ± 1)
PEGDA-80 TFSI-0.5 POP-11	134 ± 3	146 ± 2	163 ± 2	126 ± 2	154 ± 2	178 ± 2
	(24 ± 1)	(21 ± 1)	(21 ± 1)	(13 ± 1)	(18 ± 1)	(9 ± 1)

Table 4.5 - Activation energies (E_a) obtained for the neat iongel and MMIMs containing azo-POPs, at different pressures.

Membrane Sample	E_a (kJ mol^{-1}) at 2 bar	E_a (kJ mol^{-1}) at 4 bar
PEGDA-80 TFSI	1.56	3.70
PEGDA-80 TFSI-0.5 POP-1	2.97	5.76
PEGDA-80 TFSI-0.5 POP-11	3.22	5.76

4.3.2.2 Effect of Pressure

The results regarding the effect of increasing pressure on the separation performance of the neat PEGDA-80 TFSI iongel and respective MMIMs containing azo-POPs are presented in Table 4.4 and Table 4.6, for the CO_2/N_2 (xCO_2=15 vol%) and CO_2/CH_4 (xCO_2=40 vol%) binary gas mixtures, respectively.

At 303 K, the CO_2 permeabilities for both binary gas mixtures slightly decreased as the pressure increased from 2 to 4 bar. The observed decrease in CO_2 permeability at an increased pressure and low temperature (303 K), can be explained by an increase in the competitive sorption between the two gas species in the mixture. It is known that, in gas mixtures, the transport of one gas species across the membrane is directly affected by the presence of other gas components, which is more pronounced for CO_2 due to its lower content in the gas mixture. This is also the reason why the CO_2/N_2 selectivity decreased at higher pressure, regardless of the temperature. In what concerns the CO_2/CH_4 gas mixture, the increase in pressure from 2 to 4 bar did not have a significant impact in the gas selectivity.

Looking at the results obtained for the CO_2/N_2 gas mixture (Table 4.4), the CO_2 permeability obtained at 4 bar and 323 and 353 K increased, when compared to the values obtained at 303 K. The decrease in permeability observed at low temperature was counteracted by an increase in temperature and consequently increase in gas diffusion. In all cases, the CO_2 permeability as well as both CO_2/N_2 and CO_2/CH_4 selectivities were considerably higher for the MMIMs containing azo-POPs, especially for azo-POP-1, since this filler presented the highest porosity (porous volume of 0.57 cm^3 g^{-1}), surface area (1100 m^2 g^{-1}) and CO_2 sorption capacity (2.3 mmol g^{-1} at 273 K).[254]

Table 4.6 - Effect of pressure on the CO_2 permeability and CO_2/CH_4 selectivity of the neat iongel and MMIMs containing azo-POPs, at 303 K and 40 vol% CO_2.

	***P* CO_2 (Barrer) (*α* CO_2/CH_4)**	
Membrane Sample	**2 bar**	**4 bar**
PEGDA-80 TFSI	207 ± 4 (8 ± 1)	191 ± 2 (7 ± 1)
PEGDA-80 TFSI-0.5 POP-1	253 ± 4 (11 ± 1)	227 ± 3 (10 ± 1)
PEGDA-80 TFSI-0.5 POP-11	238 ± 2 (11 ± 1)	220 ± 2 (10 ± 1)

4.3.2.3 Effect of Relative Humidity

Figure 4.6 a) and b) and Figure 4.7 a) and b) display the effect of the presence of humidity on the CO_2/N_2 and CO_2/CH_4 separations, respectively, for the selected iongel membranes. It is worth mentioning that the tested iongel membranes were pre-equilibrated at the desired water activity, prior to the permeation experiments, as described in section 2.3. The permeability values obtained at RH of 11 and 21% were compared with the results obtained for the dry binary gas mixtures, at 15 vol% CO_2 for CO_2/N_2 and 40 vol% CO_2 for CO_2/CH_4. For both separations, the CO_2 permeability increased as the RH present in the gas mixture increased, for all tested iongel membranes. The increase in CO_2 permeability with increasing humidity was more significant for the PEGDA-80TFSI-0.5 POP-1 membrane, while the neat iongel displayed the lowest increase. Regarding the CO_2/N_2 separation, the CO_2 permeability obtained for the neat PEGDA-80TFSI iongel at 21% of RH was, on average, 1.5 times higher than that obtained under dry conditions. On the other hand, at 21% of RH, the CO_2 permeability increased around 2.7 times for the MMIM containing azo-POP-1 and around 2.3 times for the one containing azo-POP-11, when compared to the dry mixed gas conditions. This behaviour can be explained by the higher hydrophilicity of the PEGDA-80TFSI-0.5 POP-1 iongel material,[254] which resulted in a higher swelling of the membrane, meaning that more water-induced plasticization occurred. Consequently, the gas molecules present in the mixture could diffuse faster and more indiscriminately across the iongel membrane. The neat PEGDA-80 TFSI iongel presented a less hydrophilic character, and even though the CO_2 permeability also increased, it was not as significant as it was for the MMIMs containing azo-POPs. On the other hand, the increase in CO_2 permeability was not so accentuated for the CO_2/CH_4 separation, but maintained the same behaviour, with the PEGDA-80TFSI-0.5 POP-1 membrane reaching the highest CO_2 permeability values.

As it can be seen from Figure 4.6 b) and Figure 4.7 b), the CO_2/N_2 and CO_2/CH_4 selectivities, respectively, obtained under humified conditions were visibly lower than those achieved with the dry binary gas mixtures. As a result of the hydrophilic character of the studied membranes and consequent swelling of the materials in the presence of humidity, the diffusion rate of the gas molecules present in

the mixture was enhanced. Moreover, CO_2 is the smallest gas molecule tested in the gas mixture, which means that it should be least affected by the changes in the membrane free volume, contrary to what happens with N_2 and CH_4, leading to a decrease of selectivity.[252] For both separations, the PEGDA-80TFSI-0.5 POP-1 membrane, which was the most hydrophilic membrane and contained the azo-POP with the highest porosity, showed the most marked decrease in selectivity, when compared to that of the remaining iongels. For the CO_2/N_2 separation, the selectivity of the PEGDA-80 TFSI-0.5 POP-1 membrane decreased from around 19, under dry conditions, down to 6 when the RH increased, while for CO_2/CH_4 it decreased from 12 to 3, on average. On the other hand, the neat iongel membrane was the least affected by variations on the RH percentage since its selectivity decreased from 13 to 5 for the CO_2/N_2 separation and from around 10 to 6 for CO_2/CH_4.

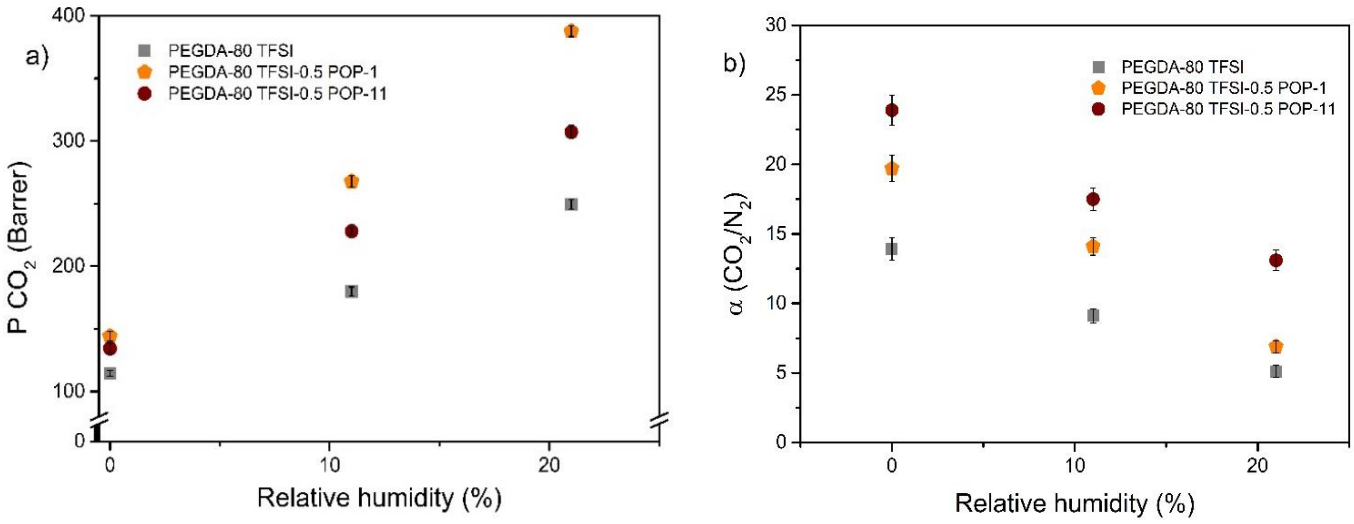

Figure 4.6 - Effect of relative humidity on the (a) CO_2 permeability and (b) CO_2/N_2 selectivity of the neat iongel and MMIMs containing azo-POPs, at 2 bar, 303 K and 15 vol% CO_2.

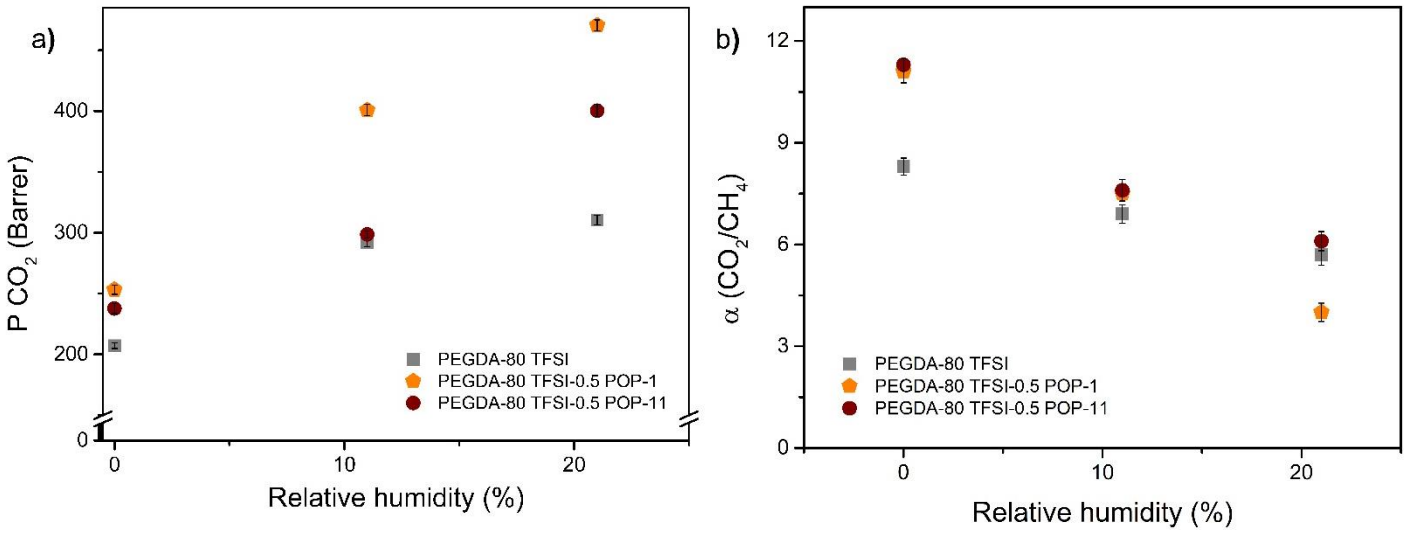

Figure 4.7 - Effect of relative humidity on the (a) CO_2 permeability and (b) CO_2/CH_4 selectivity of the neat iongel and MMIMs containing azo-POPs, at 2 bar, 303 K and 40 vol% CO_2.

4.4 Conclusions

The influence of temperature, pressure, and RH on the CO_2/N_2 and CO_2/CH_4 gas separations of MMIMs containing azo-POP-1 and azo-POP-11 was assessed. First, MMIMs containing four different azo-POPs were subjected to different saturated salt solutions, revealing that at lower a_w (up to 0.21) both single CO_2 permeabilities and CO_2/N_2 and CO_2/CH_4 ideal selectivities were improved. Conversely, higher values of a_w (up to 0.76) resulted in a significant decrease of gas diffusivity and solubility, lowering the single CO_2 permeability and ideal selectivities.

From the binary gas mixtures permeation experiments, it was found that increasing temperature promotes higher CO_2 permeability, while the CO_2/N_2 selectivity was not significantly impacted. It was also observed that, at low temperature (303 K), the CO_2 permeability decreases with increasing pressure (from 2 to 4 bar), which was not observed at higher temperatures (323 and 353 K). In the presence of water in the gas feed stream, the CO_2 permeability is significantly increased, due to the water-induced plasticization of the iongel material, which also led to a considerable decrease in both CO_2/N_2 and CO_2/CH_4 selectivities.

Under both dry and humidified gas conditions, the MMIMs containing azo-POP-1 and azo-POP-11 maintained a higher CO_2 permeability and selectivity, when compared to those of the neat iongel, due the increased porosity and higher CO_2 affinity attributed to the presence of azo functional groups in the POP structure.

The evaluation of parameters, such as pressure, temperature and RH of the gas feed stream, is a crucial step in terms of the design of gas separation processes, since the choice of materials to

fabricate gas separation membranes depends on their performance. Therefore, this work provided a thorough evaluation of the performance of MMIMs under relevant experimental conditions, which is of vital importance before considering these membranes for a potential process scale-up.

5

CO_2 SEPARATION PERFORMANCE OF UV-CROSS-LINKED IONGEL MEMBRANES CONTAINING METAL ORGANIC FRAMEWORKS

This chapter is part of the following publication: Ana R. Nabais, Vítor D. Alves, João G. Crespo, Liliana C. Tomé and Luísa A. Neves "CO_2 separation performance of UV-cross-linked iongel membranes containing metal organic frameworks" (in preparation)

Summary

The development of mixed matrix iongel membranes (MMIMs), combining a high ionic liquid (IL) content with porous fillers is a promising strategy to prepare materials with improved CO_2 separation efficiencies. In particular, metal organic frameworks (MOFs) have been widely studied for gas separation processes due to their undeniable versatility, high porosity and surface areas, and CO_2 sorption capacity. In this work, the MOFs Cu(BTC), MIL-53 and MOF-177 were selected to develop MMIMs using a fast and straightforward solvent-free UV polymerization process. Dense defect-free membranes were obtained, with a suitable thermal stability within the temperature range of interest (298-473 K), however with a significant loss of mechanical stability upon the incorporation of the different MOFs. It was also found that the porosity parameters, as well as the CO_2 sorption capacity, of the selected MOFs had a major influence on the CO_2 separation performance of the prepared membranes, showing very distinct behaviours. The best performing MMIM, containing 10 wt% Cu(BTC), was tested under mixed gas conditions for the CO_2/N_2 and CO_2/CH_4 separations under experimental conditions close to those of the industrial gas streams. It was found that, for both gas mixtures, the separation performance of the MMIMs containing 10 wt% Cu(BTC) is considerably affected by the temperature and RH of the feed gas stream. In all cases, the MMIM showed better separation performances than the neat PEGDA-80 TFSI iongel, with an improvement in CO_2 permeability with minimal or zero sacrifice of selectivity.

5.1 Introduction

During the last years, it became clear that the development of mixed matrix membranes (MMMs) is one of the most promising strategies for the design of membrane materials for gas separation processes, since it combines the easy processability and mechanical endurance of polymers with the thermal, chemical stability and high selectivity of inorganic or organic fillers.[66,211,270] The physical and chemical nature of the filler particles play an important role in the preparation, morphology and overall performance of the MMMs. However, it has been demonstrated that the incorporation of inorganic or hybrid organic/inorganic particles into a polymer matrix might lead to morphological defects, namely as a result of the poor adhesion at the interface between the different components, where unselective voids may occur.[271]

A promising strategy concerns the use of ionic liquids (ILs) to increase the compatibility at the materials' interface. ILs can be used to coat the surface of the inorganic or organic/inorganic solid particles or be dispersed in the polymer membrane along with the filler to improve the adherence between materials.[271] Besides improving the membranes' structure, ILs are known to have high CO_2 affinity. The versatility of ILs, along with their designable nature and chemical and thermal stabilities, boosted these materials to be widely used for the preparation of membranes.[9,66,116] In this context, polymer iongel membranes take advantage of the high IL content present in their structure, where usually it is the predominant component, while a polymer matrix is used to provide the necessary mechanical support.[9,10,168] In our first work, iongel membranes with an IL content up to 80 wt% were prepared in a self-standing form, to be used in gas separation processes.[136] The ILs combining the $[C_2mim]^+$ cation and four different anions ($[TFSI]^-$, $[FSI]^-$, $[C(CN)_3]^-$ and $[B(CN)_4]^-$) were selected to design the iongel membranes using poly(ethylene glycol) diacrylate (PEGDA) as polymer network. The iongel containing 80 wt% $[C_2mim][TFSI]$ IL showed the best compromise between CO_2 separation performance and thermal/mechanical stability,[136] and thus, this system was chosen to continue our studies regarding the development of novel MMIMs.

Our first approach towards the development of MMIMs consisted on the incorporation of an inorganic filler into the PEGDA-TFSI system containing 60 wt% $[C_2mim][TFSI]$ IL.[253] Different concentrations (0.2, 0.5, 1, 2.5, 5 and 7.5 wt%) of the montmorillonite (MMT) nanoclay were incorporated with the main purpose of improving the mechanical stability of the resulting membranes. The results showed that the high IL content of iongel membranes can significantly hinder their mechanical stability, however, at an optimal loading of 1 wt% MMT, the mechanical properties were considerably improved. On the other hand, even though the CO_2 permeability continuously increased at higher MMT loadings, a loss in the CO_2/N_2, CO_2/CH_4 and CO_2/H_2 ideal selectivities was observed for loadings higher than 0.5 wt%. Remarkably, due to the improved mechanical stability of the prepared iongels, it was possible to raise the IL content to 80 wt% and prepare self-standing MMIMs with improved CO_2 separation performances (up to 132 Barrer and CO_2/N_2 ideal selectivities up to 9, for a 7.5 wt% loading).[253] More

recently, we reported the synthesis of azo-porous organic polymers (azo-POPs), which are entirely organic materials with high CO_2 sorption capacities. The new azo-POPs synthesized for the first time, were used as fillers in PEGDA-TFSI system to improve their CO_2 separation performance.[254] Azo-POP-1 and azo-POP-11 showed the best separation performances, by increasing the permeability in 45 and 30%, respectively, when compared to the neat PEGDA-80 TFSI iongel, as well as significant improvements in the CO_2/N_2 (65 and 141%, respectively) and CO_2/H_2 (76 and 94%, respectively) ideal selectivities.

In the present work, we selected a different class of porous fillers, metal organic frameworks (MOFs), to prepare MMIMs by free radical UV polymerization. MOFs are inorganic-organic crystalline porous materials, composed by a metal ion or metal clusters coordinated to organic linkers to form two- or three-dimensional frameworks.[82] These porous materials are known for their versatility, since the choice of the metal ion and organic linkers can lead to almost unlimited structural and chemical features, which can be tuned towards a specific application. In the context of gas separation, the possible high surface areas and controlled porous volume of MOFs are of extreme importance as it can dictate the separation performance of membranes. Due to their hybrid nature, the use of MOFs combines the most interesting features of organic and inorganic materials: high affinity for CO_2 and improved gas selectivity arising from the inorganic metal clusters with the compatibility between the solid particles and the organic polymer matrix, provided by the organic linkers.[82,272,273] Herein, we studied the impact of three different MOFs (Cu(BTC), MIL-53 and MOF-177), and respective loadings (5 and 10 wt%) on the CO_2 separation performance of iongel membranes, combining 80 wt% [C_2mim][TFSI] IL and 20 wt% PEGDA. First, the morphology, thermal stability, mechanical properties and chemical structure of the prepared MMIMs were assessed through several characterization techniques and the separation performance was evaluated under ideal conditions, using pure gases (CO_2, N_2 and CH_4) at low temperature and pressure. In addition, the best performing MMIM was tested under experimental conditions closer to those of an industrial gas stream, in terms of gas composition, temperature and pressure aiming a more realistic assessment of its potential for the proposed application.

5.2 Experimental Section

5.2.1 Materials

Poly(ethylene glycol) diacrylate (PEGDA, M_n 575 g mol^{-1}) and 2-hydroxy-2-methylpropiophenone (DAROCUR®, 97 wt% pure) were purchased by Sigma-Aldrich (Portugal). The IL 1-ethyl-3-methylimidazolium bis(trifluoromethylsulfonyl) imide ([C_2mim][TFSI], 99 wt% pure) was supplied by Iolitec GmbH (Germany). Carbon dioxide, CO_2 (99.998% purity), nitrogen, N_2 (99.99% purity), methane, CH_4 (99.99% purity) and helium, He (>99% purity) gases were supplied by Praxair (Portugal). MOFs Cu(BTC), MIL-53(Al) and MOF-177 were synthesized by BASF SE (Germany) and

supplied by Sigma Aldrich (Portugal), as Basolite® C300, Basolite® A100 and Basolite® Z377, respectively. Table 5.1 summarizes the characteristics of the MOFs used in this work.

Table 5.1 - Characteristics of the MOFs used in this work. [274–280]

MOF	BET Surface area (m^2 g^{-1})	Pore diameter (Å)	Porous volume (cm^3 g^{-1})	CO_2 sorption capacity (mmol g^{-1}) at 1 bar and 293-303 K
Cu(BTC)	1 300-1 800	9	0.50	3.5-8
MIL-53	1 100-1 300	9	0.62	Approx. 1.5
MOF-177	4 500	11	1.60	0.8-0.95

5.2.2 Preparation of Mixed Matrix Iongel Membranes (MMIMs)

The preparation of the MMIMs started by dispersing the desired loading (5 and 10 wt% over the total iongel weight) of each MOF (Cu(BTC), MIL-53 and MOF-177) in 80 wt% of [C_2mim][TFSI] IL (4:1 mass ratio – IL:PEGDA). It should be noted that 10 wt% was found to be the maximum loading that was possible to disperse in the IL without the need of using additional solvents. The solutions were left stirring overnight at room temperature. Afterwards, 20 wt% of PEGDA was added and the resulting solution was left stirring for 1 hour, at room temperature. Then, 3 wt% of DAROCUR® (above the PEGDA mass) was added to the solution to act as photoinitiator of the polymerization reaction. The final solutions were poured between two Rain-X™-coated quartz plates, with a spacer in between to ensure a homogeneous thickness of around 100 µm. The final assembly was placed under a UV light with a wavelength of 365 nm^{-1} and intensity of 1.8 mW cm^{-2}, for 10 minutes. Finally, self-standing iongels were peeled off from the plates and characterized.

A schematic representation of the preparation of the iongels can be found in Figure 5.1.

To perform the gas permeation experiments without compromising the mechanical integrity of the materials, composite iongel membranes were prepared. The iongel solutions were poured on top of a pre-wetted porous polyamide (PA) filter (Sartorius™, supplied by Fisher Scientific) with a pore size of 0.22 µm. The support was immersed in deionized water before the solution was casted on top of it, to minimize the pore filling from the iongel solution into the porous support. The final composite mixed matrix iongels were then dried at 333 K to remove the water trapped inside the support. Thus, it was considered that the results obtained from the gas permeation experiments correspond solely to the iongel dense layer.

For the sake of clarity, the MMIMs were designated as PEGDA-80 TFSI-XX MOF, according to the loading (XX) and MOF used.

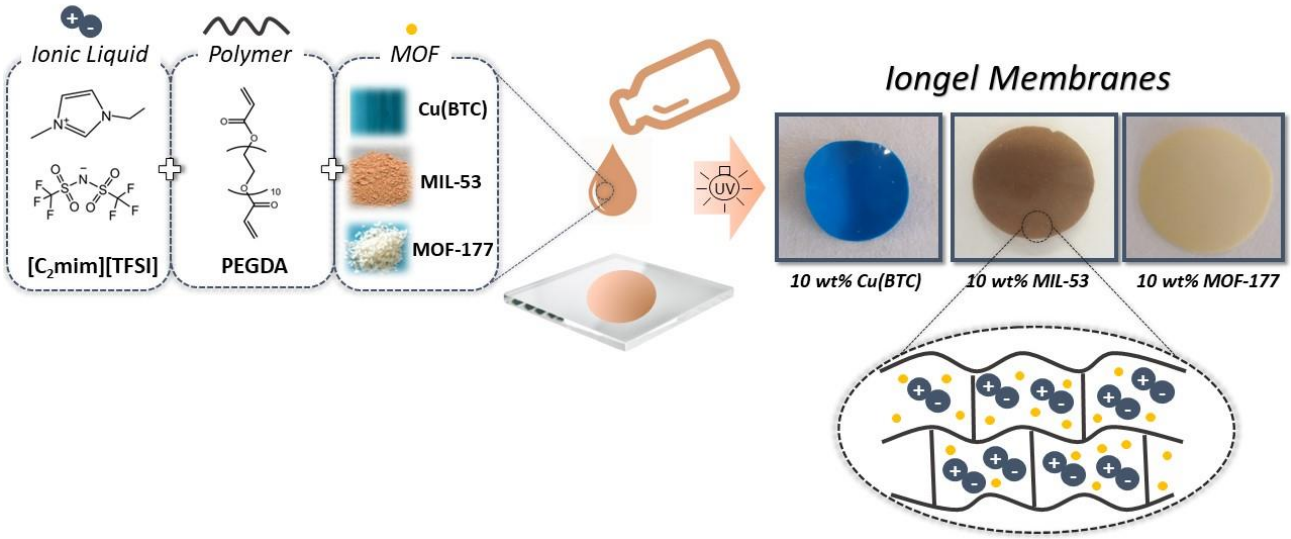

Figure 5.1 - Schematic representation of the preparation of the MMIMs containing MOFs.

5.2.3 Scanning Electron Microscopy (SEM)

The surface and cross section images of the prepared MMIMs containing different MOFs were obtained by SEM. Only the MMIMs containing 10 wt% loading of each MOF are reported in this work, since this was the highest loading used. The samples were coated with a thin Pd/Au layer, before the analysis, to induce charge under the electron beam. The SEM images were acquired with a JOEL 7001F scanning electron microscope (USA) with an electron beam intensity of 10 kV.

5.2.4 Fourier Transform Infrared-Attenuated Total Reflectance spectroscopy (FTIR-ATR)

Fourier Transform Infrared-Attenuated Total Reflectance (FTIR-ATR) spectroscopy was performed to analyze the chemical structure of the prepared iongel membranes and to verify the extent of the polymerization reaction, as well as possible interactions occurring between the materials components. The spectra were obtained using a Perkin Elmer Spectrum Two spectrometer, by collecting 10 scans from 4000 to 400 cm^{-1}.

5.2.5 Contact Angle Measurements

The contact angles of the prepared membranes were measured to evaluate the hydrophilicity of the materials, using the sessile drop method. To conduct the measurements, a drop of distilled water was deposited on the iongel surface. For each sample, 10 frames were acquired with 1 second intervals,

and at least 3 samples of each iongel were analyzed. Frames were acquired and processed by a CAM100 (KSV Instrument Ltd., Finland) and the mean contact angle was obtained.

5.2.6 Mechanical Properties

The mechanical properties of the prepared self-stading MMIMs were evaluated through puncture tests, using a TA XT Plus Texture Analyzer (Stable Micro Systems, UK). The iongel samples with 45 mm of diameter were punctured through a 10 mm hole, with a cylindrical probe with 2 mm of diameter at the constant speed of 1 mm s^{-1}, at room temperature. For each sample, 4 replicates were performed, and the mean tensile strength, normalized tensile strength with membrane thickness and elongation at break were obtained, according to the following equations:

$$\sigma = \frac{F}{A} \tag{5.1}$$

where σ is the puncture strength (Pa), F is the force applied by the probe (N) and A is the cross-sectional area of the probe (m^2). In order to compare the results, the puncture strength was normalized with the thickness of each iongel, following Equation 5.2:

$$\sigma_n = \frac{\sigma}{l} \tag{5.2}$$

where σ_n is the normalized puncture strength (MPa mm^{-1}) and l is the thickness of the iongel membrane (mm). The elongation at break given by Equation 5.3 was also determined.

$$\varepsilon\,(\%) = \left(\frac{\sqrt{h^2 - d^2} - h}{h}\right) \times 100 \tag{5.3}$$

where ε represents the elongation at break (%), h is the radius of the iongel exposed in the cylindrical hole (mm) and d is the distance between the point of contact to the point of rupture (mm). The Young's modulus of the tested MMIMs was obtained from the initial slope of the graphic representation of the puncture strength (σ) as a function of the elongation at break (ε).

5.2.7 Thermogravimetric Analysis (TGA)

To evaluate the thermal stability of the neat MOFs and prepared MMIMs, thermogravimetric analysis was performed, using a Lass EVO TGA-DTA/DSC 1600 °C PG from Setaram KEP Technologies (France). The experiments were conducted from around 298 to 773 K, at a heating rate

of 10 K min^{-1}, under a constant argon flow of 40 mL min^{-1}. The T_{onset} was determined, as the temperature at which the baseline slope changes.

5.2.8 Gas Permeation Experiments

5.2.8.1 Pure Gases

Pure gas permeation experiments were performed for CO_2, N_2, CH_4, according to a previously described procedure.[16] The MMIMs were placed inside a stainless-steel cell composed of two distinct compartments, the feed and permeate. The temperature of the experiments was maintained at 303 K, in a water bath. All permeation experiments were performed at a transmembrane pressure of 0.7 bar and three replicates of each membrane were tested. The permeability of the single gas through the membrane was calculated through the acquired data of pressure over time, on both compartments, according to the following equation:

$$\frac{1}{\beta} \times \ln\left(\frac{\Delta p_0}{\Delta \mathrm{p}}\right) = P \times \frac{t}{l} \tag{5.4}$$

where Δp_0 and Δp (bar) are the pressure variations between feed and permeate compartments of the cell from the starting point of the experiment and over time, respectively, P ($m^2\ s^{-1}$) is the permeability of the iongel (1 Barrer = 1×10^{-10} cm^3 (STP) cm $cm^{-2}\ s^{-1}\ cmHg^{-1}$ = 8.3×10^{-13} $m^2\ s^{-1}$ [235]), t is time (s), l is the thickness of the iongel layer (m) and β is the geometric parameter of the cell (m^{-1}), given by Equation 5.5.

$$\beta = \mathrm{A}\left(\frac{1}{\mathrm{V_{feed}}} + \frac{1}{\mathrm{V_{perm}}}\right) \tag{5.5}$$

where A is the membrane area (m^2), V_{feed} and V_{perm} are the volumes of the feed and permeate compartments (m^3), respectively. The permeability of the iongel was obtained from the slope of $1/\beta\ ln(\Delta p_0/\Delta p)$ as a function of t/l. The ideal selectivity of the tested iongels is given by Equation 5.6.

$$\alpha_{\mathrm{A}/\mathrm{B}} = \frac{\mathrm{P_A}}{\mathrm{P}_B} \tag{5.6}$$

5.2.8.2 Binary Gas Mixtures

Binary gas mixtures experiments for CO_2/N_2 and CO_2/CH_4 mixtures were performed to determine the permeability and selectivity of the prepared iongels, under mixed conditions. The

experiments were carried out at different conditions, depending on the gas pair. The experimental conditions used to carry out the gas mixtures experiments, listed in Table 5.2, were selected with the goal of mimicking, as much as possible, the real conditions of a flue gas (CO_2/N_2) and biogas (CO_2/CH_4) streams. In the case of the flue gas stream, the temperature was raised from 303 to 353 K, to evaluate the performance of the iongel membranes at a temperature closer to the real temperature of the process. Following the same train of thought, the relative humidity (RH) in the feed gas stream was set at 11 vol%. A schematic representation of the experimental setup and a detailed description of the procedure can be found in a previous work.[281] Briefly, the experimental setup is composed by a stainless-steel cell split in two identical compartments, designated as feed and permeate, where the membrane to be tested is placed in between. The membrane module is placed inside an oven (Venticell MMM, Germany) with controlled temperature (TC). He was used as sweep gas (MFC4) during the experiments to maintain a constant gas flow on the permeate compartment, of 5 mL min^{-1}. Feed, retentate and permeate concentrations were analyzed using an Agilent gas chromatograph (GC) 7890B. The permeability of each gas was calculated according to the following equations:

$$j_i = \frac{F^f_{total} \cdot y^f_i}{A} \tag{5.7}$$

$$\Delta p_i = p^f \cdot y_i^f - p^p \cdot y_i^p \tag{5.8}$$

$$P_i = \frac{j_i \cdot l}{\Delta p_i} \tag{5.9}$$

where j_i is the molar flux of gas i (mol m^{-2} s^{-1}), F is the gas molar flow rate (mol s^{-1}), y^f and y^p are the gas molar fractions on the feed and permeate side, respectively, A is the membrane area (m^2), Δp represents the driving force between feed and permeate sides (Pa), p^f and p^p are the pressures (Pa) in the feed and permeate sides, respectively, l is the thickness of the iongel layer (m) and P is the membrane permeability for gas i (mol m^{-1} Pa^{-1} s^{-1}).

Table 5.2 - Experimental conditions of the gas mixtures permeation experiments.

Separation	Temperature (K)	Pressure (bar)	CO_2 composition (vol%)	H_2O content (%)
CO_2/N_2 (flue gas)	303, 353	2	15	0 and 11
CO_2/CH_4 (biogas)	303	2	40	0 and 11

5.3 Results and Discussion

5.3.1 Scanning Electron Microscopy (SEM)

To evaluate the morphology of the prepared MMIMs, SEM images of the top surface and cross section were analysed and are depicted in Figure 5.2. More specifically, the MMIMs containing 10 wt% loading of each MOF were analysed to detect any possible agglomerations or defects caused by the highest concentration of solid particles. All membranes presented a dense and defect-free structure, both at the surface and cross section. It may be assumed that the high IL content in the iongel prevented possible defects and formation of voids, which is a common problem when inorganic or partially inorganic particles are incorporated into a polymer matrix. Despite not being shown here, similar morphologies were obtained for the MMIMs containing lower MOF loadings (5 wt%). The observed morphologies indicate a good compatibility between all the materials and a good dispersion of the MOF particles in the IL, during the MMIM preparation, without the need of solvents.

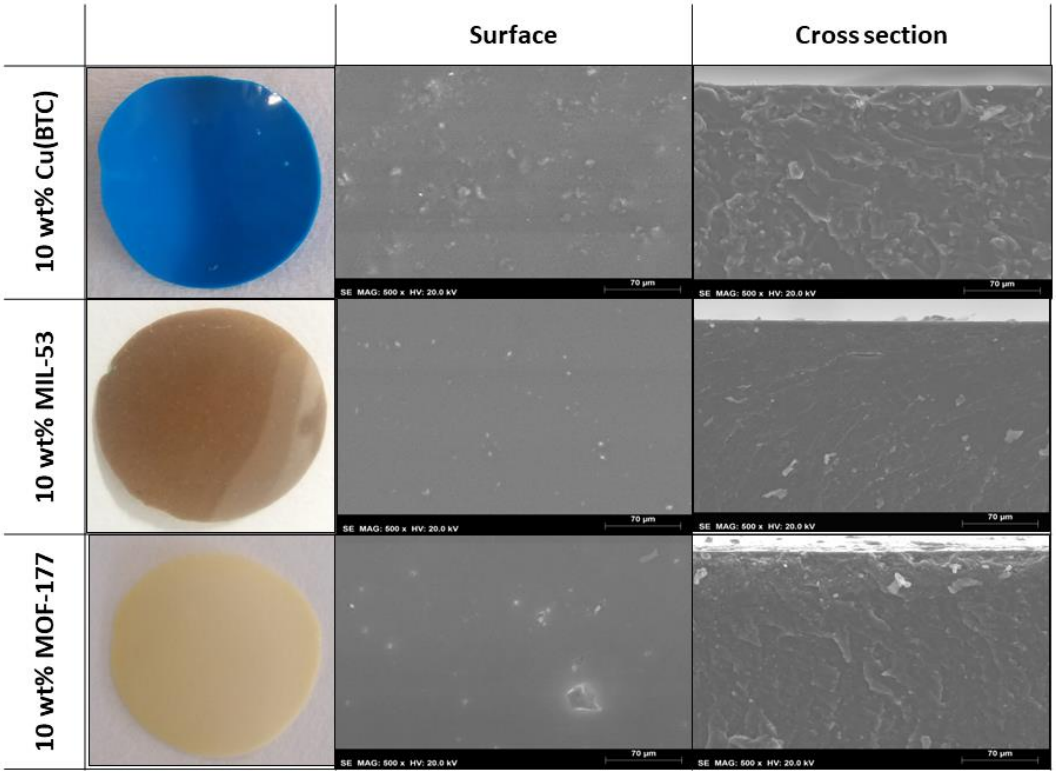

Figure 5.2 - SEM images of the surface and cross section of the MMIMs containing 10 wt% MOF.

5.3.2 FTIR-ATR

The chemical structures of the selected MOFs (Cu(BTC), MIL-53 and MOF-177) and the respective MMIMs were confirmed by FTIR-ATR spectroscopy and the respective spectra are displayed in Figure 5.3 a) and b), respectively.

The FTIR-ATR spectra of the MOFs (Figure 5.3 a)) used in this work are in accordance with what has been previously reported in the literature. [276,282,283] For Cu(BTC), the region between 1635 and 1365 cm^{-1} was assigned to the carboxylate groups of the organic benzene-1,3,5-tricarboxylic acid (BTC) linkers. Below this region, the peak at 1107 cm^{-1} and the peaks at 758 and 725 cm^{-1} corresponded to the in- and out-of-plane C-H bending modes, respectively, associated to the aromatic ring present in the BTC linker of Cu(BTC).[282] Looking at the FTIR-ATR spectrum of MIL-53, the peaks observed at 1582 and 1509 cm^{-1} were characteristic of the asymmetric CO_2 stretching vibrations of the carboxylic groups, coordinated to aluminium. At 1417 cm^{-1}, the peak corresponding to the symmetric CO_2 stretching vibration can also be observed.[276,283] The MOF-177 spectrum shows peaks between 1584 and 1411 cm^{-1}, assigned to the O-CO vibrational stretching of the dicarboxylic groups. The peaks observed in the region between 853 and 670 cm^{-1} were assigned to the ring vibrations of the 1,3,5-benzenetribenzoate (BTB) organic linkers.

Regarding the FTIR-ATR spectra obtained for the prepared MMIMs, the absence of visible peaks at 1635 and 1619 cm^{-1}, corresponding to the C=C symmetric and asymmetric stretching, respectively, from the terminal acrylate groups of PEGDA, confirmed the high extension of the polymerization reaction. The bands observed at 2940 and 278 cm^{-1} corresponded to the C-H stretching, while the peak at around 1730 cm^{-1} was attributed to the C=O symmetric stretching. As for the [C_2mim][TFSI] IL, the bands between 3160 and 3120 cm^{-1} and the peak at 1460 cm^{-1} were attributed, respectively, to the CH_2 stretching and CH_3 bending vibrations of the imidazolium cation. Moreover, the bands at 1343, 1178, 1132 and 1049 cm^{-1} were assigned to the $[TFSI]^-$ anion of the IL. It should be noted that the bands and peaks of the most characteristic functional groups of the different MOFs could not be easily detected in the FTIR-ATR spectra of the prepared MMIMs, since most of them were overlapped with those of the neat PEGDA-80 TFSI iongel.

In any case, slight changes in the FTIR-ATR spectra of the MMIMs, compared to that of the neat PEGDA-80 TFSI iongel confirmed the presence of the different fillers. In particular, for the PEGDA-80 TFSI-10 Cu(BTC) membrane, small peaks can be observed at 1636 cm^{-1} and around 740 cm^{-1}, corresponding to the carboxylate groups and aromatic rings of the BTC linker, respectively. Regarding the PEGDA-80 TFSI-10 MIL-53, the presence of the MOF particles were confirmed by the small peaks observed at 1677, 1509, 754 and 470 cm^{-1}. Finally, looking at the PEGDA-80 TFSI-10 MOF-177 spectra, the appearance of small peaks around 1700 and 1608 cm^{-1} confirmed the presence of the MOF-177 porous particles.

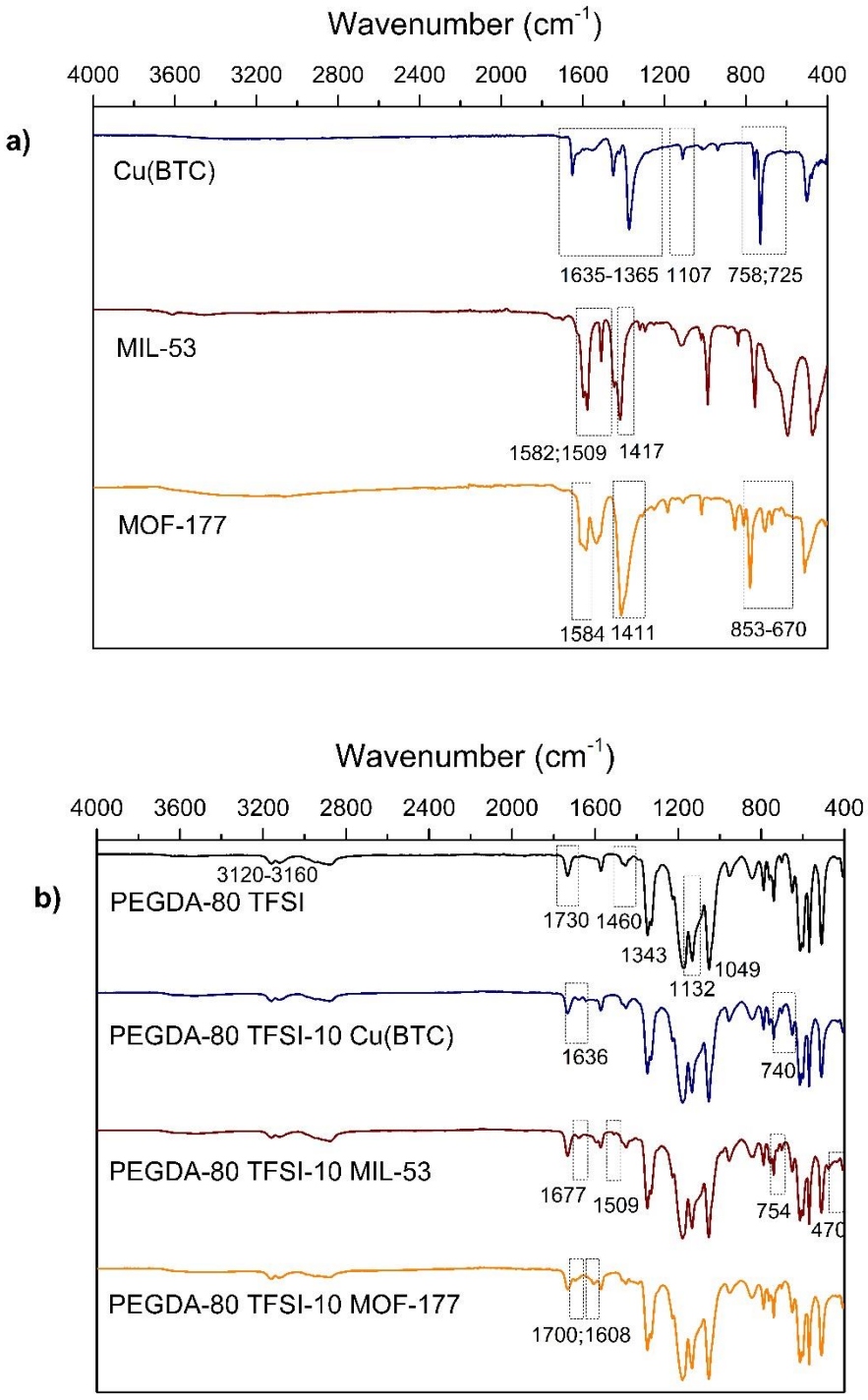

Figure 5.3 - FTIR-ATR spectra of the (a) MOFs and (b) neat PEGDA-80 TFSI iongel and MMIMs with 10 wt% MOF loading.

5.3.3 Contact Angle Measurements

The contact angles of the prepared neat PEGDA-80 TFSI iongel and MMIM containing 5 and 10 wt% of the different MOFs are summarized in Table 5.3. All measurements were carried out using distilled water, meaning that a contact angle below 90° represents a hydrophilic material, otherwise it can be considered to have a more hydrophobic nature.

As it can be perceived from Table 5.3, all the iongel membranes, including the neat PEGDA-80 TFSI, presented a hydrophilic nature. The PEGDA monomer is composed of hydrophilic ethylene oxide units and hydrophobic acrylate units. Previous works, where the contact angles of PEGDA-based materials (i.e. hydrogels) were measured, confirmed the hydrophilic nature of PEGDA, with values lower that the one obtained in this work (61.9°).[284,285] The combination of PEGDA with a hydrophobic IL, in this case the [C_2mim][TFSI] IL, reduced the hydrophilic character of the iongel, increasing the value obtained for the contact angle of the neat PEGDA-80 TFSI iongel. However, the contact angle decreased upon the incorporation of the different MOFs, since they possess a more hydrophilic nature compared to the neat iongel. The increase in MOF loading had a slight influence in the contact angle of the prepared MMIMs, since it decreased from 43.9 to 38.9° for Cu(BTC) and from 38.2 to 35.5° for the iongels containing MOF-177. In the case of MIL-53, the contact angle only slightly increased by around 2.5° when the MIL-53 loading increased from 5 to 10 wt% but maintaining its hydrophilic character. The hydrophilic nature of the prepared MMIMs might represent an advantage regarding the separation performance of the materials since, in general, the solubility of CO_2 in hydrophilic materials is higher than in less hydrophilic/more hydrophobic ones.[183]

Table 5.3 - Contact angles of the neat PEGDA-80 TFSI iongel and MMIMs prepared in this work.

Membrane Sample	Contact Angle (°)
PEGDA-80 TFSI	61.9 ± 2.2
PEGDA-80 TFSI- 5 Cu(BTC)	43.9 ± 0.3
PEGDA-80 TFSI- 10 Cu(BTC)	38.9 ± 0.3
PEGDA-80 TFSI- 5 MIL-53	37.8 ± 0.2
PEGDA-80 TFSI- 10 MIL-53	40.4 ± 0.2
PEGDA-80 TFSI- 5 MOF-177	38.7 ± 0.1
PEGDA-80 TFSI- 10 MOF-177	35.5 ± 0.4

5.3.4 Mechanical Properties

The normalized puncture strength, elongation at break and Young's modulus obtained through the puncture tests performed with the MMIMs are provided in Table 5.4.

The highest puncture strength was obtained for the neat PEGDA-TFSI iongel, at 3.1 MPa mm^{-1}, and this value decreased after incorporation of the different MOFs. Usually, the incorporation of MOFs is known for decreasing the mechanical stability of mixed matrix membranes, by interfering with the membranes structure. The presence of the solid particles decreases the free volume available in the membrane, causing a reduction in the polymer chains mobility and increasing its brittleness and fragility.[275] This effect was significantly more pronounced for the MMIMs containing 5 and 10 wt% MOF-177, where the puncture strength decreased to 0.54 and 0.50 MPa mm^{-1}, respectively. On the other hand, the MMIMs containing MIL-53 presented the highest puncture strength. The normalized puncture strength also increased from 1.9 MPa mm^{-1} to 2.6 MPa mm^{-1} with increasing MIL-53 loading from 5 wt% to to 10 wt%, respectively. A similar behaviour had already been observed for PIL/IL/MOF membranes containing MIL-53, suggesting that the chemical nature of this particular MOF (MIL-53) is more compatible with the PIL/IL ionic materials and it is capable of establishing stronger interactions.[114]

The elongation at break of the MMIMs was also lower that of the neat PEGDA-80 TFSI iongel, meaning that the incorporation of the different MOFs reduced the membranes' ability to elongate before rupture, due to the aforementioned decrease in the polymer chains mobility. Once again, the highest elongation at break amongst the MMIMs was obtained for the ones containing MIL-53, reaching 14% at 5 wt% MOF loading.

In order to evaluate how easily these materials can be stretched and deformed, the Young's modulus values of the prepared iongel membranes were also evaluated. Except for the MMIM containing Cu(BTC), where the Young's modulus did not change significantly with the loading, it can be seen that, for MIL-53 and MOF-177, higher loadings resulted in higher values of Young's modulus. This behaviour confirmed that there was a good interfacial adhesion between the MOF particles and the iongel matrix.

Table 5.4 - Normalized puncture strength, elongation at break and Young's modulus of the neat PEGDA-80 TFSI iongel and MMIMs studied in this work.

Membrane Sample	Normalized puncture strength (MPa mm^{-1})	Elongation at break (%)	Young's modulus (MPa)
PEGDA-80 TFSI	3.1 ± 0.1	19.0 ± 0.1	1.7 ± 0.1
PEGDA-80 TFSI- 5 Cu(BTC)	0.6 ± 0.0	3.6 ± 0.8	1.5 ± 0.2
PEGDA-80 TFSI- 10 Cu(BTC)	1.2 ± 0.0	9.7 ± 0.3	1.4 ± 0.0
PEGDA-80 TFSI- 5 MIL-53	1.9 ± 0.1	14.1 ± 0.2	1.5 ± 0.0
PEGDA-80 TFSI- 10 MIL-53	2.6 ± 0.4	10.8 ± 1.6	2.5 ± 0.0
PEGDA-80 TFSI- 5 MOF-177	0.5 ± 0.1	4.5 ± 0.3	1.3 ± 0.0
PEGDA-80 TFSI- 10 MOF-177	0.5 ± 0.1	1.9 ± 0.2	3.0 ± 0.1

5.3.5 Thermogravimetric Analysis (TGA)

The thermogravimetric analysis of the prepared MMIMs and the neat materials in bulk ([C_2mim][TFSI] IL, PEGDA, Cu(BTC), MIL-53 and MOF-177) was performed to evaluate their thermal stability and potential to be used in gas separation processes. Table 5.5 presents the T_{onset} (temperature at which the baseline slope changes) obtained for the prepared MMIMs. The T_{onset} of the neat [C_2mim][TFSI] IL (685 K) and PEGDA (642 K) were previously reported in our previous works.[253,254] To better understand the degradation steps of the prepared membranes, the thermogravimetric profiles of the MMIMs containing 10 wt% of each MOF, as well as of the neat iongel, are presented in Figure 5.4. The PEGDA-80 TFSI iongel presented a T_{onset} of 661 K, which was in the range of values of the neat iongel components, PEGDA and [C_2mim][TFSI] IL, and was in agreement with what has been previously obtained.[253,254] All the MMIMs exhibited a small weight loss (lower than 4 wt%), until 473 K, which can be attributed to the loss of residual moisture trapped in the iongel structure, as it can be seen in Figure 5.4. Moreover, each sample presented a degradation profile with two decomposition steps. In the case of the MMIMs containing Cu(BTC), the first degradation step corresponded to the MOF decomposition (which starts at 603 K), while the second stage corresponded to the degradation of PEGDA and IL, that decomposed at higher temperatures. MIL-53 presented the highest T_{onset} among all MOFs (822 K). For MMIMs containing MIL-53 and MOF-177, the first degradation step was attributed to the PEGDA degradation (which decomposed at around 642 K), while the second step corresponded to the degradation of the IL [253,254] and, subsequently, the MOF particles at higher temperatures. Above these temperatures, a continuous degradation of the material was observed.

Considering the conditions of the gas streams studied in this work, it can be considered that the prepared MMIMs presented a suitable thermal stability, since no significant weight loss was observed in the temperature range of interest (up to 393 K).

Table 5.5 - T_{onset} obtained for the MOFs, neat PEGDA-80 TFSI iongel and MMIMs studied in this work.

Membrane Sample	T_{onset} 1 (K)	T_{onset} 2 (K)
Cu(BTC)	605	N/D
MIL-53	822	N/D
MOF-177	688	N/D
PEGDA-80 TFSI	661	N/D
PEGDA-80 TFSI- 5 Cu(BTC)	633	698
PEGDA-80 TFSI- 10 Cu(BTC)	603	653
PEGDA-80 TFSI- 5 MIL-53	641	698
PEGDA-80 TFSI- 10 MIL-53	613	678
PEGDA-80 TFSI- 5 MOF-177	642	698
PEGDA-80 TFSI- 10 MOF-177	635	698

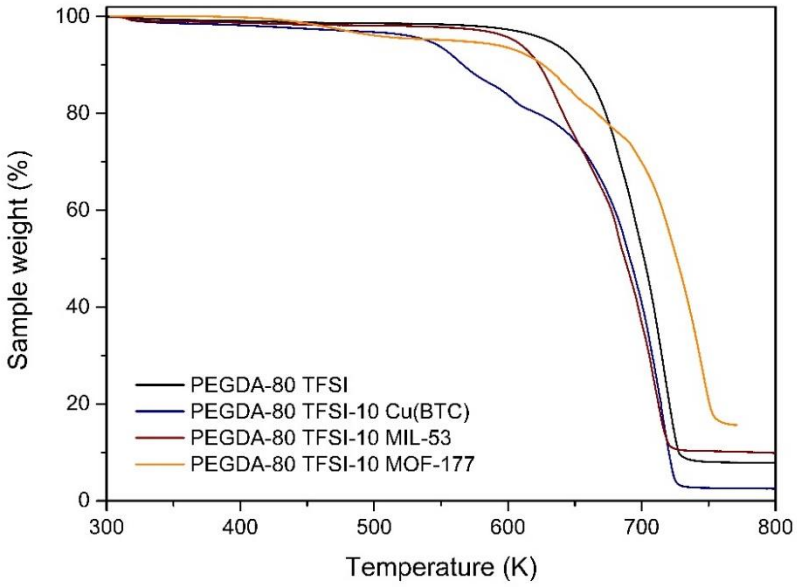

Figure 5.4 - Thermogravimetric profiles of the neat PEGDA-80 TFSI iongel and MMIMs containing 10 wt% MOF.

5.3.6 Gas Permeation Experiments

5.3.6.1 Pure Gases

Pure gas permeation experiments were carried out with CO_2, N_2 and CH_4 to evaluate the gas transport properties of the prepared MMIMs containing different loadings (5 and 10 wt%) of the selected MOFs, namely (Cu(BTC), MIL-53 and MOF-177). The results, in terms of CO_2 permeability and ideal

selectivities, obtained for the neat PEGDA-80 TFSI and MMIMs can be found in Table 5.6. To make a better comparison between the results obtained with the different MOFs, the experimental data was plotted against the CO_2/N_2 and CO_2/CH_4 Robeson upper bounds, as illustrated in Figure 5.5 a) and b), respectively. For both gas pairs, the MMIMs presented higher values of CO_2 permeabilities and ideal selectivities, when compared to the neat PEGDA-80 TFSI iongel. The highest CO_2 permeability was obtained for the MMIMs containing Cu(BTC), where a permeability of 290 Barrer was achieved at 10 wt% loading. Among the three MOFs studied, Cu(BTC) presented the highest CO_2 sorption capacity, ranging from 3.6 to 8 mmol CO_2 g^{-1} (at 1 bar and around 298-303 K), according to what has been reported in the literature,[279,280] and can be observed in Table 5.1. Conversely, the lowest CO_2 permeability was obtained with 10 wt% MIL-53, at 189 Barrer, meaning that the permeability was much more governed by the sorption capacities of the MOFs than by their porosity parameters.

Table 5.6 - CO_2 permeability and CO_2/N_2 and CO_2/CH_4 ideal selectivities obtained for the neat PEGDA-80 TFSI iongel and MMIMs.

Membrane Sample	***P*** **CO_2 (Barrer)**	***α*** **(CO_2/N_2)**	***α*** **(CO_2/CH_4)**
PEGDA-80 TFSI	62 ± 2	17 ± 1	10 ± 1
PEGDA-80 TFSI- 5 Cu(BTC)	251 ± 6	21 ± 3	10 ± 1
PEGDA-80 TFSI- 10 Cu(BTC)	290 ± 4	31 ± 3	19 ± 2
PEGDA-80 TFSI- 5 MIL-53	181 ± 6	23 ± 5	14 ± 3
PEGDA-80 TFSI- 10 MIL-53	126 ± 5	28 ± 2	19 ± 1
PEGDA-80 TFSI- 5 MOF-177	185 ± 4	28 ± 2	15 ± 1
PEGDA-80 TFSI- 10 MOF-177	209 ± 4	19 ± 2	11 ± 1

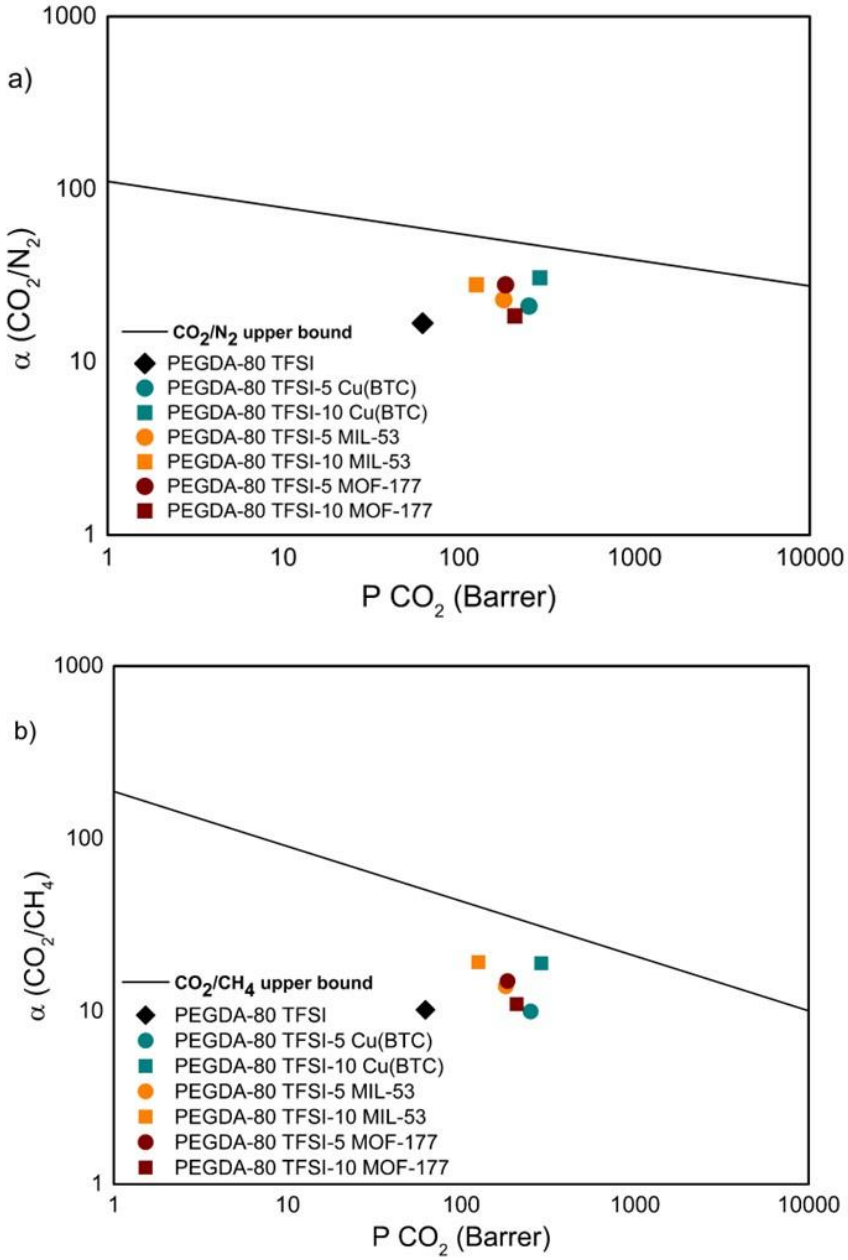

Figure 5.5 – (a) CO_2/N_2 and (b) CO_2/CH_4 ideal selectivities as a function of CO_2 permeability obtained for the neat PEGDA-80 TFSI iongel and MMIMs.

For the MMIMs containing Cu(BTC), the CO_2 permeability increased with increasing MOF loading, from 251 to 290 Barrer. Following the same behaviour, the CO_2/N_2 and CO_2/CH_4 ideal selectivities also increased, from 21 to 31 and from 10 to around 19, respectively. It is known that MOF particles provide an extra porous network to the membrane matrix and higher diffusion rates, which consequently improves the gas permeability. On the other hand, the quadrupole moment of CO_2 (-1.4×10^{-35} C m^2) has stronger interaction with the Cu sites, compared to CH_4 and N_2. Therefore, the

preferential CO_2 sorption capacity of Cu(BTC) ensured a solubility based discrimination between the gas molecules, improving the selectivity of the membranes with increasing the MOF loading.[286] This improvement could also be driven by the increased iongel membrane hydrophilicity at higher MOF loadings (Table 5.3).

The iongel membranes containing MIL-53 showed decreasing CO_2 permeabilities, from 181 down to 126 Barrer. At 10 wt% loading, the level of dispersion of the MIL-53 particles in the IL was lower and more challenging, compared to the other MOFs. It was observed that the MIL-53 particles formed some aggregates, even in the powdered form prior to the membrane fabrication. This observation difficulted a homogeneous dispersion of the MIL-53 particles, possibly creating a more tortuous path and hindering the transport of the gas molecules across the membrane. However, it should be noted that these aggregates were not detect in the SEM images. It should also be mentioned that the decrease in CO_2 permeability followed the decrease of the iongel hydrophilicity when the MIL-53 loading was increased from 5 to 10 wt%. Interestingly, as the MIL-53 loading increased, the ideal selectivities for both gas pairs (Table 5.6) slightly increased from 23 to 28 for CO_2/N_2 and from 14 to 19 for CO_2/CH_4. Even though the transport rate of the gas molecules across the membrane was lowered due to the presence of more unevenly dispersed MOF particles, the strong CO_2 quadrupole moment could induce specific interactions with the hydroxyl groups located at the metal-oxygen-metal link of MIL-53, which did not happen for N_2 and CH_4.[287] Moreover, the transport of N_2 and CH_4, which are larger molecules was more affected by the lower dispersion level of the MOF particles compared to smaller gas molecules as CO_2. Therefore, only low loadings of MIL-53 should be considered when preparing solvent-free MMIMs for gas separation, as the higher loadings (10 wt%) could be a disadvantage.

The MMIMs containing MOF-177, presented an increased CO_2 permeability as the MOF loading also increased from 5 to 10 wt%. Similar to what was observed for the MMIMs containing Cu(BTC), the higher porosity induced by the MOF particles and their affinity for CO_2 enhanced the transport of the gas molecules across the membrane, improving both solubility and diffusivity. It also followed the tendency of higher CO_2 permeability for more hydrophilic materials (Table 5.3). Conversely, the CO_2/N_2 and CO_2/CH_4 ideal selectivities decreased from 28 to 19 and from 15 to 11, respectively, as the MOF-177 loading increased (Table 5.6). Even though MOF-177 presented a higher affinity for CO_2 compared to N_2 and CH_4, it also presented higher porosity characteristics, compared to the other MOFs tested (Table 5.2), with a pore diameter of 11 Å and a porous volume of 1.6 $cm^3\,g^{-1}$, which is around three times higher than those of Cu(BTC) and MIL-53. This indicates that increasing MOF-177 load had a more significant impact in the gas diffusion rather than in gas solubility, resulting in the observed lower ideal selectivities for CO_2/N_2 and CO_2/CH_4 gas pairs. Although the incorporation of MOFs in iongel membranes containing such a high amount of IL (80 wt%) has not been deeply explored yet, there are a few works reported in literature that can be used for comparison, to understand the potential of the prepared MMIMs. For example, in our previous work, poly(ionic liquid)-based membranes, containing 40 wt% of similar ILs (also combining fluorinated anions) and varying loadings of different MOFs (MOF-5, Cu(BTC), MIL-53 and ZIF-8), showed lower separation performances (with the highest CO_2

permeability at 89 barrer) compared to the iongel membranes proposed in the present work.[114,115] In addition, Li and co-workers [147] studied iongel membranes combining Pebax® as polymer matrix, 80 wt% [C_4mim][TFSI] IL and 15 wt% ZIF-8, that showed separation performances similar to the ones reported in the present work, with a maximum CO_2 permeability of 231 Barrer and a CO_2/N_2 and CO_2/CH_4 ideal selectivities of 27 and 15, respectively. Nonetheless, the authors used higher MOF loadings and resorted to the use of solvents to prepare the Pebax®-based membranes.[147]

Overall, it is possible to conclude that for both CO_2/N_2 and CO_2/CH_4 gas pairs, the MMIM containing 10 wt% Cu(BTC) showed the best compromise between CO_2 permeability and ideal selectivity, being the result that fell closer to both Robeson upper bounds (Figure 5.4).

5.3.6.2 Binary gas mixtures

The MMIMs containing 10 wt% Cu(BTC) were selected to be tested under mixed gas conditions, as it presented the best compromise between permeability and ideal selectivities for both CO_2/N_2 and CO_2/CH_4 separations. The PEGDA-80 TFSI-10 Cu(BTC) iongel was tested for CO_2/N_2 (flue gas) and CO_2/CH_4 (biogas) binary gas mixtures, according to the experimental conditions shown in Table 5.2, to make a more realistic assessment. Considering that the pressure of both CO_2/N_2 and CO_2/CH_4 (biogas) streams is relatively low, the pressure of the conducted experiments was set at 2 bar, and only the influence of temperature and RH in the feed gas stream was assessed. The results obtained for the gas permeation of CO_2/N_2 and CO_2/CH_4 gas mixture can be found in Figure 5.6 a) and b) and Figure 5.7 a) and b), respectively.

In what concerns the CO_2/N_2 separation (Figure 5.6), it can be seen that the CO_2 permeability and selectivity at a CO_2 feed composition of 15 vol% were lower (216 Barrer and selectivity of 13) than those obtained with pure gas stream (240 Barrer and selectivity of 26), due to competitive sorption effects. A similar behaviour was obtained for the CO_2/CH_4 separation with a decrease in CO_2 permeability from 312 (selectivity of 13) to 301 Barrer (selectivity of 10), when the CO_2 feed composition decreased from 100 to 40 vol%, respectively. For both separations, the results obtained for the MMIM containing 10wt% Cu(BTC) were considerably higher than those obtained for the neat PEGDA-80 TFSI iongel membranes, under the same experimental conditions.[281] For instance, at 15 vol% CO_2, the CO_2 permeability of the PEGDA-80 TFSI iongel membrane reached 115 Barrer in the CO_2/N_2 mixture, which increased 87% (up to 216 Barrer) after the incorporation of Cu(BTC), while maintaining a similar selectivity (13). For the CO_2/CH_4 separation an increase in permeability of 45% (up to 301) was also observed, without sacrificing gas selectivity (around 10).

Looking at Figure 5.6, it can be seen that the presence of RH in the gas stream also had a significant impact on the permeability and selectivity. At a RH = 11 vol%, the CO_2 permeability substantially increased from 216 Barrer under dry conditions to 412 Barrer. This value was significantly higher than that obtained for the neat PEGDA-80 TFSI iongel (180 Barrer).[281] The high hydrophilic character of the PEGDA-80 TFSI-10 Cu(BTC) iongel membrane allowed for a high swelling degree of

the membrane, meaning a higher water-induced plasticization could occur. As a result, gas molecules diffused much faster and indiscriminately across the membrane. However, since CO_2 is the smallest gas molecule, its diffusion rate was not as affected by the presence of humidity as those of larger molecules, such as N_2, leading to the observed decrease in selectivity from 13 to 10. The same conclusions were drawn from the results obtained for the CO_2/CH_4 separation, where the CO_2 permeability increased from 301 to 409 Barrer, while the selectivity decreased from 10 to 7.

Additionally, considering the temperature conditions of a flue gas stream, the influence of this parameter was also studied for the CO_2/N_2 binary gas mixture, under dry conditions and 15 vol% CO_2 in the feed stream (Figure 5.6). It was found that the CO_2 permeability increased from 216 to 239 Barrer, when the temperature was raised to 353 K, while the selectivity slightly decreased from 13 to 11. It is known that temperature has opposite effects on the gas permeability. On one hand, an increase in temperature has a negative impact on gas solubility, while the gas diffusivity tends to increase, due to a higher kinetic energy of the molecules. Considering that the CO_2 permeability increased with increasing temperature, it can be concluded that the gas transport on the iongel membrane was more diffusion-controlled at higher temperatures. [266,269] It should be mentioned that, since the pressure of the flue gas and biogas streams is relatively low, the influence of different experimental pressures was not studied in this work.

For both separations, it was concluded that the separation performance of the MMIMs containing 10 wt% Cu(BTC) was considerably affected by the experimental conditions, emphasizing the relevance of studying different parameters, such as temperature and RH. Nonetheless, in all cases, the MMIM showed better separation performances than the neat PEGDA-80 TFSI iongel, with an improvement in CO_2 permeability with minimal or zero sacrifice of gas selectivity.

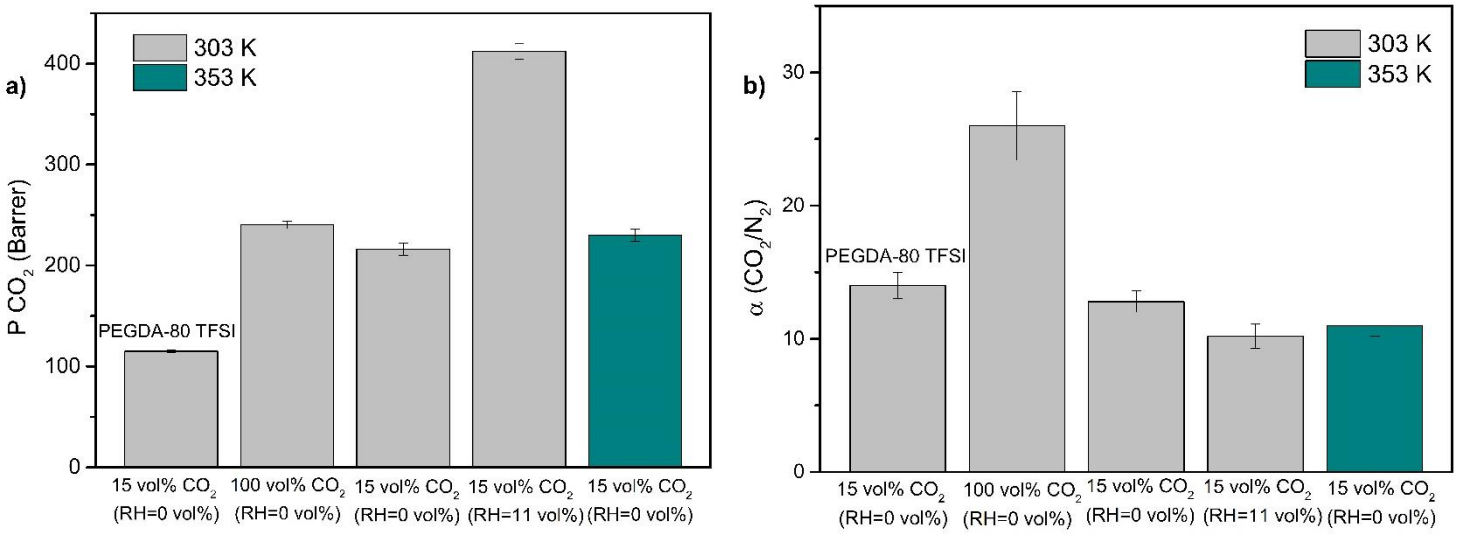

Figure 5.6 - (a) CO_2 permeability and (b) CO_2/N_2 selectivity of the neat PEGDA-80 TFSI iongel (for comparison) and MMIM containing 10 wt% Cu(BTC), at 2 bar and different experimental conditions of temperature and RH.

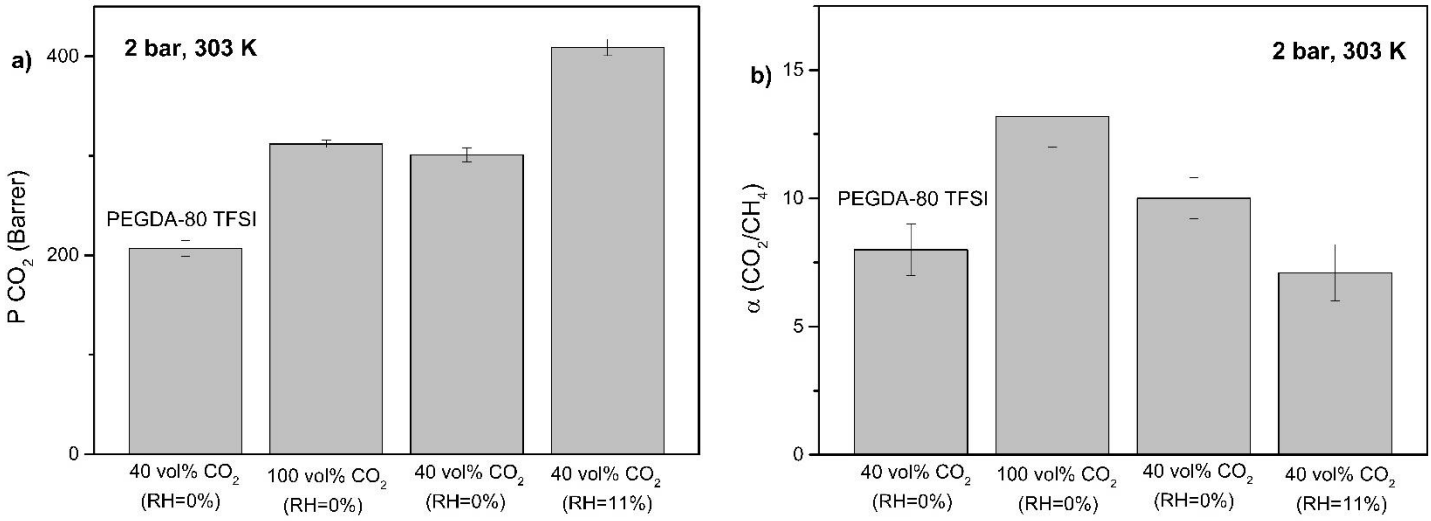

Figure 5.7 - (a) CO_2 permeability and (b) CO_2/CH_4 selectivity of the neat PEGDA-80 TFSI iongel (for comparison) and MMIM containing 10 wt% Cu(BTC), at 2 bar and different experimental conditions of RH.

5.4 Conclusions

The MOFs Cu(BTC), MIL-53 and MOF-177 were successfully used to develop MMIMs with loadings up to 10 wt% by a solvent-free UV polymerization. The high IL content (80 wt%) allowed the preparation of iongel membranes without defects or the formation of unselective voids, which is a challenge in the fabrication of mixed matrix membranes containing inorganic or partially inorganic solid particles. The presence of MOF particles contributes to an increased brittleness of the membranes, except for the MMIMs containing MIL-53, which become more resistant in terms of puncture strength. All the MMIMs showed suitable thermal stability for the proposed gas separation applications. From the pure gas permeation experiments with CO_2, N_2 and CH_4 at 0.7 bar and 303 K, it was found that the CO_2 adsorption capacity and porosity parameters of each MOF play an important role in the separation performance, since different behaviours were observed when increasing the MOF loading into the iongel structure. The MMIMs containing 10 wt% Cu(BTC) disclosed the best compromise between CO_2 permeability (290 Barrer) and ideal selectivity (29 for CO_2/N_2 and 19 for CO_2/CH_4), for both separations. Gas mixture permeation experiments were also carried out to make a more realistic assessment of the potential of the PEGDA-80 TFSI-10 Cu(BTC) MMIM. It was found that the CO_2 permeability markedly increased in the presence of 11vol% RH, from 301 and 216 Barrer under dry conditions to 409 and 412 Barrer for the CO_2/N_2 and CO_2/CH_4 gas mixtures, respectively. Moreover, the temperature (303-353 K) also showed to have an important effect on the CO_2/N_2 separation, with an increase in CO_2 permeability from 216 to 239 Barrer, and similar selectivities. Overall, the MMIM containing 10 wt% Cu(BTC) showed

higher CO_2 permeabilities, for both separations, than those obtained for the neat PEGDA-80 TFSI iongel membrane, without compromising the selectivity. This observation, along with the high thermal stability of MMIMs, indicates that the incorporation of MOFs, in particular Cu(BTC) represents an advantage in the design of iongel membranes for gas separation.

6

POLY(IONIC LIQUID)-BASED SEMI-INTERPENETRATING POLYMER NETWORKS IN THE DEVELOPMENT OF MIXED MATRIX IONGEL MEMBRANES FOR CO_2 SEPARATION

This chapter is part of the following publication: Ana R. Nabais, Vítor D. Alves, David Mecerreyes, João G. Crespo, Luísa A. Neves and Liliana C. Tomé, "Poly(ionic liquid)-based semi-interpenetrating polymer networks in the development of mixed matrix iongel membranes for CO_2 separation" (under preparation)

Summary

In this work, new semi-interpenetrating polymer networks (sIPNs) based on poly(ionic liquid)s (PILs) and a non-ionic polymer network (poly(ethylene glycol) diacrylate, PEGDA) were used in the design of iongel membranes for gas separation applications. Three new PILs, based on poly(diallyldimethylammonium) (PDADMA) and the monomers sulfonyl(trifluoromethane sulfonyl)imide methacrylate ($[MTFSI]^-$), sulfopropyl methacrylate ($[MSPM]^-$) and 4-styrenesulfonate ($[MSS]^-$) as counter-anions, were first synthesized and then, mixed with PEGDA and 80 wt% of $[C_2mim][TFSI]$ IL. The resulting formulations were used to prepare iongels by free-radical UV polymerization and their film-forming ability was assessed. In order to obtain homogenous sIPN iongel materials, the PDAMA-MTFSI was selected and novel mixed matrix iongel membranes (MMIMs) were developed by incorporating different fillers. The influence of inorganic (nanoclay MMT), organic (azo-porous organic polymers – azo-POP-1 and azo-POP-11) and "hybrid" (metal organic frameworks – Cu(BTC) and MIL-53) materials on the CO_2/N_2 and CO_2/CH_4 separation performances of the prepared MMIMs was evaluated.

The use of an ionic polymer (PDADMA-MTFSI) contributed to a higher affinity of the resulting sIPN iongel membrane towards CO_2, compared to the results obtained when only employing a non-ionic

polymer network (PEGDA). Among all the fillers studied, Cu(BTC) (at 10 wt% loading) revealed the best compromise between permeability (319 Barrer) and selectivity (30 for CO_2/N_2 and 23 for CO_2/CH_4). This MMIM containing 10 wt% Cu(BTC) was further tested under mixed gas conditions, at experimental parameters close to those of flue gas and biogas streams. Temperature (303 K and 353K) and relative humidity (11 vol%) revealed to have a significant influence in the separation performance of the iongels, by increasing the CO_2 permeability, at the expense of gas selectivity.

6.1 Introduction

Different strategies have been used to develop highly functional and efficient membranes for gas separation. In this context, ionic liquids (ILs) have been deeply exploited due to their versatile and tunable properties.[2] The most explored strategy to prepare IL-based membranes was through the development of supported ionic liquid membranes (SILMs), where the IL is trapped inside the pores of a support by capillary forces. However, the challenges and drawbacks related to the stability of the IL inside the pores of the support led to the development of a different class of membranes, where poly(ionic liquid)s (PILs) are blended with free ILs to form PIL/IL composites.[2] This strategy allows for the preparation of IL-based membranes with enhanced CO_2 separation properties, while maintaining the stability of the IL inside the polymer matrix. Ideally, to maximize the separation performance, the IL content in PIL/IL composite membranes should be as high as possible.[93] However, it has been observed that, particularly through the solvent evaporation method, only a limited maximum amount of IL (between 40 and 60 wt%) can be blended with the linear PILs before the stability of the PIL/IL membrane started to be compromised.[105,107,110,114,207]

More recently, strategies such as the use of cross-linked iongels [59,199,288] and interpenetrating polymer networks (IPNs) have been explored to fabricate gas separation membranes with high IL contents (> 60 wt%).[289] The definition of an IPN presupposes two or more networks, which are partially interlaced, on a molecular scale, and cannot be separated, unless chemical bonds are broken. [290] Under this definition, there are different subclasses of IPN-derived materials, such as the case of semi-IPNs (sIPNs) comprising one or more polymer networks and one or more linear/branched polymer(s). These materials are characterized by the penetration, on a molecular scale, of at least one of the networks by at least some of the linear/branched chains. [290,291] The main idea behind the development of sIPNs is to combine the properties of each polymer species, while ideally overcoming some of their weaknesses.

The sIPN strategy has been used by different authors to develop gas separation membranes. Saimani *et al*.[292] prepared asymmetric sIPN membranes comprising poly(ether imide) (PEI) and poly(ethylene glycol) diacrylate (PEGDA). The PEI/PEGDA sIPNs reached selectivities comparable to the most selective material for CO_2/N_2 (PEGDA) and CO_2/CH_4 (PEI) gas pairs. The best results were achieved with a PEGDA content of 6 wt%, where CO_2/N_2 and CO_2/CH_4 selectivities reached 50 and 43, respectively, while a CO_2 permeance (ratio between permeability and membrane thickness) of 2.5 GPU was obtained.[292] Zhang *et al*.[293] incorporated linear polyvinyl acetate (PVAc) into a cross-linked PIL. It

was observed that an increase in the PIL content resulted in gradually higher gas permeabilities, reaching a CO_2 permeability of 36.1 Barrer and a CO_2/N_2 selectivity of 59.6 with 50 wt% PIL.[293] By entwining poly(ethylene oxide) (PEO) with linear polyimides, Kline *et al*.[294] develop sIPN membranes with improved mechanical stability, compared to that of the pure PEO membrane. The incorporation of PEO into the linear polyimides and utilizing low PEO networks crosslinking density represented an advantage for CO_2 permeability, as well as both CO_2/N_2 and CO_2/H_2 ideal selectivities.[294] Kim and co-workers[295] used poly(glycidylmethacrylate-g-polypropylene)-co-poly(oxyethylene methacrylate) (PGP-POEM) and Pebax®-1657 to develop sIPN. Compared to the neat Pebax®-1657 membrane, the sIPN of 40 wt% PGP-POEM showed an enhancement of 2.5 times in CO_2 permeability (reaching 237 Barrer) and similar CO_2/N_2 selectivity (around 39).[295] In a slightly different approach, Lee *et al*.[296] prepared thermally rearranged sIPN gas separation membranes by combining bismaleamic acid with hydroxyl polyimide. The authors observed an improvement in the plasticization resistance for the sIPN membranes, under high pressure and natural gas environments. Moreover, a CO_2 permeability of 4112 Barrer was achieved, with a CO_2/CH_4 ideal selectivity of 20.[296]

Even though the above-mentioned studies do not include the use of ILs, they certainly provide an insight into the potential of using sIPNs to prepare membranes for gas separation. On the other hand, Gouveia *et al*.[289] developed sIPN membranes containing different ILs. The sIPNs comprised PEO network and linear nitrile butadiene rubber (NBR), as well as up to 66 wt% of $[C_2mim][C(CN)_3]$, $[C_2mim][TFSI]$ and $[C_2mim][FSI]$ ILs. The highest CO_2/N_2 selectivity was achieved with the sIPN membrane combining the $[C_2mim][C(CN)_3]$ IL, while the one with $[C_2mim][FSI]$ IL showed the highest CO_2 and N_2 permeabilities. Additionally, at 66 wt% $[C_2mim][FSI]$ IL, the sIPN membrane reached a CO_2 permeability of 727 Barrer and a CO_2/H_2 selectivity of 11.[289]

Bearing in mind our previous works on iongel membranes comprised of $[C_2mim][TFSI]$ IL (60 to 80 wt%), PEGDA as polymer matrix, and different fillers (*i.e.* nanoclays [253] and azo-porous organic polymers [254]), in this work we develop sIPNs made of PDADMA poly(ionic liquid)s and PEGDA, to act as polymer matrix of iongels with 80 wt% of $[C_2mim][TFSI]$ IL. The combination of PEGDA with PDADMA poly(ionic liquid)s, bearing the sulfonyl(trifluoromethane sulfonyl)imide methacrylate - $[MTFSI]^-$, sulfopropyl methacrylate - $[MSPM]^-$ or 4-styrenesulfonate - $[MSS]^-$ counter-anions, is expected to improve the separation performance of the previously prepared PEGDA-based iongel membranes due to the ionic nature of the PIL and its affinity towards CO_2. First, the membrane forming ability, as well as the compatibility between the new synthesized PILs and the $[C_2mim][TFSI]$ IL, were studied. Afterwards, the best sIPN was characterized and used to prepare MMIMs containing different fillers. In particular, a nanoclay (MMT), two different azo-POPs (azo-POP-1 and azo-POP-11) and two metal organic frameworks (Cu(BTC) and MIL-53) were selected.[253,254] Pure CO_2, N_2 and CH_4 permeation experiments were performed and the best performing MMIM was also tested under mixed gas conditions, at experimental conditions close to reality for flue gas (CO_2/N_2) and biogas (CO_2/CH_4) streams.

6.2 Experimental Section

6.2.1 Materials

Poly(diallyldimethylammonium) chloride solution (PDADMA-Cl), average Mw 400,000–500,000 g mol^{-1}, 20 wt% in H_2O), poly(ethylene glycol) diacrylate (PEGDA, M_n 575 g mol^{-1}) and 2-hydroxy-2-methylpropiophenone (DAROCUR®, 97 wt% pure) were purchased by Sigma-Aldrich (Portugal). The IL 1-ethyl-3-methylimidazolium bis(trifluoromethylsulfonyl) imide ([C_2mim][TFSI], 99 wt% pure) was supplied by Iolitec GmbH (Germany). The metal organic frameworks (MOFs), Cu(BTC) and MIL-53(Al) were synthesized by BASF SE (Germany) and supplied by Sigma Aldrich (Portugal) as Basolite® C300 and Basolite® A100, respectively. The nanoclay Nanomer® I.34TCN, montmorillonite (MMT) clay surface modified with 25–30 wt% methyl dihydroxyethyl hydrogenated tallow ammonium was obtained from Sigma-Aldrich (Portugal). The azo-porous organic polymers, Azo-POP-1 and azo-POP-11, were synthesized according to a previously described procedure.[254]

Lithium sulfonyl(trifluoromethane sulfonyl)imide methacrylate (LiMTFSI) was supplied by Specific Polymers (France), while the 3-sulfopropyl methacrylate potassium (KSPM) salt and the sodium 4-styrenesulfonate (NaSS) were provided by Sigma-Aldrich (Spain).

Carbon dioxide, CO_2 (99.998% purity), nitrogen, N_2 (99.99% purity) methane, CH_4 (99.99% purity) and helium, He (>99% purity) gases were supplied by Praxair (Portugal).

6.2.2 Synthesis of Poly(ionic liquid)s (PILs)

Three different PILs were synthesized, bearing the poly(diallyldimethylammonium) (PDADMA) as polycation, and different monomers as counter-anions, namely sulfonyl(trifluoromethane sulfonyl)imide methacrylate - $[MTFSI]^-$, 3-sulfopropyl methacrylate - $[MSPM]^-$ or 4-styrenesulfonate - $[MSS]^-$.

The PDADMA-MTFSI was synthesized through an ion exchange reaction in water. First, 3 g of lithium sulfonyl(trifluoromethane sulfonyl) imide methacrylate salt, LiMTFSI, and 7 g of the poly(diallyldimethylammonium chloride), PDADMA-Cl solution were dissolved, in 9 and 7 mL of distilled water, respectively. Afterwards, the LiMTFSI aqueous solution was dropwise added to the PDADMA-Cl solution, under constant stirring. The resulting PIL (*i.e.* PDADMA-MTFSI), immediately started to precipitate. The solution containing the PDADMA-MTFSI was left stirring for 1 hour and then filtered under vacuum and washed with water. The obtained solid polymer was re-dissolved in acetone, then re-precipitated in water, filtered under vacuum, and dried overnight at 303 K.

Regarding the synthesis of PDADMA-MSPM, 3 g of potassium 3-sulfopropyl methacrylate salt (KSPM) were dissolved in 50 mL of methanol. Simultaneously, 2 g of PDADMA-Cl were dissolved in 40 mL of methanol. The solutions were mixed and kept under stirring at room temperature for 3 hours. The methanol was then evaporated by rotary evaporation at 303 K and 100 mL of ethanol was added. The resulting solution was stirred until complete polymer dissolution was obtained. This final solution was

kept in a fridge overnight and then filtered under vacuum to separate the KCl. The excess of ethanol was evaporated by rotary evaporation until complete polymer precipitation. The remaining solvent was removed with N_2 flow. Finally, the obtained solid PDADMA-MSPM was dried under vacuum at room temperature.

The synthesis of PDADMA-MSS started by dissolving 2 g of sodium 4-styrenesulfonate (NaSS) in 70 mL of methanol and 2 g of PDADMA-Cl in 40 mL of the same solvent. The solutions were mixed together and kept stirring at room temperature for 3 hours. Methanol was evaporated by rotary evaporation at 303 K. Afterwards, 100 mL of ethanol were added, and the solution remained stirring overnight to achieve complete polymer dissolution. The solution was kept in a fridge overnight to precipitate the NaCl and centrifugated twice (at 1200 rpm and 277 K, for 45 min) to separate the NaCl precipitated. The ethanol was evaporated by rotary evaporation and the obtained PDADMA-MSS was dried under vacuum at room temperature.

To confirm the chemical structure of the obtained PILs, Fourier Transform Infrared-Attenuated Total Reflectance spectroscopy (FTIR-ATR) and Nuclear Magnetic Resonance (^{1}H-NMR) were performed. The results are presented in Appendix D (Figure D.1 and Figure D.2-D.4, respectively). The chemical structures of the synthesized PILs with different monomers as counter-anions are illustrated in Figure 6.1.

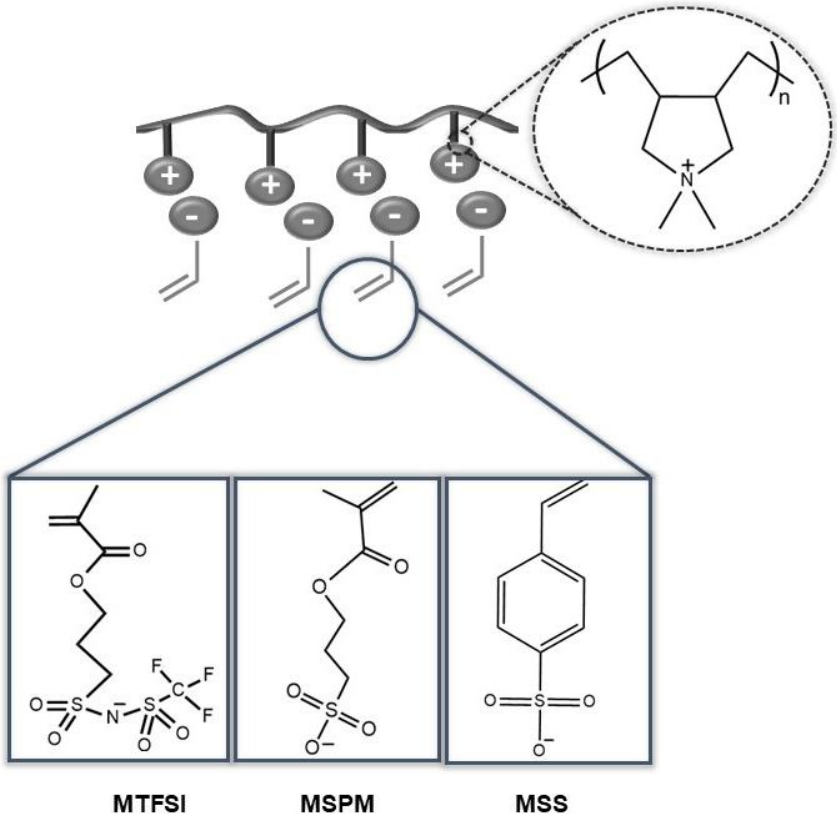

Figure 6.1 - Schematic representation of the synthesized poly(ionic liquid)s (PILs) comprised of PDADMA and different monomers as counter-anions.

6.2.3 Preparation of PIL-based sIPN Iongel Membranes

With the intent of preparing sIPN iongel membranes, 20 wt% of each PIL was dissolved in the appropriate solvent, that is 3% (w/v) ethanol for PDADMA-MSPM and PDADMA-MSS, and 20% (w/v) acetonitrile for PDADMA-MTFSI. After complete PIL dissolution, 80 wt% [C_2mim][TFSI] IL and 20 wt% PEGDA (relative to the PIL weight) were added to the PIL solution. During the addition of IL/PEGDA to both the PDADMA-MSPM and PDADMA-MSS solutions, an immediate precipitation was observed (see Figure D.5 and Figure D.6, Appendix D). This might be attributed to the occurrence of ion exchanges reactions between the SO_3^- groups of the PILs and the $[TFSI]^-$ anion of the IL. Considering that the resulting PILs, now containing the $[TFSI]^-$ as counter-anion, are insoluble in ethanol, they precipitated as white solids in the solution. In view of this, the ethanol was left to evaporate, and the resulting powders were redissolved in acetonitrile. Then, 3 wt% of photoinitiator DAROCUR® was added and the formulations were exposed to UV light (wavelength of 365 nm^{-1} and intensity of 1.8 mW cm^{-2}) for 10 minutes. However, it was not possible to prepare solid iongel membranes, since only liquid/gel-like materials were obtained (see Figure D.5 and Figure D.6, Appendix D).

In what concerns the PDADMA-MTFSI solution, it was mixed with the IL/PEGDA solution and left stirring without any evidence of the formation of solid precipitate. The acetonitrile solution was left to evaporate until a viscous solution was obtained and then 3 wt% of photoinitiator DAROCUR® was added. The final solution was casted between two Rain-X™-coated quartz plates, with a spacer in between with a thickness of around 100 µm, and exposed to the same UV light for 10 min. In this case, a free-standing iongel was obtained. Therefore, the PDADMA-MTFSI based sIPN system was selected to further design mixed matrix iongel membranes (MMIMs) by the incorporation of different fillers. Note that the neat PDADMA-MTFSI/PEGDA sIPN iongel membrane containing 80 wt% [C_2mim][TFSI] IL is designated as “sIPN-80 IL” throughout the manuscript and its preparation is illustrated in Figure 6.2.

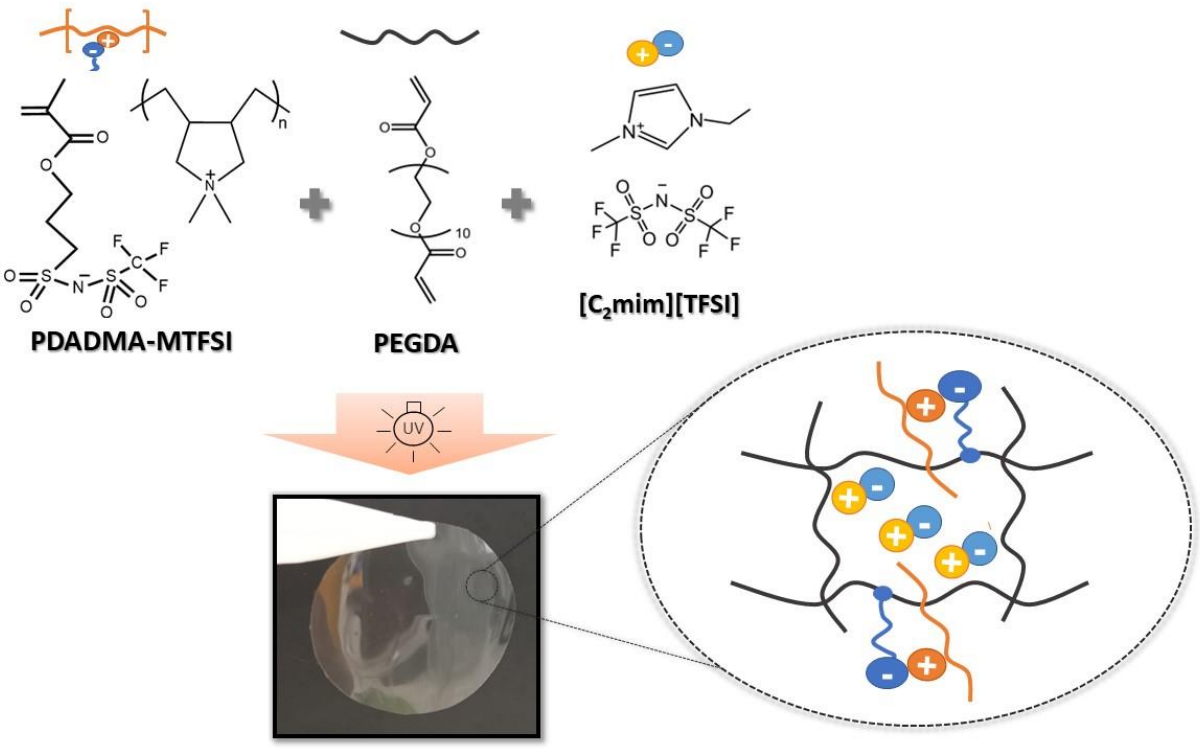

Figure 6.2 - Schematic representation of the preparation and structure of the sIPN-80 IL iongel membrane.

6.2.4 Preparation of Mixed Matrix Iongel Membranes (MMIMs)

The MMIMs were prepared using diverse fillers at different loadings. Regarding the incorporation of azo-POPs, the MMIMs were prepared containing 0.5 wt% of azo-POP-1 and azo-POP-11, to make a direct comparison with the results obtained in our previous works.[254] The azo-POP loading was then increased to 5 wt%, which was found to be the maximum amount of azo-POP that can be dispersed in the IL. For the MOF-containing MMIMs, Cu(BTC) and MIL-53 were selected and a loading of 5 wt% was first used to make a direct comparison with the PEGDA-based iongels containing the same MOFs, previously studied.[297] In particular, the loading of Cu(BTC) in the MMIMs was then increased to 10 wt% (maximum loading) to evaluate the influence in the separation performance of the materials. On the other hand, the MIL-53 loading was set at only 5 wt% to prepare the MMIMs, since higher loadings resulted in a poor dispersion of the particles and created visible agglomerates in the membrane. The MMT loading was also set at 5 wt%, in order to make a direct comparison between all the different fillers studied in this work.

The MMIMs were prepared by free-radical UV polymerization. First, 20 wt% of PDADMA-MTFSI was dissolved in 20% (w/v) of acetonitrile and left stirring until complete dissolution. Simultaneously, the respective loading of each filler was dispersed in 80 wt% [C_2mim][TFSI] IL, and left stirring overnight to obtain an homogeneous solution. Then, 20 wt% of PEGDA (relative to the PDADMA-MTFSI weight) was added to the IL/filler solutions and left stirring. After a homogeneous solution was obtained, the PIL

solution in acetonitrile was mixed with the IL/filler/PEGDA mixture. The obtained solution was left to evaporate the excess of acetonitrile, under stirring, until a viscous solution was obtained. Around 3 wt% of photoinitiator DAROCUR® was added to the solution before casting. The final solutions were poured on top of a pre-wetted porous polyamide (PA) filter (Sartorius™, supplied by Fisher Scientific) with a pore size of 0.22 µm. Note that the support was immersed in deionized water, prior to casting, to minimize the pore filling from the iongel solution into the porous support. The iongel solution/support system was closed between two Rain-X™-coated quartz plates, with a spacer in between to ensure a homogeneous thickness of around 100 µm. The final assembly was placed under a UV light with a wavelength of 365 nm^{-1} and intensity of 1.8 mW cm^{-2}, for 10 minutes. The obtained composite MMIMs were then dried at 333 K to remove the water trapped inside the support. Therefore, it was considered that the results obtained from the gas permeation experiments correspond solely to the iongel dense layer.

6.2.5 Membrane Characterization

6.2.5.1 Scanning Electron Microscopy (SEM)

Images of the cross-section of the prepared sIPN-80 IL membrane and MMIMs were acquired with a JEOL 7001F scanning electron microscope (FEG-SEM), with an electron beam intensity of 10 kV. The iongel samples were coated with a thin Pd/Au conductive layer, to induce charge under the electron beam.

6.2.5.2 Fourier Transform Infrared-Attenuated Total Reflectance spectroscopy (FTIR-ATR)

The FTIR-ATR spectroscopy analysis was performed to confirm the chemical structure of the PIL PDADMA-MTFSI, [C_2mim][TFSI] IL, PEGDA, and sIPN-80 IL iongel and respective MMIMs. This analysis was also used to verify the occurrence of the polymerization reaction in the sIPN-80 IL membrane and to determine if there were any interactions being established between the different iongel components. The FTIR spectra were obtained using a Perkin Elmer Spectrum Two spectrometer, that collected 10 scans from 4000 to 400 cm^{-1}.

6.2.5.3 Contact Angles Measurements

The water contact angle of the sIPN-80 IL iongel membrane and MMIMs were measured to evaluate the hydrophilicity of the material. The contact angles were measured by manually depositing a drop of distilled water on the iongel's surface. Three different samples were used, and, for each sample, 10 frames were acquired in 1 second intervals. The frames were processed by a CAM100 (KSV

Instruments LTD, Finland) software. The drop shape was fitted to mathematical equations and the mean water contact angle was obtained.

6.2.5.4 Mechanical Properties

The mechanical properties of the neat sIPN-80 IL iongel and MMIMs were determined by puncture tests. The tests were carried out using a TA XT Plus Texture Analyzer (Stable Micro Systems, Godalming, UK) by puncturing each membrane through a hole (diameter of 10 mm) with a cylindrical probe with 2 mm of diameter at a rate of 1 mm s^{-1}, at room temperature. The puncture strength was determined according to Equation (6.1)

$$\sigma = \frac{F}{A} \tag{6.1}$$

where σ is the puncture strength (Pa), F is the maximum force applied by the probe (N) and A is the cross-sectional area of the probe (m^2). To compare the results without the influence of the iongel thickness, the puncture strength was normalized following Equation (6.2)

$$\sigma_n = \frac{\sigma}{l} \tag{6.2}$$

where σ_n is the normalized puncture strength (MPa mm^{-1}) and l is the thickness (100 µm) of the iongel (mm). The elongation at break given by Equation (6.3) was also determined.

$$\varepsilon\,(\%) = \left(\frac{\sqrt{h^2 - d^2} - h}{h}\right) \times 100 \tag{6.3}$$

where ε is the elongation at break (%), h is the radius of the iongel exposed in the cylindrical hole of the sample holder (mm) and d is the distance of the probe from the point of contact to the point of puncture (mm). For each sample, at least three replicates were performed and the mean values of puncture strength and elongation at break are reported.

6.2.5.5 Pure Gas Permeation Experiments

Single gas permeation experiments were carried out for CO_2, N_2 and CH_4, using a gas permeation setup described elsewhere.[16] The experiments were performed at 303 K, by placing the permeation cell in a water bath where the temperature was controlled by a thermostat (Corio C, Julabo, Germany). The permeation cell, composed by two compartments (feed and permeate), was first pressurized with the pure gas to be tested and, once the pressure was stabilized, the experiments began by applying a transmembrane pressure difference of around 0.7 bar. The pressure of each cell

compartment, over time, was measured by two transducers (Jumo type 404327, Germany), and recorded by the PicoLog software.

The data collected throughout the experiment allowed for the determination of the permeability of the iongel membranes, according to the following equation:

$$\frac{1}{\beta} \times \ln\left(\frac{\Delta p_0}{\Delta p}\right) = P \times \frac{t}{l} \tag{6.4}$$

where Δp_0 and Δp (bar) are the pressure variations in the feed and permeate compartments at the beginning of the experiment and over time, respectively, P is the permeability of the iongel ($m^2\ s^{-1}$, where 1 Barrer = 1×10^{-10} cm^3 (STP) cm $cm^{-2}\ s^{-1}\ cmHg^{-1}$ = 8.3×10^{-13} $m^2\ s^{-1}$), t is the time (s), l is the thickness of the iongel layer (m) and β is the geometric parameter of the cell (m^{-1}), given by:

$$\beta = A\left(\frac{1}{V_{feed}} + \frac{1}{V_{perm}}\right) \tag{6.5}$$

where A is the membrane area (m^2), V_{feed} and V_{perm} represent the volumes of the feed and permeate compartments (m^3), respectively. The permeability of the membranes was obtained from the slope when plotting $1/\beta\ ln(\Delta p_0/\Delta p)$ as a function of t/l. The ideal selectivity of the iongel is given by:

$$\alpha_{A/B} = \frac{P_A}{P_B} \tag{6.6}$$

where α is the ideal selectivity, P_A and P_B are the permeabilities of the most and least permeable gas species, respectively.

6.2.5.6 Gas Mixtures Permeation Experiments

Binary gas mixtures experiments for CO_2/N_2 and CO_2/CH_4 mixtures were carried out to determine the permeability and selectivity of the prepared membranes. The experiments were carried out at different conditions,[297] depending on the gas pair, to mimic, as much as possible, the real conditions of a flue gas (CO_2/N_2) and biogas (CO_2/CH_4) streams. For CO_2/N_2, the experiments were carried out at 2 bar of pressure and temperature between 303-353 K with 15 vol% of CO_2 in feed, while for CO_2/CH_4, the experiments were conducted at 2 bar and 303 K, at 40 vol% CO_2 in feed stream. Moreover, for both gas streams, the effect of a RH of 11 vol% in the feed gas stream was also assessed. Since the pressure of both gas streams is relatively low, the influence of this parameter was not considered in this work, and the experimental pressure was set at 2 bar.

A schematic representation of the experimental setup and a detailed description of the procedure can be found elsewhere.[281] The experimental apparatus is composed by a stainless-steel cell divided in two identical compartments, defined as feed and permeate, and the membrane to be tested is placed in between. The membrane module is placed inside an oven (Venticell MMM, Germany) with controlled temperature (TC). Retentate and permeate concentrations were analyzed using an Agilent gas chromatograph (GC) 7890B, where He was used as the gas carrier, equipped with a thermal conductivity detector (TCD), maintained at 473 K. The experiments were carried out until a constant permeate flow and composition were achieved. The permeability of each gas was calculated according to the following equations:

$$j_i = \frac{F^f_{total} \cdot y^f_i}{A} \tag{6.7}$$

$$\Delta p_i = p^f \cdot y_i^f - p^p \cdot y_i^p \tag{6.8}$$

$$P_i = \frac{j_i \cdot L}{\Delta p_i} \tag{6.9}$$

where j_i is the molar flux of gas i (mol m^{-2} s^{-1}), F is the gas molar flow rate (mol s^{-1}), y^f and y^p are the gas molar fractions on the feed and permeate side, respectively, A is the membrane area (m^2), Δp represents the driving force between feed and permeate sides (Pa), p^f and p^p are the pressures (Pa) in the feed and permeate sides, respectively, l is the thickness of the iongel layer (m) and P is the membrane permeability for gas i (mol m^{-1} Pa^{-1} s^{-1}).

6.3 Results and Discussion

6.3.1 SEM

Figure 6.3 displays the SEM cross-sectional images of the sIPN-80 IL iongel membrane and respective MMIMs containing the highest loading of each filler. The SEM surface images can be found in Figure D.7 of Appendix D. The sIPN-80 IL iongel membrane presented a smooth and defect-free structure, demonstrating the compatibility between the sIPN matrix and the IL. The MMIMs presented different morphologies, depending on the filler incorporated. The cross-sectional images of the MMIMs containing 5 wt% of azo-POP-1 and azo-POP-11presented less smooth morphologies, especially in the case of azo-POP-11. Considering that azo-POPs are entirely organic (composed mainly of N and C atoms), these materials are significantly lightweight. Consequently, these fillers occupied more volume in the solution, when compared to the MMT or MOFs and thus, were more prone to form some agglomerates. Oppositely, the SEM images of the MMIMs containing MOFs showed a smoother cross-section, particularly for Cu(BTC), even at the highest loading (10 wt%).

The reliefs observed in the structures of the different MMIMs were caused by the freezing under liquid nitrogen, during the sample preparation.

In all cases, dense morphologies were obtained, without observable defects, which was mainly attributed to the good compatibility between the material components.

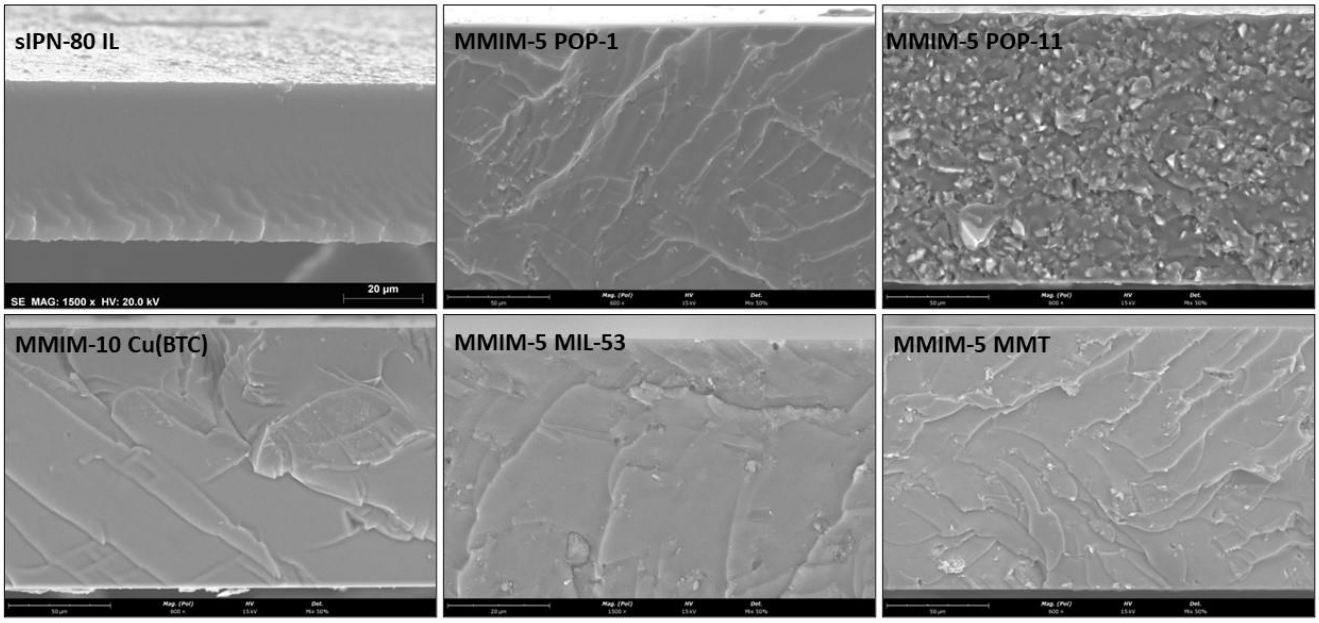

Figure 6.3 - SEM cross-section images of the neat sIPN-80 IL iongel and MMIMs containing different fillers.

6.3.2 FTIR-ATR

The FTIR-ATR spectra of the neat sIPN-80 IL membrane and its starting materials can be found in Figure 6.4 a), while the spectra of the different MMIMs are shown in Figure 6.4 b). The detailed descriptions of the spectra obtained for PEGDA, [C_2mim][TFSI] IL, MMT, azo-POPs and MOFs have been previously reported.[253,254,297]

Regarding the PDADMA-MTFSI spectra, the band at around 2940 cm^{-1} originated from the polycation backbone, while the peak at 1711 cm^{-1} corresponded to the C=O stretching. The peak at 1634 cm^{-1} was be attributed to the methacrylate group, and the peaks between 1310 and 1044 cm^{-1} were attributed to the C-F stretching vibrations arising from the counter-anion.

Several characteristic peaks of the starting materials can be observed in the spectrum of sIPN-80 IL (Figure 6.4 a)). The peaks at 1050 and 509 cm^{-1} corresponded to the [C_2mim][TFSI] IL, while the peaks observed at 1714 and 609 were attributed to the presence of the PDADMA-MTFSI.

Additionally, the absence of the peak at around 1634 and 1619 cm^{-1} in this spectrum confirmed the high degree of polymerization of the polymer networks.

From Figure 6.4 b), it is not possible to clearly distinguish all the characteristic peaks of the fillers in the analyzed MMIMs, due to overlapping and the low concentration of fillers, particularly in the

case of azo-POPs. Nonetheless, the influence of MMT in the MMIM-5 MMT iongel spectrum can be observed at 1090 and 450 cm^{-1}, while the small peaks at 1640 and 1630 cm^{-1} in the MMIM-10 Cu(BTC) and MMIM-5 MIL-53 spectra, confirming the presence of the respective MOFs in the iongel membrane. Similar to the sIPN-80 IL, the absence of the peak at around 1634 and 1619 cm^{-1} in the spectra of MMIMs also confirmed the high degree of the polymerization reaction.

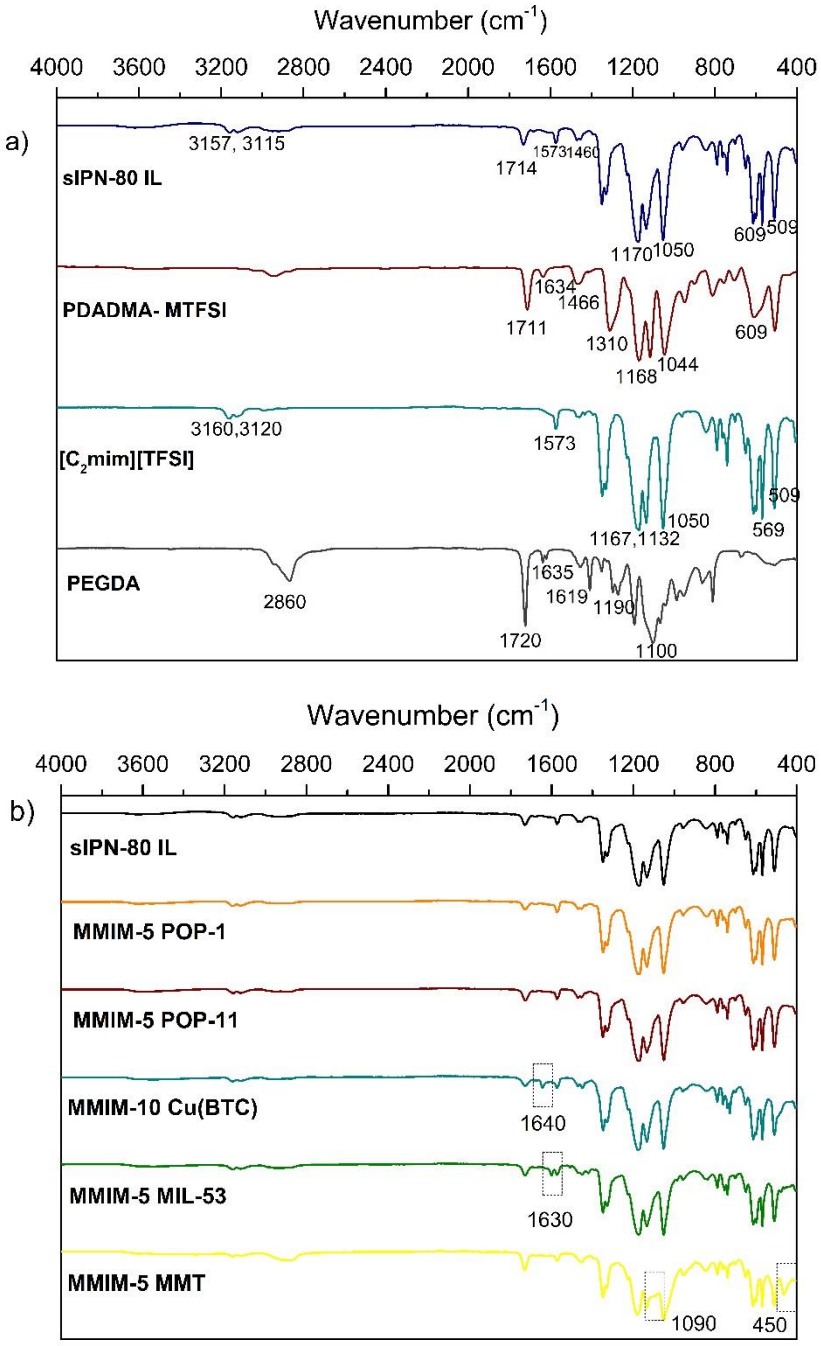

Figure 6.4 - FTIR-ATR spectra of the (a) starting materials and neat sIPN-80 IL membrane and (b) MMIMs containing different fillers.

6.3.3 Contact Angles Measurements

The mean contact angles obtained for the neat sIPN-80 IL and respective MMIMs containing different fillers are presented in Table 6.1. The contact angle for the sIPN-80 IL reached 40.4°, indicating the hydrophilic character of the material. Moreover, the sIPN-80 IL iongel revealed a more hydrophilic character, when compared to the results previously obtained for the PEGDA-80 TFSI membrane (61.9°).[254] The prepared MMIMs also presented a hydrophilic nature, with mean contact angles below 40°, and below that of the neat sIPN-80 IL, probably due to the hydrophilicity of the different fillers. The increase in the filler loading increased the hydrophilicity of the MMIMs. The MMIM-10 Cu(BTC) showed the highest hydrophilicity, with a mean contact angle of 34.2°. All the MMIMs presented in Table 6.1 showed lower contact angles than those observed for the iongel membranes combining only PEGDA as polymer matrix and MMT,[253] azo-POPs,[254] and MOFs.[297] The more hydrophilic nature of the sIPN-based iongel membranes can be an advantage regarding their gas separation performance, since CO_2 has a higher solubility in hydrophilic materials than in more hydrophobic ones.[183]

Table 6.1 - Contact angles obtained for all the iongel membranes prepared in this work.

Membrane Sample	Mean Contact Angle (°)
sIPN-80 IL	40.4 ± 0.9
MMIM-0.5 POP-1	37.5 ± 0.3
MMIM-5 POP-1	35.6 ± 0.4
MMIM-0.5 POP-11	38.2 ± 0.3
MMIM-5 POP-11	36.7 ± 0.7
MMIM-5 Cu(BTC)	38.1 ± 0.6
MMIM-10 Cu(BTC)	34.2 ± 0.5
MMIM-5 MIL-53	37.8 ± 0.2
MMIM-5 MMT	39.8 ± 0.2

6.3.4 Mechanical Properties

Even though the sIPN-based iongel membranes prepared in this work were tested in gas permeation experiments with a porous polyamide support (with a pore size of 0.2 µm), the mechanical properties of the self-standing membranes, with a thickness of around 100 µm, were determined, to understand the influence of the different fillers.

The normalized puncture strength (considering a membrane thickness around 100 µm) and elongation at break of all the prepared sIPN-based iongel membranes are provided in Table 6.2. The puncture strength obtained for the neat sIPN-80 IL iongel was quite low (0.8 MPa mm^{-1}) and lower than the value for the PEGDA-80 TFSI iongel (3.1 MPa mm^{-1}), even though it presented a higher flexibility (elongation at break of 35.5 %, opposed to 19.0).[297] The increased elongation resulted from the well interpenetrated PEGDA and PDADMA-MTFSI network. It is interesting to observe that the puncture

strength of the MMIMs generally increased upon the incorporation of the different fillers. Similar behaviours were also observed for MMIMs containing MMT[253] and MIL-53.[297] In fact, these two fillers provided the highest puncture strength, among all the prepared MMIMs. It is known that the incorporation of fillers in a polymer matrix usually results in poorer mechanical properties.[298,299] However, such behaviour was not observed for the iongel membranes reported herein. Given the fragility of the neat sIPN-80 IL iongel, it is possible that the different fillers acted as a reinforcement of the mechanical stability of the membranes, by creating a more cohesive structure. In addition, it shows that the solid particles were well dispersed throughout the iongel matrix, without the creation of weak spots. Conversely, the incorporation of the different fillers also resulted in lower elongation at break. This means that, even though the MMIMs were more resistant to applied external forces, they were also less flexible, since the internal cohesion was higher.

Overall, it can be concluded that the addition of different fillers in the sIPN-80 IL iongel poses an advantage in terms of the membrane mechanical stability.

Table 6.2 - Normalized puncture strength and elongation at break obtained for all the iongel membranes prepared in this work.

Membrane Sample	Normalized Puncture Strength (MPa mm^{-1})	Elongation at Break (%)
sIPN-80 IL	0.8 ± 0.1	35.5 ± 0.1
MMIM-0.5 POP-1	1.7 ± 0.2	10.3 ± 1.1
MMIM-5 POP-1	1.9 ± 0.1	10.8 ± 0.7
MMIM-0.5 POP-11	0.7 ± 0.2	3.8 ± 0.9
MMIM-5 POP-11	1.1 ± 0.1	4.7 ± 0.3
MMIM-5 Cu(BTC)	1.9 ± 0.1	6.5 ± 0.2
MMIM-10 Cu(BTC)	2.0 ± 0.2	4.0 ± 0.3
MMIM-5 MIL-53	2.8 ± 0.2	9.5 ± 0.8
MMIM-5 MMT	2.3 ± 0.3	3.0 ± 1.1

6.3.5 Pure gas permeation experiments

Table 6.3 presents the results obtained from the pure gas permeation experiments, for the CO_2/N_2 and CO_2/CH_4 separations. To make a more direct comparison between the results and evaluate the overall performance of the MMIMs, the experimental data was plotted against the respective Robeson upper bounds (Figure 6.5 a) and b)).

The neat sIPN-80 IL membranes presented a CO_2 permeability of 122 Barrer, and CO_2/N_2 and CO_2/CH_4 ideal selectivities of 17 and 10, respectively. Compared to the iongel membrane composed of only the non-ionic polymer network PEGDA,[254] the use of PDADMA-MTFSI represents a clear advantage in terms of gas separation, since the permeability increased almost twice, from 62 to 122 Barrer.[254] The ionic nature of the PIL, along with the presence of the fluorinated $[TFSI]^-$ counter-anion

structure, which is the same as the one present in the IL, contributed to a higher affinity of the iongel towards CO_2, leading to the observed increase in permeability. Nevertheless, the CO_2/N_2 and CO_2/CH_4 ideal selectivities of the sIPN-80 IL were similar to those of the non-ionic PEGDA-80 TFSI iongel membrane.[254] The influence of the different fillers on the separation performance of the prepared MMIMs will be discussed in the following subsections, according to the type of filler.

6.3.5.1 Nanoclay MMT

In this work, 5 wt% MMT was used to prepare MMIMs, because it is possible to prevent the formation of large particles agglomerates at this concentration. At higher loadings, the particle agglomerations were more visible and influenced the iongel structure and the gas separation performance.

The MMIM containing 5 wt% MMT achieved a permeability of 219 Barrer, and CO_2/N_2 and CO_2/CH_4 ideal selectivities of 9 and 5, respectively. The CO_2 permeability suffered a significant increase, compared to the neat sIPN-80 IL membrane, but the CO_2/N_2 ideal selectivity decreased from around 17 to 9 and from 10 to 5 for CO_2/CH_4. Considering that the selected nanoclay MMT does not possess a significant affinity for CO_2,[253] it can be concluded that the incorporation of the nanoparticles had influence only in the diffusion of the gas molecules, while the effect on solubility was less pronounced. The presence of the solid non-porous particles increases the fractional free volume (FFV) of the polymer, leading to higher gas diffusion rates and, consequently, permeability. This effect was more pronounced for the larger molecules (N_2 and CH_4), resulting in lower ideal selectivities. Unlike what happened for the remaining MMIMs, the one containing 5 wt% MMT presented a lower ideal selectivity than the sIPN-80 IL membrane.

Overall, the separation performance of the MMIMs combining the sIPN and MMT was higher than that of the PEGDA and MMT iongel membranes, regardless of the MMT loading.[253]

6.3.5.2 Azo-POPs

Taking into account the previously obtained results,[254] azo-POP-1 and azo-POP-11 were selected to be incorporated into the sIPN-80 IL material. First, the 0.5 wt% loading provided the basis for comparison with the PEGDA iongel membranes previously developed.[254] An increase in the azo-POP loading from 0.5 to 5 wt% helped understanding the influence of the filler loading in the performance of the MMIMs.

For the MMIMs containing 0.5 wt% azo-POP the CO_2 permeability reached 151 Barrer for azo-POP-1 and 150 for azo-POP-11. In both cases, the CO_2 permeability was higher than those achieved with the PEGDA-based iongels, combining the same azo-POPs (91 and 80 Barrer, respectively), mainly due to the presence of the ionic PDADMA-MTFSI poly(ionic liquid). Conversely, the CO_2/N_2 ideal selectivity decreased (from 28 to 18 for azo-POP-1 and from 41 to 22 for azo-POP-11), while the

CO_2/CH_4 slightly increased in both cases (from 11 to 16 for azo-POP-1 and from 12 to 14) for azo-POP-11. [254]

When the azo-POP loading increased from 0.5 to 5 wt%, the CO_2 permeability also increased. For azo-POP-1, the CO_2 permeability increased from 151 to 197 Barrer, while the azo-POP-11 increased the CO_2 permeability from 150 to 330 Barrer. Additionally, the ideal selectivities also increased, for both gas pairs (Table 6.3), regardless of the azo-POP used. The higher CO_2 permeabilities and ideal selectivities were attributed to, on one hand, the increase in porosity due to the presence of the porous fillers, which provided higher gas diffusion rates through the iongel and also to the azo functional groups, which are known for their high affinity towards CO_2.[227,229,230,238,300] The highest CO_2 permeability was achieved for azo-POP-11 (330 Barrer), while the highest CO_2/N_2 and CO_2/CH_4 ideal selectivities were obtained at 5 wt% azo-POP-1 (28 and 20, respectively).

Looking at Figure 6.5 the best compromise between CO_2 permeability and ideal selectivity was obtained with the MMIMs containing 5 wt% azo-POP-1, since this experimental point falls closer to the upper bound, in both gas pairs separations.

6.3.5.3 MOFs

In what concerns the development of MMIMs containing MOFs, Cu(BTC) and MIL-53 were selected. Note that, in the case of MIL-53, it was not possible to increase the loading beyond 5 wt%, due to issues in the dispersion of the solid particles in the IL and the occurrence of agglomerations.

For the MMIMs combining Cu(BTC), and regardless of the loading, the CO_2 permeability as well as the ideal selectivities for both gas pairs (Table 6.3), were higher than the results obtained for the neat sIPN-80 IL membrane. The increase in Cu(BTC) loading from 5 to 10 wt%, led to an increase in CO_2 permeability from 269 to 319 Barrer, respectively. The ideal selectivities also increased, for both gas separations. Compared to our previous work,[297] the same 5 wt% Cu(BTC) loading, resulted in a higher separation performance, both in terms of CO_2 permeability and ideal selectivities. The CO_2 permeability increased from 251 to 269 Barrer, while the CO_2/N_2 and CO_2/CH_4 ideal selectivities increased from 21 to 24 and from 10 to 16, respectively, in the presence of the ionic polymer matrix.

The incorporation of 5 wt% MIL-53 increased the CO_2 permeability from 122 Barrer to 171 Barrer. Additionally, the ideal selectivities increased from 17 to 28 for CO_2/N_2 and from 10 to 17 for CO_2/CH_4. The same trend was observed previously in,[297] regarding the development of MMIMs based on PEGDA network, $[C_2mim][TFSI]$ IL and different MOFs (Cu(BTC), MIL-53 and MOF-177). Moreover, the results obtained for the MMIMs combining the sIPN and MIL-53 were higher, in terms of ideal selectivities, than those of the MMIMs composed of PEGDA,[297] with similar CO_2 permeabilities, probably due to the ionic character of the sIPN.

These improvements over the neat sIPN-80 IL membrane can be attributed to the porosity provided by the MOFs Cu(BTC) and MIL-53 (pore diameters of 9 Å and porous volume of 0.50 and 0.62 cm^3g^{-1}, respectively), and to the CO_2 quadrupole moment that induced strong interactions with the

hydroxyl groups located at the metal-oxygen-metal ligand of MIL-53 and the interactions between CO_2 and the Cu sites of Cu(BTC).

Looking at the results obtained for the MMIMs containing MOFs, it can be concluded that the one containing 10 wt% Cu(BTC) achieved the best separation performance, since it combines the best relation between permeability (319 Barrer) and ideal selectivities (30 and 23 for CO_2/N_2 and CO_2/CH_4 separations). In fact, the MMIM containing 10 wt% Cu(BTC) showed the best separation result among all the iongel membranes prepared, being the one that falls closer to both Robeson upper bounds (Figure 6.5).

Table 6.3 - CO_2 permeabilities and CO_2/N_2 and CO_2/CH_4 ideal selectivities of the prepared iongel membranes.

Membrane Sample	*P* CO_2 (Barrer)	*α* (CO_2/N_2)	*α* (CO_2/CH_4)
sIPN-80 IL	122 ± 2	17 ± 1	10 ± 1
MMIM-0.5 POP-1	151 ± 3	18 ± 1	16 ± 2
MMIM-5 POP-1	197 ± 2	28 ± 2	20 ± 2
MMIM-0.5 POP-11	150 ± 2	22 ± 2	14 ± 2
MMIM-5 POP-11	330 ± 4	23 ± 2	15 ± 2
MMIM-5 Cu(BTC)	269 ± 2	24 ± 1	16 ± 1
MMIM-10 Cu(BTC)	319 ± 2	30 ± 2	23 ± 1
MMIM-5 MIL-53	171 ± 3	28 ± 2	17 ± 2
MMIM-5 MMT	219 ± 3	9 ± 2	5 ± 2

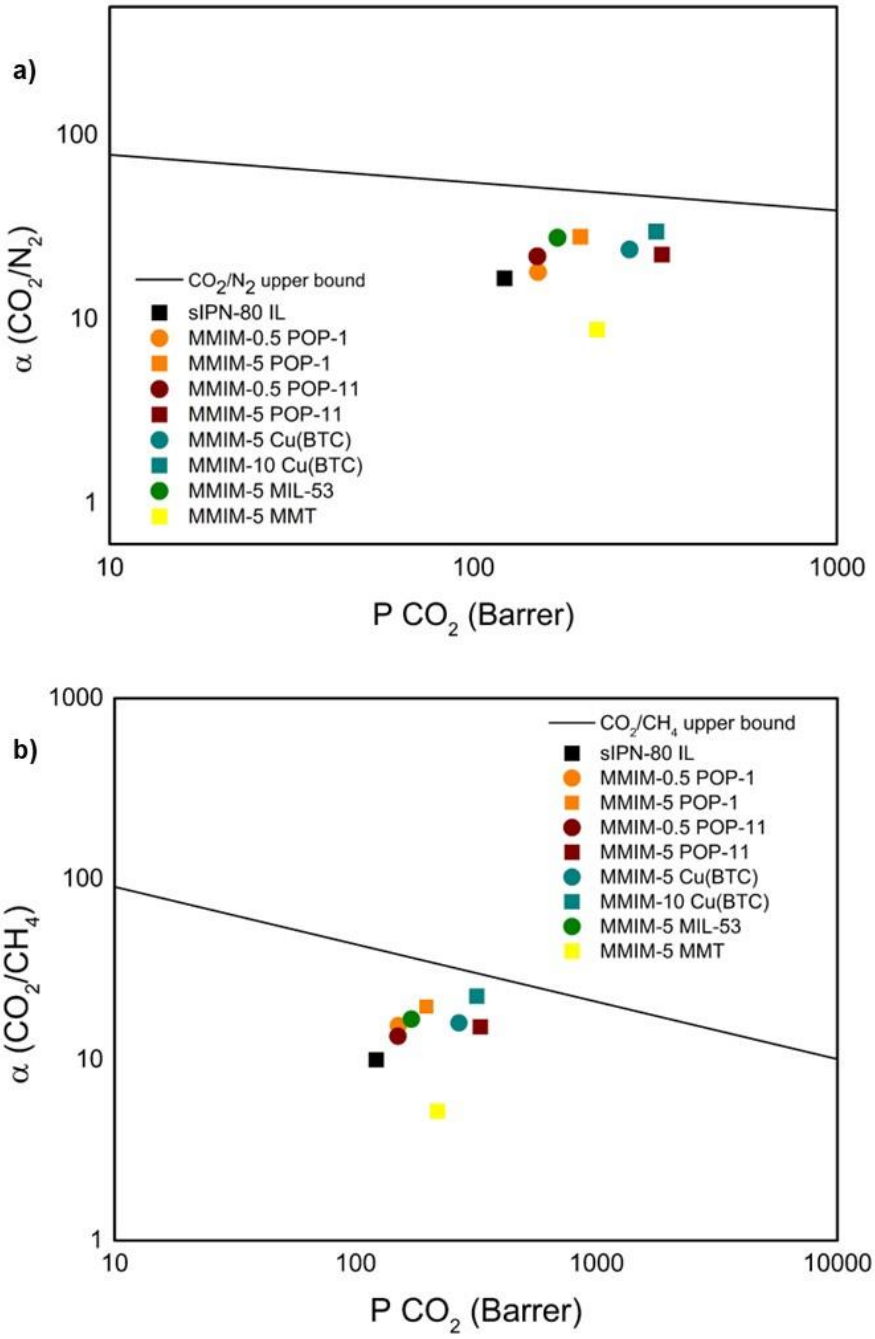

Figure 6.5 – (a) CO_2/N_2 and (b) CO_2/CH_4 ideal selectivities a function of the CO_2 permeability, for all iongel membranes prepared in this work.

6.3.6 Gas Mixtures Permeation Experiments

The MMIM-10 Cu(BTC) iongel membrane was selected to be tested under gas mixture conditions. For the CO_2/N_2 separation, the experiments were conducted at 303 and 353 K and 2 bar of pressure, with 15 vol% CO_2 in feed. The CO_2/CH_4 separation was carried out at 303 K and 2 bar, with

40 vol% CO_2 in feed. For both separations, the influence of relative humidity (RH) was also studied, by carrying out gas permeation experiments with a RH of 11 vol%, at 303 K and 2 bar. The CO_2 permeability and CO_2/N_2 and CO_2/CH_4 selectivities values obtained for the MMIMs containing 10% Cu(BTC) are provided in Table 6.4 and Table 6.5, respectively. For comparison purposes, the results previously obtained for the PEGDA-80 IL membrane containing the same MOF, and tested under the same experimental conditions, are also presented.

Regarding the CO_2/N_2 separation (Table 6.4), the sIPN-80 IL membrane reached a CO_2 permeability of around 132 Barrer and a selectivity of 14, at 303 K and dry conditions. These values were higher than those of the PEGDA-80 TFSI iongel,[281] where the CO_2 permeability reached 115 Barrer, with a selectivity of 14, under the same experimental conditions. In the presence of 11 vol% of RH, the CO_2 permeability increased, up to 193 Barrer, due to the water-induced plasticization of the polymer chains. This effect increased the diffusion rate of the gas molecules, indiscriminately, which also led to the observed decrease in selectivity. When the temperature was further raised to 353 K (under dry conditions), the CO_2 permeability increased from 132 to 144 Barrer, while the selectivity decreased down to 10. This can also be explained by an increase in the gas diffusivity since, at higher temperatures, the gas transport through the iongel membranes is more diffusion-controlled, as previously discussed.[281,297]

The same conclusions can be drawn from the results obtained for the MMIM-10 Cu(BTC) (Table 6.4). Higher permeabilities and selectivities were achieved upon the incorporation of Cu(BTC) into the sIPN-80 IL iongel, due to the high affinity and adsorption capacity of the filler. Compared to the previously obtained results,[297] the use of a sIPN to prepare the MMIM-10 Cu(BTC) presents a clear advantage over the use of only PEGDA network. For instance, at RH=11 vol%, the sIPN-based MMIM containing 10 wt% Cu(BTC) presented slightly higher CO_2 permeability (416 Barrer) and CO_2/N_2 selectivity (15), due to its more hydrophilic nature, induced by the use of the sIPN.

Similar trends were found for the iongel membranes tested for the CO_2/CH_4 separation (Table 6.5). Under dry conditions, the sIPN-80 IL iongel reached a CO_2 permeability of 215 Barrer coupled with a selectivity of 9.2, which are slightly higher than those of PEGDA-80 IL,[281] in which only PEGDA was used as polymer network (P CO_2= 207 Barrer and CO_2/CH_4 selectivity of 8). Comparable to what was found for the CO_2/N_2 separation, at RH=11 vol%, the CO_2 permeability further increased to 297 Barrer, at the expense of the CO_2/CH_4 selectivity, which decreased to 7. Regardless of the experimental conditions, the separation performance of the iongel was enhanced upon the incorporation of 10 wt% Cu(BTC), in terms of both the CO_2 permeability and CO_2/CH_4 selectivity. Compared to the PEGDA-80 TFSI-10 Cu(BTC),[297] the sIPN-based MMIM-10 Cu(BTC) achieved similar or higher CO_2 permeabilities and selectivities (Table 6.5).

Table 6.4 - CO_2 permeability and CO_2/N_2 selectivities obtained for the neat sIPN-80 IL iongel and MMIM containing 10 wt% Cu(BTC).

Membrane Sample	2 bar					
	303 K (RH=0 vol%)		303 K (RH=11 vol%)		353 K (RH=0 vol%)	
	P **CO_2 (Barrer)**	***α*** **CO_2/N_2**	***P*** **CO_2 (Barrer)**	***α*** **CO_2/N_2**	***P*** **CO_2 (Barrer)**	**α CO_2/N_2**
sIPN-80 IL	132 ± 3	14 ± 1	193 ± 2	11 ± 1	144 ± 5	10 ± 1
MMIM-10 Cu(BTC)	281 ± 3	23 ± 1	416 ± 3	15 ± 4	290 ± 4	20 ± 1
PEGDA-80 TFSI-10 Cu(BTC)*	216 ± 6	13 ± 1	412 ± 8	10 ± 1	230 ± 6	11 ± 1

* results previously obtained.[297]

Table 6.5 - CO_2 permeability and CO_2/CH_4 selectivities obtained for the neat sIPN-80 IL iongel and MMIM containing 10 wt% Cu(BTC).

Membrane Sample	2 bar			
	303 K (RH=0 vol%)		303 K (RH=11 vol%)	
	P **CO_2 (Barrer)**	***α*** **CO_2/CH_4**	***P*** **CO_2 (Barrer)**	***α*** **CO_2/CH_4**
sIPN-80 IL	215 ± 2	9 ± 1	297 ± 5	7 ± 1
MMIM-10 Cu(BTC)	326 ± 4	15 ± 2	386 ± 7	13 ± 2
PEGDA-80 TFSI-10 Cu(BTC)*	301 ± 7	10 ± 1	409 ± 8	7 ± 1

* results previously obtained. [297]

6.4 Conclusions

Three new poly(ionic liquid)s were synthesized in this work, containing different anions: sulfonyl(trifluoromethane sulfonyl)imide methacrylate ($[MTFSI]^-$), sulfopropyl methacrylate ($[MSPM]^-$) or 4-styrenesulfonate ($[MSS]^-$) and their ability to form free-standing iongel membranes containing 80 wt% $[C_2mim][TFSI]$ IL was assessed. It was found that in terms of the polymer synthesis and compatibility with the iongel components, the PIL containing the $[MTFSI]^-$ anion (PDADMA-MTFSI) was the most suitable to fabricate iongel membranes.

The sIPN iongel membranes were prepared by UV polymerization using 20 wt% of PDADMA-MTFSI, PEGDA and 80 wt% of $[C_2mim][TFSI]$ IL. Moreover, different fillers (inorganic – MMT, organic – azo-POP-1 and azo-POP-11 and hybrid – Cu(BTC) and MIL-53) were incorporated into the selected sIPN iongel to prepare MMIMs with loading ranging from 0.5 to 10 wt%, depending on the filler used. The characterization results revealed a good compatibility between all the materials, and dense defect-free structures were obtained. Interestingly, the mechanical properties of the MMIMs improved upon the

incorporation of the different fillers since they provided more rigidity to the structure. However, such rigidity lowered the elongation at break of the materials, making them less flexible.

The MMIMs were tested in single gas permeation experiments, for CO_2/N_2 and CO_2/CH_4 separations. The nanoclay MMT showed the lowest separation performance, with a significant decrease in selectivity, for both separations, compared to the neat sIPN iongel. The best compromise between permeability and selectivity was achieved with the sIPN-based MMIM containing 10 wt% Cu(BTC), where both parameters were improved compared to the neat iongel. The best performing MMIM was also tested under mixed gas conditions. The presence of RH (11 vol%) revealed to have a significant impact on the CO_2 permeability, but a negative effect on the gas selectivity. The same behaviour was observed when the temperature raised from 303 to 353 K (under dry conditions).

Both the neat sIPN-80 IL iongel and respective MMIM with 10 wt% Cu(BTC) showed better gas separation performances, when compared to the iongel membranes (neat and bearing the same MOF) comprised of the non-ionic polymer network PEGDA, tested under the same experimental conditions.

Finally, it can be concluded that the use of an ionic sIPN based on a poly(ionic liquid) can be an interesting strategy to prepare MMIMs for gas separation, with improved separation properties and mechanical properties.

7

GENERAL CONCLUSIONS AND FUTURE WORK

The main goal of the work developed throughout this PhD project was to design Mixed Matrix Iongel Membranes (MMIMs) combining different types of solid fillers (inorganic, organic and "hybrid" organic/inorganic) to improve the overall performance of the developed membranes, especially in terms of their gas separation properties, thermal and mechanical stabilities. The main achievements and conclusions obtained in this PhD project are highlighted in the current chapter. Additionally, some suggestions for future work are also discussed, including some strategies that might be used to further improve the performance of the membranes studied throughout this work. Finally, some considerations and opportunities will also be discussed, in a more general perspective, for future research directions.

7.1 General conclusions

The main conclusions obtained throughout this work can be divided in four main topics, depending on the filler or, as in Chapter 6, on the polymer matrix used to fabricate the MMIMs.

Although iongel membranes present undeniable advantages for CO_2 separation applications, mainly due to the high load of IL that may be achieved, this characteristic can also represent one of the biggest drawbacks in the preparation and use of these membranes by compromising their mechanical stability. Aiming at overcoming this issue, an inorganic nanoclay, montmorillonite (MMT), known for its ability to reinforce the mechanical stability of different materials was incorporated in PEGDA iongel membranes with a starting [C_2mim][TFSI] IL content of 60 wt% (Chapter 2). The MMT loading was systematically increased from 0.2 to 7.5 wt%. The overall mechanical properties of the fabricated MMIMs were indeed improved, and an optimal loading of 1 wt% MMT was found. Despite a deterioration of the mechanical properties at higher MMT loadings (> 1 wt%), the MMIMs still presented better overall stability compared to the neat iongel membrane. While the CO_2 permeability of the MMIMs increased with increasing MMT loading, the ideal selectivities of CO_2/N_2, CO_2/CH_4 and CO_2/H_2 separations remained similar or decreased. This is a direct consequence of the negligible MMT affinity towards CO_2, acting only as an enhancer in the gas diffusivity. Nonetheless, the mechanical reinforcement provided

by the nanoclay allowed to further increase the IL content to 80 wt%, which consequently resulted in a better dispersion of the MMT particles and better separation performances of the free-standing membranes. Even though the main goal of Chapter 2 was achieved with the improvement of the mechanical stability, the lack of affinity towards CO_2 does not enable these MMIMs to be considered for gas separation applications, since they fall short compared to others reported in the literature. Even so, the results obtained may be a step towards the development of strategies to overcome the low mechanical stability of iongel membranes.

Bearing in mind the above-mentioned results regarding the MMT-containing MMIMs and the necessity to improve the separation performance, completely organic porous organic polymers containing azo functional groups (azo-POPs) were considered in Chapter 3. Given their novelty, a full characterization of these materials (azo-POP-1, azo-POP-10, azo-POP-11 and azo-POP-12) was performed, in terms of their porosity parameters, thermal stability and CO_2 sorption capacity, since these are determinant factors in the choice of any filler to fabricate membranes for gas separation processes. Dense, defect-free and thermally stable membranes combining these azo-POPs with 80 wt% [C_2mim][TFSI] IL and 20 wt% PEGDA were obtained through a rapid and solvent-free UV polymerization process. Even though a low loading of each azo-POP was used in the fabrication of the MMIMs (0.5 wt%), a significant improvement on the permeability and ideal selectivities of the CO_2/N_2, CO_2/CH_4 and CO_2/H_2 separations was achieved, with significant contribution from the presence of the azo functional groups that are known for their "CO_2-philic" properties. It was also found that the azo-POP structure had great influence in the gas separation, especially for azo-POP-1 that presented the highest porosity and CO_2 adsorption capacity, leading to the highest gas permeability achieved in this chapter.

Despite the encouraging progress achieved in Chapter 3, a more realistic assessment of the performance of the fabricated MMIMs containing azo-POPs was needed. It is known that the separation performance of membranes is highly influenced by the experimental conditions, such as temperature, pressure and presence of water vapour. Gas permeability and selectivity differ greatly from pure gas permeation tests to gas mixtures under realistic/industrial conditions. Chapter 4 presented a thorough evaluation of the influence of increasing temperature and pressure and a specific RH in feed gas stream on the gas separation performance of the best performing MMIMs tested under pure gas conditions in Chapter 3. The first step was the evaluation of the influence of different water activities when the MMIMs containing azo-POP-1 or azo-POP-11 were subjected to different saturated salt solutions and tested under pure gas conditions. Interestingly, it was found that low water activities (up to 0.21) promoted an increase in both CO_2 permeability and CO_2/N_2 and CO_2/CH_4 ideal selectivities. Under CO_2/N_2 mixed gas conditions, an increase in temperature (303, 323 and 353 K) led to an increase on CO_2 permeability, without a significant impact in selectivity. On the other hand, at lower temperatures, the increase in pressure had a negative impact on the gas permeability. The presence of water vapour on the CO_2/N_2 gas mixture also had a significant effect on the membranes' performance. It was found that the CO_2 permeability greatly increased, at the expense of selectivity. In any case, the MMIMs containing azo-POPs performed better than the neat PEGDA-80 TFSI iongel, despite the experimental conditions. The results obtained in this chapter confirmed that it is of vital importance to study the effect of different

experimental conditions, similar to those of the industrial gas streams. Moreover, it also confirmed the initial hypothesis that azo-POPs are suitable materials to be incorporated into iongel matrices to improve their gas separation performance.

To take advantage of the higher surface areas and CO_2 sorption capacities of MOFs, compared to the previously selected azo-POPs, Cu(BTC), MIL-53 and ZIF-8 were incorporated into de PEGDA-80 TFSI iongel. MOF loadings up to 10 wt% were observed to be the maximum amount of MOF that is possible to incorporate into this iongel matrix, without compromising the smooth and defect-free structures. Interestingly, oppositely to what usually happens in mixed matrix membranes, the incorporation of MIL-53 had a positive effect on the mechanical properties of the MMIMs, that became more mechanically stable. Under pure gas conditions, the tested MMIMs showed different behaviours, depending on the MOF used, with the best results being obtained when 10 wt% Cu(BTC) was incorporated into the PEGDA-80 TFSI iongel. Then, the Cu(BTC)-containing MMIM at 10 wt% loading was tested for CO_2/N_2 and CO_2/CH_4 gas mixtures, and it was found that the incorporation of Cu(BTC) lead to a significant improvement in CO_2 permeability, while the selectivity was maintained.

The final step in this PhD thesis towards the design of MMIMs with improved separation performances was the use of a different polymer matrix, a semi interpenetrating polymer network (sIPN), combining PEGDA and a PIL. Considering the results obtained from the previous chapters, the fillers that resulted in the best performing MMIMs were selected to be incorporated into the sIPN-based iongel and characterized. An optimal loading was found for nanoclay MMT, azo-POP-1, azo-POP-11, Cu(BTC) and MIL-53. Remarkably, the selected fillers allowed for the preparation of more mechanically resistant MMIMs, compared to the neat sIPN-80 IL iongel membrane, which was one of the goals of this PhD thesis.

As expected, the presence of an ionic polymer (PIL) in the iongel structure contributed to a higher affinity of the membrane towards CO_2, which was further improved upon the incorporation of the different fillers. Following what was observed in Chapters 3 and 5, the azo-POPs and MOFs embedded into the sIPN-based iongels lead to higher separation efficiencies, under pure gas conditions, with the best overall result being achieved at 10 wt% Cu(BTC). Under dry and humidified mixed gas conditions, the sIPN-based MMIMs containing 10 wt% Cu(BTC) showed higher values of CO_2 permeability and higher or similar values of CO_2/N_2 and CO_2/CH_4 selectivities, compared to those obtained with the PEGDA-based MMIM, tested under the same conditions on Chapter 5. These findings confirmed that the use of an ionic sIPN as polymer matrix was a suitable strategy to develop advanced iongel membranes, while the incorporation of Cu(BTC) revealed to be an interesting alternative to design MMIMs with improved thermal and mechanical properties as well as CO_2 separation performances.

It is clear that the development of iongel membranes represents a step forward in the design of IL-based membranes for gas separation. Especially compared to SILMs, iongel membranes are able to achieve similar separation performances, due to the high IL content, while providing considerably higher stabilities, under different experimental conditions. The use of different polymer matrices and the incorporation of solid fillers can further boost the fabrication of MMIMs with better gas transport

properties and, in some cases, enhanced mechanical stabilities. In this thesis, it was also found that, besides the filler, the polymer matrix also plays an important role in the membranes' performance.

Figure 7.1 a) and b) presents some of the most relevant results reported in the literature, for the CO_2/N_2 and CO_2/CH_4 separations, respectively, for the different types of IL-based membranes.[23,25,101–103,105–108,112,114,115,33,135–137,139,141,142,160,189,194,195,34,196,301–309,40,310–313,45,60,62,94,99]

Overall, the results obtained in this thesis fall among those already reported in the literature, especially considering the reported MMIMs,[119,147–150,152,157], our own previous works,[114,115] and those described in Chapter 1, without achieving the desired higher values of permeability and selectivities, as it can be seen in Figure 7.1 a) and b). Nonetheless, for CO_2/N_2 the results fall above or close to the respective upper bounds. Despite the fact that an improvement in the performance of the proposed MMIMs is still needed, it should be highlighted that the present work not only reports the use of different polymer matrices and fillers in MMIMs that had not been reported yet, such as a semi-interpenetrating polymer network, the nanoclay MMT and azo-POPs but it also presents a detailed study of the influence of different experimental conditions on this class of membranes, which is still lacking in the literature. Moreover, in Chapter 2 a successful strategy was used to improve the mechanical stability of the iongels, which is one of the main challenges regarding these materials. It can be concluded that throughout the presented chapters, there is a continuous improvement of the MMIMs properties, especially in terms of their separation performance, from Chapter 2 to Chapter 6, where the sIPN-based MMIM presented the best results achieved in the thesis.

Throughout this thesis, the separation performance of the prepared MMIMs have been reported in terms of permeability and selectivity. However, from an industrial perspective, the concept of permeance (ratio between permeability and membrane thickness) is much more relevant than permeability since it gives a more accurate idea of the gas permeation rate through a certain membrane area. Considering that in this thesis MMIMs were prepared with selective layers with around 100 µm of thickness, their permeances are considerably lower than what is desirable.

Most membranes are evaluated as dense films (between 50 and 150 µm of thickness), but from the technological and industrial point of view, thin films with a selective layer of 0.1-1 µm of thickness, supported on a highly permeable porous support are much more commercially attractive.[314] A thin selective layer will allow a reduction in the membrane area required and higher permeances.[314] Nowadays, polymer materials such as polymers of intrinsic microporosity (PIMs) and thermal rearranged (TR) polymers have shown some of the highest permeances achieved so far, which are considerably higher than those obtained with IL-based membranes. Nonetheless, the development of IL-based membranes presents an important advantage, since the use of highly permeable-high free volume materials, such as PIMs and TR polymers, can lead to a fast physical aging over time, especially when fabricated as thin films.[65] It has been reported that thin film polymer membranes can lose around 25% of their permeance in the first few days and 25% more over the following couple of weeks, due to a reordering of the polymer chains and loss of free volume.[314] While it is known that achieving high gas permeability/permeance and selectivity is usually the main focus of the development of membranes for

CO_2 separation, these parameters may not be able to compensate the fast aging and degradation of the materials. The MMIMs developed in this thesis, and particularly the ones reported in Chapter 6 using sIPNs, can represent a step forward in the design of advanced IL-based membranes, able to overcome some of the issues of the mentioned polymer membranes. In Chapter 6, the use of a charged polymer matrix containing an anion structurally similar to the IL allows for a high stability of the IL inside the iongel matrix, even at higher temperatures, while the used fillers (especially Cu(BTC)) further boost their separation performances and mechanical stability. The fabrication of the same MMIMs with thinner selective layers may help achieve gas separation performances closer to those of other highly permeable materials, while overcoming their fast-aging process.

Despite the progress made throughout each chapter of this thesis, there are still some challenges that need to be answered and additional steps that need to be considered in the future towards the development of MMIMs for gas separation applications at a larger scale. Some suggestions for future research are given in the next section.

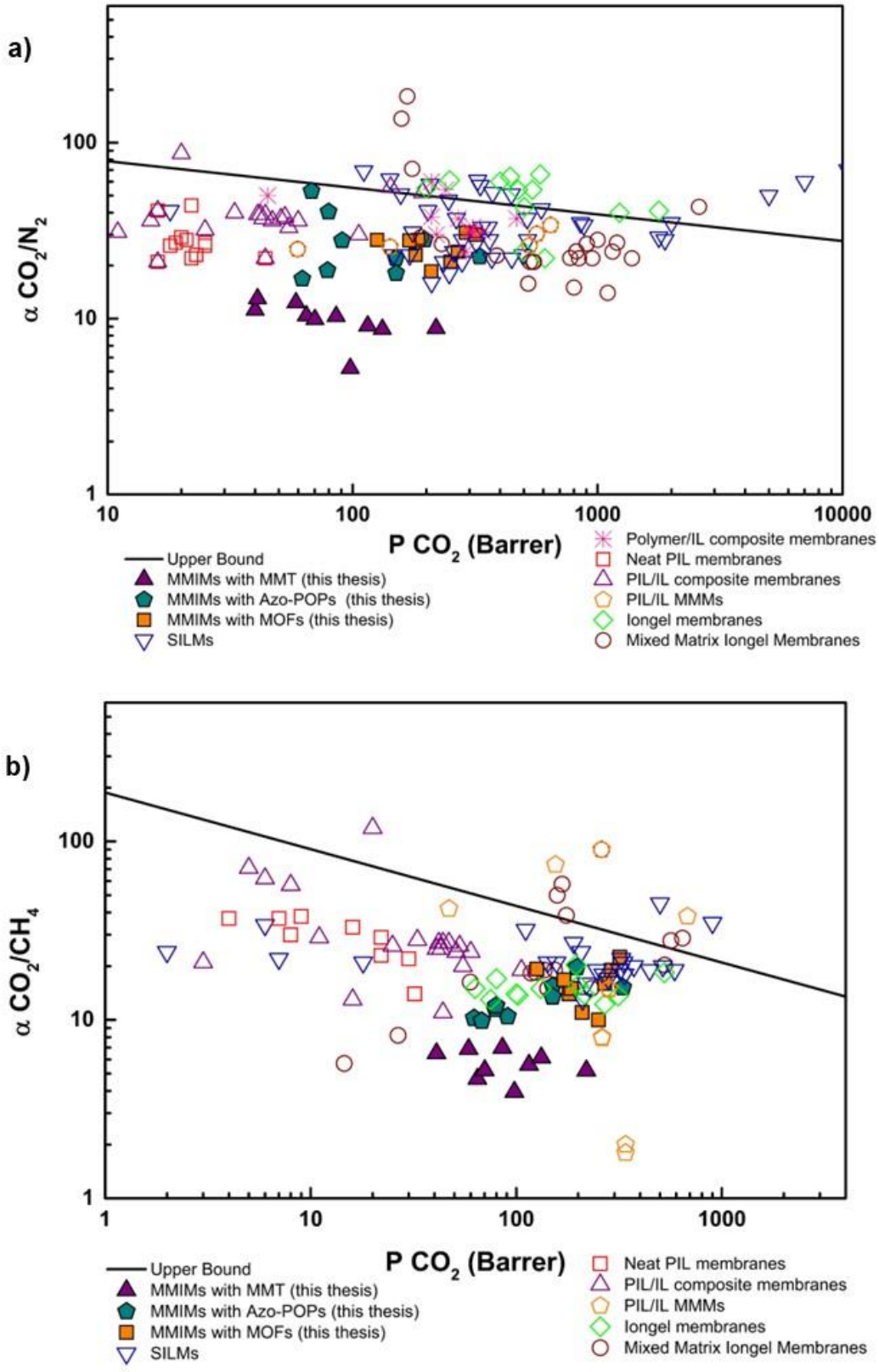

Figure 7.1 – (a) CO_2/N_2 and (b) CO_2/CH_4 upper bounds for comparison between the results obtained throughout this thesis for MMIMs (with MMT, azo-POPs and MOFs) and others reported in the literature for IL-based membranes.

7.2 Suggestions for future work

Regarding the future steps on the development of MMIMs, some suggestions can be considered:

1. The separation performance of iongel membranes can be further improved by selecting different materials. In this thesis, only the [C_2mim][TFSI] IL was considered for the fabrication of membranes. Different ILs can be considered, for instance, with functional groups able to promote an active transport of the CO_2 molecules;
2. Despite the improvements in the mechanical properties of self-standing iongel membranes achieved with an inorganic nanoclay (MMT), further research regarding different nanoparticles, with higher solubilities for CO_2 should be carried out. Another strategy involves the use of a porous support as a mechanical support, where the iongel layer is coated on top, as described throughout Chapters 3 to 6 in this thesis. To further maximize the gas permeance, the iongel layer should be as thin as possible;
3. The use of ILs can pose a challenge in the scale-up of the MMIMs, due to the cost of the materials. An alternative could involve the use of deep eutectic solvents (DES), which are cheaper and simple to synthesize, and have also shown high CO_2 solubilities, depending on their structure;
4. Throughout this thesis, it was shown that the experimental conditions have a significant impact in the MMIMs separation performance. Besides temperature, pressure, presence of water vapour and feed gas composition, the presence of minor components (impurities) in the gas mixtures should also be considered;
5. In addition to the above-mentioned experimental conditions, the physical aging of the prepared membranes should also be evaluated through long-term gas permeation experiments, to evaluate the modifications and stability of the materials.
6. Finally, the design of the MMIMs should be scaled up from flat to a hollow fiber configuration, to make this technology more attractive from an industrial and commercial point of view.

REFERENCES

1 Z. Lei, B. Chen, Y. M. Koo and D. R. Macfarlane, *Chem. Rev.*, 2017, **117**, 6633–6635.

2 L. C. Tomé and I. M. Marrucho, *Chem. Soc. Rev.*, 2016, **45**, 2785–2824.

3 R. L. Vekariya, *J. Mol. Liq.*, 2017, **227**, 44.

4 M. C. Bubalo, K. Radošević, I. R. Redovniković, I. Slivac and V. G. Srček, *Arh. Hig. Rada Toksikol.*, 2017, **68**, 171–179.

5 M. Aghaie, N. Rezaei and S. Zendehboudi, *Renew. Sustain. Energy Rev.*, 2018, **96**, 502–525.

6 Y. Zhang, S. Zhang, X. Lu, Q. Zhou, W. Fan and X. P. Zhang, *Chem. - A Eur. J.*, 2009, **15**, 3003–3011.

7 E. D. Bates, R. D. Mayton, I. Ntai and J. H. Davis, *JA*, 2002, **124**, 2001–2002.

8 B. Engineering, V. Uni, N. Dame, B. E. Gurkan, J. C. De Fuente, E. M. Mindrup, L. E. Ficke, B. F. Goodrich, E. A. Price, W. F. Schneider and J. F. Brennecke, *J. Am. Chem. Soc.*, 2010, **132**, 2116–2117.

9 K. Friess, P. Izák, M. Kárászová, M. Pasichnyk, M. Lanč, D. Nikolaeva, P. Luis and J. C. Jansen, *Membranes (Basel).*, 2021, **11**, 1–58.

10 M. G. Cowan, D. L. Gin and R. D. Noble, *Acc. Chem. Res.*, 2016, **49**, 724–732.

11 Z. Dai, R. D. Noble, D. L. Gin, X. Zhang and L. Deng, *J. Membr. Sci.*, 2016, **497**, 1–20.

12 L. J. Lozano, C. Godínez, A. P. de los Ríos, F. J. Hernández-Fernández, S. Sánchez-Segado and F. J. Alguacil, *J. Memb. Sci.*, 2011, **376**, 1–14.

13 C. Myers, H. Pennline, D. Luebke, J. Ilconich, J. N. K. Dixon, E. J. Maginn and J. F. Brennecke, *J. Memb. Sci.*, 2008, **322**, 28–31.

14 P. Scovazzo, J. Kieft, D. A. Finan, C. Koval, D. DuBois and R. Noble, *J. Memb. Sci.*, 2004, **238**, 57–63.

15 F. J. Hernández-Fernández, A. P. de los Ríos, F. Tomás-Alonso, J. M. Palacios and G. Víllora, *J. Memb. Sci.*, 2009, **341**, 172–177.

16 L. A. Neves, J. G. Crespo and I. M. Coelhoso, *J. Membr. Sci.*, 2010, **357**, 160–170.

17 A. A. Akhmetshina, I. M. Davletbaeva, E. S. Grebenschikova, I. I. Zaripov, C. F. Martins, L. A. Neves and I. V Vorotyntsev, *Membranes (Basel).*, 2016, **6**, 1–18.

18 X. Yan, S. Anguille, M. Bendahan and P. Moulin, *Sep. Purif. Technol.*, 2019, **222**, 230–253.

19 P. Scovazzo, A. E. . Visser, J. H. Davis, R. D. . Rogers, C. A. . Koval, D. L. . DuBois and R. D. Noble, *Am. Chem. Soc.*, 2002, **818**, 69–87.

20 W. H. Lai, D. K. Wang, H. H. Tseng and M. Y. Wey, *J. CO2 Util.*, 2022, **56**, 101871.

21 S. Wickramanayake, D. Hopkinson, C. Myers, L. Hong, J. Feng, Y. Seol, D. Plasynski, M. Zeh and D. Luebke, *J. Memb. Sci.*, 2014, **470**, 52–59.

22 D. H. Kim, I. H. Baek, S. U. Hong and H. K. Lee, *J. Memb. Sci.*, 2011, **372**, 346–354.

23 L. C. Tomé, D. J. S. Patinha, R. Ferreira, H. Garcia, C. S. Pereira, C. S. R. Freire, L. P. N. Rebelo and I. M. Marrucho, *ChemSusChem*, 2014, **7**, 110–113.

24 M. Y. Abdelrahim, C. F. Martins, L. A. Neves, C. Capasso, C. T. Supuran, I. M. Coelhoso, J. G. Crespo and M. Barboiu, *J. Memb. Sci.*, 2017, **528**, 225–230.

25 L. A. Neves, N. Nemestóthy, V. D. Alves, P. Cserjési, K. Bélafi-Bakó and I. M. Coelhoso, *Desalination*, 2009, **240**, 311–315.

26 J. Albo, E. Santos, L. A. Neves, S. P. Simeonov, C. A. M. Afonso, J. G. Crespo and A. Irabien, *Sep. Purif. Technol.*, 2012, **97**, 26–33.

27 P. S. Kulkarni, L. A. Neves, I. M. Coelhoso, C. A. M. Afonso and G. Crespo, *Environ. Sci. Technol.*, 2012, **46**, 462–468.

28 L. A. Neves, C. Afonso, I. M. Coelhoso and J. G. Crespo, *Sep. Purif. Technol.*, 2012, **97**, 34–41.

29 R. Couto, L. Neves, P. Simões and I. Coelhoso, *Membranes (Basel).*, 2015, **5**, 13–21.

30 L. A. Neves, J. Benavente, I. M. Coelhoso and J. G. Crespo, *J. Memb. Sci.*, 2010, **347**, 42–52.

31 H. Karkhanechi, S. Salmani and M. Asghari, *ChemBioEng Rev.*, 2015, **2**, 290–302.

32 M. A. Malik, M. A. Hashim and F. Nabi, *Chem. Eng. J.*, 2011, **171**, 242–254.

33 J. E. Bara, C. J. Gabriel, S. Lessmann, T. K. Carlisle, A. Finotello, D. L. Gin and R. D. Noble, *Ind. Eng. Chem. Res.*, 2007, **46**, 5380–5386.

34 J. E. Bara, C. J. Gabriel, T. K. Carlisle, D. E. Camper, A. Finotello, D. L. Gin and R. D. Noble, *Chem. Eng. J.*, 2009, **147**, 43–50.

35 S. M. Mahurin, T. Dai, J. S. Yeary, H. Luo and S. Dai, *Ind. Eng. Chem. Res.*, 2011, **50**, 14061–14069.

36 H. Ying and R. E. Baltus, *Ind. Eng. Chem. Res.*, 2007, **46**, 8166–8175.

37 S. D. Hojniak, A. L. Khan, O. Hollo, B. Kirchner, I. F. J. Vankelecom, W. Dehaen and K. Binnemans, *J. Phys. Chem. B*, 2013, **117**, 15131–15140.

38 S. M. Mahurin, P. C. Hillesheim, J. S. Yeary, D. E. Jiang and S. Dai, *RSC Adv.*, 2012, **2**, 11813–11819.

39 P. C. Hillesheim, J. A. Singh, S. M. Mahurin, P. F. Fulvio, Y. Oyola, X. Zhu, D. Jiang and S. Dai, *RSC Adv.*, 2013, **3**, 3981–3989.

40 P. C. Hillesheim, S. M. Mahurin, P. F. Fulvio, J. S. Yeary, Y. Oyola, D. E. Jiang and S. Dai, *Ind. Eng. Chem. Res.*, 2012, **51**, 11530–11537.

41 K. Huang, X. M. Zhang, Y. X. Li, Y. T. Wu and X. B. Hu, *J. Memb. Sci.*, 2014, **471**, 227–236.

42 R. Condemarin and P. Scovazzo, *Chem. Eng. J.*, 2009, **147**, 51–57.

43 A. B. Pereiro, L. C. Tomé, S. Martinho, L. P. N. Rebelo and I. M. Marrucho, *Ind. Eng. Chem. Res.*, 2013, **52**, 4994–5001.
44 S. M. Mahurin, J. S. Lee, G. A. Baker, H. Luo and S. Dai, *J. Memb. Sci.*, 2010, **353**, 177–183.
45 L. C. Tomé, C. Florindo, C. S. R. Freire, L. P. N. Rebelo and I. M. Marrucho, *Phys. Chem. Chem. Phys.*, 2014, **16**, 17172–17182.
46 S. Hanioka, T. Maruyama, T. Sotani, M. Teramoto, H. Matsuyama, K. Nakashima, M. Hanaki, F. Kubota and M. Goto, *J. Memb. Sci.*, 2008, **314**, 1–4.
47 S. Kasahara, E. Kamio and H. Matsuyama, *J. Memb. Sci.*, 2014, **454**, 155–162.
48 S. Kasahara, E. Kamio, T. Ishigami and H. Matsuyama, *J. Memb. Sci.*, 2012, **415**–**416**, 168–175.
49 S. Kasahara, E. Kamio, T. Ishigami and H. Matsuyama, *Chem. Commun.*, 2012, **48**, 6903–6905.
50 P. Scovazzo, *J. Memb. Sci.*, 2009, **343**, 199–211.
51 P. Scovazzo, D. Havard, M. McShea, S. Mixon and D. Morgan, *J. Memb. Sci.*, 2009, **327**, 41–48.
52 P. Bernardo, J. C. Jansen, F. Bazzarelli, F. Tasselli, A. Fuoco, K. Friess, P. Izák, V. Jarmarová, M. Kačírková and G. Clarizia, *Sep. Purif. Technol.*, 2012, **97**, 73–82.
53 B. Lam, M. Wei, L. Zhu, S. Luo, R. Guo, A. Morisato, P. Alexandridis and H. Lin, *Polymer (Guildf).*, 2016, **89**, 1–11.
54 A. F. Ismail, N. Ridzuan and S. A. Rahman, *Membr. Sci. Technol.*, 2002, **24 (Suppl.**, 1025–1043.
55 L. M. Robeson, *J. Membr. Sci.*, 2008, **320**, 390–400.
56 S. Uk Hong, D. Park, Y. Ko and I. Baek, *Chem. Commun.*, 2009, **1**, 7227.
57 J. C. Jansen, K. Friess, G. Clarizia, J. Schauer and P. Izák, *Macromolecules*, 2011, **44**, 39–45.
58 P. Uchytil, J. Schauer, R. Petrychkovych, K. Setnickova and S. Y. Suen, *J. Memb. Sci.*, 2011, **383**, 262–271.
59 E. M. Erdni-Goryaev, A. Y. Alent'Ev, N. A. Belov, D. O. Ponkratov, A. S. Shaplov, E. I. Lozinskaya and Y. S. Vygodskii, *Pet. Chem.*, 2012, **52**, 494–498.
60 H. Z. Chen, P. Li and T. S. Chung, *Int. J. Hydrogen Energy*, 2012, **37**, 11796–11804.
61 K. Friess, J. C. Jansen, F. Bazzarelli, P. Izák, V. Jarmarová, M. Kačírková, J. Schauer, G. Clarizia and P. Bernardo, *J. Memb. Sci.*, 2012, **415**–**416**, 801–809.
62 S. Uk Hong, D. Park, Y. Ko and I. Baek, *Chem. Commun.*, 2009, **1**, 7227–7229.
63 H. Z. Chen, P. Li and T. S. Chung, *Int. J. Hydrogen Energy*, 2012, **37**, 11796–11804.
64 L. Liang, Q. Gan and P. Nancarrow, *J. Memb. Sci.*, 2014, **450**, 407–417.
65 Z. Dai, R. D. Noble, D. L. Gin, X. Zhang and L. Deng, *J. Memb. Sci.*, 2016, **497**, 1–20.
66 A. R. Nabais, L. A. Neves and L. C. Tomé, *ACS Appl. Polym. Mater.*, 2022, **4**, 3098–3119.
67 B. Yang, H. Jiang, L. Bai, Y. Bai, T. Song and X. Zhang, *Int. J. Greenh. Gas Control*, 2022, **121**, 103796.
68 S. Raeissi and C. J. Peters, *Green Chem.*, 2009, **11**, 185–19.
69 C. Cadena, J. L. Anthony, J. K. Shah, T. I. Morrow, J. F. Brennecke and E. J. Maginn, *J. Am. Chem. Soc.*, 2004, **126**, 5300–5308.

70 D. Bastani, N. Esmaeili and M. Asadollahi, *J. Ind. Eng. Chem.*, 2013, **19**, 375–393.
71 S. Li, J. L. Falconer and R. D. Noble, *Adv. Mater.*, 2006, **18**, 2601–2603.
72 Y. Li and J. Yu, *Nat. Rev. Mater.*, 2021, **6**, 1156–1174.
73 N. Kosinov, J. Gascon, F. Kapteijn and E. J. M. Hensen, *J. Memb. Sci.*, 2016, **499**, 65–79.
74 M. M. Zagho, M. K. Hassan, M. Khraisheh, M. Al, A. Al-maadeed and S. Nazarenko, *Chem. Eng. J. Adv.*, 2021, **6**, 100091.
75 R. Shindo, M. Kishida, H. Sawa, T. Kidesaki, S. Sato, S. Kanehashi and K. Nagai, *J. Memb. Sci.*, 2014, **454**, 330–338.
76 D. F. Mohshim, H. Mukhtar and Z. Man, *Sep. Purif. Technol.*, 2018, **196**, 20–26.
77 H. C. J. Zhou and S. Kitagawa, *Chem. Soc. Rev.*, 2014, **43**, 5415–5418.
78 S. Mandal, S. Natarajan, P. Mani and A. Pankajakshan, *Adv. Funct. Mater.*, 2021, **31**, 1–22.
79 B. Zornoza, C. Tellez, J. Coronas, J. Gascon and F. Kapteijn, *Microporous Mesoporous Mater.*, 2013, **166**, 67–78.
80 B. S. T. Meek, J. A. Greathouse and M. D. Allendorf, *Adv. Mater.*, 2011, **23**, 249–267.
81 H. B. Tanh Jeazet, C. Staudt and C. Janiak, *Dalt. Trans.*, 2012, **41**, 14003–14027.
82 R. Lin, B. Villacorta Hernandez, L. Ge and Z. Zhu, *J. Mater. Chem. A*, 2018, **6**, 293–312.
83 H. Dou, B. Jiang, M. Xu, Z. Zhang, G. Wen, F. Peng, A. Yu, Z. Bai, Y. Sun, L. Zhang, Z. Jiang and Z. Chen, *Angew. Chemie - Int. Ed.*, 2019, **58**, 13969–13975.
84 A. R. Kamble, C. M. Patel and Z. V. P. Murthy, *J. Environ. Manage.*, 2020, **262**, 110256.
85 J. Yuan, D. Mecerreyes and M. Antonietti, *Prog. Polym. Sci.*, 2013, **38**, 1009–1036.
86 R. Marcilla, J. A. Blazquez, J. Rodriguez, J. A. Pomposo and D. Mecerreyes, *J. Polym. Sci. Part A Polym. Chem.*, 2004, **42**, 208–212.
87 M. Hirao, K. Ito and H. Ohno, *Electrochim. Acta*, 2000, **45**, 1291–1294.
88 M. D. Green and T. E. Long, *Polym. Rev.*, 2009, **49**, 291–314.
89 R. Marcilla, J. A. Blazquez, R. Fernandez, H. Grande, J. A. Pomposo and D. Mecerreyes, *Macromol. Chem. Phys.*, 2005, **206**, 299–304.
90 W. Ogihara, S. Washiro, H. Nakajima and H. Ohno, *Electrochim. Acta*, 2006, **51**, 2614–2619.
91 A. L. Pont, R. Marcilla, I. De Meatza, H. Grande and D. Mecerreyes, *J. Power Sources*, 2009, **188**, 558–563.
92 D. Mecerreyes, *Prog. Polym. Sci.*, 2011, **36**, 1629–1648.
93 J. E. Bara, S. Lessmann, C. J. Gabriel, E. S. Hatakeyama, R. D. Noble and D. L. Gin, *Ind. Eng. Chem. Res.*, 2007, **46**, 5397–5404.
94 J. E. Bara, C. J. Gabriel, E. S. Hatakeyama, T. K. Carlisle, S. Lessmann, R. D. Noble and D. L. Gin, *J. Memb. Sci.*, 2008, **321**, 3–7.
95 W. J. Horne, M. A. Andrews, M. S. Shannon, K. L. Terrill, J. D. Moon, S. S. Hayward and J. E. Bara, *Sep. Purif. Technol.*, 2015, **155**, 89–95.
96 P. Li, D. R. Paul and T.-S. Chung, *Green Chem.*, 2012, **14**, 1052–1063.
97 T. K. Carlisle, E. F. Wiesenauer, G. D. Nicodemus, D. L. Gin and R. D. Noble, *Ind. Eng. Chem. Res.*, 2013, **52**, 1023–1032.

98 H. Cong, B. Yu, J. Tang and X. S. Zhao, *J. Polym. Res.*, 2012, **19**, 4–9.

99 J. E. Bara, E. S. Hatakeyama, D. L. Gin and R. D. Noble, *Polym. Adv. Technol.*, 2008, **19**, 1415–1420.

100 J. E. Bara, D. L. Gin and R. D. Noble, *Ind. Eng. Chem. Res.*, 2008, **47**, 9919–9924.

101 J. E. Bara, R. D. Noble and D. L. Gin, *Ind. Eng. Chem. Res.*, 2009, **48**, 4607–4610.

102 J. Zhou, M. M. Mok, M. G. Cowan, W. M. Mcdanel, T. K. Carlisle, D. L. Gin and R. D. Noble, *Ind. Eng. Chem. Res.*, 2014, **53**, 20064–20067.

103 T. K. Carlisle, W. M. McDanel, M. G. Cowan, R. D. Noble and D. L. Gin, *Chem. Mater.*, 2014, **26**, 1294–1296.

104 T. K. Carlisle, G. D. Nicodemus, D. L. Gin and R. D. Noble, *J. Memb. Sci.*, 2012, **397**–**398**, 24–37.

105 L. C. Tomé, D. Mecerreyes, C. S. R. Freire, L. P. N. Rebelo and I. M. Marrucho, *J. Membr. Sci.*, 2013, **428**, 260–266.

106 L. C. Tomé, M. A. Aboudzadeh, L. P. N. Rebelo, C. S. R. Freire, D. Mecerreyes and I. M. Marrucho, *J. Mater. Chem. A*, 2013, **1**, 10403–10411.

107 L. C. Tomé, M. Isik, C. S. R. Freire, D. Mecerreyes and I. M. Marrucho, *J. Membr. Sci.*, 2015, **483**, 155–165.

108 L. C. Tomé, D. C. Guerreiro, R. M. Teodoro, V. D. Alves and I. M. Marrucho, *J. Membr. Sci.*, 2018, **549**, 267–274.

109 A. S. L. Gouveia, L. Ventaja, L. C. Tomé and I. M. Marrucho, *Membranes (Basel).*, 2018, **8**, 124.

110 A. S. L. Gouveia, E. Malcaitè, E. I. Lozinskaya, A. S. Shaplov, L. C. Tomé and I. M. Marrucho, *ACS Sustain. Chem. Eng.*, 2020, **8**, 7087–7096.

111 Y. C. Hudiono, T. K. Carlisle, J. E. Bara, Y. Zhang, D. L. Gin and R. D. Noble, *J. Membr. Sci.*, 2010, **350**, 117–123.

112 Z. V. Singh, M. G. Cowan, W. M. McDanel, Y. Luo, R. Zhou, D. L. Gin and R. D. Noble, *J. Membr. Sci.*, 2016, **509**, 149–155.

113 C. A. Dunn, Z. Shi, R. Zhou, D. L. Gin and R. D. Noble, *Ind. Eng. Chem. Res.*, 2019, **58**, 4704–4708.

114 A. R. Nabais, A. P. S. Martins, V. D. Alves, J. G. Crespo, I. M. Marrucho, L. C. Tomé and L. A. Neves, *Sep. Purif. Technol.*, 2019, **222**, 168–176.

115 A. M. Sampaio, A. R. Nabais, L. C. Tomé and L. A. Neves, *Ind. Eng. Chem. Res.*, 2020, **59**, 308–317.

116 L. C. Tomé, L. Porcarelli, J. E. Bara, M. Forsyth and D. Mecerreyes, *Mater. Horizons*, 2021, **8**, 3239–3265.

117 J. Le Bideau, L. Viau and A. Vioux, *Chem. Soc. Rev.*, 2011, **40**, 907–925.

118 J. M. Chem, M. Oubaha, A. Kavanagh, A. Gorin, G. Bickauskaite, R. Byrne and M. Farsari, *J. Mater. Chem.*, 2012, **22**, 10552–10559.

119 E. Kamio, T. Yasui, Y. Iida, J. P. Gong and H. Matsuyama, *Adv. Mater.*, 2017, **29**, 1–8.

120 L. Yu, S. Guo, Y. Li, X. Lan, D. Wu, R. Li, S. Wu and X. Hu, *Adv. Energy Mater.*, 2019, **9**,

1900257.

121 A. Su, P. Guo, J. Li, D. Kan, Q. Pang, T. Li, J. Sun, G. Chen and Y. Wei, *J. Mater. Chem. A*, 2020, **8**, 4775.

122 H. Li, Z. Feng, K. Zhao, Z. Wang, J. Liu, J. Liu and H. Song, *Nanoscale*, 2019, **11**, 3689–3700.

123 X. Liu, B. He, Z. Wang, H. Tang, T. Su and Q. Wang, *Sci. Rep.*, 2014, **4**, 1–7.

124 C. Lu and X. Chen, *Materials (Basel).*, 2020, **13**, 1–7.

125 S. M. Villa, V. M. Mazzola, T. Santaniello, E. Locatelli, M. Maturi, L. Migliorini, C. Lenardi, M. C. Franchini and P. Milani, *ACS Macro Lett.*, 2019, **8**, 414–420.

126 Z. Dai, L. Ansaloni, J. J. Ryan, R. J. Spontak and L. Deng, *J. Memb. Sci.*, 2019, **588**, 117193.

127 H. Gao, L. Bai, J. Han, B. Yang, S. Zhang and X. Zhang, *Chem. Commun.*, 2018, **54**, 12671–12685.

128 B. A. Voss, J. E. Bara, D. L. Gin and R. D. Noble, *Chem. Mater.*, 2009, **21**, 3027–3029.

129 Y. Gu, E. L. Cussler and T. P. Lodge, *J. Memb. Sci.*, 2012, **423**–**424**, 20–26.

130 W. Fam, J. Mansouri, H. Li and V. Chen, *J. Memb. Sci.*, 2017, **537**, 54–68.

131 A. M. Lopez, M. G. Cowan, D. L. Gin and R. D. Noble, *J. Chem. Eng. Data*, 2018, **63**, 1154–1162.

132 Y. Gu and T. P. Lodge, *Macromolecules*, 2011, **44**, 1732–1736.

133 A. Ito, T. Yasuda, T. Yoshioka, A. Yoshida, X. Li, K. Hashimoto, K. Nagai, M. Shibayama and M. Watanabe, *Macromolecules*, 2018, **51**, 7112–7120.

134 M. S. Mittenthal, B. S. Flowers, J. E. Bara, J. W. Whitley, S. K. Spear, J. D. Roveda, D. A. Wallace, M. S. Shannon, R. Holler, R. Martens and D. T. Daly, *Ind. Eng. Chem. Res.*, 2017, **56**, 5055–5069.

135 V. A. Kusuma, M. K. Macala, J. Liu, A. M. Marti, R. J. Hirsch, L. J. Hill and D. Hopkinson, *J. Memb. Sci.*, 2018, **545**, 292–300.

136 A. P. S. Martins, A. F. De Añastro, J. L. Olmedo-Martínez, A. R. Nabais, L. A. Neves, D. Mecerreyes and L. C. Tomé, *Membranes (Basel).*, 2020, **10**, 46.

137 W. M. McDanel, M. G. Cowan, N. O. Chisholm, D. L. Gin and R. D. Noble, *J. Memb. Sci.*, 2015, **492**, 303–311.

138 F. Moghadam, E. Kamio, T. Yoshioka and H. Matsuyama, *J. Memb. Sci.*, 2017, **530**, 166–175.

139 I. Kammakakam, J. E. Bara, E. M. Jackson, J. Lertxundi, D. Mecerreyes and L. C. Tomé, *ACS Sustain. Chem. Eng.*, 2020, **8**, 5954–5965.

140 R. M. Teodoro, L. C. Tomé, D. Mantione, D. Mecerreyes and I. M. Marrucho, *J. Memb. Sci.*, 2018, **552**, 341–348.

141 H. Lin, T. Kai, B. D. Freeman, S. Kalakkunnath and D. S. Kalika, *Macromolecules*, 2005, **38**, 8381–8393.

142 V. A. Kusuma, M. K. Macala, J. S. Baker and D. Hopkinson, *Ind. Eng. Chem. Res.*, 2018, **57**, 11658–11667.

143 S. Zeng, X. Zhang, L. Bai, X. Zhang, H. Wang, J. Wang, D. Bao, M. Li, X. Liu and S. Zhang, *Chem. Rev.*, 2017, **117**, 9625–9673.

144 S. Zhang, J. Zhang, Y. Zhang and Y. Deng, *Chem. Rev.*, 2017, **2**, 6755–6833.
145 G. Dong, H. Li and V. Chen, *J. Mater. Chem.*, 2013, **1**, 4610–4630.
146 L. Ma, F. Svec, Y. Lv and T. Tan, *Chemistry (Easton).*, 2019, **14**, 3502–3514.
147 M. Li, X. Zhang, S. Zeng, L. Bai, H. Gao, J. Deng, Q. Yang and S. Zhang, *RSC Adv.*, 2017, **7**, 6422–6431.
148 F. Ranjbaran, E. Kamio and H. Matsuyama, *J. Memb. Sci.*, 2017, **544**, 252–260.
149 F. Ranjbaran, E. Kamio and H. Matsuyama, *Ind. Eng. Chem. Res.*, 2017, **56**, 12763–12772.
150 E. Kamio, M. Minakata, Y. Iida, T. Yasui, A. Matsuoka and H. Matsuyama, *Polym. J.*, 2021, **53**, 137–147.
151 J. Zhang, E. Kamio, A. Matsuoka, K. Nakagawa, T. Yoshioka and H. Matsuyama, *Ind. Eng. Chem. Res.*, 2021, **60**, 12640–12649.
152 J. Zhang, E. Kamio, M. Kinoshita, A. Matsuoka, K. Nakagawa, T. Yoshioka and H. Matsuyama, *Ind. Eng. Chem. Res.*, 2021, **60**, 12698–12708.
153 F. Pitsch, F. F. Krull, F. Agel, P. Schulz, P. Wasserscheid, T. Melin and M. Wessling, *Adv. Mater.*, 2012, **24**, 4306–4310.
154 M. Fallanza, A. Ortiz, D. Gorri and I. Ortiz, *J. Memb. Sci.*, 2013, **444**, 164–172.
155 J. H. Lee, J. Hong, J. H. Kim, Y. S. Kang and S. W. Kang, *Chem. Commun.*, 2012, **48**, 5298–5300.
156 W. Fam, J. Mansouri, H. Li, J. Hou and V. Chen, *Ind. Eng. Chem. Res.*, 2019, **58**, 3304–3313.
157 E. Ghasemi Estahbanati, M. Omidkhah and A. Ebadi Amooghin, *ACS Appl. Mater. Interfaces*, 2017, **9**, 10094–10105.
158 S. Singh, A. M. Varghese, D. Reinalda and G. N. Karanikolos, *J. CO2 Util.*, 2021, **49**, 101544.
159 Z. Qiao, S. Zhao, J. Wang, S. Wang, Z. Wang and M. D. Guiver, *Angew. Chemie - Int. Ed.*, 2016, **55**, 9321–9325.
160 A. Jamil, M. Zulfiqar, U. Arshad, S. Mahmood, T. Iqbal, S. Rafiq and M. Z. Iqbal, *Adv. Polym. Technol.*, 2020, **2020**, 1–12.
161 M. Smiglak, J. M. Pringle, X. Lu, L. Han, S. Zhang, H. Gao, D. R. Mac Farlane and R. D. Rogers, *Chem. Commun.*, 2014, **50**, 9228–9250.
162 N. V. Plechkova and K. R. Seddon, *Chem. Soc. Rev.*, 2008, **37**, 123–150.
163 L. Porcarelli, A. S. Shaplov, M. Salsamendi, J. R. Nair, Y. S. Vygodskii, D. Mecerreyes and C. Gerbaldi, *ACS Appl. Mater. Interfaces*, 2016, **8**, 10350–10359.
164 H. Mohammed, A. Al-Othman, P. Nancarrow, Y. Elsayed and M. Tawalbeh, *Int. J. Hydrogen Energy*, 2021, **46**, 4857–4869.
165 H. Karimi-Maleh, C. T. Fakude, N. Mabuba, G. M. Peleyeju and O. A. Arotiba, *J. Colloid Interface Sci.*, 2019, **554**, 603–610.
166 S. Velasco-Bosom, N. Karam, A. Carnicer-Lombarte, J. Gurke, N. Casado, L. C. Tomé, D. Mecerreyes and G. G. Malliaras, *Adv. Healthc. Mater.*, 2021, **10**, 10–15.
167 S. T. Chen, M. N. Renny, L. C. Tomé, J. L. Olmedo-Martínez, E. Udabe, E. P. W. Jenkins, D. Mecerreyes, G. G. Malliaras, R. R. McLeod and C. M. Proctor, *Adv. Sci.*, 2021, **8**, 1–9.

168 L. C. Tomé, L. Porcarelli, J. E. Bara, M. Forsyth and D. Mecerreyes, *Mater. Horizons*, 2021, **8**, 3239–3265.
169 A. Guyomard-Lack, N. Buchtová, B. Humbert and J. Le Bideau, *Phys. Chem. Chem. Phys.*, 2015, **17**, 23947–23951.
170 T. Zhou, X. Gao, F. Lu, N. Sun and L. Zheng, *New J. Chem.*, 2016, **40**, 1169–1174.
171 S. A. M. Noor, P. M. Bayley, M. Forsyth and D. R. MacFarlane, *Electrochim. Acta*, 2013, **91**, 219–226.
172 K. Ueno, K. Hata, T. Katakabe, M. Kondoh and M. Watanabe, *J. Phys. Chem. B*, 2008, **112**, 9013–9019.
173 J. H. Ri, J. Jin, J. Xu, T. Peng and K. Il Ryu, *Electrochim. Acta*, 2016, **201**, 251–259.
174 Z. V. Singh, M. G. Cowan, W. M. McDanel, Y. Luo, R. Zhou, D. L. Gin and R. D. Noble, *J. Memb. Sci.*, 2016, **509**, 149–155.
175 S. Wang, X. Li, H. Wu, Z. Tian, Q. Xin, G. He, D. Peng, S. Chen, Y. Yin, Z. Jiang and M. D. Guiver, *Energy Environ. Sci.*, 2016, **9**, 1863–1890.
176 B. Monteiro, A. R. Nabais, M. H. Casimiro, A. P. S. Martins, R. O. Francisco, L. A. Neves and C. C. L. Pereira, *Membranes (Basel).*, 2018, **8**, 93.
177 J. Shen, M. Zhang, G. Liu, K. Guan and W. Jin, *AIChE J.*, 2016, **62**, 2843–2852.
178 Z. Amini and M. Asghari, *Appl. Clay Sci.*, 2018, **166**, 230–241.
179 A. Jamil, O. P. Ching and A. B. M. Shariff, *Chem. Eng. Technol.*, 2016, **39**, 1393–1405.
180 A. V. Noskov, O. V. Alekseeva, V. D. Shibaeva and A. V. Agafonov, *RSC Adv.*, 2020, **10**, 34885–34894.
181 S. Sinha Ray, in *Clay-containing Polymer Nanocomposites: From Fundamentals to Real Applications*, Elsevier, First edit., 2013, pp. 1–24.
182 A. Jamil, O. P. Ching and A. B. M. Shariff, *Appl. Mech. Mater.*, 2014, **625**, 690–695.
183 M. Mulder, *Basic principles of membrane technology 2nd ed.*, Kluwer Academic Publishers, The Netherlands, Second., 1996.
184 G. Defontaine, A. Barichard, S. Letaief, C. Feng, T. Matsuura and C. Detellier, *J. Colloid Interface Sci.*, 2010, **343**, 622–627.
185 J. J. Parajó, T. Teijeira, J. Fernández, J. Salgado and M. Villanueva, *J. Chem. Thermodyn.*, 2017, **112**, 105–113.
186 S. A. Hashemifard, A. F. Ismail and T. Matsuura, *Chem. Eng. J.*, 2011, **170**, 316–325.
187 N. Ghaemi, S. S. Madaeni, A. Alizadeh, H. Rajabi and P. Daraei, *J. Memb. Sci.*, 2011, **382**, 135–147.
188 S. Mahmoudian, M. U. Wahit, A. F. Ismail and A. A. Yussuf, *Carbohydr. Polym.*, 2012, **88**, 1251–1257.
189 M. Behroozi and M. Pakizeh, *J. Appl. Polym. Sci.*, 2017, **134**, 1–11.
190 A. Jamil, P. C. Oh and A. M. Shariff, *Sep. Purif. Technol.*, 2018, **206**, 256–267.
191 B. W. Rowe, L. M. Robeson, B. D. Freeman and D. R. Paul, *J. Membr. Sci.*, 2010, **360**, 58–69.
192 Y. C. Hudiono, T. K. Carlisle, A. L. LaFrate, D. L. Gin and R. D. Noble, *J. Membr. Sci.*, 2011,

370, 141–148.

193 H. R. Mahdavi, N. Azizi, M. Arzani and T. Mohammadi, *J. Nat. Gas Sci. Eng.*, 2017, **46**, 275–288.

194 W. Fam, J. Mansouri, H. Li and V. Chen, *J. Memb. Sci.*, 2017, **537**, 54–68.

195 K. Friess, M. Lanč, K. Pilnáček, V. Fíla, O. Vopička, Z. Sedláková, M. G. Cowan, W. M. McDanel, R. D. Noble, D. L. Gin and P. Izak, *J. Memb. Sci.*, 2017, **528**, 64–71.

196 A. Ito, T. Yasuda, X. Ma and M. Watanabe, *Polym. J.*, 2017, **49**, 671–676.

197 K. E. O'Harra, I. Kammakakam, E. M. Devriese, D. M. Noll, J. E. Bara and E. M. Jackson, *Membranes (Basel).*, 2019, **9**, 79.

198 J. Zhou, M. M. Mok, M. G. Cowan, W. M. Mcdanel, T. K. Carlisle, D. L. Gin and R. D. Noble, *Ind. Eng. Chem. Res.*, 2014, **53**, 20064–20067.

199 J. Yin, C. Zhang, Y. Yu, T. Hao, H. Wang, X. Ding and J. Meng, *J. Memb. Sci.*, 2020, **593**, 117405.

200 I. Kammakakam, J. E. Bara, E. M. Jackson, J. Lertxundi, D. Mecerreyes and L. C. Tomé, *ACS Sustain. Chem. Eng.*, 2020, **8**, 5954–5965.

201 J. Deng, J. Yu, Z. Dai and L. Deng, *Ind. Eng. Chem. Res.*, 2019, **58**, 5261–5268.

202 J. Xu, Z. Wang, Z. Qiao, H. Wu, S. Dong, S. Zhao and J. Wang, *J. Memb. Sci.*, 2019, **581**, 195–213.

203 A. R. Kamble, C. M. Patel and Z. V. P. Murthy, *Renew. Sustain. Energy Rev.*, 2021, **145**, 111062.

204 M. Kárászová, B. Zach, Z. Petrusová, V. Červenka, M. Bobák, M. Šyc and P. Izák, *Sep. Purif. Technol.*, 2020, **238**, 116448.

205 M. Klepić, K. Setničková, M. Lanč, M. Žák, P. Izák, M. Dendisová, A. Fuoco, J. C. Jansen and K. Friess, *J. Memb. Sci.*, 2020, **597**, 117623.

206 M. Galizia, W. S. Chi, Z. P. Smith, T. C. Merkel, R. W. Baker and B. D. Freeman, *Macromolecules*, 2017, **50**, 7809–7843.

207 L. C. Tomé, A. S. L. Gouveia, M. A. Ab Ranii, P. D. Lickiss, T. Welton and I. M. Marrucho, *Ind. Eng. Chem. Res.*, 2017, **56**, 2229–2239.

208 M. Klepić, A. Fuoco, M. Monteleone, E. Esposito, K. Friess, Z. Petrusová, P. Izák and J. C. Jansen, *Polymers (Basel).*, 2020, **12**, 890.

209 L. Hao, P. Li, T. Yang and T. S. Chung, *J. Memb. Sci.*, 2013, **436**, 221–231.

210 W. Fam, J. Mansouri, H. Li, J. Hou and V. Chen, *ACS Appl. Mater. Interfaces*, 2018, **10**, 7389–7400.

211 S. Kanehashi and C. A. Scholes, *Front. Chem. Sci. Eng.*, 2020, **14**, 460–469.

212 M. Chawla, H. Saulat, M. Masood Khan, M. Mahmood Khan, S. Rafiq, L. Cheng, T. Iqbal, M. I. Rasheed, M. Z. Farooq, M. Saeed, N. M. Ahmad, M. B. Khan Niazi, S. Saqib, F. Jamil, A. Mukhtar and N. Muhammad, *Chem. Eng. Technol.*, 2020, **43**, 184–199.

213 K. K. Wong and Z. A. Jawad, *J. Polym. Res.*, 2019, **26**, 1–18.

214 S. Y. Ding, J. Gao, Q. Wang, Y. Zhang, W. G. Song, C. Y. Su and W. Wang, *J. Am. Chem. Soc.*, 2011, **133**, 19816–19822.

215 L. Stegbauer, K. Schwinghammer and B. V. Lotsch, *Chem. Sci.*, 2014, **5**, 2789–2793.
216 Q. Fang, S. Gu, J. Zheng, Z. Zhuang, S. Qiu and Y. Yan, *Angew. Chemie*, 2014, **126**, 2922–2926.
217 S. Wan, F. Gándara, A. Asano, H. Furukawa, A. Saeki, S. K. Dey, L. Liao, M. W. Ambrogio, Y. Y. Botros, X. Duan, S. Seki, J. F. Stoddart and O. M. Yaghi, *Chem. Mater.*, 2011, **23**, 4094–4097.
218 X. H. Liu, C. Z. Guan, D. Wang and L. J. Wan, *Adv. Mater.*, 2014, **26**, 6912–6920.
219 M. Dogru, M. Handloser, F. Auras, T. Kunz, D. Medina, A. Hartschuh, P. Knochel and T. Bein, *Angew. Chemie*, 2013, **125**, 2992–2996.
220 G. Das, B. P. Biswal, S. Kandambeth, V. Venkatesh, G. Kaur, M. Addicoat, T. Heine, S. Verma and R. Banerjee, *Chem. Sci.*, 2015, **6**, 3931–3939.
221 A. Nagai, X. Chen, X. Feng, X. Ding, Z. Guo and D. Jiang, *Angew. Chemie*, 2013, **125**, 3858–3862.
222 S. Dalapati, S. Jin, J. Gao, Y. Xu, A. Nagai and D. Jiang, *J. Am. Chem. Soc.*, 2013, **135**, 17310–17313.
223 J. T. Yu, Z. Chen, J. Sun, Z. T. Huang and Q. Y. Zheng, *J. Mater. Chem.*, 2012, **22**, 5369–5373.
224 C. J. Doonan, D. J. Tranchemontagne, T. G. Glover, J. R. Hunt and O. M. Yaghi, *Nat. Chem.*, 2010, **2**, 235–238.
225 S. S. Han, H. Furukawa, O. M. Yaghi and W. A. G. Iii, *JACS Commun.*, 2008, **105**, 11580–11581.
226 G. Ma, Heping; Ren, Hao; Meng, Shuang; Yan, Zhuojun; Zhao, Huanyu; Sun, Fuxing; Zhu, *Chem. Commun.*, 2013, **49**, 9773–9775.
227 P. Arab, E. Parrish, T. Islamoğlu and H. M. El-Kaderi, *J. Mater. Chem. A*, 2015, **3**, 20586–20594.
228 L. Zou, Y. Sun, S. Che, X. Yang, X. Wang, M. Bosch, Q. Wang, H. Li, M. Smith, S. Yuan, Z. Perry and H. C. Zhou, *Adv. Mater.*, 2017, **29**, 1–35.
229 J. Lu and J. Zhang, *J. Mater. Chem. A*, 2014, **2**, 13831–13834.
230 Z. Yang, H. Zhang, B. Yu, Y. Zhao, Z. Ma, G. Ji, B. Han and Z. Liu, *Chem. Commun.*, 2015, **51**, 11576–11579.
231 R. He, S. Cong, S. Xu, S. Han, H. Guo, Z. Liang, J. Wang and Y. Zhang, *J. Memb. Sci.*, 2021, **624**, 119081.
232 J. X. Zhou, X. S. Luo, X. Liu, Y. Qiao, P. Wang, D. Mecerreyes, N. Bogliotti, S. L. Chen and M. H. Huang, *J. Mater. Chem. A*, 2018, **6**, 5608–5612.
233 F. Chen, G. Tian, L. Shi, S. Qi and D. Wu, *RSC Adv.*, 2012, **2**, 12879–12885.
234 A. F. M. El-Mahdy, M. G. Mohamed, T. H. Mansoure, H. H. Yu, T. Chen and S. W. Kuo, *Chem. Commun.*, 2019, **55**, 14890–14893.
235 E. L. Cussler, *Fundamentals of Mass Transfer*, Cambridge University Press, New York, Third edit., 2009.
236 R. Selyanchyn, M. Ariyoshi and S. Fujikawa, *Membranes (Basel).*, 2018, **8**, 121.
237 J. M. S. Henis and M. K. Tripodi, *J. Memb. Sci.*, 1981, **8**, 233–246.
238 H. A. Patel, S. Hyun Je, J. Park, D. P. Chen, Y. Jung, C. T. Yavuz and A. Coskun, *Nat. Commun.*,

2013, **4**, 1–8.

239 P. M. Budd, E. S. Elabas, B. S. Ghanem, S. Makhseed, N. B. McKeown, K. J. Msayib, C. E. Tattershall and D. Wang, *Adv. Mater.*, 2004, **16**, 456–459.

240 J. Jeromenok and J. Weber, *Langmuir*, 2013, **29**, 12982–12989.

241 H. X. Fu, Z. H. Zhang, W. Fan, S. Wang, Y. Liu and M. H. Huang, *J. Mater. Chem. A*, 2019, **7**, 15048–15053.

242 S. Q. Peng, B. Zhang, W. Fan, S. Wang, Z. H. Zhang, Y. Liu, S. L. Chen and M. H. Huang, *Polym. Chem.*, 2020, **11**, 6429–6434.

243 M. Thommes, K. Kaneko, A. V. Neimark, J. P. Olivier, F. Rodriguez-Reinoso, J. Rouquerol and K. S. W. Sing, *Pure Appl. Chem.*, 2015, **87**, 1051–1069.

244 P. Arab, M. G. Rabbani, A. K. Sekizkardes, T. Islamoğlu and H. M. El-Kaderi, *Chem. Mater.*, 2014, **26**, 1385–1392.

245 K. Hosaka, J. Tagami, Y. Nishitani, M. Yoshiyama, M. Carrilho, F. R. Tay, K. A. Agee and D. H. Pashley, *Eur. J. Oral Sci.*, 2007, **115**, 239–245.

246 A. Hassan, N. A. Rahman and R. Yahya, *Fibers Polym.*, 2012, **13**, 899–906.

247 A. R. Nabais, R. P. P. L. Ribeiro, J. P. B. Mota, V. D. Alves, I. A. A. C. Esteves and L. A. Neves, *Sep. Purif. Technol.*, 2018, **202**, 174–184.

248 A. Brunetti, F. Scura, G. Barbieri and E. Drioli, *J. Memb. Sci.*, 2010, **359**, 115–125.

249 M. Rezakazemi, A. Ebadi Amooghin, M. M. Montazer-Rahmati, A. F. Ismail and T. Matsuura, *Prog. Polym. Sci.*, 2014, **39**, 817–861.

250 S. R. Reijerkerk, K. Nijmeijer, C. P. Ribeiro, B. D. Freeman and M. Wessling, *J. Memb. Sci.*, 2011, **367**, 33–44.

251 E. Lasseuguette, R. Malpass-Evans, M. Carta, N. B. McKeown and M. C. Ferrari, *Membranes (Basel).*, 2018, **8**, 1–11.

252 J. D. Moon, H. Borjigin, R. Liu, R. M. Joseph, J. S. Riffle, B. D. Freeman and D. R. Paul, *J. Memb. Sci.*, 2021, **639**, 119758.

253 A. R. Nabais, R. O. Francisco, V. D. Alves, L. A. Neves and L. C. Tomé, *Membranes (Basel).*, 2021, **11**, 998.

254 A. R. Nabais, S. Ahmed, M. Younis, J. Zhou, F. Freitas, D. Mecerreyes, G. J. Crespo, M. Huang, L. A. Neves and L. C. Tomé, *J. Memb. Sci.*, 2022, **660**, 120840.

255 B. P. Spigarelli and S. K. Kawatra, *J. CO2 Util.*, 2013, **1**, 69–87.

256 S. D. Kenarsari, D. Yang, G. Jiang, S. Zhang, J. Wang, A. G. Russell, Q. Wei and M. Fan, *RSC Adv.*, 2013, **3**, 22739–22773.

257 R. Khalilpour, K. Mumford, H. Zhai, A. Abbas, G. Stevens and E. S. Rubin, *J. Clean. Prod.*, 2015, **103**, 286–300.

258 A. Brunetti, E. Drioli, Y. M. Lee and G. Barbieri, *J. Memb. Sci.*, 2014, **454**, 305–315.

259 R. W. Baker and K. Lokhandwala, *Ind. Eng. Chem. Res.*, 2008, **47**, 2109–2121.

260 T. E. Rufford, S. Smart, G. C. Y. Watson, B. F. Graham, J. Boxall, J. C. Diniz da Costa and E. F. May, *J. Pet. Sci. Eng.*, 2012, **94**–**95**, 123–154.

261 L. Deng and M. B. Hägg, *Int. J. Greenh. Gas Control*, 2010, **4**, 638–646.
262 L. Greenspan, *J. Res. Natl. Bur. Stand. A. Phys. Chem.*, 1977, **81**, 89–96.
263 G. Q. Chen, C. A. Scholes, G. G. Qiao and S. E. Kentish, *J. Memb. Sci.*, 2011, **379**, 479–487.
264 C. A. Scholes, J. Jin, G. W. Stevens and S. E. Kentish, *J. Polym. Sci. Part B Polym. Phys.*, 2015, **53**, 719–728.
265 R. Sander, *Atmos. Chem. Phys.*, 2015, **15**, 4399–4981.
266 B. Zhang, C. Yang, Y. Zheng, Y. Wu, C. Song, Q. Liu and Z. Wang, *J. Memb. Sci.*, 2021, **627**, 119239.
267 A. S. L. Gouveia, M. Yáñez, V. D. Alves, J. Palomar, C. Moya, D. Gorri, L. C. Tomé and I. M. Marrucho, *Sep. Purif. Technol.*, 2021, **259**, 118113.
268 S. A. Gulmus and L. Yilmaz, *J. Polym. Sci. Part B Polym. Phys.*, 2007, **45**, 3025–3033.
269 C. K. Yeom, S. H. Lee and J. M. Lee, *J. Appl. Polym. Sci.*, 2000, **78**, 179–189.
270 M. R. A. Hamid and H. K. Jeong, *Korean J. Chem. Eng.*, 2018, **35**, 1577–1600.
271 N. N. R. Ahmad, C. P. Leo, A. W. Mohammad, N. Shaari and W. L. Ang, *Int. J. Energy Res.*, 2021, **45**, 9800–9830.
272 C. Wang and R. Patel, *Membr. J.*, 2021, **31**, 1–15.
273 E. Adatoz, A. K. Avci and S. Keskin, *Sep. Purif. Technol.*, 2015, **152**, 207–237.
274 J. A. Mason, K. Sumida, Z. R. Herm, R. Krishna and J. R. Long, *Energy Environ. Sci.*, 2011, **4**, 3030–3040.
275 S. Basu, A. Cano-Odena and I. F. J. Vankelecom, *Sep. Purif. Technol.*, 2011, **81**, 31–40.
276 R. Abedini, M. Omidkhah and F. Dorosti, *Int. J. Hydrog. Energy*, 2014, **39**, 7897–7909.
277 Z. Liang, M. Marshall and A. L. Chaffee, *Energy Fuels*, 2009, **23**, 2785–2789.
278 B. C. R. Camacho, R. P. P. L. Ribeiro, I. A. A. C. Esteves and J. P. B. Mota, *Sep. Purif. Technol.*, 2015, **141**, 150–159.
279 S. Shang, Z. Tao, C. Yang, A. Hanif, L. Li, D. C. W. Tsang, Q. Gu and J. Shang, *Chem. Eng. J.*, 2020, **393**, 124666.
280 Y. Zhang, H. Wibowo, L. Zhong, M. Horttanainen, Z. Wang, C. Yu and M. Yan, *Sep. Purif. Technol.*, 2021, **279**, 119644.
281 A. R. Nabais, P. Ortiz-Albo, J.-X. Zhou, M.-H. Huang, D. Mecerreyes, J. G. Crespo, L. C. Tomé and L. A. Neves, *Chapter 4 - Submitt.*
282 Z. Dong, Z. Mi, W. Shi, H. Jiang, Y. Zheng and K. Yang, *RSC Adv.*, 2017, **7**, 55504–55512.
283 X. Y. Chen, H. Vinh-Thang, D. Rodrigue and S. Kaliaguine, *Ind. Eng. Chem. Res.*, 2012, **51**, 6895–6906.
284 Z. Yang, H. Peng, W. Wang and T. Liu, *J. Appl. Polym. Sci.*, 2010, **116**, 2658–2667.
285 H. Ju, B. D. McCloskey, A. C. Sagle, V. A. Kusuma and B. D. Freeman, *J. Memb. Sci.*, 2009, **330**, 180–188.
286 S. Shahid and K. Nijmeijer, *J. Membr. Sci.*, 2014, **470**, 166–177.
287 P. Rallapalli, K. P. Prasanth, D. Patil, R. S. Somani, R. V. Jasra and H. C. Bajaj, *J. Porous Mater.*, 2011, **18**, 205–210.

288 I. Kammakakam, J. E. Bara and E. M. Jackson, *ACS Appl. Polym. Mater.*, 2020, **2**, 5067–5076.
289 A. S. L. Gouveia, E. Bumenn, K. Rohtlaid, A. Michaud, T. M. Vieira, V. D. Alves, L. C. Tomé, C. Plesse and I. M. Marrucho, *Sep. Purif. Technol.*, 2021, **274**, 118437.
290 L. Chikh, V. Delhorbe and O. Fichet, *J. Memb. Sci.*, 2011, **368**, 1–17.
291 E. S. Dragan, *Chem. Eng. J.*, 2014, **243**, 572–590.
292 S. Saimani, M. M. Dal-Cin, A. Kumar and D. M. Kingston, *J. Memb. Sci.*, 2010, **362**, 353–359.
293 C. Zhang, W. Zhang, H. Gao, Y. Bai, Y. Sun and Y. Chen, *J. Memb. Sci.*, 2017, **528**, 72–81.
294 G. K. Kline, Q. Zhang, J. R. Weidman and R. Guo, *J. Memb. Sci.*, 2017, **544**, 143–150.
295 N. U. Kim, B. J. Park, M. S. Park, J. T. Park and J. H. Kim, *Chem. Eng. J.*, 2019, **360**, 1468–1476.
296 W. H. Lee, J. G. Seong, J. Y. Bae, H. H. Wang, S. J. Moon, J. T. Jung, Y. S. Do, H. Kang, C. H. Park and Y. M. Lee, *J. Memb. Sci.*, 2021, **625**, 119157.
297 A. R. Nabais, V. D. Alves, J. G. Crespo, L. C. Tomé and L. A. Neves, *Chapter 5 - prep.*
298 S. Basu, A. L. Khan, A. Cano-Odena, C. Liu and I. F. J. Vankelecom, *Chem. Soc. Rev.*, 2010, **39**, 750–768.
299 S. Basu, A. Cano-odena and I. F. J. Vankelecom, *J. Membr. Sci.*, 2010, **362**, 478–487.
300 M. M. Abdelnaby, T. A. Saleh, M. Zeama, M. A. Abdalla, H. M. Ahmed and M. A. Habib, *ACS Omega*, 2022, **7**, 14535–14543.
301 A. K. Zulhairun, A. F. Ismail, T. Matsuura, M. S. Abdullah and A. Mustafa, *Chem. Eng. J.*, 2014, **241**, 495–503.
302 Z. Qiao, S. Zhao, J. Wang, S. Wang, Z. Wang and M. D. Guiver, *Angew. Chemie - Int. Ed.*, 2016, **55**, 9321–9325.
303 J. Albo, E. Santos, L. A. Neves, S. P. Simeonov, C. A. M. Afonso, J. G. Crespo and A. Irabien, *Sep. Purif. Technol.*, 2012, **97**, 26–33.
304 S. M. Mahurin, T. Dai, J. S. Yeary, H. Luo and S. Dai, *Ind. Eng. Chem. Res.*, 2011, **50**, 14061–14069.
305 S. M. Mahurin, J. S. Yeary, S. N. Baker, D. en Jiang, S. Dai and G. A. Baker, *J. Memb. Sci.*, 2012, **401**–**402**, 61–67.
306 E. Santos, J. Albo and A. Irabien, *J. Memb. Sci.*, 2014, **452**, 277–283.
307 S. Kasahara, E. Kamio, T. Ishigami and H. Matsuyama, *J. Memb. Sci.*, 2012, **415**–**416**, 168–175.
308 S. V. Shaligram, P. P. Wadgaonkar and U. K. Kharul, *J. Memb. Sci.*, 2015, **493**, 403–413.
309 F. Moghadam, E. Kamio, A. Yoshizumi and H. Matsuyama, *Chem. Commun.*, 2015, **51**, 13658–13661.
310 N. Shahkaramipour, M. Adibi, A. A. Seifkordi and Y. Fazli, *J. Memb. Sci.*, 2014, **455**, 229–235.
311 L. C. Tomé, D. J. S. Patinha, C. S. R. Freire, L. P. N. Rebelo and I. M. Marrucho, *RSC Adv.*, 2013, **3**, 12220–12229.
312 R. M. Teodoro, L. C. Tomé, D. Mantione, D. Mecerreyes and I. M. Marrucho, *J. Memb. Sci.*, 2018, **552**, 341–348.

313 S. Kasahara, E. Kamio, A. Yoshizumi and H. Matsuyama, *Chem. Commun.*, 2014, **50**, 2996–2999.

314 R. W. Baker and B. T. Low, *Macromolecules*, 2014, **47**, 6999–7013.

A

APPENDIX: POLY(ETHYLENE GLYCOL) DIACRYLATE IONGEL MEMBRANES REINFORCED WITH NANOCLAYS FOR CO_2 SEPARATION

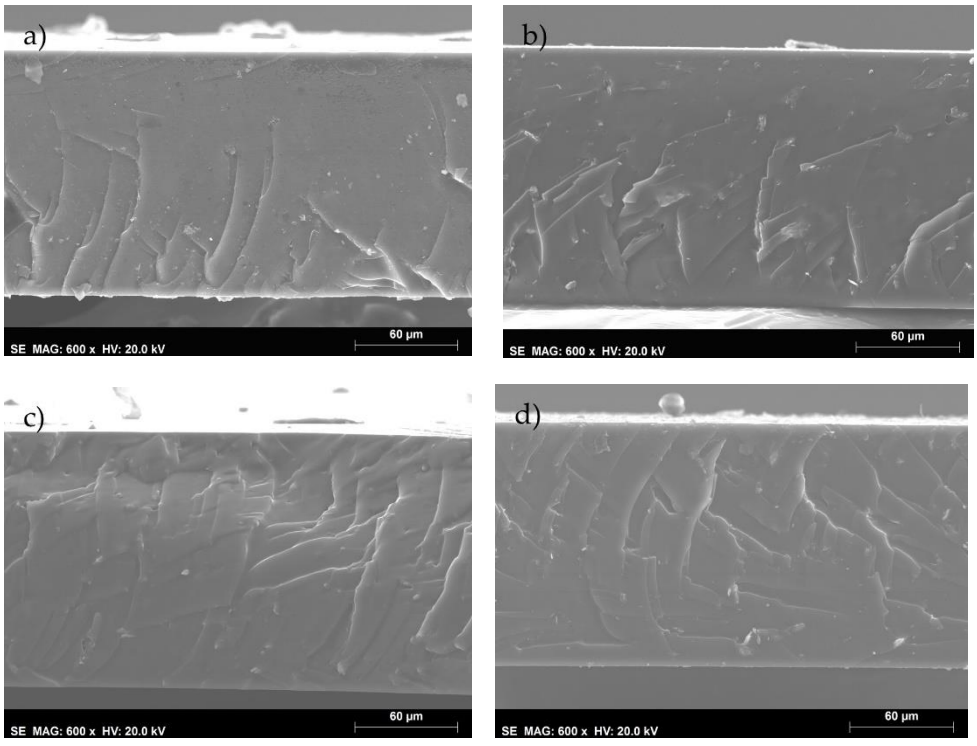

Figure A.1 – SEM images of the iongels containing (a) 0.5, (b) 1, (c) 2.5 and (d) 5 wt% MMT

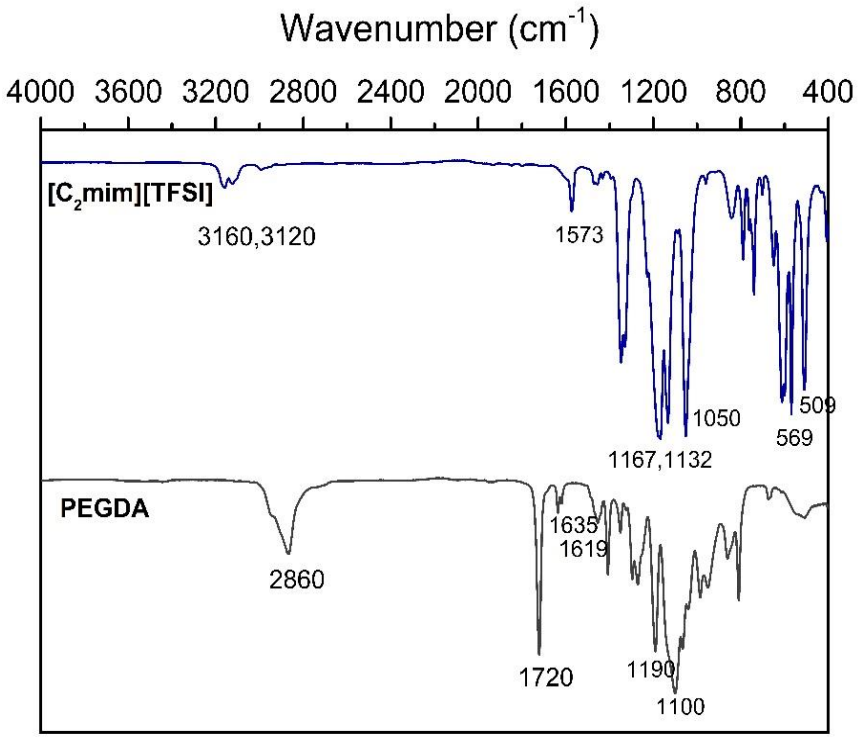

Figure A.2 – FTIR-ATR spectra of the [C_2mim][TFSI] IL and PEGDA network

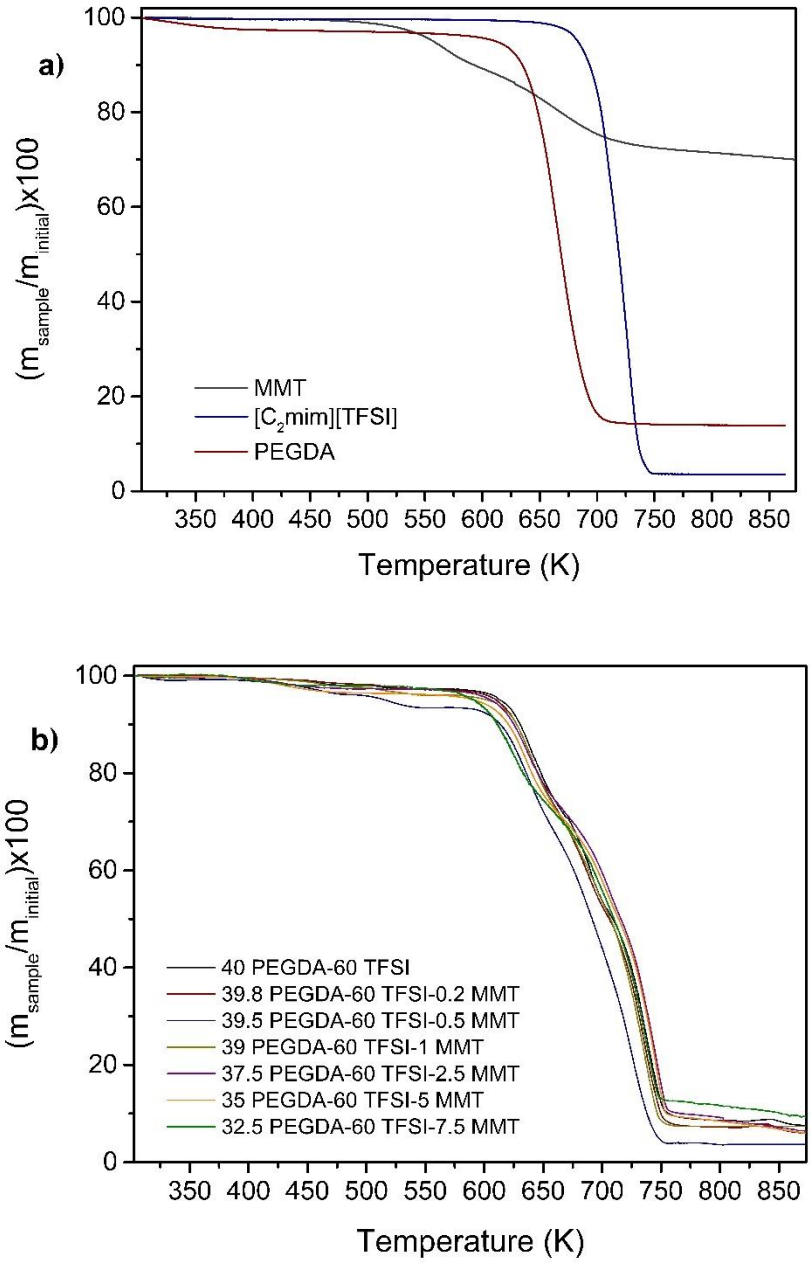

Figure A.3 - Thermogravimetric profiles of the (a) neat iongel components and (b) neat 40 PEGDA-60 TFSI iongel and MMIMs with different MMT contents.

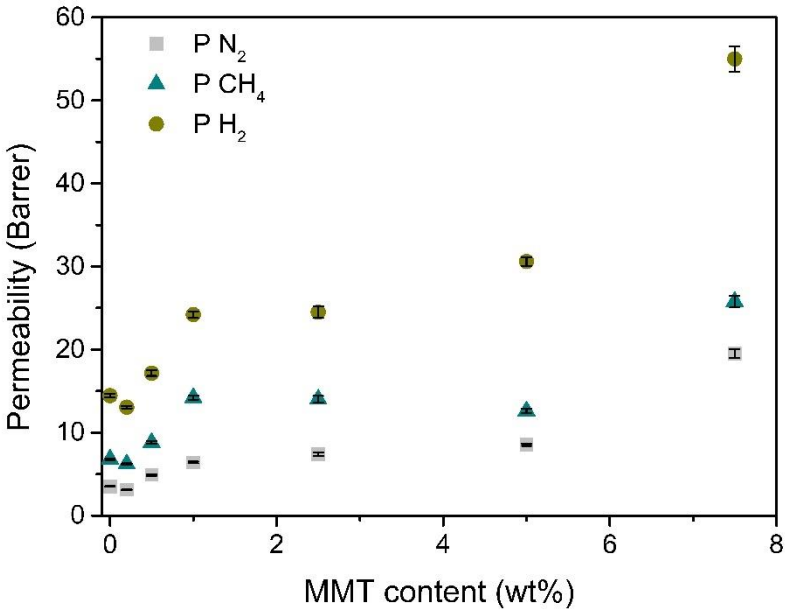

Figure A.4 - N_2, CH_4 and H_2 permeabilities obtained for the prepared neat 40 PEGDA-60 TFSI iongel and MMIMs, as a function of the MMT content.

B

APPENDIX: MIXED MATRIX MEMBRANES BASED ON IONIC LIQUIDS AND POROUS ORGANIC POLYMERS FOR SELECTIVE CO_2 SEPARATION

B.1 Synthesis of azo-POPs Monomers

Monomer 1, tetra (4-nitrophenyl) methane was obtained following the three-step procedure reported by Huang *et al*.,[232] as represented in Figure B.1, 3.25g of triphenylchloromethane was mixed with 9.75 mL of aniline and magnetically stirred at 473 K for 3h. After the solution cooled down to 363 K, 9.7 mL of methanol and 5 mL of concentrated HCl were added and the mixture was stirred at 363 K for another 5 h. The final mixture was cooled down to room temperature, filtered and washed with water and ethanol (3x100 mL) until light purple solid particles were obtained (86.5% yield). 3.75g of tetraphenylmethane aniline (hydrochloride) and 25 mL of acetonitrile were mixed with 9.38 mL of hypophosphite and 13.75 mL of HCl under magnetic stirring at 313 K. Subsequently, a sodium nitrite aqueous solution was slowly poured (10 M) into the previous solution, and the final solution was left stirring for 6h. The mixture was filtered and washed with water and ethanol (3x100 mL) and finally a white solid was obtained after vacuum drying.

Nitration of tetraphenyl methane was carried out by modifying a known procedure.[232] To 13.5 mL of nitric acid cooled down to 233 K, 2.5g of tetraphenylmethane were added in portions within 90 min. The reaction mixture was stirred for 30 min at 233 K before 4.3 mL of acetic anhydride and 8.5 mL of glacial acetic acid were added and left stirring for another 90 min. Finally, the obtained solid was washed with glacial acetic acid (2x100 mL) followed by water (3x100 mL) and THF (2x100 mL). The targeted monomer 1 was obtained as a yellow solid with a yield of 60%.

To synthesize the remaining monomers (Figure B.2), a solution of NaH (4 mmol) was fractionally added to 1 mmol of diamine moiety, phenylene diamine (monomer 2), benzidine (monomer 3) or terphenyl diamine (monomer 4) in DMSO (10 mL), followed by a dropwise addition of p-fluoro nitrobenzene (4.4 mmol). The reaction mixture was stirred for 4 h at 418 K and, after cooling, it was poured into 50 mL of methanol. The precipitated product was collected by filtration and dried to obtain the targeted yellow/orange solid particles (85% yield).

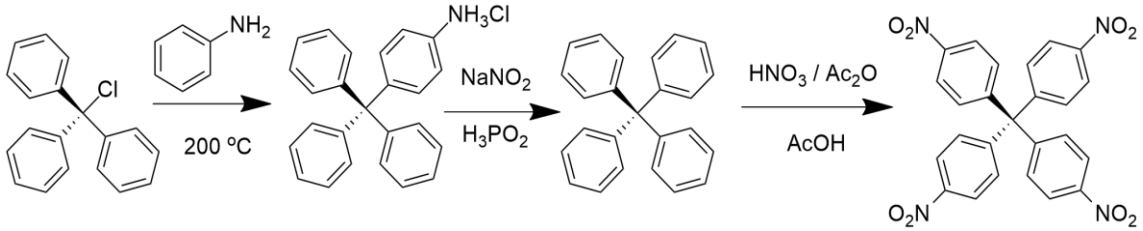

Figure B.1 - Synthesis of tetranitro-phenylmethane (monomer 1).

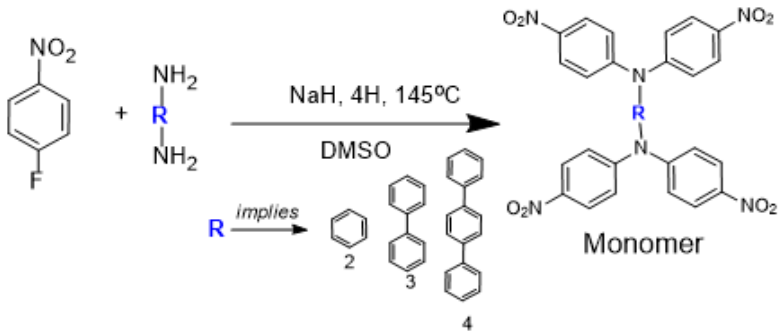

Figure B.2 - Synthesis of tetranitro-phenylene diamine (monomer 2), tetranitrobenzidine (monomer 3) and tetranitroterphenyl diamine (monomer 4).

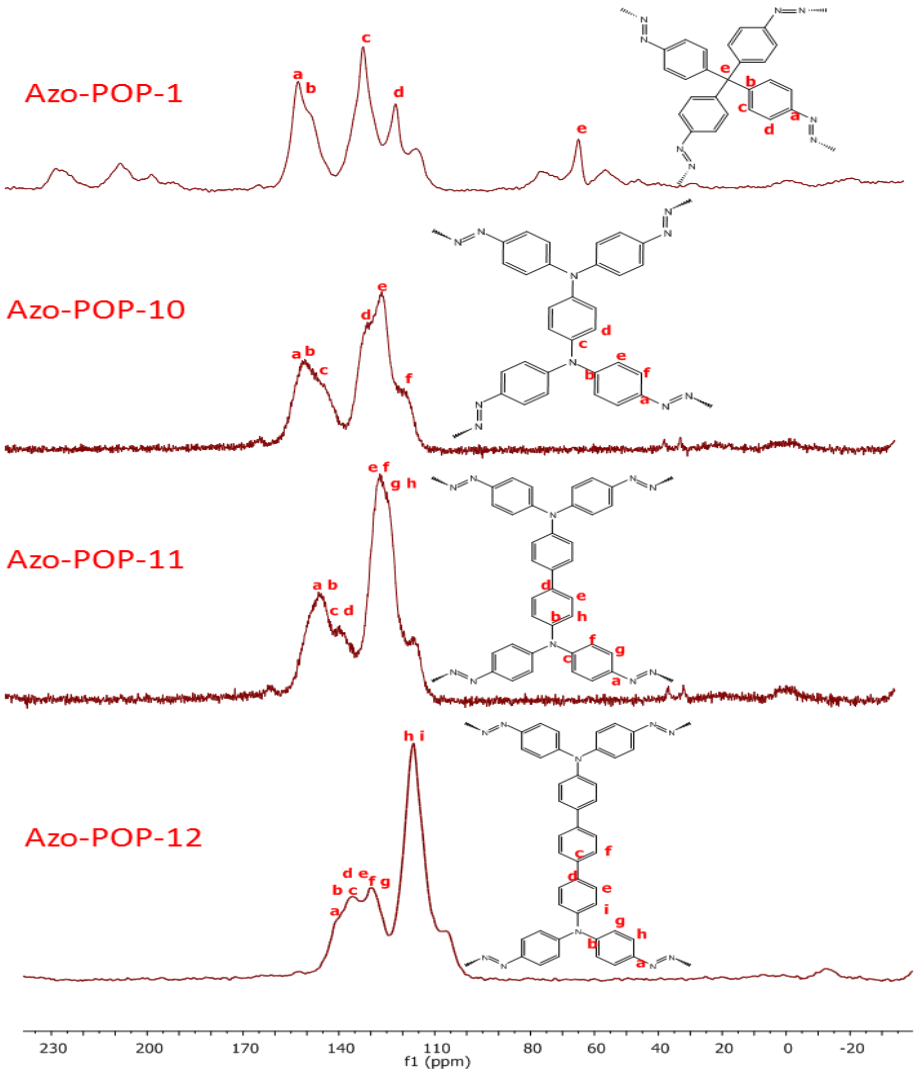

Figure B.3 - The ^{13}C CP/MS NMR of azo-POP-1, azo-POP-10, azo-POP-11 and azo-POP-12.

B.2 ^{1}H NMR of the Prepared Azo-POPs

Monomer 1

^{1}H-NMR(400 MHz, DMSO-d6) δ (ppm): 8.20 d (8H); 7.57 d (8H). FT-IR (cm-1): 3111 (vw), 3081 (vw), 1606(w), 1591 (w), 1494 (m), 1340 (vs), 1301 (m), 1109 (m),

Monomer 2

^{1}H NMR (DMSO-d_6, 400 MHz): δ (ppm) (DMSO-6d) 8.18-8.20 d(8H), 7.32 s(4H) and 7.26-7.29 d(4H). IR(cm^{-1}): 3069(s), 1580(s), 1485(s), 1302(s), 1106(s).

Monomer 3

^{1}H NMR (DMSO-d_6, 400 MHz): δ (ppm) (DMSO-6d) 8.18-8.20 d(8H), 7.80-7.82 d(4H), 7.31-7.34 d(4H) and 7.22-7.25 d(8H). IR(cm^{-1}): 3080(s), 1580(s), 1491(s), 1329(s), 1112(s).

Monomer 4

^{1}H NMR (DMSO-d_6, 400 MHz): δ (ppm) (DMSO-6d) 8.19-8.21 d(8H), 7.85-7.86 d(4H), 7.82 (s,4H) 7.35-7.33 d(4H) and 7.27-7.25 d(8H). IR(cm^{-1}): 3030(s), 1587(s), 1489(s), 1312(s), 1160(s).

Table B.1 - Experimental and theoretical data of Elemental Analysis of azo-POPs.

Sample	Actual Percentage				Theoretical Percentage			
	% of C	*% of H*	*% of N*	*C/N ratio*	*% of C*	*% of H*	*% of N*	*C/N ratio*
Azo-POP-1	75.75	75.75	14.41	5.26	80.63	4.33	15.04	5.36
Azo-POP-10	67.73	4.30	16.29	4.22	77.58	4.31	18.10	4.28
Azo-POP-11	74.06	4.14	14.44	5.12	80.00	4.44	15.50	5.16
Azo-POP-12	75.49	4.54	13.23	5.70	81.80	4.50	13.06	6.01

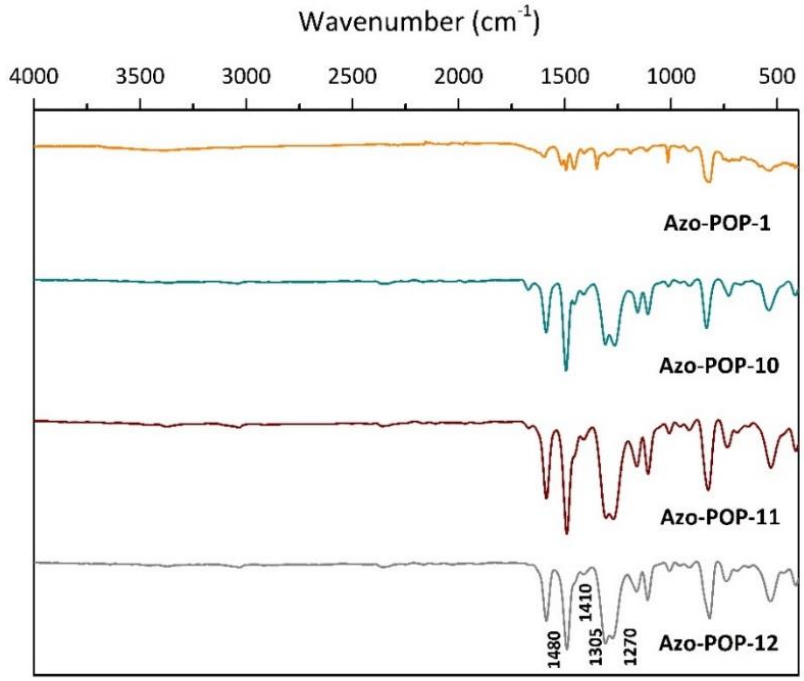

Figure B.4 – FTIR-ATR spectra of azo-POP-1, azo-POP-10, azo-POP-11 and azo-POP-12.

Table B.2 - Onset (T_{onset}) and decomposition (T_{dec}) temperatures of neat the component (PEGDA and IL) and respective iongel, as well as the prepared MMIMs containing different azo-POPs.

Membrane Sample	T_{onset} (K)	T_{dec} (K)
PEGDA	642	669
[C_2mim][TFSI] IL	688	719
PEGDA-80 TFSI	661	702
PEGDA-80 TFSI-0.5 POP-1	610	700
PEGDA-80 TFSI-0.5 POP-10	617	696
PEGDA-80 TFSI-0.5 POP-11	624	688
PEGDA-80 TFSI-0.5 POP-12	626	686

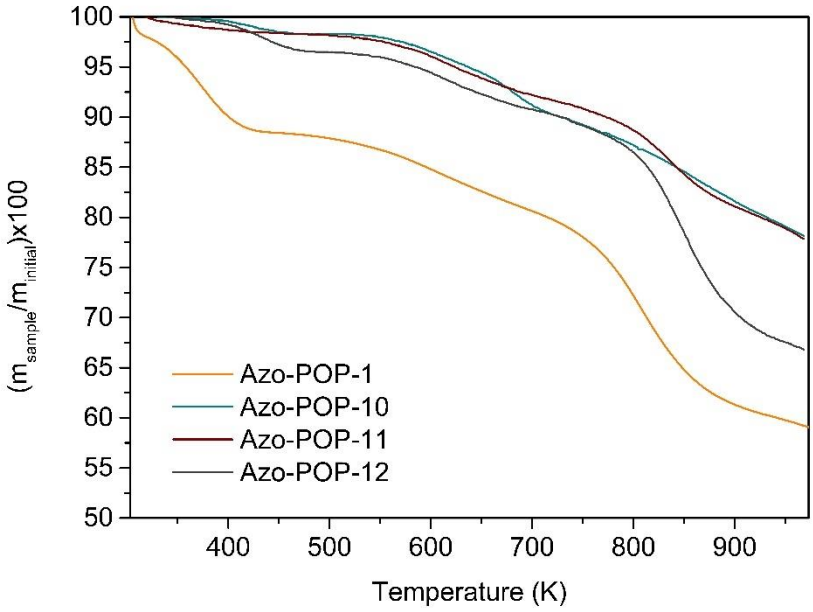

Figure B.5 - Thermogravimetric profiles of the azo-POPs synthesized in this work.

Table B.3 - CO_2 permeability and CO_2/N_2, CO_2/CH_4 and CO_2/H_2 ideal selectivities of the prepared composite membranes, in which the different MMIMs materials are supported on top of a porous polyamide filter.

Composite Membrane	P_t CO_2 (Barrer)	α_t (CO_2/N_2)	α_t (CO_2/CH_4)	α_t (CO_2/H_2)
PEGDA-80 TFSI	111 ± 4	18 ± 2	11 ± 1	6 ± 1
PEGDA-80 TFSI-0.5 POP-1	158 ± 5	28 ± 2	11 ± 2	12 ± 2
PEGDA-80 TFSI-0.5 POP-10	139 ± 4	20 ± 3	12 ± 1	11 ± 2
PEGDA-80 TFSI-0.5 POP-11	140 ± 5	40 ± 3	13 ± 1	11 ± 3
PEGDA-80 TFSI-0.5 POP-12	120 ± 3	52 ± 4	10 ± 2	12 ± 1

C

APPENDIX: MIXED MATRIX IONGEL MEMBRANES CONTAINING AZO-POROUS ORGANIC POLYMERS: INFLUENCE OF TEMPERATURE, PRESSURE AND WATER VAPOUR ON CO_2 SEPARATION

Table C.1 - CO_2 permeability and CO_2/N_2 selectivity as a function of vol% CO_2, pressure, and temperature, for the PEGDA-80 TFSI iongel

	***P* CO_2 (Barrer) (α CO_2/N_2)**					
	2 bar			**4 bar**		
Vol% CO_2	**303**	**323**	**353**	**303**	**323**	**353**
5	118 ± 1 (11 ± 1)	122 ± 2 (12 ± 1)	125 ± 1 (12 ± 1)	119 ± 12 (10 ± 1)	148 ± 2 (15 ± 1)	157 ± 3 (6 ± 1)
10	116 ± 1 (12 ± 1)	121 ± 2 (11 ± 1)	126 ± 2 (12 ± 1)	112 ± 1 (9 ± 1)	146 ± 2 (15 ± 1)	160 ± 2 (7 ± 1)
15	115 ± 1 (14 ± 1)	124 ± 2 (11 ± 1)	127 ± 2 (12 ± 1)	116 ± 2 (9 ± 1)	147 ± 3 (16 ± 1)	168 ± 2 (6 ± 1)
30	110 ± 2 (13 ± 1)	117 ± 3 (13 ± 1)	123 ± 1 (11 ± 1)	104 ± 1 (10 ± 1)	130 ± 2 (16 ± 1)	144 ± 1 (6 ± 1)

Table C.2 - CO_2 permeability and CO_2/N_2 selectivity as a function of vol% CO_2, pressure, and temperature, for the PEGDA-80 TFSI-0.5 POP-1.

	***P* CO_2 (Barrer) (α CO_2/N_2)**					
	2 bar			**4 bar**		
Vol% CO_2	**303**	**323**	**353**	**303**	**323**	**353**
5	142 ± 2 (19 ± 1)	154 ± 3 (19 ± 1)	170 ± 3 (18 ± 1)	138 ± 2 (14 ± 1)	160 ± 2 (16 ± 1)	175 ± 2 (10 ± 1)
10	150 ± 2 (21 ± 1)	158 ± 2 (19 ± 1)	167 ± 3 (17 ± 1)	144 ± 3 (15 ± 1)	165 ± 3 (16 ± 1)	175 ± 1 (12 ± 1)
15	144 ± 2 (20 ± 1)	158 ± 2 (19 ± 1)	172 ± 2 (17 ± 1)	140 ± 2 (15 ± 1)	168 ± 2 (16 ± 1)	174 ± 3 (19 ± 1)
30	135 ± 2 (20 ± 1)	141 ± 2 (17 ± 1)	166 ± 2 (18 ± 1)	128 ± 2 (13 ± 1)	146 ± 3 (17 ± 1)	157 ± 2 (10 ± 1)

Table C.3 - CO_2 permeability and CO_2/N_2 selectivity as a function of vol% CO_2, pressure, and temperature, for the PEGDA-80 TFSI-0.5 POP-11

	***P* CO_2 (Barrer) (α CO_2/N_2)**					
	2 bar			**4 bar**		
Vol% CO_2	**303**	**323**	**353**	**303**	**323**	**353**
5	130 ± 3 (25 ± 1)	137 ± 3 (23 ± 1)	154 ± 3 (21 ± 1)	125 ± 3 (14 ± 1)	158 ± 3 (17 ± 1)	167 ± 2 (8 ± 1)
10	132 ± 3 (25 ± 1)	144 ± 2 (22 ± 1)	158 ± 3 (21 ± 1)	127 ± 2 (13 ± 1)	153 ± 3 (18 ± 1)	170 ± 1 (8 ± 1)
15	134 ± 3 (24 ± 1)	146 ± 2 (21 ± 1)	163 ± 2 (21 ± 1)	126 ± 2 (13 ± 1)	154 ± 2 (18 ± 1)	178 ± 2 (9 ± 1)
30	123 ± 2 (24 ± 1)	133 ± 3 (22 ± 1)	147 ± 2 (21 ± 1)	107 ± 3 (15 ± 1)	140 ± 3 (17 ± 1)	159 ± 3 (9 ± 1)

Table C.4 - CO_2 permeability and CO_2/CH_4 selectivity as a function of vol% CO_2 and pressure, for the PEGDA-80 TFSI iongel.

	***P* CO_2 (Barrer) (α CO_2/CH_4)**	
Vol% CO_2	**2 bar**	**4 bar**
10	197 ± 3	185 ± 3
	(11 ± 1)	(10 ± 1)
20	201 ± 2	188 ± 3
	(10 ± 1)	(8 ± 1)
30	211 ± 3	190 ± 2
	(10 ± 1)	(9 ± 1)
40	207 ± 4	191 ± 2
	(8 ± 1)	(7 ± 1)

Table C.5 - CO_2 permeability and CO_2/CH_4 selectivity as a function of vol% CO_2 and pressure, for the PEGDA-80 TFSI-0.5 POP-1.

	***P* CO_2 (Barrer) (α CO_2/CH_4)**	
Vol% CO_2	**2 bar**	**4 bar**
10	245 ± 2	227 ± 3
	(12 ± 2)	(10 ± 1)
20	247 ± 3	226 ± 3
	(11 ± 1)	(9 ± 1)
30	246 ± 2	235 ± 3
	(13 ± 1)	(11 ± 1)
40	253 ± 4	227 ± 3
	(11 ± 1)	(10 ± 1)

Table C.6 - CO_2 permeability and CO_2/CH_4 selectivity as a function of vol% CO_2, and pressure, for the PEGDA-80 TFSI-0.5 POP-11

	***P* CO_2 (Barrer) (*α* CO_2/CH_4)**	
Vol% CO_2	**2 bar**	**4 bar**
10	224 ± 2	216 ± 3
	(11 ± 1)	(11 ± 1)
20	234 ± 3	216 ± 2
	(12 ± 1)	(12 ± 1)
30	237 ± 3	219 ± 3
	(12 ± 1)	(10 ± 1)
40	238 ± 2	220 ± 2
	(11 ± 1)	(10 ± 1)

Table C.7 - CO_2 permeability and CO_2/N_2 selectivity as a function of vol% CO_2 and RH, for the PEGDA-80 TFSI iongel.

	***P* CO_2 (Barrer) (*α* CO_2/N_2)**		
Vol% CO_2	**RH= 0%**	**RH= 11%**	**RH= 21%**
5	117 ± 2	206 ± 1	239 ± 3
	(11 ± 1)	(10 ± 1)	(5 ± 1)
10	116 ± 2	205 ± 2	245 ± 2
	(12 ± 1)	(9 ± 1)	(6 ± 1)
15	115 ± 2	180 ± 2	250 ± 2
	(14 ± 1)	(9 ± 1)	(5 ± 1)
30	110 ± 2	207 ± 3	253 ± 2
	(13 ± 1)	(8 ± 1)	(5 ± 1)

Table C.8 - CO_2 permeability and CO_2/N_2 selectivity as a function of vol% CO_2 and RH, for the PEGDA-80 TFSI-0.5 POP-1.

	***P* CO_2 (Barrer)** ***(α* CO_2/N_2)**		
Vol% CO_2	**RH= 0%**	**RH= 11%**	**RH= 21%**
5	142 ± 1	254 ± 2	378 ± 2
	(19 ± 1)	(16 ± 1)	(7 ± 1)
10	150 ± 2	264 ± 3	387 ± 3
	(21 ± 1)	(15 ± 1)	(6 ± 1)
15	144 ± 4	268 ± 5	388 ± 4
	(20 ± 1)	(14 ± 1)	(7 ± 1)
30	135 ± 3	269 ± 3	396 ± 4
	(20 ± 1)	(15 ± 1)	(7 ± 1)

Table C.9 - CO_2 permeability and CO_2/N_2 selectivity as a function of vol% CO_2 and RH, for the PEGDA-80 TFSI-0.5 POP-11.

	***P* CO_2 (Barrer)** ***(α* CO_2/N_2)**		
Vol% CO_2	**RH= 0%**	**RH= 11%**	**RH= 21%**
5	142 ± 1	254 ± 2	378 ± 2
	(19 ± 1)	(16 ± 1)	(7 ± 1)
10	150 ± 2	264 ± 3	387 ± 3
	(21 ± 1)	(15 ± 1)	(6 ± 1)
15	144 ± 4	268 ± 5	388 ± 4
	(20 ± 1)	(14 ± 1)	(7 ± 1)
30	135 ± 3	269 ± 3	396 ± 4
	(20 ± 1)	(15 ± 1)	(7 ± 1)

Table C.10 - CO_2 permeability and CO_2/CH_4 selectivity as a function of vol% CO_2 and RH, for the PEGDA-80 TFSI iongel.

	***P* CO_2 (Barrer)** ***(α* CO_2/CH_4)**		
Vol% CO_2	**RH= 0%**	**RH= 11%**	**RH= 21%**
10	197 ± 3	229 ± 3	270 ± 3
	(11 ± 1)	(9 ± 1)	(6 ± 1)
20	201 ± 2	291 ± 3	313 ± 2
	(10 ± 1)	(8 ± 1)	(6 ± 1)
30	211 ± 3	296 ± 3	312 ± 2
	(10 ± 1)	(7 ± 1)	(6 ± 1)
40	207 ± 2	292 ± 4	310 ± 4
	(8 ± 1)	(7 ± 1)	(6 ± 1)

Table C.11 - CO_2 permeability and CO_2/CH_4 selectivity as a function of vol% CO_2 and RH, for the PEGDA-80 TFSI-0.5 POP-1.

	***P* CO_2 (Barrer)** ***(α* CO_2/CH_4)**		
Vol% CO_2	**RH= 0%**	**RH= 11%**	**RH= 21%**
10	245 ± 2	392 ± 2	431 ± 4
	(12 ± 1)	(7 ± 1)	(4 ± 1)
20	247 ± 4	403 ± 2	454 ± 2
	(11 ± 1)	(7 ± 1)	(4 ± 1)
30	246 ± 2	398 ± 2	462 ± 2
	(13 ± 1)	(8 ± 1)	(5 ± 1)
40	253 ± 4	401 ± 5	471 ± 4
	(11 ± 1)	(8 ± 1)	(4 ± 1)

Table C.12 - CO_2 permeability and CO_2/CH_4 selectivity as a function of vol% CO_2 and RH, for the PEGDA-80 TFSI-0.5 POP-11.

	***P* CO_2 (Barrer)** ***(α* CO_2/CH_4)**		
Vol% CO_2	**RH= 0%**	**RH= 11%**	**RH= 21%**
10	224 ± 2	254 ± 4	398 ± 4
	(11 ± 1)	(8 ± 1)	(5 ± 1)
20	234 ± 1	269 ± 2	402 ± 3
	(12 ± 1)	(7 ± 1)	(6 ± 1)
30	237 ± 4	288 ± 2	403 ± 2
	(12 ± 1)	(8 ± 1)	(6 ± 1)
40	238 ± 4	299 ± 3	400 ± 5
	(11 ± 1)	(8 ± 1)	(6 ± 1)

D

APPENDIX: POLY(IONIC LIQUID) BASED SEMI-INTERPENETRATING POLYMER NETWORKS IN THE DEVELOPMENT OF MIXED MATRIX IONGEL MEMBRANES FOR CO_2 SEPARATION

D.1 Fourier Transform Infrared-Attenuated Total Reflectance spectroscpy (FTIR-ATR)

Figure D.1 displays the IR spectra obtained for the synthesized PDADMA-MSPM and PDADMA-MSS.

Looking at the FTIR-ATR spectrum of PDADMA-MSPM, the band between around 3050 and 2950 cm^{-1} were attributed to the cationic backbone. The peaks observed at 1710 and 1634 cm^{-1} were attributed to the C=O stretching vibration from the methacrylate group. Additionally, the peaks observed at 1162 and 1029 cm^{-1} originated from the asymmetric and symmetric vibrations of the SO_3^- functional group. The IR spectrum obtained for PDADMA-MSS presented a band between 3020 and 2935, which was attributed to the cationic backbone of the polymer structure. At 1182 and 1031 cm^{-1} two peaks can be observed, which were assigned to the asymmetric and symmetric vibrations of the SO_3^- group. The peaks observed at 1117 and 733 cm^{-1} were assigned to the in-plane and out-of-plane skeleton bending vibrations of the benzene ring, respectively. Moreover, the peak observed at 671 cm^{-1} corresponds to the out-of-plane bending vibrations of the -CH groups in the benzene ring.

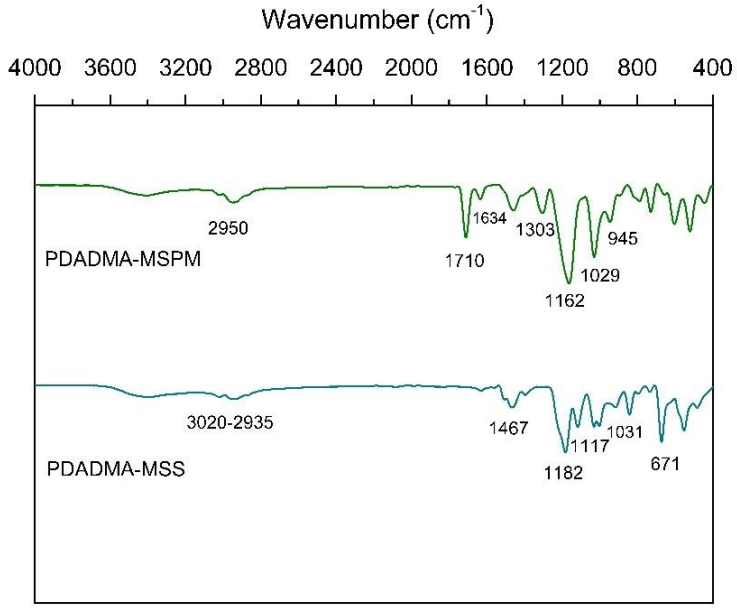

Figure D.1 - FTIR-ATR spectra obtained for the synthesized PDADMA-MSPM and PDADMA-MSS.

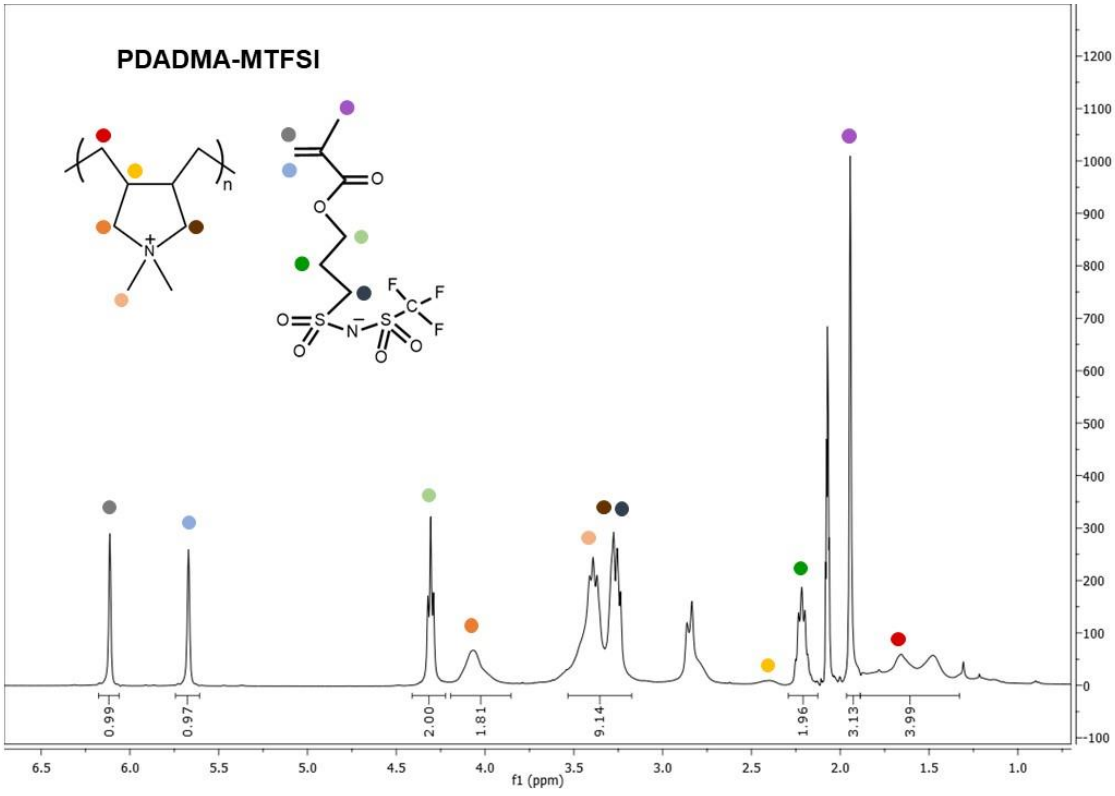

Figure D.2 - ^{1}H-NMR spectrum of PDADMA-MTFSI.

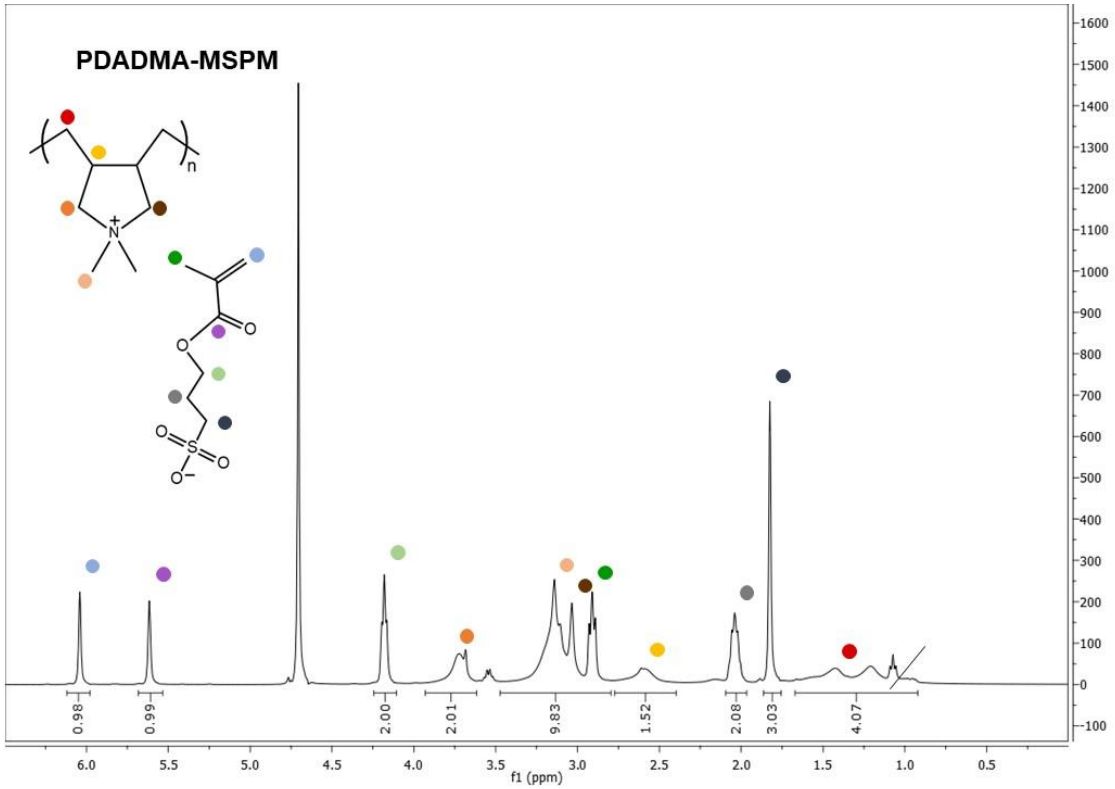

Figure D.3 - ^{1}H-NMR spectrum of PDADMA-MSPM.

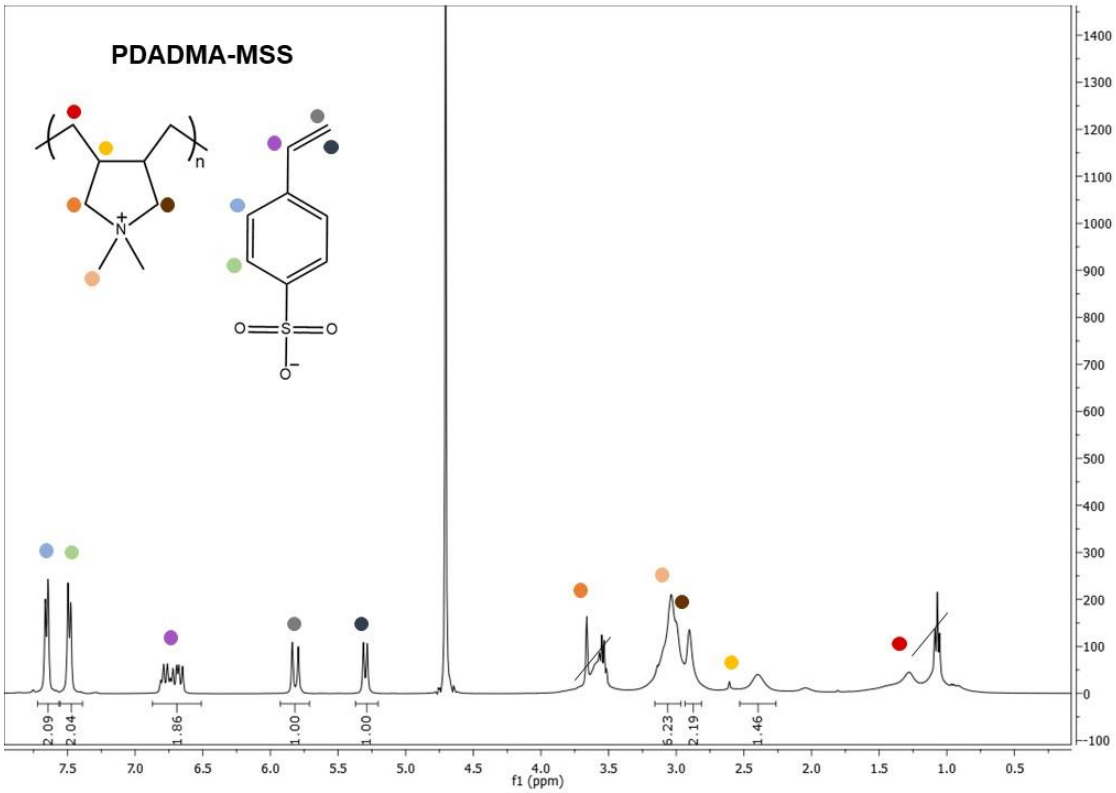

Figure D.4 - ^{1}H-NMR spectrum of PDADMA-MSS.

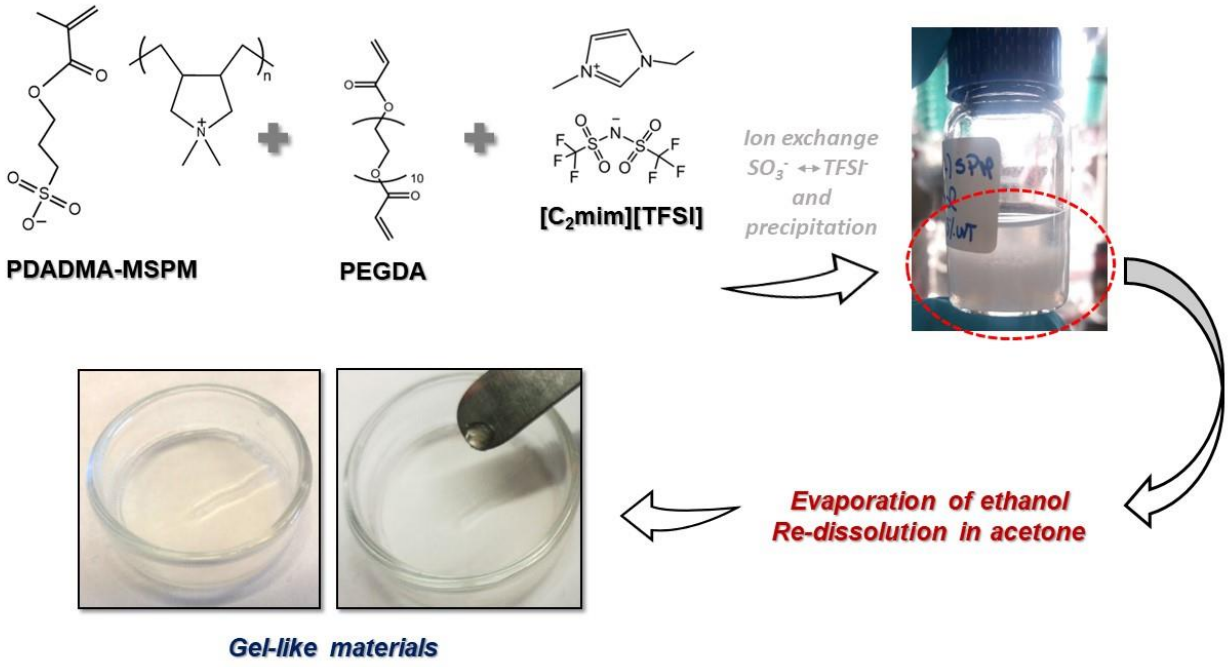

Figure D.5 - Schematic representation of the preparation of the sIPN-based iongel containing the MSPM anionic monomer.

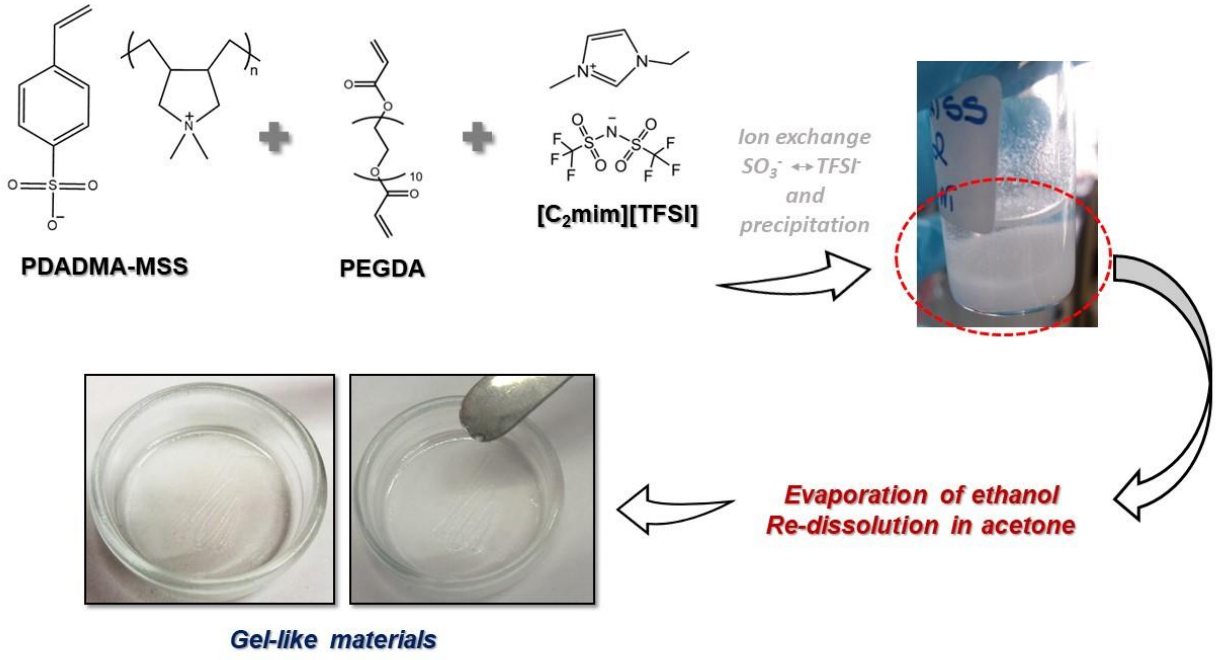

Figure D.6 - Schematic representation of the preparation of the sIPN-based iongel containing the MSS anionic monomer.

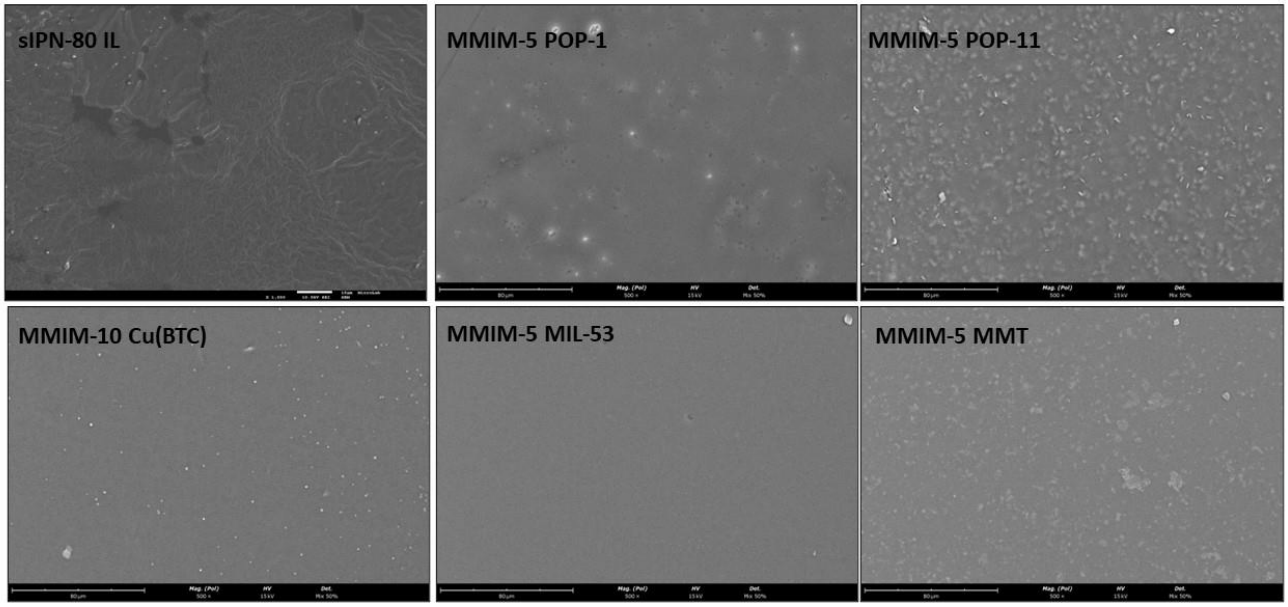

Figure D.7 - SEM surface images of the neat sIPN-80 IL and MMIMs prepared in this work.

ANA RITA MILEU MOTA NABAIS

DEVELOPMENT OF MIXED MATRIX IONGEL MEMBRANES FOR CO_2 SEPARATION

NOVA SCHOOL OF SCIENCE & TECHNOLOGY

2023

ANA RITA MILEU MOTA NABAIS

DEVELOPMENT OF MIXED MATRIX IONGEL MEMBRANES FOR CO_2 SEPARATION